INVESTIGATION INTO MECHANICAL AND TRIBOLOGICAL BEHAVIOR OF BIOMASS BASED CARBON BLACK FILLED EPOXY COMPOSITE

A THESIS SUBMITTED IN PARTIAL FULFILMENT OF THE REQUIREMENTSFOR THE DEGREE OF

Doctor of Philosophy
in
Mechanical Engineering

By

SHAKUNTALA OJHA

Department of Mechanical Engineering
National Institute of Technology
Rourkela - 769008

July-2015

INVESTIGATION INTO MECHANICAL AND TRIBOLOGICAL BEHAVIOR OF BIOMASS BASED CARBON BLACK FILLED EPOXY COMPOSITE

A THESIS SUBMITTED IN PARTIAL FULFILMENT OF THE REQUIREMENTSFOR THE DEGREE OF

Doctor of Philosophy
in
Mechanical Engineering

By

SHAKUNTALA OJHA

Under the Guidance of

Prof. S.K. Acharya

Department of Mechanical Engineering
National Institute of Technology
Rourkela - 769008
July-2015

Dedicated to
my parents

TABLE OF CONTENTS

DEPARTMENT OF MECHANICAL ENGINEERING
NATIONAL INSTITUTE OF TECHNOLOGY,
ROURKELA, ODISHA,
INDIA-769008

CERTIFICATE

This is to certify that the thesis entitled "**Investigation into mechanical and tribological behavior of biomass based carbon black filled epoxy composite**" submitted to the National Institute of Technology, Rourkela by **Mrs. Shakuntala Ojha**, Roll No. **511-ME-119** for the award of the Degree of Doctor of Philosophy in Mechanical Engineering is a record of bonafide research work carried out by her under my supervision and guidance. The results presented in this thesis has not been, to the best of my knowledge, submitted to any other University or Institute for the award of any degree or diploma.

The thesis, in my opinion, has reached the standards fulfilling the requirement for the award of the degree of **Doctor of Philosophy** in accordance with regulations of the Institute.

Dr. S. K. Acharya
Professor
Dept. of Mechanical Engineering
National Institute of Technology
Rourkela – 769008

ACKNOWLEDGEMENT

I would like to express my special appreciation and thanks to my advisors **Dr. S.K. Acharya,** Professor, Dept. of Mechanical Engineering, NIT, Rourkela for suggesting the topic of my thesis and their ready and able guidance throughout the course of my work.

I express my sincere thanks to Director NIT Rourkela **Prof. Sunil Kumar Sarangi** and **Prof. S.S. Mohapatra,** Head of the Department of Mechanical Engineering for providing all academic and administrative help during the course of my work.

The guidance, review and critical suggestion of the Doctoral scrutiny Committee (DSC) during various presentations and review meeting comprising of **Prof. S.S. Mohapatra**, **Prof. R.K. Behera**, **Prof. M. Kumar** and **Prof. D. Sarkar** are acknowledged. I also express my thanks to **Prof. S.K. Pratihar** of Ceramic Engineering Department for his help during my experimental work in the laboratory.

Last but not least, I would like to pay high regards to my father **Mr. Khageswar Ojha** and my mother **Mrs. Sanjukta Ojha** for their blessing, guidance and supports**.** This work could have been a distant dream if I did not get the moral encouragement and support from my spouse **Dr. Raghavendra Gujjala** throughout my research work and lifting me uphill this phase of life. This thesis is the outcome of the sincere prayers and dedicated support of my family.

Finally I wish to acknowledge the support given to me by all the PhD and M-tech Scholars of Tribology Laboratory during the course of my work also my special thanks to **Dhanajaya M**. My special thanks go to **Miss. Suneeta kumari** and **Miss Basu** for her unconditional help to see this work in this form.

Date: **(Shakuntala Ojha)**

ABSTRACT

Over the last few years, ecological concern and global warming has initiated a considerable interest in using natural materials to produce green products and reduce anthropogenic carbon dioxide emissions by all possible means. Kyoto protocol has further highlighted this issue by which many countries including India has committed to reduce combined CO_2, CH_4 and N_2O emissions. India and China are becoming important players in the Global GHG arena. The CO_2 emission in these countries increased by 9% and 6% respectively in 2011, relative to the previous years of their share in global CO_2 emission now equals that of Organization for Economic Co-operation and Development (OECD).

In the present scenario, natural fibers have excellent potential to reduce not only CO_2 emissions but also save non-renewable resources by substituting glass fiber reinforcements in plastic composites. Traditionally, glass fibers/wool has been extensively used as building insulation material and reinforcement in auto sector thermoplastics. However, environmental performance of glass fiber mat thermoplastics (GMTs) has several drawbacks due to extensive energy consumption and potential health risks during production and handling. Glass fibers cause severe abrasion to process equipment and their composites may transform into sharp splints during collision causing extra injuries to passengers. Moreover GMTs are non-recyclable and their incineration generates clinker like mass that is hard to dispose off except land filling.

There are many potential natural resources, which India has in abundance. Most of it comes from the forest and agriculture. Wood apple (Aegle marmelos) belongs of family rutaceae is highly reputed medicinal tree. Its fruit is commonly known as the "Stone apple" or "Bael". It is an indigenous fruit of India and found abundantly in sub-Himalayan forest, Bengal central, south India, Sri Lanka, Pakistan, Bangladesh, Burma, and Thailand. The peel of the fruit is very hard. Wood apple shell contains 39.54% cellulose, 26.06% hemicellulose, and 30.86% lignin. Coconut (Cocos nucifera) is a member of the palm family. The coconut palm is used for decoration as well as for culinary and non-culinary uses; virtually every part of the coconut palm has some human use. Coconut shell is non-food part of coconut, which is hard lignocellulosic

agro-waste. Coconut shell consists of 30.04% cellulose, 20.16% hemicellulose, and 25.76% lignin.If the density (low) of these materials is taken in to consideration, then its specific stiffness and strength are comparable to the respective quantities of glass fibers. The wood apple shell and coconut shell composites can be very cost-effective material especially for pipe lines carrying coal dust, slurries, desert structure, low cost housing, boats/sporting equipment, partition boards, doors and window panels.

As far as composite industries are concerned in recent period, carbon has been one of the outstanding elements that have revolutionized science of materials. Carbon provides the materials with excellent properties for a wide range of industrial applications. From carbon we receive the strongest fibers (carbon fibers), to one of the best solid lubricants (graphite), one of the best electrically leading materials (graphite electrodes), the best structural material for high temperature tribological application (carbon–carbon composites), one of the best porous absorbers (activated carbon), an essentially non-crystalline impermeable material (vitreous carbon), the hardest material (diamond), and now the most fascinating material, the fullerenes. All these forms are made by meticulously choosing the raw materials and processing conditions

Over the last century the production of carbon black (CB) is found to be relatively very expensive, which is produced by incomplete combustion of oil feed stocks. As a result the focus is now shifting towards agricultural waste products which are found to be good source of raw materials for the production of CB. This CB is produced by the pyrolysis of coal, wood, coconut shell, oil palm shell, jute, banana, bamboo, and other lignocellulosic biomass based materials which are carbonaceous in nature and rich in organic materials. Such agricultural by-products are usually inexpensive, for which the effective utilization has not been tried so far. It is unlikely that the use of products made from renewable resources will provide a complete solution to the pressing problems of industrial society.

The activated carbon was introduced for the first time industrially in the first part of the 20^{th} century, Activated carbon is a trade name for a carbonaceous adsorbent, which can be prepared from a large number of carbonaceous raw materials including agricultural and forestry residues by either a physical method or a chemical method. The most commercial products are made from agricultural waste such as coconut shell, bamboo, wood, sawdust, hard shell, nut shells and fruit pits.

Therefore the present research work has been under taken with an objective to produce carbon and activated carbon from the natural waste (wood apple shell and coconut shell) in the laboratory by utilizing the method of pyrolysis process. It is also planned to use these raw, carbon and activated carbon as reinforcing material in polymer composite of different weight fraction 5, 10, 15 and 20wt%. Direct usage of natural filler alone in polymer composite is inadequate in satisfactorily tackling all the technical needs of a fibre reinforced composite. It is reported that if natural fibre are carbonized to remove the waste material (volatiles and moisture) and increase the carbon percentage the strength of the composites are increased.

In this work an attempt has also been made to prepare carbon and activated carbon from wood apple shell and coconut shell. Efforts are made to study the effect of carbonization temperature on the tensile strength, flexural strength, tensile modulus and flexural modulus of the composite. Experiment is also carried out to study the erosive wear behavior of the composite developed. Effect of different parameters like impingement angle and velocity on the erosive wear behavior of carbon and activated carbon composite has also been studied and reported in the thesis. The test results indicate that there is an increase in both tensile and flexural and as well as the modulus for raw, carbonous and activated carbon of wood apple and coconut particulate filled composites. The trend observed for both wood apple and coconut particulate are almost same and the trend is raw<carbon black (400°C<600°C<800°C)<activated carbon black (800°C). The erosion efficiency (η) values obtained experimentally also confirm that the raw particulates (wood apple and coconut) composite exhibit semi ductile erosion response whereas carbonized and activated carbon reinforced composites exhibited semi-brittle and brittle response. .

LIST OF FIGURES

LIST OF TABLES

Chapter 1

Introduction

1.1 BACKGROUND

Over the last few years, ecological concern and global warming has initiated a considerable interest in using natural materials to produce green products and reduce anthropogenic carbon dioxide emissions by all possible means. Kyoto protocol has further highlighted this issue by which many countries including India has committed to reduce combined CO_2, CH_4 and N_2O emissions.

India and China are becoming important players in the Global GHG arena. The CO_2 emission in these countries increased by 9% and 6% respectively in 2011, relative to the previous years of their share in global CO_2 emission now equals that of OECD [1]. Figure 1.1 shows the level of CO_2 emission [2] over time from 1990 to 2011, for the six largest emitters in the world.

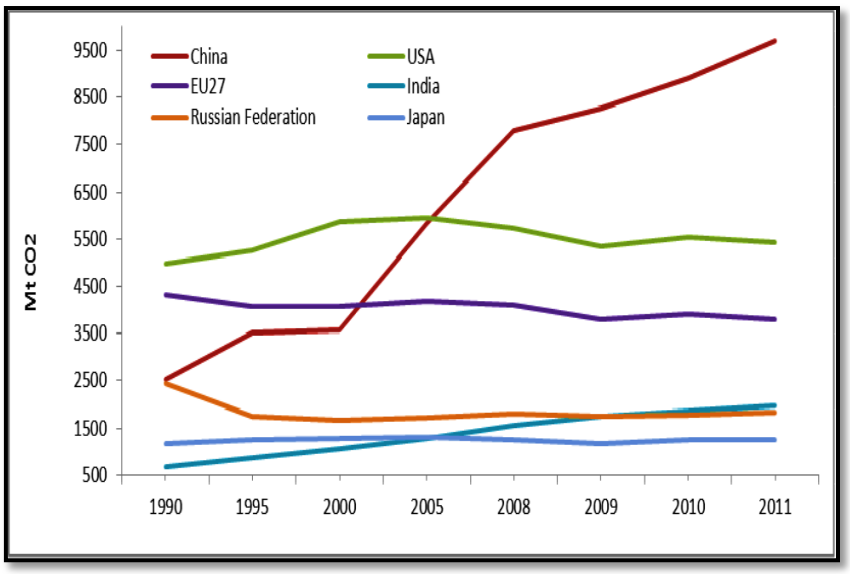

Figure 1.1 CO_2 emissions per capital [1, 2]

While in the past India has been below Russia and Japan, its upward and steadily increasing CO_2 emissions trend has exceeded both of these countries. In 2008, India was the fifth largest emitter of GHG in the world and in 2011 it was already the fourth emitter in terms of CO_2 alone (see Figure 1.1), overtaking Russia to a position behind China, the USA and the EU-27. A report released by the Government of India, which forecasts the Indian production of GHG based on five different models, shows that India's GHG will be between 4 and 7 billion tons in 2030 [3]. However, the per

capita GHG in 2030, estimated to be between 2.8 and 5 tonnes CO_2-eq, will still be below the global average 25 years prior. Four out of the five studies in this report estimate that the per capita emissions will stay below 4 tonnes. Despite the fact that India, like China, refuses to engage in emissions cuts through international binding agreements, the country is said to adopt an innovative market-based scheme (PAT) as part of the National Action Plan for Climate Change, to promote energy efficiency, based on certificates for meeting energy efficiency targets and allowing for their trading [4]. The mandatory energy efficiency scheme, planned to commence in 2014 aims to reduce the emissions intensity by 20%, to 25% of the 2005 level, by 2020. The scheme will cover eight sectors responsible for 54% of India's energy consumption [5].

In the present scenario, natural fibers have excellent potential to reduce not only CO_2 emissions but also save non-renewable resources by substituting glass fiber reinforcements in plastic composites. Traditionally, glass fibers/wool has been extensively used as building insulation material and reinforcement in auto sector thermoplastics. However, environmental performance of glass fiber mat thermoplastics (GMTs) has several drawbacks due to extensive energy consumption and potential health risks during production and handling. Glass fibers cause severe abrasion to process equipment and their composites may transform into sharp splints during collision causing extra injuries to passengers. Moreover GMTs are non-recyclable and their incineration generates clinker like mass that is hard to dispose off except land filling.

On the other hand, natural fibers are being explored more extensively by research institutions and automobile companies as environmental friendly alternative for the use of glass fibers. Most of the bast fibers being studied are obtained from naturally growing plants of flax, hemp, and kenaf. These fibers are renewable, non-abrasive to process equipment and can be incinerated at the end of their life cycle for energy recovery as they possess a good deal of calorific value. They are also very much safe during handling and less suspected to affect lungs during processing and use.

As far as composite industries are concerned in recent period, carbon has been one of the outstanding elements that have revolutionized science of materials. Carbon provides the materials with excellent properties for a wide range of industrial applications [6, 7]. From carbon we receive the strongest fibers (carbon fibers), to one

of the best solid lubricants (graphite), one of the best electrically leading materials (graphite electrodes), the best structural material for high temperature tribological application (carbon–carbon composites), one of the best porous absorbers (activated carbon), an essentially non-crystalline impermeable material (vitreous carbon), the hardest material (diamond), and now the most fascinating material, the fullerenes. All these forms are made by meticulously choosing the raw materials and processing conditions [8].

Over the last century the production of CB is found to be relatively very expensive, which is produced by incomplete combustion of oil feed stocks [9]. As a result the focus is now shifting towards agricultural waste products which are found to be good source of raw materials for the production of CB. This CB is produced by the pyrolysis of coal, wood, coconut shell, oil palm shell, jute, banana, bamboo, and other lignocellulosic biomass based materials which are carbonaceous in nature and rich in organic materials. Such agricultural by-products are usually inexpensive, for which the effective utilization has not been tried so far. It is unlikely that the use of products made from renewable resources will provide a complete solution to the pressing problems of industrial society.

1.2 CARBON BLACK

Carbon black is a material produced by incomplete combustion of heavy petroleum products such as FCC tar, coal tar, ethylene cracking tar and a small amount from vegetable oil.

The enormous majority of carbon black finds its use as reinforcement in vulcanized rubber goods, including more than two-thirds for tires alone [10]. On the other hand, carbonaceous material also plays a major role as pigments for coating, plastics, ink, and inkjet applications [11, 12]. Another commercial value of carbon finds its use in waste water treatment and heavy metal removal process. The separation technology by its adsorption capabilities has been known as carbon great utilization for decades [13].

It is found from the literature that Carbon black is extensively used as filler material in polymer industry due to its own qualities and characteristics [14]. The

properties of carbon used in the composites depend mostly on the origin, processing conditions, and chemical treatments. These fillers are to be added to polymers for obtaining the desirable properties and improve the products service qualities. Also, the high potential of carbon gives an impact in the thermoset polymer industry whose utility is growing rapidly in civil and construction sectors. Some of the benefits of carbon are its use as a UV stabilizer, electric conductivity, weather resistance, and modifying the mechanical properties of the carbon filled composites. As examples of this is the carbon black filled polyethylene composites usein pipelines in extreme weather conditions, while polypropylene geotextiles carbon black composites are used for soil reinforcement and for many construction purposes [15].Carbon black composites could also endure wide thermal ranges, making them valuable in thermo-mechanical applications such as the automotive industry [16].

Although commercially available carbon blacks are obtained from thermal cracking of natural gas and furnace black produced by incomplete combustion of oil feed stocks [17]. This carbon black is relatively expensive due to its dependence on the decrease in the supply of crude oil. It is therefore crucial to develop sustainable alternative source of carbon from renewable resources.Biomass is the only renewable source of carbon which can be converted to solid, liquid and gaseous product through various conversion processes. Currently, biomass provides about 14% of the world's energy consumption [18], but still large quantities of biomass have no specific use.They are burnt in open air or are dumped, which generate pollutants including dust and acid rain gases such as sulfur dioxide and nitrogen oxides.

1.3 ACTIVATED CARBON (AC)

The activated carbon was introduced for the first time industrially in the first part of the 20th century, when the activated carbon of the plant was produced for use in the reinforcing. Since then, Activated carbon has been used in many industries [19].Activated carbon is a trade name for a carbonaceous adsorbent, which can be prepared from a large number of carbonaceous raw materials including agricultural and forestry residuesby either a physical method or a chemical method [20].

The most commercial products are made from agricultural waste such as coconut shell, bamboo, wood, sawdust, hard shell, nut shells, fruit pits,. The selection

of the raw material to produce activated carbon depends on its end-use or design specifications, since different raw materials will produce activated carbon with different properties. Activated carbonobtained from hard wood is preferable for adsorptionbecause charcoal obtained from soft wood, such aspinewood, is very unstable and readily crumbles. It hasbeen reported that the best grades of AC are obtained from the shell material.

1.4 POLYMERIC COMPOSITE

Polymeric materials have been finding great potentials in the industry as a class of important engineering materials. For centuries, the use of polymers in everyday life has become important part of human life. The growth of polymer starts in the early 19^{th} century with the development of celluloid, a hard plastic which is formed from nitrocellulose. The development of polymer technology was slow until 1930s, before the material such as phenol, vinyl, polystyrene and polyester were developed. After the development of these materials, the polymer research has taken an enormous growth that is still going on. Polymers are rapidly developing materials with the attractive advantages of low density and cost compared to metals and ceramics. Generally, polymers are very large molecules consisting of many small molecules called monomers or repeating units that can be linked together to form long chains and are known as macromolecules. A typical polymer may include tens of thousands of monomers. This specific long chain like structures is responsible for their fascinating properties with a wide range of the versatility of polymers for years in different fields of consumer durables, electrical and electronic equipment, aerospace, packaging, medical equipment, automobiles and other engineering applications.

Reinforcements are needed to provide additional strength for polymers. The addition reinforcements into polymers is termed as “polymer matrix composite” or shortly PMCs. PMCs are engineering materials consists of two or more significantly different physical or chemical properties of constituent materials separated by distinct interface. Upon the combination of this material, a material with properties different from the individual characteristics is produce. The matrix phase of the PMCs is generally thermoset or thermoplastic materials.

Thermoset resins are the materials which undergo chemical reactions when heating that crosslink the entire polymer chains into a three dimensional network and tends to have high dimensional stability, high temperature and good resistance to solvents. Thermoset resins are irreversible process which includes phenol formaldehyde, unsaturated polyester, vinyl ester, polypropylene, acrylonitrile-butadiene-styrene, polyamide, polyetherimide etc. Upon heating the thermoplastics to the process temperature, the materials can be formed into any shape. Thermoplastic materials offer a great advantage from a manufacturing point of view, because it is easier and faster in processing compared to thermoset resins which attract high volume industries such as automotive industries. The reinforcement phase of PMCs is particulate or fibrous type of reinforcements. The particulate reinforcements are composed of particles which include titanium di-oxide, calcium carbonate, kaolin, zinc oxide, talc, potassium titanate, carbon black etc. The fibrous types of reinforcements are glass fibers, carbon fibers, aramid fibers, kelvar etc. Due to available of wide variety of matrix and reinforcements, the design potentials are greater in terms of low weight, corrosion resistance, dimensional stability, quick assembly etc. than the other composites such as metal matrix or ceramic matrix composites.

Polymer based composite materials are becoming essential part of today's materials and have successfully substituted the traditional materials in most applications where high strength to weight ratio, high tensile strength at elevated temperatures, high creep resistance, high toughness, light weight, good surface finish, low cost etc. are required. Due to the better properties of polymer composites, these materials are used extensively in engineering components and play a key role in the sectors such as automobile, aircraft, electronics, packaging, healthcare, construction, defense etc. For the past few decades, polymer composites have generated wide interest in tribo-engineering applications and used in fabricate mechanical components such asbushes, gears, bearing cages, cams etc. due to their special property of self-lubrication, corrosion resistance, light weight etc. The polymer composite materials are well suited for non-lubricated condition and it is the key factor for this material selection in tribological applications [21].

Extensive studies [22-29] have carried out by various researchers for the synthesis and characterization of carbon black and activated carbon prepared from various biomasses. There use in various industrial applications is well documented.

Going through the available information on the utilization of carbon black derived from biomass, it is seen that some of the natural fibers are carbonaceous in nature and reach on organic materials. This biomass can be converted to carbon black and activated carbon which can be used as filler for making light weight polymer composite. This will give an effective means for proper and optimum utilization of large quantities of unwanted low value agricultural residues and underutilized crop in to useful high value product.

1.5 ORGANIZATION OF THESIS

The present research work has been under taken to fabricate carbon black and activated carbon black particles from wood apple and coconut shell in the laboratory by utilizing the method of pyrolysis. It is also planned to use these carbon fillers as reinforcing material in polymer composite and also to investigate the effect of the carbonization and activation on tensile strength, flexural strength, tensile modulus and flexural modulus of the composite. Experiment was also carried out to study the erosive wear behavior of the composite developed. In addition the carbonization and activation effect on the erosive wear behavior of composite has also been studied and reported in the thesis.

In the second chapter detail discussion of properties and structure of natural fibers, carbon black and a literature review designed to provide a summary of the work related to present investigation are presented.

In the third chapter detail discussion on the characterization of the raw, carbon black and activated carbon black of wood apple and coconut shell particles have been presented.

In the fourth chapter mechanical characterization of raw, carbon black and activated carbon black particulate obtained from wood apple and coconut shell has been studied.

In the fifth chapter the solid particle wear response of raw wood apple and coconut particulate composite with different weight percentage, various impact angle and various velocities has been studied.

Sixth chapter discusses solid particle erosion wear behavior of the carbon black (various carbonization temperatures i.e. 400°°C, 600°°C and 800°C) and activated carbon black (activation temperature 800°C) composite of both wood apple and coconut shell particulate composite has been studied.

In the seventh chapter conclusions have been drawn from the above studies mentioning scope for the future work.

Chapter 2

Literature Survey

2.1 INTRODUCTION

The purpose of this literature review is to provide back ground information on the issue to be considered in this thesis and to emphasize the relevance of the present study. This treatise embraces various aspects of carbonaceous materials obtained from lignocellulosic materials with special reference to their mechanical and tribological behavior.

The topics include brief review:

- **Natural fiber a source of carbonaceous material**
- **On carbon black and activated carbon**
- **On Processing of activated carbon**
- **Methods of Activation**
- **Factors Affecting Activated Carbon Production**
- **Characterization of carbon black and activated carbon black**
- **On wear and its classification**

Composites materials have emerged as a major class of structural elements and are either used or being considered as substitutions for metals/traditional material in aerospace, automotive and other industries. The outstanding features of fiber reinforced polymer composites (FRPs) are their high specific stiffness, high specific strength and controlled anisotropy, which make them very attractive structural materials. Other advantages of composites are light weight, good corrosion resistance, impact resistance, fatigue strength and flexibility in design capabilities. A unique feature of composites is that the characteristics of the finished product can be tailored to a specific engineering requirement by a careful selection of matrix and reinforcement type. FRP composite materials consist of two or more chemically distinct constituents have a distinct interface separating them. It has a unique combination of properties that are noticeably different from the constituent properties. Generally, a discontinuous phase (reinforcement) is embedded into a continuous phase (matrix). Polymer based composite materials (PMC) or FRP constitutes a major category of composites materials with a wide range of applications. They offer very attractive properties, which can be tailored to the specific requirements by careful selection the fiber, matrix,

fiber configuration (short, long, strength, woven, braided, laminated, etc.) and fiber surface treatment. PMCs exhibit desirable physical and chemical properties that include lightweight coupled with high stiffness and strength along the direction of the reinforcing fiber, dimensional stability, temperature and chemical resistance and relatively easy processing. The role of matrix in a fiber-reinforced composite is to

- ✓ Transfer stresses between the fibers
- ✓ Provide a barrier against an adverse environment
- ✓ Protect the surface of fibers from mechanical abrasion

Specifically, lignocellulosic wastes are a low-cost natural carbon source for the synthesis of several materials including the production of activated carbons. In this context, it is convenient to remark that natural resources play a dominant role in the economic activities and the utilization of lignocellulosic wastes for the synthesis of valuable commercial products may contribute to the economic development and to prevent environment pollution especially in developing countries [30]. Therefore, lignocellulosic materials are considered as an interesting and important natural resource for production of activated carbons based on the fact that several billion tons of these materials are available [30, 31]. Actually, these precursors are considered as the most appropriate candidates for a cost-effective preparation of activated carbons [32].

2.2 NATURAL FIBER A SOURCE OF CARBONACEOUS MATERIAL

The terrestrial plants can be classified into three taxonomic groups in general, namely, soft wood trees, hard wood trees and the grasses. Plant tissue is made up of lignocellulosic material. The lignocellulosic material consists of plant cell wall and also the intracellular substances. The cell wall is made up of holocellulose which is a combination of cellulose and hemicellulose and lignin. In general, the intracellular substances are termed as extractives based on the analytical method of extraction. The above mentioned components, namely, lignin, cellulose and extractives are known to vary in chemical structure and initial carbon content. The cellulose is a linear polymer of glucose with a theoretical carbon content of 44.4 %. Lignin is a three dimensional polymer of aromatic alcohols with a carbon content of 60 – 63%. As a result the carbon content of a lignocellulosic material is dependent on the relative abundance of its

constituents. Thus it can be said that greater the carbon content of the lignocellulosic precursor greater will be the carbon content of the char.

2.2.1 Cellulose

Cellulose is considered to be the most abundant renewable polymer on Earth [33]. This structural material is naturally organized as microfibrils linked together to form cellulose fibers. It is biosynthesized by a number of living organisms ranging from higher to lower plants, some amoebae, sea animals, bacteria and fungi [34]. Cellulose consists of a linear homopolysaccharide composed of β-D-glucopyranose units linked together by β-1-4-linkages [35]is shown in figure 2.1. Each monomer bears three hydroxyl groups. It is therefore obvious that these hydroxyl groups and their ability to form hydrogen bonds play a major role in directing the crystalline packing and also governing the physical properties of cellulose [36].

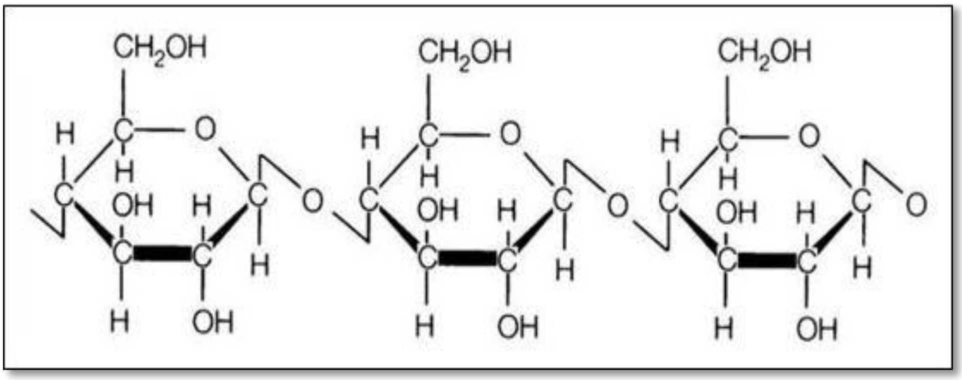

Figure 2.1 Molecular structures of cellulose and the (β 1→4) glycoside bond

2.2.2 Hemicellulose

The term hemicellulose is a collective term. It is used to represent a family of polysaccharides such as arabino-xylans, gluco-mannans, galactans, and others that are found in the plant cell wall and have different composition and structure depending on their source and the extraction method.

The most common type of polymers that belongs to the hemicellulose family of polysaccharides is xylan. As shown in figure 2.2, the molecule of a xylan involves 1->4 linkages of xylopyranosyl units with α-(4-O)-methyl-D-glucuronopyranosyl units attached to a hydroxylase units. The result is a branched polymer chain that is mainly

composed of five carbon sugar monomers, xylose, and to a lesser extent six carbon sugar monomers such as glucose.

Important aspects of the structure and composition of hemicellulose are the lack of crystalline structure, mainly due to the highly branched structure, and the presence of acetyl groups connected to the polymer chain [37].

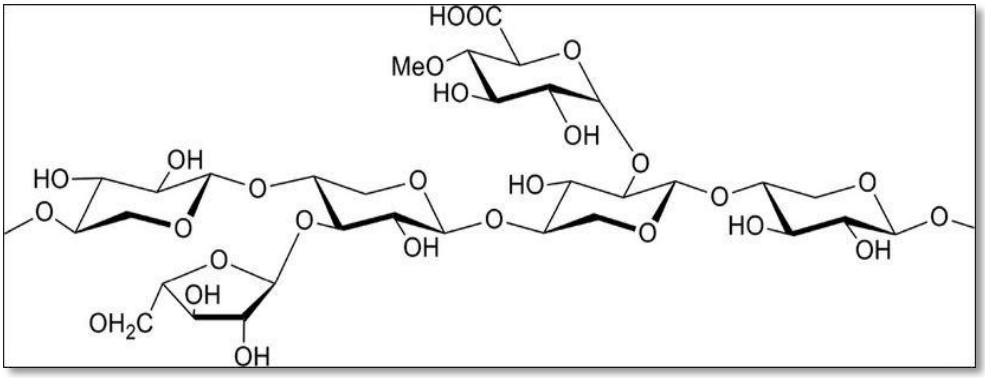

Figure 2.2 A schematic representation of the hemicellulose backbone of arborescent plants

2.2.3 Lignin

Second to cellulose, lignin is one of the most abundant bio macromolecule in the world. In trees, lignin gives stiffness to the cell wall and, hence, contributes to the mechanical strength of the wood.Lignin is the most complex natural polymer. It is an amorphous three-dimensional polymer with phenylpropane units as the predominant building blocks is shown in figure 2.3. More specifically, p-coumaryl alcohol, coniferyl alcohol and sinapyl alcohol (0) are the ones most commonly encountered.

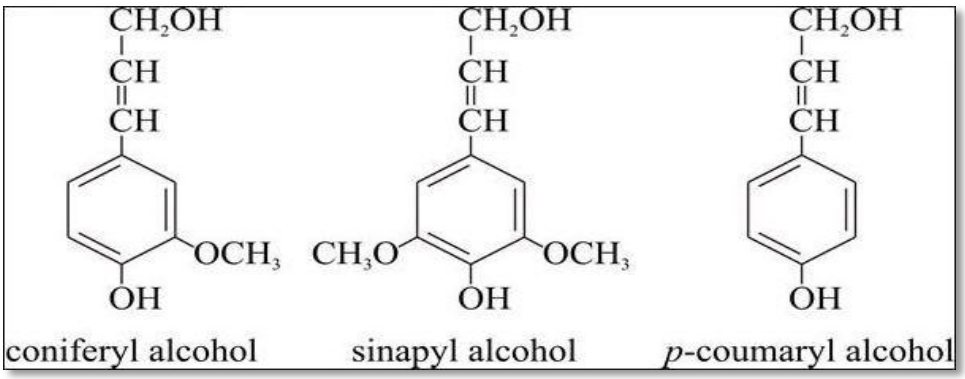

Figure 2.3 The three phenyl propane monomers in lignin

Dividing higher plants into two categories, hardwood (angiosperm) and softwood (gymnosperm), it has been identified that lignin from softwood is made up of

more than 90% ofconiferyl alcohol with the remaining being mainly p-coumaryl alcohol units. Contrary to softwoods, lignin contained in hardwood is made up of varying ratios of coniferyl and sinapyl alcohol type of units.

Lignin in wood behaves as an insoluble three-dimensional network. It plays an important role in the cell's endurance and development, as it affects the transport of water, nutrients and metabolites in the plant cell. It acts as binder between cells creating a composite material that has a remarkable resistance to impact, compression and bending.

2.2.4 Pectin

Pectin is a complex branched structure of acidic structural polysaccharides, found in fruits and bast fibers. The majority of the structure consists of homopolymeric partially methylated poly-α-(1-4)-D-galacturonic acid residues, but there are substantial 'hairy' non-gelling areas of alternating α-(1-2)-L-rhamnosyl-α-(1-4)-Dgalacturonosyl sections containing branch-points with mostly neutral side chains (1-20 residues) of mainly L-arabinose and D-galactose (rhamnogalacturonan-I). Pectin is the most hydrophilic compound in plant fibres due to the carboxylic acid groups and is easily degraded by de-fibrated with fungi [38]. Pectin along with lignin and hemicelluloses present in natural fibers can be hydrolyzed at elevated temperatures is shown in figure 2.4.

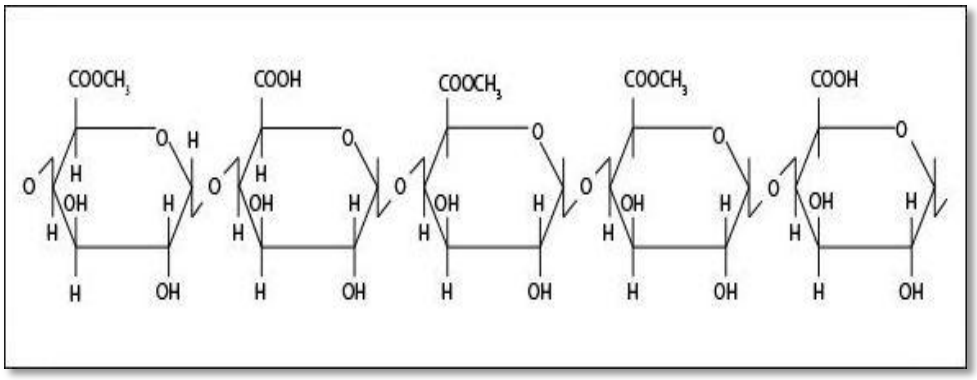

Figure 2.4 Basic unit of pectin: Poly-α-(1-4)-D-galacturonic acid

2.3 ON CARBON BLACK AND ACTIVATED CARBON

Carbon materials are unique and versatile in their performance. They have major industrial significance. Activated carbon is a material with high porosity consisting of hydrophobic graphene layer as well as hydrophilic surface functional groups making them beneficial for sorption and catalytic applications. The applications and manufacturing method of activated carbon black have also been discussed in the previous chapter.

Thermochemical decomposition of organic matter in the absence of oxygen at high temperature is termed as pyrolysis. The main process-related parameters are peak temperature, pressure, heating rate, residence time, and heat transfer rates. Particle size and shape, physical properties, composition (lignin, cellulose, hemicellulose, etc.) and ash content are most important feedstock properties which influence the properties of the final product [39].

Lignocellulosic materials have been and will be with mankind forever and they hold a promise of renewable and inexhaustible supply of carbon materials provided suitable methods of production are developed. In addition they are more evenly distributed throughout the globe relative to either coal or petroleum. Thus these lignocellulosic materials are a good source of natural resources for the generation of carbon materials rather than fossil fuels.

The demand for activated carbon is increasing owing to the increased utility of the carbon materials in pollution control. As a result, cost of activated carbon is also growing depending on the application. Designing ways for the production of activated carbon through economic ways is the need of the hour. A range of low cost, easily available, carbon rich and low ash precursors and sources are being explored for the production of carbon materials.

Most of the commercial activated carbons are either coal based [40, 41] or petroleum pitch based [42] which are prone to exhaustion. Their global distribution is non-uniform. As the applications of activated carbon are immense, the gap between demand and supply is ever widening. This may in due course result in scarcity of the material in addition to becoming expensive. This situation necessitates the need for the

exploration of new sources of carbon materials with desired physicochemical properties namely, high specific surface area, micro or mesoporosity or both, depending on the end application, surface functionality, thermal stability, carbon purity, adsorptive capacity and chemical composition (inherent or induced presence of hetero atoms like B, N, S and P).

Hence various kinds of agricultural by-products have been extensively investigated for fast pyrolysis, including corn stover, switchgrass, logging residue, coconut shell, sugarcane bagasse, nutshells, forest residues and tobacco stems [43-46]. In some countries, these products are considered as wastes and have caused significant disposal problems. Their utilization in the carbon industries is a viable solution to this environmental issue. Such agricultural by-products are usually inexpensive, for which the effective utilization has been desired. The raw materials used are nonrenewable. Therefore, all possible sources should be investigated. Therefore the preparation of activated carbon with high surface area from agricultural by-product is a very interesting subject.

2.4 ON PROCESSING OF ACTIVATED CARBON

The processing of activated carbon basically involves selection of parameters that effecting the activated carbon production, carbonization process and types of activation. Basically, there are two different methods in the preparation of activated carbon; single step pyrolysis and two step pyrolysis.

Single step pyrolysis usually applied in the preparation of activated carbon using **chemical activation** method. Two step pyrolysis is usually applied in the preparation of activated carbon using **physicalactivation** method. The product quality of two step pyrolysis is better compared to the single step pyrolysis.

The choice of activation method is also depending upon the starting material and whether a low or high density, powdered or granular carbon is desired. Figure 2.5 shows a block diagram and the summary of comparison for both procedures used in the preparation of activated carbon.

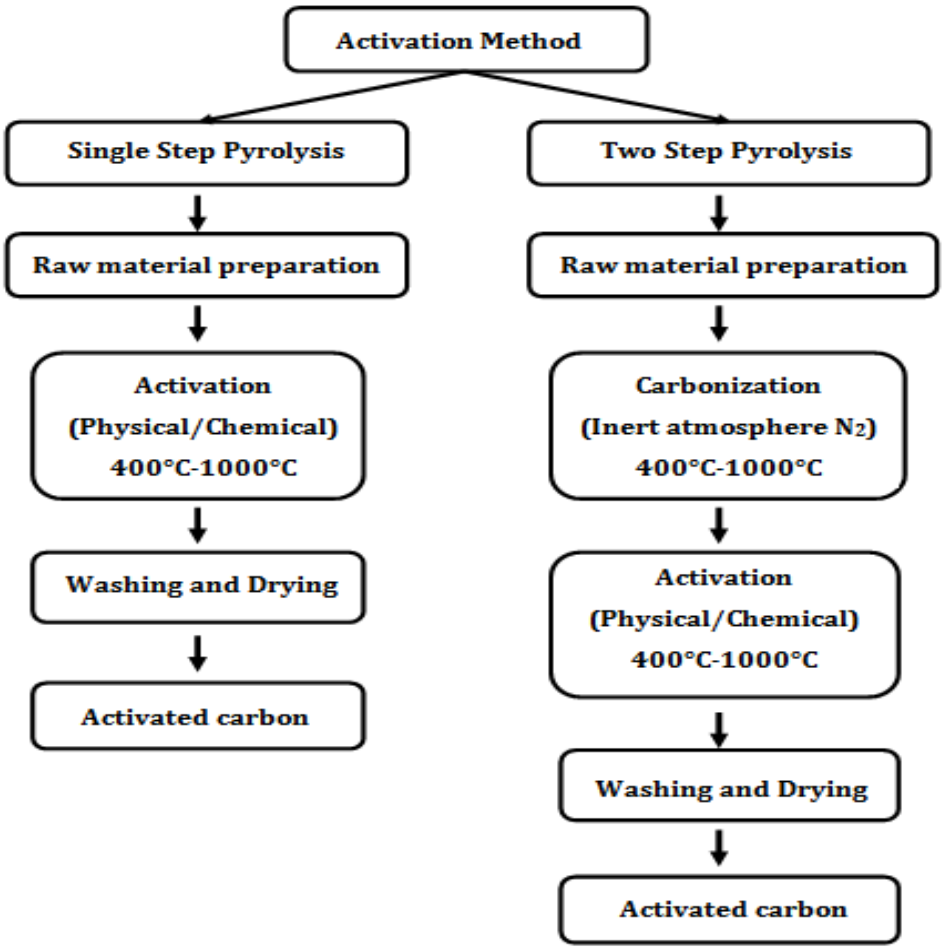

Figure 2.5 Block diagram and comparison of boththe procedures used in the preparation of activated carbon

2.4.1 Single Step Pyrolysis Method

Single step pyrolysis means that the carbonaceous raw material from the beginning comes in contact with the chemical activating agent or physical activating agent, so that both carbonization and activation occur simultaneously at the same temperature.

2.4.2 Two-step Pyrolysis Method

In two-steps pyrolysis method carbonization and activation are not carried out simultaneously, but in distinct steps.It is a conventional manufacturing process for activated carbon. The overall process usually consists of two steps:

1. Thermal pyrolysis or carbonization at a relatively low temperature (typically 400°C-800°C) in the presence of nitrogen or helium to break down the cross-linkage between carbon atoms
2. Thermal activation or physical activation or gasification of carbon black or carbonized of raw material at 800°C-1000°C for further development of the porosity

2.5 METHODS OF ACTIVATION

All the available methods of activation can be classified in to two types, namely, physical activation or chemical activation depending on whether a gaseous or solid activating agent is used. Each of these methods has its own merits and demerits.

2.5.1 Physical/ Thermal Activation

The production of activated carbon by physical activation can be done using two methods. These methods are called single step pyrolysis and two-step pyrolysis depending on whether the carbonization and activation processes occur simultaneous or in the separate steps.

2.5.1.1 Pyrolysis or carbonization

In the first step, the pyrolysis (so-called carbonization) of the carbonaceous precursor [47] at elevated temperatures (500°C-1000°C) under inert atmosphere. The terms carbonization means to transformation of organic matter to elemental carbon at high temperature in the absence of oxygen which goals the maximization the carbon black product forms from the parent material and the increase carbon content for the activated carbon production.

During carbonization process, most of the non- carbon elements, hydrogen and oxygen are first removed in gaseous form by pyrolytic decomposition of the starting materials [48] and the free atoms of elementary carbon are grouped into organized crystallographic formations known as elementary graphite crystallites. This process drives off the volatiles matter to form carbon black. The residue that contains mostly carbon is called carbonized material or carbon black. Three products are obtained from the decomposition of raw material namely: carbon black, tar and product gas. At the

time of the carbonization, hundreds of co-current reactions occur because of the complex and the heterogeneous origin of the lignocellulosic biomass.

The carbon black obtained normally has low surface area and adsorption capacity since the porous structure is not well developed. As a result this porous is not enough for most of the adsorption processes. For this purpose the carbonization step is followed by activation process for increasing the porous structure, widened the existing micropores and mesopores of carbon black particles. The temperature, heating rate, atmosphere that reactions takes place in, catalyst usage, reactor configuration and carbonization time are the important process parameters in the pyrolysis or carbonization process that should be carefully selected and controlled.

2.5.1.2 Thermal Activation

In process of carbonization, a carbon skeleton with a rudimentary porous structure is formed which is known as carbon black. The pores of the produced carbon black can be blocked by the tar formed in thermal process and result in a low adsorption capacity. Therefore, physical or thermal activation after the carbonization process is required to remove the blockage caused by tar. Subsequently, in the second stage the resulting carbon black are subjected to a partial and controlled gasification at a higher temperature.

Thermal activation involves the contact between the carbon black and activating agent followed by reaction between the surface carbons on the pores and the activating agent. These agents extract carbon atoms from the structure of the porous carbon.

Thermal activation is performed by an oxidizing agent such as CO_2, steam, O_2 or a mixture of them at elevated temperatures to produce the final activated carbons with well-developed and accessible internal structures. The most important effects of the activation step are: the formation of micropores and mesopores and the increase of the volume and the diameter of existing pores. This is known as the physical method and is widely used in industry.

Physical activation uses gaseous activation agents and does not produce waste water this method is considered to be an environmentally benign technology. But all is

not well with this process. It takes long time and much energy for producing micro porous activated carbon through physical activation methods. Also another inherent drawback of this method is that large amount of internal carbon mass is eliminated to obtain well-developed pore structure.

2.5.2 Chemical Activation

The production of activated carbon by chemical activation generally prepared using single step pyrolysis method. Chemical activation involves the impregnation of the carbonized material by mixing it with an excess amount of a given chemical activating agent, usually in the form of concentrated solution. It allows both pyrolysis and activation to be integrated into a single, relatively lower temperature process in the absence of oxygen [49]. Then the pyrolyzed product is cooled and washed with distilled water or by mild acid to extrude the rest of the activating agent and the agent are recycled. Various dehydrating oractivating agents are: H_2SO_4, $ZnCl_2$, H_3PO_4, KOH, and NaOH etc. is applied in chemical activation process [50] .Other chemicals that can also be used include ferric iron carbonates of alkali metals and potassium sulphide.

2.6 FACTORS AFFECTING ACTIVATED CARBON PRODUCTION

2.6.1 Raw material

Most organic materials rich in carbon that do not fuse upon carbonization can be used as raw material for the manufacture of AC [51]. The selection of raw material for preparation of porous carbon, several factors are taken into consideration. The factors are:

- High carbon content
- Low in inorganic content (i.e. low ash)
- High density and sufficient volatile content
- The stability of supply in the countries
- Potential extent of activation
- Inexpensive material
- Low degradation upon storage

Low content in organic materials is important to produce AC with low ash content, but relatively high volatile content is also needed for the control of the manufacturing process.

2.6.2 Temperature

Temperature, particularly the final activation temperature, affects the characteristic of the activated carbon produced. Generally, commercial activated carbon usually conducted at temperature above 800°C in a mixture of steam and CO_2 [52]. Activation temperature significantly affects the production yield of activated carbon and also the surface area of activated carbon. The temperature usually used between 110°C-200°C. Previously, Haimour and Emeish [53] suggested that the percentage of volatile matter decreased with an increase of carbonization temperature and the variation of this parameter was optimized between 200°C and 800°C due to rapid carbonization occurring in this region.

It is also unsuitable to prepare activated carbon when carbonization temperature was more than 800°C since the successive decreased in volatile matter is minimal above this range. This was accompanied with an increase of fixed carbon and ash content which may be attributed to the removal of volatile matter in the material during carbonization process.

Another notable feature that showed the effect of activation temperature on the activated carbon properties is the BET surface area. As the activation temperature increased, the BET surface area also increased. This may be attributed to the development of new pores as a result of volatile matter released and the widening of existing ones as the activation temperature become higher.

2.6.3 Activation time

Besides activation temperature, the activation time also affects the carbonization process and properties of activated carbon. From previous study, the activation times normally used were from 1 hour to 3 hour. As the time increased, the percentage of yield decreased gradually and the BET surface area also increased. This result is possibly due to the volatilization of organic materials from raw material, which results in formation of activated carbon.

2.6.4 Physical Structure of Activated Carbon

The structure studies of Franklin [54] on carbonized materials showed two distinct well defined classes; non-graphitizing carbons and graphitizing carbon (Figure 2.6).

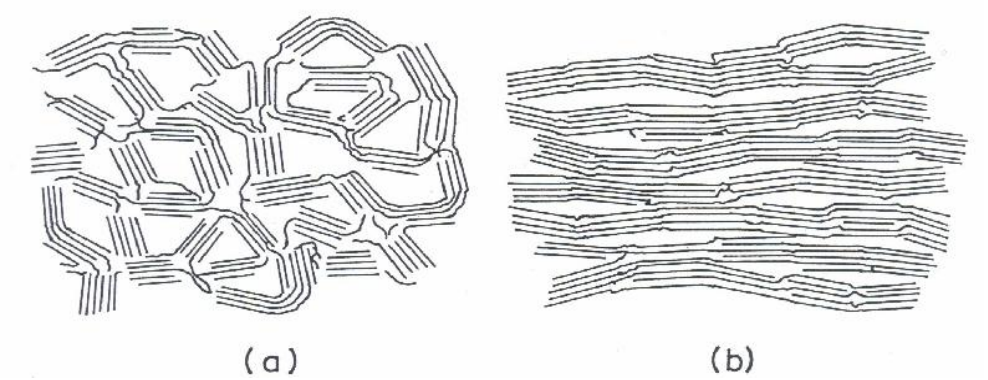

Figure 2.6 Schematic Representation of (a) Non-graphitizing and (b) Graphitizing Structure of activated Carbon [55]

In general, the non-graphitizing carbons are formed from substances containing little hydrogen or more oxygen. On heating such substances, at low temperature develops a strong system of cross linking of crystallites forming porous mass. The graphitizing carbons are prepared from substances containing more hydrogen. The crystallites remain relatively mobile during the early stages of carbonization and cross linking is much weaker. As a result, softer and less porous carbon is obtained.

2.7 CHARACTERIZATION OF CARBON BLACK AND ACTIVATED CARBON

Carbon black is an intense black powder made by incomplete combustion or thermal cracking of a hydrocarbon feedstock. Based on the manufacturing method, it is classified as furnace black, produced by burning oil in 50% air; thermal black, produced through thermal decomposition of methane; and channel black, obtained through direct combustion of fossil fuels or municipal waste. The main uses of carbon black are in the rubber industry, as an additive in manufacturing of tires, and as the principal ingredient in ink, paint, and copy machines toners.

The technology for producing carbon black has various degrees of complexity, depending on the specific requirements of the end-use application. When used in less demanding applications, carbon black is a low cost commodity produced on large scale and with few restrictive controls during fabrication. However, it takes a high level of technology to produce high quality carbon black materials suitable for obtaining stable dispersions in water- or solvent-based media, as required in ink and paint industries.

Carbon black is composed of nanometer-sized primary particles which are bonded together to form primary aggregates of various shapes and structure; the primary aggregates may cluster into larger agglomerates, forming fluffy, free-flowing powders, or may be bonded into beads.

Both physical and chemical properties of carbon black affect its dispersibility. Among the physical properties, the most important are those associated with the size, shape, and distribution of primary particles and aggregates. The particle size describes the "fineness" of the carbon black, and is inversely related to the surface area. Small particle size (or high surface area) determines increased blackness, tint, UV protection, and electrical conductivity, but reduces dispersibility. The structure describes the cluster morphology of primary aggregates, which can be either more compact (low structure) or more open (high structure). In general, low structure carbons are more difficult to disperse because of strong attractive forces acting between primary aggregates that cause packing together into larger clusters.

A very important factor that affects dispersibility of carbon blacks is their surface chemistry. Various amounts of adsorbed oxygen are present on the surface of all carbons. Oxygen is found in surface functional groups of various chemical nature (carboxylic, phenolic, quinonic or lactonic groups) that result from slow, uncontrolled oxidation of the carbon surface in contact with air. The presence of chemical functionalities on carbon black is beneficial for dispersion because chemical groups improve the wetting of the surface, and help localizing electric charges that stabilize the dispersion. Thus, all other properties being equal, carbon blacks with higher volatile content would disperse easier than thatwith lower volatile content. However, not all surface functional groups on carbon black are identical; the response of surface groups (or their acid-base character) is an important factor that affects water dispersibility of various carbons.

Among these factors, the physical factors (particle size and aggregate structure) are expected to show stability and reproducibility in time. In contrast, the surface chemistry is more dynamic, very sensitive to the environment (or sample history) and less reproducible. All carbons have a tendency to react with oxygen and moisture from air and to oxidize slowly at the surface. When freshly produced, and protected from contact with air, the pristine carbon surface is hydrophobic; it has basic pH and reducing properties in aqueous media. After prolonged contact with air and moisture, carbons become surface-oxidized; they are less hydrophobic; impart acidic pH in aqueous solutions, and no longer may exhibit reducing properties. Some carbon blacksare specially post-treated under oxidizing conditions in order to increase their hydrophilic character and water dispersibility.

2.7.1 Methods available for Carbon Black Characterization

A large selection of characterization methods is available for quantification of physical and chemical properties that affect dispersibility of carbon blacks.

Electron microscopy is used to visualize the aggregate shape and to characterize the average size and morphology of primary particles. The ASTM method D3849-04 covers the morphological characterization of carbon black primary aggregates based on transmission electron microscopy [56]. Image processing software is used to derive the mean particle and aggregate size of carbon black in a dry state.

Nitrogen adsorption measurements at liquid nitrogen temperature are used to characterize the total surface area based on the Brunauer, Emmett, and Teller (BET) theory [57] of multilayer gas adsorption. Additional information include evaluation of external surface area based on the statistical thickness method, evaluation of the total volume of micropores (pore with widths smaller than 2 nm) based on adsorption potential theories [58] and the pore size distribution based on the density functional theory (DFT) method [59]. The ASTM method D 6556-04 covers only the determination of total and external surface area [60] by nitrogen adsorption [61]. The other determinations are available in commercial software packages fromall manufacturers of advanced gas adsorption equipment on the market.

A method for structure characterization of carbon black is based on determination of the oil absorption number (OAN), and is covered by ASTM D 2414-05. It is based on detecting the volume of paraffin oil or dibuthylphthalate that, by incorporation to carbon black powder, suffices to change the state from free powder to a semi plastic agglomerate state. The oil absorption number is related to processing and vulcanizate properties of rubber compounds containing carbon black. High OAN values correlate roughly with high structure aggregates. The method is specific for characterization of carbon black additives for rubber industry, and requires the use ofspecial equipment (absorptometer) [62]. We have not used the OAN method in this study.

Chemical methods for characterization of carbon blacks comprise methods for measuring impurity content and methods for characterization of surface chemistry.

Several methods are available for elemental analysis of impurities in carbon. The analysis of sulfur, oxygen and nitrogen content in carbon black is possible using combustion techniques (for S) and inert gas fusion techniques (for O and N) available on commercial instruments equipped with infrared gas analyzers. Analysis of other impurities in carbon black and of elements present in trace concentrations is possible by high resolution glow discharge mass spectrometry (HR-GDMS). In this method the solid sample is atomized by sputtering in low pressure DC plasma and extracted into the mass analyzer for separation and detection.

The volatile content of carbon is a measure of oxygen surface complexes that may be present. It is obtainable by thermogravimetric analysis of carbon samples in a flow of inert gas or under vacuum. Upon heating, oxygen surface complexes decompose to yield CO_2 and CO.

Surface chemistry plays a decisive role in dispersing carbon blacks. However, a method for unequivocal identification and quantification of surface functional groups on carbons is not actually available; all existing methods provide limited information and should be considered as complementary to each other. Among physical methods for surface analysis of carbons, two methods enjoy large popularity: X-ray photoelectron spectroscopy (XPS) and Fourier-transform infrared (FTIR) spectroscopy.

The XPS method (also known as ESCA – electron spectroscopy for chemical analysis) is a powerful method for elemental analysis of the surface layer (0–10 nm) of inorganic materials. The method is based on surface excitation of the sample's surface withmonochromatic X-rays and energy analysis of photoelectrons ejected from the sample. High resolution XPS could also be used to identify bonding or oxidation states of specific elements.

The use of IR spectra for identification of chemical groups is well established as a chemical detection method. However, the applicability of FTIR spectroscopy for analysis of surface groups on carbons is limited by the very high absorption of infrared radiation by carbons. This can be circumvented by using highly diluted carbon samples in an inert matrix, but this drastically lowers the signal/noise ratio and the quality of IR spectra.

A chemical method for identification and quantification of acid-base groups on carbons is based on potentiometric titration in an aqueous electrolyte. The pH-volume converted into a proton binding isotherm that relates the amount of protons bound (or released) to (from) the surface as a function of pH; this is by itself a measure of surface charge evolution on carbon as a function of solution pH. One more step of data processing allows for the derivation of the continuous spectrum of acidity constants (or pK_{α} spectrum) of the carbon surface. The assignment of surface chemical groups is based on comparison with known acid strengths of the main organic functions.

Extensive studies have been carried out by various researchers for the synthesis and characterizationof carbons black from different feedstocks and have been used as reinforcement in polymer to fabricate carbon black polymer composite.

In the compounding of rubber products, fillers are major additives. Incorporation of such additives into the rubber matrix enhances properties such as tensile strength, modulus, tear strength, abrasion resistance, stiffness and possibility. The cost of the manufactured rubber product is also significantly reduced [63]. In the vulcanization of rubber, carbon black is the main filler in use; however, because of the origin of carbon black from petroleum, carbon black causes pollution, and gives the rubber a black color but the filler is costly [64].

Agricultural by-products as fillers have also been investigated by many authors. This included banana peel, rice husk, spent mango, bean seed skin, groundnut shell [65], cocoa pod and rubber seed shell [63], and short pine apple leaf fiber [66], ash rice husk [67]. In addition, the processing of these composite materials is flexible, economical, and ecological and it is possible to use the same machinery employed with other traditional fillers.

Aguele et al. [68] made a comparative analysis on physical properties of polymer composites reinforced with uncarbonised and carbonized coir. In this study three reinforcements such as carbon black, uncarbonised coir (UC) and carbonized coir (CC) were used separately with natural rubber (NR) to prepare the polymer composites. The results obtained from the tests for the NR-UC composites were compared with those of NR-CC and also with those of NR-CB composites. It was observed that as far as hardness is concerned, its value increases for UC, CC fillers as well as for carbon black filled composites as compared to unfilled composite with different weight fraction of fillers. As far as tensile strength and modulus are concerned a higher value was observed for carbon black filled composite when compared with UC and CC composites.

Onyeagoro [69] studied the cure characteristics and physico-mechanical properties of carbonized bamboo fiber filled natural rubber vulcanizates. In the experiment bamboo fibers were carbonized at 600°C and used as particulate filler in natural rubber vulcanizates whereas maleic anhydride-grafted-polyisoprene was used as a compatibilizer. Results obtained showed that carbonized bamboo fiber filled vulcanizates shows improvement in the cure properties over the non-compatibilized vulcanizates. Carbon black exhibited higher tensile strength, modulus, hardness and elongation at break in the vulcanizates than carbonized bamboo fibre.

Hwanget al. [70] prepared a novel polymer membrane composite using activated carbon (AC) and polyethylene glycol (PEG), which were added into polyphenylsulfone (PPSU)/polyetherimide (PEI) polymers. The results showed that the addition of AC significantly affected the membrane morphology, pore size distribution, porosity, and chemical properties. With this increase in AC concentration, the filtration flux and permeability of the AC/PPSU/PEI/PEG composite membrane improved.

The effect of filler carbonization temperature on the tensile properties of natural rubber compounds filled with cassava (Manihotesculenta) peel carbon filler was reported by Stella et al. [71]. Their reports revealed that the physico-mechanical properties of the composites were greatly influenced by filler loading and filler carbonization temperature.

Imoisil et al. [72] was investigated the mechanical and end use properties of natural rubber reinforced rice-husk/carbon black hybrid filler composite. The result showed that tensile strengths, compression strength, abrasion resistance and hardness properties of the vulcanizate improves with increase in carbon black content, while elongation at break decreases with increase in carbon black content.

Abdul Khalil et al. [22] derived carbon black from various carbonaceous materials such as bamboo stem, coconut shells and oil pal empty fiber bunch by pyrolysis of fibers at 700°C. The experimental results showed that the carbon black epoxy composites exhibited better flexural properties than the neat epoxy, which can be attributed to better adhesion between the carbon black particles and epoxy resin. Also carbon black particles show well-developed porosities and were predominantly made up of micropores.

Extensive studies have also been carried out on the preparation of activated carbon black from various carbonaceous materials using chemical and physical methods.

Olowoyo et al. [73] prepared activated carbon from palm-kernel shell; coconut shell, ground nut shell and obeche wood and investigate their physical properties. The higher apparent density, lower moisture content and lower ash content were observed for palm-kernel shell and coconut shell activated carbon than groundnut shell and obeche wood activated carbon. In terms of particles size distribution Palm-kernel shell and coconut shell are found to be better.

Ismail et al. [74] prepared activated carbon from the natural biomaterial durian (Duriozibethinus) seed; using phosphoric acid (H_3PO_4) as the activating agent and found thatmost outstanding carbon with the highest surface area of 2123m^2/g was

achieved using an impregnation ratio of 2, an activation temperature of 600°C for 4h and a heating rate of 1°C/min.

Activated carbon with high surface area from carbonized tobacco stems with K_2CO_3 activation by microwave radiation were investigated by Li et al [45] and evaluated the effect of microwave radiation time and K_2CO_3/C ratio on the yield and adsorption capacities of activated carbons. Surface area, micropores volume and pore size distribution (PSD) of the carbons were determined bythe BET, H-K and DFT methods. Results showed that activated carbons content about 59.98% of micropores and a small number of mesopores and macrospores.

Azevedo et al. [75] prepared micro porous activated carbon samples from coconut shells (low-cost lignocellulose waste), using chemical activation with zinc chloride followed by physical activation. They have the opinion that activated carbons obtained from the above method may be used as potential adsorbents for natural gas storage applications.

Lot of studies has also been carried out for specific application of carbon black particles in various industrial situations using various conditions of carbonization and activation processes and few of the literatures are summarized in Table 2.1.

2.7.2 Advantages of Zinc chloride chemical agent over other chemical agents

The activation with $ZnCl_2$ gave the highest yield percentage. Moreover, the $ZnCl_2$ activated product has the highest iodine value, indicating that its pore surface and structure were the best developed. Zinc chloride is capable to absorb arsenics. It gives best products with absorption capacities, highest BET surface area, pore volume, low ash content and highest carbon content. Thus, $ZnCl_2$ was chosen as the activating agent for subsequent experiments.

Table 2.1 Survey table on research carried out on various conditions of carbonization and activation processes with specific application

Author	Year	Raw Material	Carbonization condition	Activation condition	Activation method	Chemical treatment	Studies/ Application	Ref
Gomez-de-Salazar et al.	2000	Peach stone	N_2, 850°C/2h, 80 mL/min, 2 °C/min	800°C/3h, 80mL/min	Physical	50% CO_2/N_2	Preparation of carbon molecular sieves by controlled oxidation treatments	76
Junichi Hayashi et al.	2002	Almond shell, Coconut shell, Oilpalm shell, Pistacho shell, Walnut shell	N_2, 473K/ 2h	1073K	Chemical	K_2CO_3	Activated carbons have been prepared from several kinds of Nutshells and characterized their surface area	77
Olivares-Marın et al.	2006	Cherry stones	N_2, 100mL/min, 10°C/min, 2h	400°C–800°C	Chemical	$ZnCl_2$	Preparation of activated carbon and characterized their properties by FTIR, BET	78
Adinata et al.	2007	Palm shell	N_2, 2.0 mL/min, 10 °C/min	600°C-1000°C	Chemical	K_2CO_3	Production of carbon molecular sieve by chemical vapor deposition (CVD) method using benzene as depositing agent	79
Wei Li et al.	2008	Coconut shell	N_2, 400°C-1000°C	900°C, 30-120min	Physical	CO_2	Effect of carbonization temperature on characteristics porosity of Coconut shell char and activated carbon	80
Thio Christine Chandra et al.	2009	Durian shell	N_2	673K–923K, 10 K/min	Chemical	KOH	Activated carbon prepared from Durian shell and characterized byBET and TGA	81
Guo et al.	2009	Coconut shell	N_2, 600°C, 2h, 10°C/min	750°C-950°C, 120-360 min	Physical	CO_2	Textural characterization of an activated carbon derived	82

							from carbonized Coconut shell charand evaluated the effect of activation temperature on BET surface area	
Ahmad	2010	Bael shell	N_2, 450°C/1h	-	-	-	Activated carbon prepared from Bael shell and used as removal of congo red (CR) dye from aqueous solution	83
Jassim et al.	2012	Iraqi Apricot Stones	N_2, 90,120 and 180min	300°C-800°C,20 C/min	Chemical	H_3PO_4	Prepared activated carbon from Iraqi apricot stones and characterized by BET and FTIR	84
Ramakrishna Gottipati et al.	2013	Aegle marmelos	N_2,400°C/1h mL/min	400°C-700°C/2h, 200mL/min	Chemical	KOH	Activated carbons prepared from Aegle marmelos shell and studied their parameter	85
El-Sayed et al.	2014	Corncob	N_2	400°C, 500°C and600°C	Chemical	H_3PO_4	Removal of methylene blue(MB)dye from aqueous solutions using corncob activated Corncob	86
Yavuz et al.	2010	olive stone			Chemical	H_3PO_4	Granular activated carbons prepared from olive stones and characterized their properties	87

2.8 ON WEAR MECHANISM AND ITS CLASSIFICATION

Wear is a process of removal of material from one or the other of two solid surfaces in the solid state contact, occurring when two solid surfaces are in sliding or rolling motion together according to Bhushan and Gupta [88]. The rate of removal is generally slow, but steady and continuous. Figure 2.7 shows the five main categories of wear and the specific wear mechanisms that occur in each category. Each specific mode of wear different from the next, and can be distinguished relatively easily.

Wear rate changes drastically in the range of 10^{-15} to $10^{-1}mm^3/Nm$, depending on operating conditions and material selections [89-95]. These results mean that design of operating conditions and selectionof materials are the keys to controlling wear. One of the ways to meet these requirements, wear maps had been proposed for prediction of wear modes and wear rates [96-97]. Wear mechanisms are described by considering complex changes during friction. In general, wear does not take place through a single wear mechanism, so understanding each wear mechanism in each mode of wear becomes important.

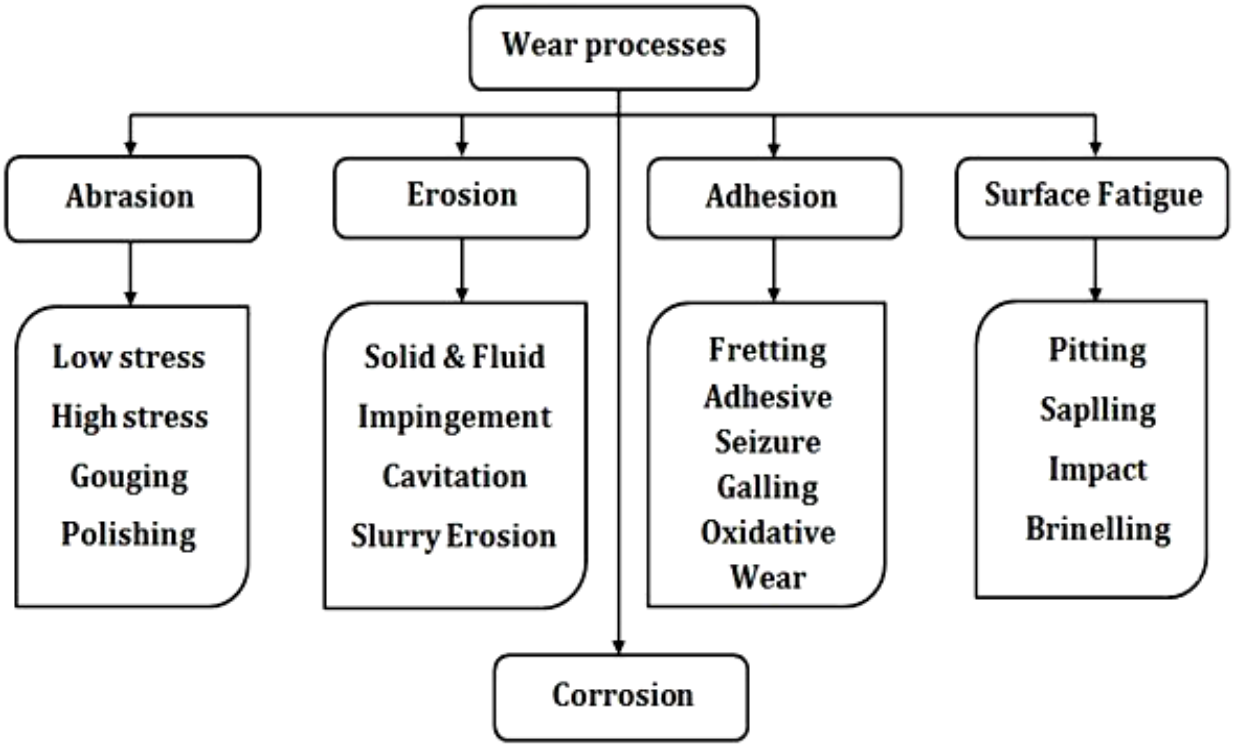

Figure 2.7 Flow chart of various wear mechanism

In order to focus on the wear mechanisms from the viewpoint of contact configurations, apparent and real contact conditions at the contact interface are introduced without particularizing about these contact configurations. Severity of contact, such as elastic contact or plastic contact, is the simplest and most direct way to think about wear mechanisms, and is a tribosystem response determined by dynamic parameters, material parameters, and atmospheric parameters. The following four wear modes are generally recognized as fundamental and major ones [98].

2.8.1 Abrasive wear

If the contact interface between two surfaces has interlocking of an inclined or curved contact, ploughing takes place in sliding. As a result of ploughing, a certain volume of surface material is removed and an abrasive groove is formed on the weaker surface. This type of wear is called abrasive wear.

A common example of this problem is the wear of shovelson earth-moving machinery. It was originally thought that abrasive wear by grits or hard asperities closely resembled cutting by a series of machine tools or a file.It can be account for most failures in practice. Hard particles or asperities that cut or groove one of the rubbing surfaces produce abrasive wear. This hard material may be originated from one of the two rubbing surfaces. In sliding mechanisms, abrasion can arise from the existing asperities on one surface (if it is harder than the other), from the generation of wear fragments which are repeatedly deformed and hence get work hardened for oxidized until they became harder than either or both of the sliding surfaces, or from the adventitious entry of hard particles, such as dirt from outside the system. The way the grits pass over the worn surface determines the nature of abrasive wear.

The literature denotes two basic modes of abrasive wear such as two-body and three-body abrasive wear. In two-body abrasive condition; one surface is harder than the other rubbing surface. Hard asperities or rigidly held grits pass over the surface like a cutting tool is shown in figure 2.8(a). In three-body abrasive condition, generally a small particle of grit or abrasive, lodges between the two softer rubbing surfaces, abrades one or both of these surfaces is shown in figure 2.8(b). It was found that three body abrasive wear is ten times slower than two-body wear.

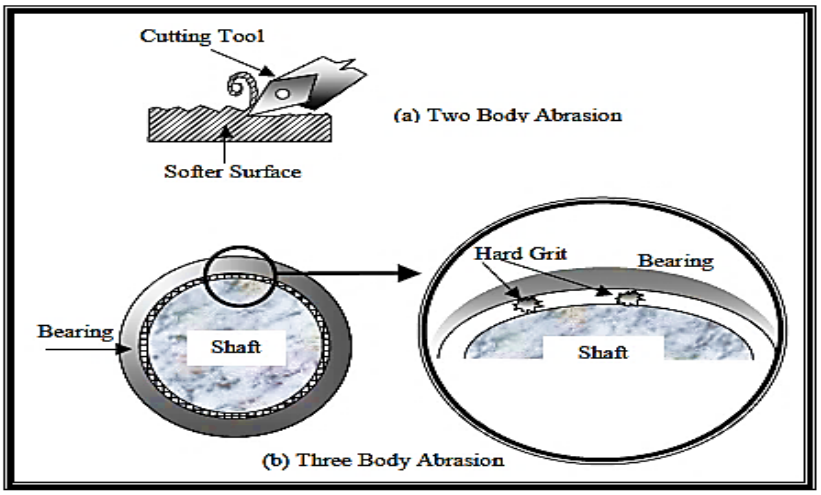

Figure 2.8 Schematic of abrasive wear phenomena [99]

2.8.2 Adhesive wear

Adhesive wear is a very serious form of wear characterized by high wear rates and a large unstable friction coefficient. It is also called galling and scuffing where interfacial adhesive junctions lock together as two surfaces slide across each other under pressure. Sliding contacts can rapidly be destroyed by adhesive wear and, in extreme cases, sliding motion may be prevented by very large coefficients of friction or seizure is shown in figure 2.9.

Most solids will adhere on contact with another solid to some extent provided certain conditions are satisfied. Adhesion between two objects casually placed together is not observed because intervening contaminant layers of oxygen, water and oil are generally present. The earth's atmosphere and terrestrial organic matter provide layers of surface contaminant on objects which suppress very effectively any adhesion between solids. Adhesion is also reduced with increasing surface roughness or hardness of the contacting bodies. Actual observation of adhesion became possible after the development of high vacuum systems which allowed surfaces free of contaminants to be prepared. Adhesion and sliding experiments performed under high vacuum showed a totally different tribological behavior of many common materials from that observed in open air.

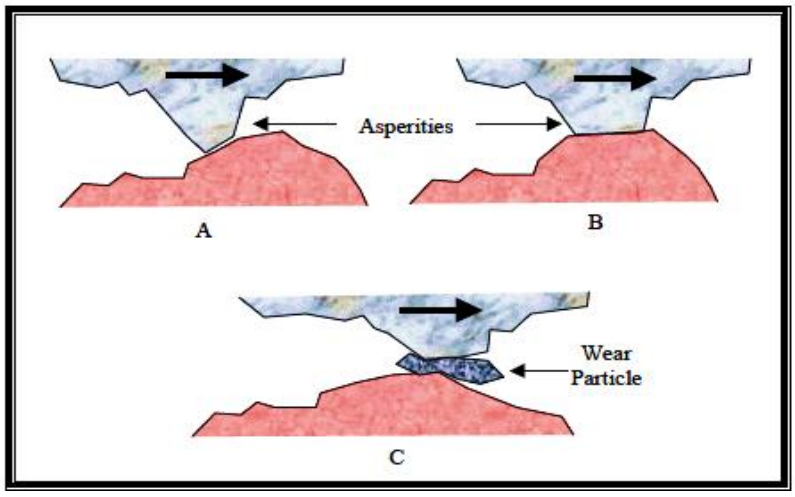

Figure 2.9 Schematic of generation of a wear particle as a result of adhesive wear process [99]

2.8.3 Erosive wear

The term 'erosive wear' refers to an unspecified number of wear mechanisms which occur when relative small particles impact against mechanical components. This definition is empirical by nature and relates more to practical considerations than to any fundamental understanding of wear.

Erosive wear is caused as a result of solid or small drops of liquid particles or gas impact against the surface of an object. The typical examples of solid particles erosive wear occurs in a wide variety of machinery and the damage to gas turbine blades when an aircraft flies through dust clouds, and the wear of pump impellers in mineral slurry processing systems. Examples include the ingestion of sand and erosion of jet engines and of helicopter blades.

Solid particle erosion is a result of the impact of a solid particle A, with the solid surface B, resulting in part of the surface B been removed is shown in figure 2.10. The solid particles or liquid drops significantly contingent on the material properties and erosion process, such as impact velocity, impact angle and particle size. Angle of impingement and movement of particle stream have significantly effect on the rate of material removal. In common superior mechanical strength of a material does not guarantee better wear resistance, hence it is required a meticulous study of material characteristics for minimization of wear. The properties of the eroding particle are also recognized as a relevant parameter in the control of this type of wear.

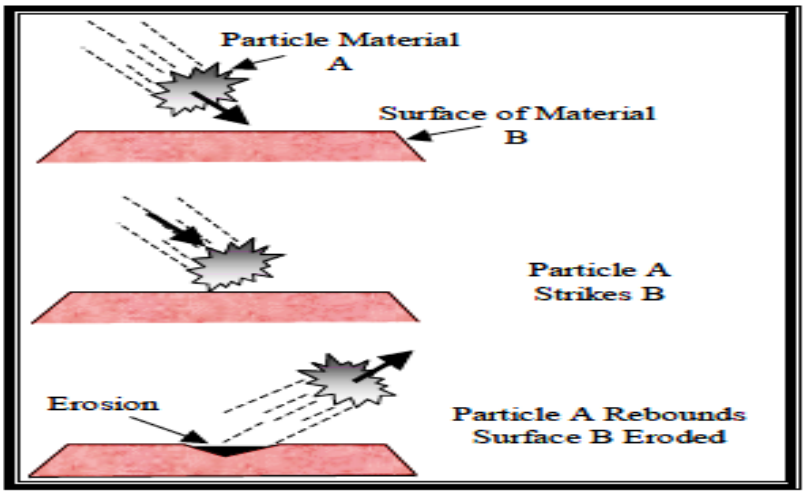

Figure 2.10 Schematic representations of the erosive wear mechanism [99]

2.8.4 Surface fatigue wear

When two surfaces slide across each other, the maximum shear stress lies some distance below the surface, causing micro cracks, which lead to failure of the component. These cracks initiate from the point where the shear stress is maximum and propagate to the surface as shown in figure 2.11.

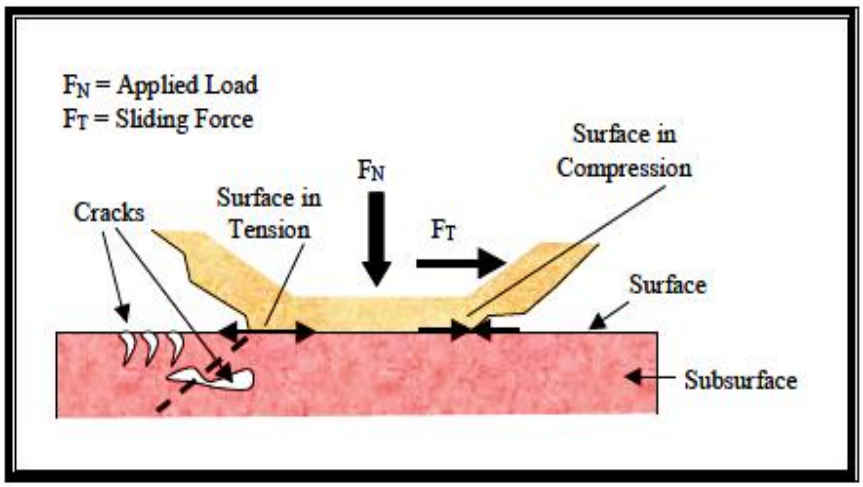

Figure 2.11 Schematic of fatigue wear, due to the formation of surface and subsurface cracks [99]

2.8.5 Corrosive wear

In corrosive wear, tribochemical reaction produces a reaction layer on the surface. At the same time, such layer is removed by friction is shown in figure 2.12. Therefore, relative growth rate and removal rate determine the wear rate of the reaction

layers and, as a result, of the bulk material. Therefore, models of the reaction layer growth and those of the layer removal become very important.

Typical examples of corrosive wear can be found in situations when overly reactive E.P. additives are used in oil (condition sometimes dubbed as 'lubricated wear' [100]) or when methanol, used as a fuel in engines, is contaminated with water and the engine experiences a rapid wear [101]. Another example of corrosive wear, extensively studied in laboratory conditions, is that of cast iron in the presence of sulphuric acid [102]. The corrosivity of sulphuric acid is verysensitive to the water content and increases with acid strength until there is less water than acid. Pure or almost pure acid is only weakly corrosive and has been used as a lubricant for chlorine compressors where oils might cause an explosion [103].

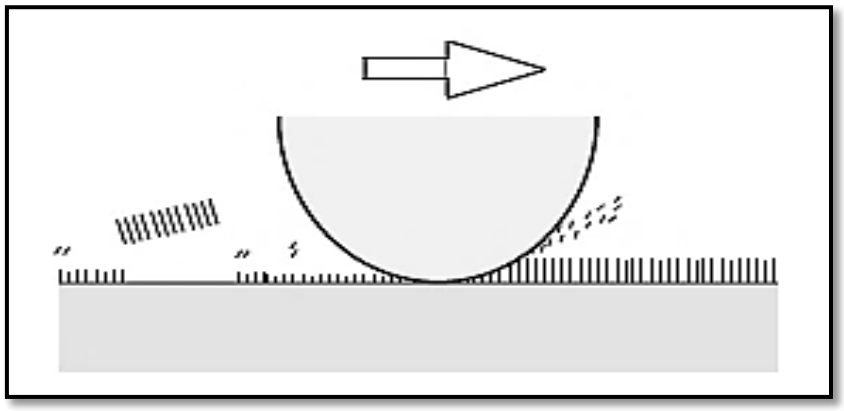

Figure 2.12 Schematic of corrosive wear, due to the formation of surface and subsurface cracks

After reviewing the existing literature available on carbon black and activated carbon with their applications efforts are put to understand the basic needs of the growing composite industry. The conclusions drawn from this is that, the literature is reach with preparation and characterization of carbon black and activated carbon from abundantly available natural fibers which are reach in carbonaceous materials and could be used as filler material for preparation of polymer composites. These fillers are cheap; nontoxic can be obtained from renewable resources, and are easily recyclable. It is also clear from this study that, study of polymer composites tribological behavior filled with carbon black and activated carbon obtained from natural fibers still remained as an unexplored area.

In view of the above the present work is under taken to prepare and characterize carbon black and activated carbon from natural fiber. It is also planned to prepare polymer composite filled with different doses of these fillers (carbon black and activated carbon).The characterization will be done by Energy Dispersive Spectroscopy (EDS), X-ray Diffraction (XRD), Fourier Transform Infrared Spectroscopy (FTIR), Thermo Gravimetric Analysis (TGA) and BET Surface Area Analysis.

The potential of the developed composite for tribological application (solid particle erosion test as per ASTM standard) have also been carried out and reported in this thesis.

Chapter 3

Preparation and Characterization of Carbon Black and Activated Carbon Black

3.1 INTRODUCTION

Composition of the raw material is an important factor that dictates the selection of precursor for carbon production. The chemical composition of the lignocellulosic fibers is constituted by three main components: hemicellulose, cellulose and lignin, which are known to present very complex structure. In case of lignocellulosic shell materials, cellulose is a major structural component of cell walls, and it provides better mechanical strength and chemical stability to plants. Celluloseis a semi crystalline polysaccharide made up of D-glucosidic bonds. A large amount of hydroxyl groups in cellulose gives hydrophilic properties to the natural fibers. Hemi-cellulose is a copolymer of different C_5 and C_6 sugar that also exist in the plant cell wall and it is strongly bound to the cellulose fibrils, presumably by hydrogen bonds. It consists of polysaccharides of comparatively low molecular weight built up from hexoses, pentoses and ironic acid residues. Lignin is polymer of aromatic compounds product through a biosynthetic process and forms a protective layer for the plant walls [104]. Lignin acts as the cementing agent in fiber, binding the cellulose fibers together. The lignin, cellulose and hemicelluloses content depend on the hard shell material. In this context chemical composition of some lignocelluloses fiber investigated by different researchers are given in Table 3.1. Most of the works carried out by these investigators are on the natural materials.

Raju [105] fabricated composite by randomly distributed chemically modified groundnut shell particles of different grain sizes and epoxy resin with volume percentages of 70:30, 65:35 and 60:40 and observed that groundnut shell based epoxy composite shows better mechanical and moisture absorption properties than epoxy composite.

Abdul Khalil [22] prepared carbon black from bamboo stem and oilpalm empty fruit bunch at 700°C carbonization temperature and used as filler in epoxy composites. The experimental result showed that carbon black filled epoxy compositeexhibited better flexural properties than the neat epoxy.

Jacob [106] fabricated natural rubber hybrid composite with untreated chopped sisal and oil palm fibers and studied the effects of concentration and modification of fiber surface in sisal/oil palm hybrid fiber reinforced rubber composites.

Table 3.1 Composition of lignocellulosic fibers in several sources on dry basis

Lignocellulosic materials	α-Cellulose (wt %)	Hemicellulose(wt %)	Lignin (wt %)	Ash (wt%)	Ref
Groundnut shell	35.7	18.7	30.2	5.9	105
Bamboo stem	46.3	23.4	22.2	1.53	22
Oil palm empty fruit bunch	50.5	29.6	17.8	3.43	22
Oil palm shell	65	-	19	2	106
Sisal	78	10	8	1	106
Coconut coir	47.7	25.9	17.8	0.8	107
Rice husk	31.3	24.3	14.3	23.5	108
Bagasse	40-46	24.5-29	12.5-20	1.5-2.4	109
Hemp	70.2-74.4	17.9-22.4	3.7-5.7	-	110
Kenaf	31-39	21.5	15-19	-	110

For the present investigation wood apple and coconut shells are being utilized for preparation of carbon black and activated carbon.

3.2 MATERIALS

Wood apple and Coconut shells were collected from locally from the investigators place.

3.2.1 Wood apple

Wood apple (Aegle marmelos) belongs of family rutaceae is highly reputed medicinal tree (Figure 3.1). Its fruit is commonly known as the “Stone apple” or “Bael”(Figure 3.2). It is an indigenous fruit of India and found abundantly in sub-Himalayan forest, Bengal central, south India., Sri Lanka, Pakistan, Bangladesh, Burma, and Thailand. It has a reputation in India for being able to grow in places that other trees cannot. It copes with a wide range of soil conditions (pH range 5-10), is tolerant of water logging and has an unusually wide temperature tolerance (from -7 °C

to 48 °C). It requires a pronounced dry season to give fruit. The peel of the fruit is very hard.

Figure 3.1 Wood apple tree

Figure 3.2 Wood apple fruit

Its color is green and becomes brown in ripening stage is shown in figure 3.3.Wood apple shell mainly consists of carbohydrate component such as cellulose, hemicellulose and lignin. Therefore wood apple shell is one such byproduct of its fruit and considered to be a waste.

Figure 3.3 Wood apple shells

Sing et al. [111]analyzed chemically the leaf, pulp and seed powder for proximate composition and found that Bael leaf, pulp and seed are good source of protein, fat, minerals, crude fibre and energy.

Researchers like Anusha et al. [112] and Ahmad et al. [113] used Bael shell carbon as an absorbent for the removal of iron or Congo red dye from waste water. Anandkumara and Mandal [113] used activated carbon prepared from non-usable Bael fruit shell (BS) as anefficient low cost adsorbent to remove the Cr (VI) toxic metal from aqueous phase.

3.2.2 Coconut

Coconut (Cocos nucifera) is a member of the palm family. The coconut palm is used for decoration as well as for culinaryand non-culinary uses; virtually every part of the coconut palm has some human use. Coconut shell is non-food part of coconut, which is hard lignocellulosic agro-waste. The coconut husk, or mesocarp, is composed of fibers called coir. The inner stone or endocarp is the hardest part of the nut called shell. Adhering to the inside wall of the endocarp is the testa, with a thick albuminous endosperm, the white and fleshy edible part of the seed. Figure 3.4 shows the photograph of coconut shell.

Figure 3.4 Coconut shells

Coconut shells have little or no economic value and their disposal is not only costly but may also cause environmental problems. Coconut shells are suitable for preparing micro porous-activated carbon due toits excellent natural structure and low ash content [114-116].

Li et al. [80] conducted series of experiment to study the effects of different carbonization temperatures (400°C, 600°C, 800°C and 1000°C) on characteristics porosity of carbonized coconut shell char. They also prepared activated carbon derived from coconut shell with different activation times (30, 60, 90 and 120min) at activation temperature of 800°C.

Samantarai et al. [117] studied the effect of different carbonization temperature on the abrasive wear behavior of carbonized rice husk char epoxy composite. The experimental results show that the wear behavior of pure epoxy improved considerable with the incorporation of carbonized char.

3.3 METHODS

3.3.1 Preparation of raw shell particles

The wood apple shell (WAS) and coconut shell (CS) used in this study were washed several times with distilled water to remove water-soluble impurities and surface adhered particles. The washed shells were then dried at 110°C for 48hour in an oven to remove excess water content and moisture. After drying the shell materials were crushed in to small pieces with the help of a crusher. The crushed pieces were

then grinded in to the powder using ball mill for 48hour. The collected powder was sieved using a sieve shaker. Separate sieve mesh sizes were used to obtain a distribution of particle sizes resulting from the crushing. The particle size chosen for this experiment was 1-212µm is shown in figure 3.5.

In the similar process coconut shell particles were also prepared is show in figure 3.6.

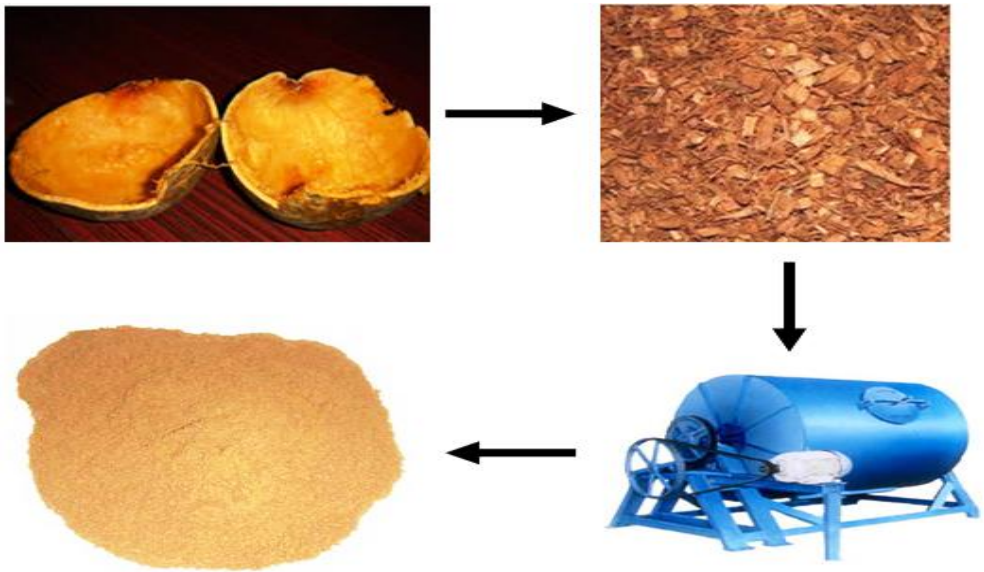

Figure 3.5 Preparation of Raw wood apple shell particles

Figure 3.6 Raw coconut shell particles

3.3.2 Processing of Carbon black particles through Carbonization (Pyrolysis)

The main purpose of carbonization process is to increase the carbon content and to create an initial porosity in the carbon black. Carbonization is carried out in a specially designed burning chamber which allows limited air supply.

WAS particles were loaded on a ceramic boat which was placed inside a muffle furnace. The shell particles were heated up to desired carbonization temperature i.e.

400°C, 600°C and 800°C at a heating rate of 5°C/min and held for at least 2hour at the same carbonization temperature under an inert atmosphere. To avoid oxidation, which could subsequently cause ashing, an inert environment was created by passing of Nitrogen gas at the time of carbonizing process. After reaching the final carbonization temperature, the samples were soaked for 1hour at this temperature and then allowed to cool in the furnace itself. The carbon black thus obtained is shown in figure 3.7(a) and for coconut shell (Figure 3.7(b)). They were ground and sieved for further analysis. The important factors that determine the quality of the carbonized product are: (i) rate of heating, (ii) final temperature and (iii) soaking time.

Figure 3.7 Photomacrograph of the sieved carbon black **(a)** wood apple shell and **(b)** coconut shell particles

3.3.3 Processing of activated carbon black

The characteristics of the activated carbon (AC) can be carried out by controlling three major variables viz. activation temperature (AT), impregnation ratio of activator to sample' (R) and, carbonization time (CT). The range of variables investigated in this study were; AT = 800°C, CT = 1h and R = 1:1, 1.5:1, 2:1 and 2.5:1.

Production of activated carbon involves the following steps:

i. Pretreatment of the raw shell
ii. Impregnation of the raw shell particles with the activator
iii. Carbonizationof the impregnated raw shell
iv. The removal of activator

3.3.3.1 Pretreatment of the raw shell particles

Pretreatment of the both wood apple and coconut shell as already mentioned art 3.3.1.

3.3.3.2 Impregnated with Zinc chloride ($ZnCl_2$) chemical activating agent

Raw material was directly impregnated with zinc chloride. About 20gm ofground and sieved shells particles were treated with 85% (wt.) zinc chloride solution at room temperature in fourdifferent weight ratios as 1:1, 1.5:1, 2:1 and 2.5:1 ($ZnCl_2$: shells). Continuous mixing of the shells with the zinc chloride solution for 24h was maintained by using a magnetic stirrer. The resulting slurry was carried out for 24h at 110°C in a hot air oven to achieve well penetration of chemical into the interior of the precursor. After this period, shells were ready for the carbonization and activation which were carried out simultaneously.In the activation process, an important factor is the degree of impregnation. It is defined as the ratio of "weight of activating agent added to the weight of raw material". Proximate analysis of activated raw wood apple and coconut shell particles based on impregnation ratio is shown in Table 3.2.

Table 3.2 Proximate analysis of activated raw wood apple and coconut shell particles based on impregnation ratio

Impregnation ratio	Wood apple shell				Coconut shell			
	Moisture %	Volatile matter %	Ash %	Fixed carbon %	Moisture %	Volatile matter %	Ash %	Fixed carbon %
1:1	3.2	4.7	4.1	88	3.3	7.1	6.86	82.74
1.5:1	3.1	3.1	3.8	90	3.8	5.56	5.87	84.77
2:1	**3**	**1.2**	**1.3**	**94.5**	**3.7**	**3**	**2.3**	**89.4**
2.5:1	3	4	6	87	4.4	5.5	4	86.1

3.3.3.3 Carbonization

The reactors were cylindrical in shape with on end closed and the other end is fitted with removable cover with 2mm hole at the center of the cover for easy escape of pyrolysis vapor of gases that generates during process.

The required numbers of reactors were placed inside muffle furnace and the furnace was heated slowly (average heating rate was 5°C/min) till the desired temperature is achieved. The furnace takes about 2 to 2.3hours to reach the desired activation temperature i.e. 800°C. Once the furnace reaches the desired temperature carbonization process starts. During the process nitrogen flow of $100cm^3min^{-1}$ STP was maintained. The process was continuous for a period of 60min. After 60min the flow of nitrogen was discontinued but the temperature of furnace was maintained at

that temperature for another 60min and then the furnace was allowed to cool. After cooling reactors were taken out from the furnace. Activated carbon were then extracted from the reactors and kept in tightly closed plastic bottle for further use.

3.3.3.4 Washing

The next step is the removal of the zinc chloride activator from the carbonization products.Tocarry out this procedure; first the pyrolysis products were grinded into fine powder and then passed through sieve shaker. Required volume of dilute 5% HCl was added to the powder particles (>100 µm) to get a liquid to solid ratio (LSR) of 10 ml/g. The mixture so obtained was then left as it is for 24hour. After 24hour supernatant liquid was decanted in a filter paper followed by three successive washings and decantation was done using distilled water.

By the end of washing, the whole carbon was transferred to the filter paper and washing was continued on the filter paper till free of chloride ion as indicated by pH test. Finally the carbon was dried at 110°C for 2hour and kept in tightly closed plastic bottles and carefully labeled. The process was repeated for different impregnation ratios such as 1:1, 1.5:1, 2:1 and 2.5:1. The detail procedure for the preparation of activated carbon black from raw material is shown in figure 3.8.

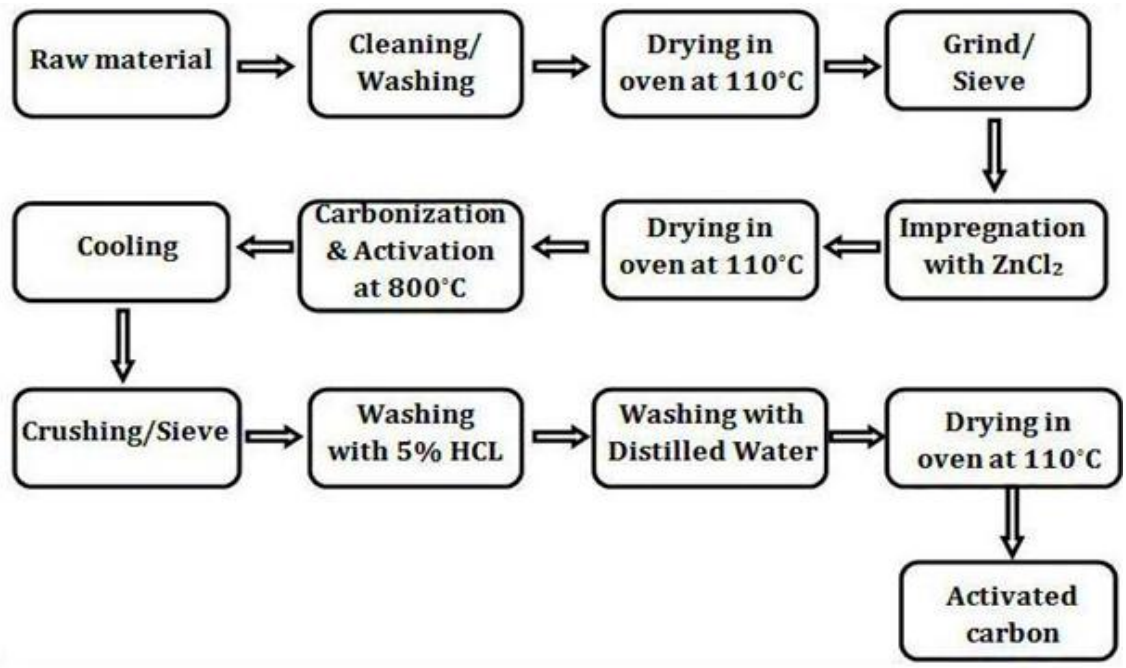

Figure 3.8 Flow diagram showing the steps for the preparation of activated carbon black

3.4 PHYSICAL CHARACTERIZATION OF PARTICLES

3.4.1 Chemical Composition

The cellulose, hemicelluloses and lignin of both wood apple and coconut shell particles were determined by using the method described in [22]. The particulates of wood apple shell were subjected to Soxhlet extraction with ethanol/toluene (1:2, v/v) for 12h, to remove the extractives. The composition (extractive, α-cellulose, hemicelluloses, lignin, and ash contents) of the particulates were analysed according to Technical Association of Pulp and Paper Industry (TAPPI) standards. Holocellulose content (α-cellulose + hemicelluloses) of the particulates was determined by treating the particulates with a $NaClO_3$ and NaOH mixture solution. The α-cellulose content of the particulates was then determined by further treating holocellulose with 17.5% NaOH to remove the hemicelluloses. The difference between the values of Holocellulose and α-cellulose gives the hemicellulose content of the particulates. The lignin content of the particulates was found by treating them with sulphuric acid solution based on TAPPI standard T222 om-83. The extractive-free samples were analysed thrice for each of the batch. In the similar process the chemical composition of coconut shell particles were also found out.

3.4.2 Proximate Analysis

Proximate analysis is one of the most important characterization methods to analyse the biofiber. It provides information on moisture, ash, volatile matter and fixed carbon content of the material in case of dry base or weight base. Traditionally, proximate analysis measures are developed following different national and international normative, such as ASTM E-871 for moisture, ASTM E-830, D-1102 or UNE-EN 14775 for ash or ASTM E-872 and ASTM E- 1755 for volatile matter determination [118-119].

In the present case the proximate analysis of shell particles has been carried out following the ASTM standards E-871, E- 1755, E-872; for moisture, ash and volatile matter respectively. Fixed carbon other than ash does not vaporize when heated in the absence of air. Fixed carbon is usually determined by subtracting the sum of the first

three values that is moisture, ash, and volatile matter (weight percent from 100 percent). So, it is very important for economic reasons to know the moisture and ash contents of the material.

Fixed carbon (%) =100-(Moisture, % + Ash, % + Volatile matter, %) (3.1)

3.4.3 Ultimate Analysis

CHNSO(CHN-932) elemental analyzers provide a means for the rapid determination of Carbon (C), Hydrogen (H), Nitrogen (N) and Sulphur (S) contents in organic matrices and other types of materials.And when sum of theses compositions is subtracted from 100, it gives oxygen percentage composition.

This analysis determines the elemental compositions of the sample and it is based on the principle of Dumas method which involves the complete and instantaneous oxidation of the sample by flash combustion. Sample is fed to the CHNSOanalyzer along with excess oxygen. Oxygen reacts with the elements present in the sample i.e. nitrogen, hydrogen, sulphur and carbon to produce nitrogen dioxide, water, sulphur dioxide and carbon dioxide. A chromatographic column is used for the separation of combustion products and these are detected by thermal conductivity detector (TCD). TCD gives an output signal proportional to the concentration of individual components. From this individual component of the elements in the sample is determined.This may include methods for reducing environmental pollution and so forth.

Oxygen (%) = 100 – (Carbon, % + Hydrogen, % + Nitrogen, % + Sulphur, %) (3.2)

3.4.4 Energy Dispersive Spectroscopy (EDS)

The elemental composition of wood apple shell particles is determined by Energy Dispersive Spectroscopy (EDS). The EDS was obtained in a ‘‘spot mode’’ in which beam is focused on a single area selected within the field of view.

3.4.5 X-ray Diffraction (XRD)

X-ray diffraction has widely been used to evaluate the crystalline structure of cellulose, since it provides a qualitative and semi-qualitative evaluation of the

amorphous and crystalline cellulosic components in a sample [120]. XRD is the most common technique used to characterize the crystalline content in a polymer structure. It is also used in particle research to characterize their critical features such as crystallite size, chemical composition and strain. The peak positions are indicative of the crystal structure and symmetry of the contributing phase. The apparatus is shown in figure 3.9.

XRD patterns of crystalline materials shows sharp peaks while that of amorphous shows single broad diffused peak. If certain amount of amorphous impurity is there, then diffraction peak will be surrounded by slightly broad peaks from amorphous.

On the basis of XRD studies activated carbon are classified in two types, based on their graphitizing ability [54]. According to the peak intensity evolution, the graphitization process can be distinctly viewed into three regions. The non-graphitization region, near-graphitization region, and graphitization region correspond to activated carbon treated below 900°C, at 1000-1100°C, and above 1200°C, respectively. The non-graphitizing carbons are hard and show a well-developed micro porous structure due to the formation of strong cross-linking between the neighboring randomly oriented elementary crystallites. Whereas, graphitizing carbons has weak cross-linking and had a less developed porous structure.

The crystal structures were measured by scanning the particle samples in the range of 5–90° of 2θ angle with a scan rate of 20/min and a step size of 0.06 by a Powder X-ray Diffractometer (PAN alytical, PW3050/60 XRD; Cu Kα anode; k= 0.154 nm) is shown in figure 3.9. High X-pert software was used to investigate the structural changes and phase transformations of the powders. The samples were gently consolidated in an aluminum holder and a graphite monochromator with 40 mA current and 40 mV voltage. The apparent crystallite thickness (L_c), the apparent layer-plane length parallel to the fiber axis (L_a), and the average interlayer spacingis‘d’indicates the packing density of carbon layers and has been estimated by using the Bragg and Scherrer formula. The formulas can be expressed as:

$$d = \frac{\lambda}{2\sin\theta} \tag{3.3}$$

Where'θ'is the Bragg angle of peaks (°), 'λ' is the wavelength of X-ray used (0.154 nm).

Figure 3.9 X-ray Diffractometer

3.4.6 Fourier Transform Infrared Spectroscopy (FTIR)

FTIR is most powerful tool for identifying chemical bond (functional group). FTIR spectra of pure compounds are like a molecular fingerprint and organic compounds have very richdetailed spectra. But it is much simpler in case of inorganic compound. The spectrum of an unknown can be identified by comparison with a known compound.

A beam of infrared light is passed through the sample and the infrared spectrum is recorded. A part of this radiation is absorbed and other part is transmitted through the sample. Amount of energy that was absorbed by each wavelength can be found out by examining the transmitted light. Thus a spectrum is produced in the form of transmittance/absorbance plotted against the wave number. This spectrum detects the infrared wavelength at which absorption occurs. When the vibrational frequency of bond and frequency of IR are same, absorption occurs. Thus, it gives an idea about the organic functional groups present in the sample.

A pure KBr (Potassium bromide) pellet and a pellet of sample mixed with KBr were prepared. KBr pellet was used as a reference. Then the sample pellet was placed in the device to obtain the IR spectrum in terms of transmittance v/s wave number plot. FTIR spectra were recorded in a range of 4000-400cm^{-1} at a resolution of 4cm^{-1} with 64 scans.

3.4.7 Thermo Gravimetric Analysis (TGA)

Thermogravimetric analysis (TGA) records the loss of weight of a sample as the temperature is raised at a uniform rate. TGA of biomass samples has been extensively used as a means ofdetermining the characteristics of the devolatilisation process. This serves as a basic study for activation process as it helps in determine working range of temperature for activation of sample. Maximum temperature, heating rate and holding time are the parameters required for analysis. TGA is used in research and testing to determine characteristics of materials such as absorbed moisture content of materials, the level of Inorganic and organic components in materials, polymers, todetermine degradation temperatures, decomposition points of explosives, and solvent residues.

Nunn et al. [121] reported that the decomposition of cellulose and lignin occurred at a wide range of 200°-400°C and 150°-750°C; furthermore the rate of decomposition was slow. Zeriouh and Belbirl [122] reported that the decomposition of hemicellulose, cellulose and lignin occurred at ranges of 180°–240°, 230°–310°, and 300°–400°C, respectively. They also reported that lignin is the first component which decomposes at low temperature (160°-170°C) and continues to decompose at low rate until approximately 900°C. Hemicellulose is the second component to start decomposing, followed by cellulose, in a narrow temperature interval from about 200° to 400°C. This is the interval in which the main decomposition takes place and accounts for the greatest decomposition in the biomass pyrolysis process consisting of degradation reactions. Beyond 400°C, the most important reaction leads to the aromatization process, at low mass loss rate [123].

This analysis is performed to study the chemical modification by the use of LINSEIS Thermowaage L81 thermogravimetric analyser (TGA) is shown in figure

3.10. According to the various researchers, the thermal stability of the particles or composite was determined mainly the decomposition of cellulose, hemicelluloses and lignin present in a biomass.

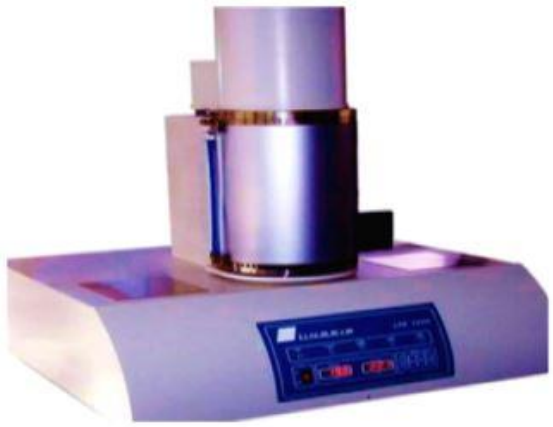

Figure 3.10 Thermogravimetric analyser (TGA)

3.4.8 Surface Area Analysis (BET) and Average particle diameter

The specific surface area of the particles is the summation of the areas of the exposed surfaces of the particles per unit mass. There is an inverse relationship between particle size and surface area. Nitrogen adsorption can be used to measure the specific surface area of a powder [124, 125]. The method of Brunauer, Emmett, and Teller (BET) is commonly used to determine the total surface area.

The average particle size can be estimated by assuming all the particles to have the same spherical shape and size. The average surface diameterof the particle, "d_{BET}", is given by:

$$d_{BET} = \frac{6}{\left(S_f \times \rho\right)} \quad (3.4)$$

Where 'S_f' is the BET specific surface area of the material in m^2/g and 'ρ'is the theoretical density in g/cm^3 [26].

3.4.9 Scanning Electron Microscope Analysis (SEM)

Scanning electron microscope uses highly energetic beam of light for produce the image of a sample by scanning it. Vacuum is maintained inside the microscope

Electron beam strikes the sample placed in the sample chamber, gets decelerated and produces a variety of signals like secondary electrons, back scattered electrons, diffracted backscattered electrons, photons, visible light and heat. The detectors detect the secondary electrons and produce visible image of the surface of the sample.

Very small amount of sample was taken in a circular disc like structure and the sample was attached to the disc by a specific tape. Then sintering of the sample was done and the sample was coated with platinum. Then sample with the disc was placed in the electron chamber of the microscope. For better quality image and for proper view of the surface the magnification of scan was varied. SEM analysis was performed using Nova Nano SEM450 at an accelerating voltage of 15 kV is shown in figure 3.11. A thin film of platinum is vacuum-evaporated onto them to enhance the conductivity of the samples before taking the photomicrographs.

Figure 3.11 Nova Nano SEM450

3.5 RESULTS AND ANALYSIS

3.5.1 Chemical Composition

As can be seen from the Table 3.3, wood apple shell particles have higher cellulose content than groundnut shell, rice husk and kenaf fiber as compared to Table

3.1. The hemicelluloses content of wood apple shell is greater than other species. The lignin content of wood apple shell is much greater than other species.

Similarly the cellulose content of coconut shell is less than other lignocellulosic materials but hemicellulose content is greater than sisal, groundnut shell and hemp fiber. Coconut shell consists of higher lignin percentage as compared tobamboo stem, oil palm shell, coconut coir, sisal, rice husk, bagasse, hemp and kenaf fiber.

The results reported in Table 3.3 indicate that wood apple shell particles contains high cellulose and lignin content than coconut shell particles, which is an important factor for preparation of activated carbon because higher the lignin content, the higher the carbon content. Therefore the wood apple shell and coconut shell is suitable for the preparation of carbon black due to high carbon content and low ash content.

Table 3.3 Chemical composition of raw shell particles

Lignocellulosic materials	α-Cellulose, wt%	Hemicellulose, wt%	Lignin, wt%	Ash, wt%
Wood apple shell	39.54	26.06	30.86	0.9
Coconut shell	30.04	20.16	25.76	1.98

3.5.2 Proximate Analysis

The content of wood apple shell is determined by proximate analysis. It may be noted that the maximum volatile matter is present in wood apple shells. The moisture content present in the raw wood apple shell particles can also be considered as water. When it is heated to high temperature the water converted to vapour. Hence, about 79.94% of the contents material which are ready to convert, of which 73.34 % is volatile matter and 6.6% is moisture content.

From figure 3.12 it is clearly observed that the fixed carbon content of raw wood apple shell particles is 19.11% and ash content of the sample is 0.95% but after pyrolytic decomposition, the carbon percentage increases drastically up to 87.43% at 800°C carbonization temperature. This is due to the extraction of non-carbon elements mainly hydrogen and oxygen in the form of gas leaving from the particles at different stages of carbonization temperature which is drastically decreases from 73.34% to 5.37%. Also it can be observed that ash percentage slightly increases at every stage of

carbonization process because in carbonization process some carbon elements are converted into ash and removed slowly from the surface of the shell particles.

Again due to chemical activation of raw particles with zinc chloride carbon percentage increases up to 94.5%. This is because of rest of the volatile substances which has a strong bond not broken at 800°C carbonization temperature, after chemical activation those are again activated due to activating agent and reacted and converted at 800°C activated temperature. After activation moisture and ash percentage in activated particles slightly decreases as compared to non-activated particles. Due to activating agent it reduce the percentage of ash formation on the surface of particles. These parameters are essential to determine the level of fillers in the polymer which effectively affect the properties of final product.

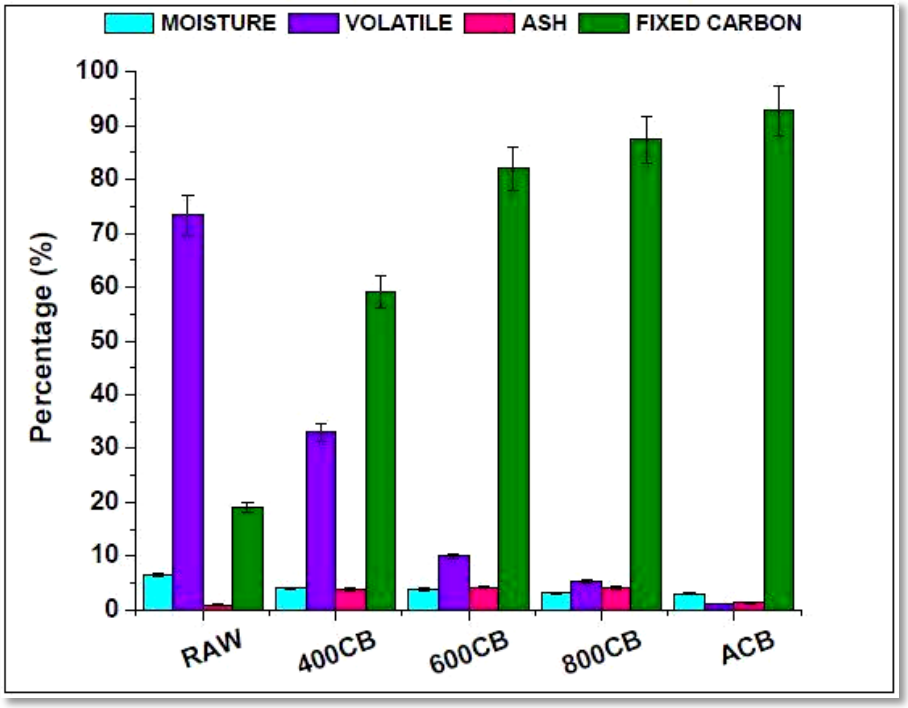

Figure 3.12 Proximate analysis of wood apple shell particulates

From proximate analysis result, it is observed that the fixed carbon percentage of raw coconut shell particles increases from 17.54% to 89.4 % after activating with chemical activating agent at 800°C activated temperature is shown in figure 3.13.

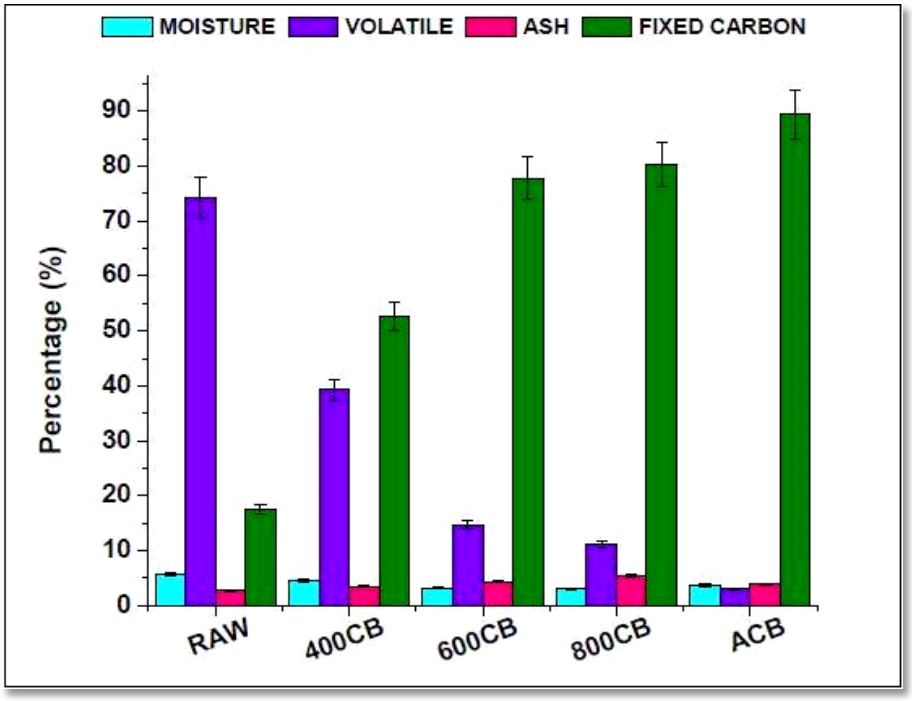

Figure 3.13 Proximate analysis of coconut shell particulates

3.5.3 Ultimate Analysis

Elemental (C, H, N, S and O) analysis of these ten samples was carried out according to the procedure explained in art 3.3.3 is given in Table 3.4 and Table 3.5 respectively. As it can be seen from the Table 3.4, raw wood apple shell particles contain about 66.387% carbon, 6.859% hydrogen, 0.632% nitrogen, 25.27% oxygen and rest amount is % of ash. As the carbonization temperature increases the carbon and nitrogen percentage also increases.The presence of oxygen and hydrogen influence the adsorptive properties of activated carbon.

Also from Table 3.5 it is clearly observed that raw coconut shell particles contain about 60.75% carbon, 6.88% hydrogen, 0.617% nitrogen, 29.87% oxygen and rest amount is % of ash.

Though after chemical activation of raw shell particles with $ZnCl_2$ at activation temperature of 800°C, there is a steep rise in the carbon concentration on activation is shown in Table 3.4 and Table 3.5. This may be due to, the fixed carbon is the major component that is left after over in addition to the volatile matter, ash and moisture content. All the four components are present as, in general a chemical reaction does not

have 100 percent conversion rate. This could also explain the reason for the sharp fall in the hydrogen as well. But the value of nitrogen has increased as the carbonization temperature increases. This is because the nitrogen gas which is used as the medium for pyrolysis as well as activation step is fixed on the surface or on the sample while the process is continuing. Oxygen in the sample naturally gets used up during the analysis and it oxidizes other elements present in the sample. The highest amount of oxygen being present in the sample really makes sense, as a large amount of oxygen in activated carbon is lost during the pyrolysis process.

Table 3.4 Ultimate analysisof wood apple shell particulates

Wood apple shell	**Element (wt% by mass basis)**				
	C	**H**	**N**	**S**	**O**
Raw	66.38	6.85	0.63	0	25.27
400°C CB	77.98	4.88	1.44	0	11.88
600°C CB	84.12	3.72	1.9	0	6.05
800°C CB	86.39	3.55	1.99	0	2.36
ACB (800°C)	88.93	3.38	2.07	0	2.03

Table 3.5 Ultimate analysisof coconut shell particles

Coconut shell	**Element (wt% by mass basis)**				
	C	**H**	**N**	**S**	**O**
Raw	60.75	6.88	0.61	0	29.87
400°C CB	67.89	5.17	1.31	0	22.62
600°C CB	78.70	4.87	2.1	0	11.25
800°C CB	83.77	3.77	2.3	0	7.75
ACB (800°C)	88.43	3.48	2.67	0	3.28

3.5.4 Energy Dispersive Spectroscopy (EDS)

The microstructure of the coconut shell particle reveals that the size and shape of the particles vary however, they can be sorted into three main groups – prismatic, spherical and fibrous.The prismatic particles consist mainly of Si and O. The spherical ones contain Si and O as well as Ca and Al. The fibrous ones consist of only C [126].

Figures 3.14(a)-(e) show the inspection spectra of wood apple shell particulate surface elements acquired for wood apple shell. The surface of raw particulates exhibit

spectra containing mainly carbon, oxygen, silica, aluminum with small amount of zirconia and calcium is shown in figure 3.14(a). Due to pyrolytic decomposition non-carbon elements are slowly removed from raw wood apple shell particulates at various carbonization temperatures i.e. 400°C, 600°C and 800°C. Hence the carbon, silicon and zirconia percentage within the raw particulates is gradually increasing which is clearly observed from the figure 3.14(b), 3.14(c) and 3.14(d).Also from the figure 3.14(e) it can be observed that after chemical activation of raw shell particulate at 800°C carbonization temperature the carbon and silicon percentage drastically increases as compared to non-activated carbon particles.

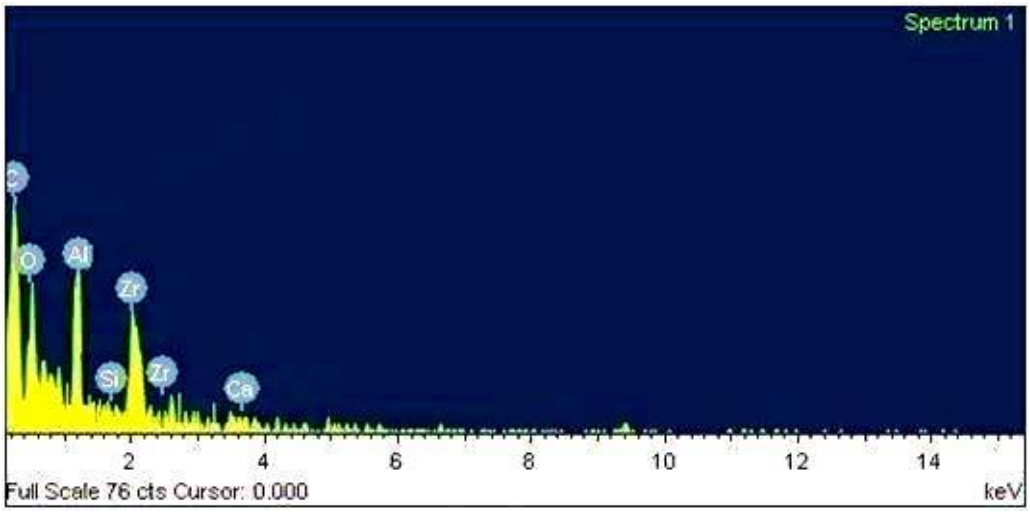

Figure 3.14(a) EDS of Raw wood apple shell particulates

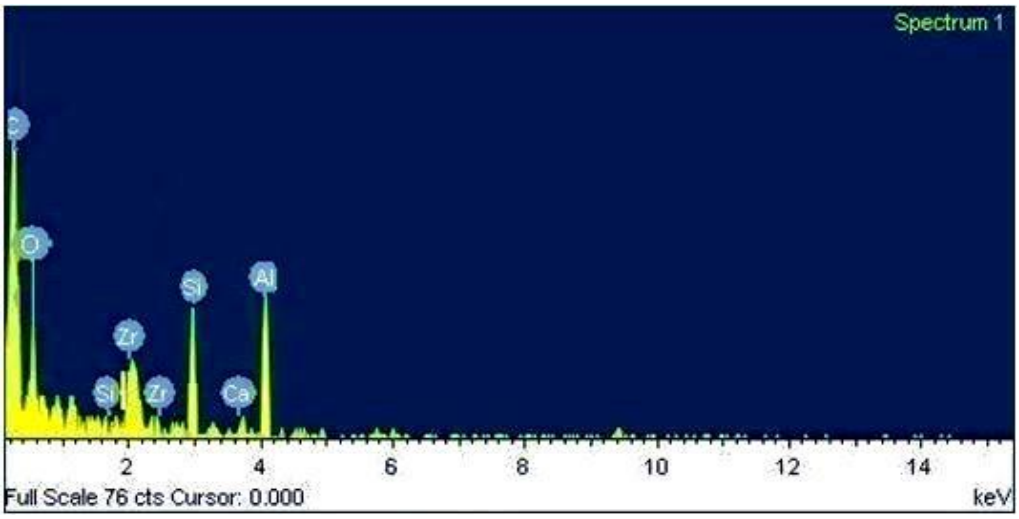

Figure 3.14(b) EDS of 400°C carbon black wood apple shell particulates

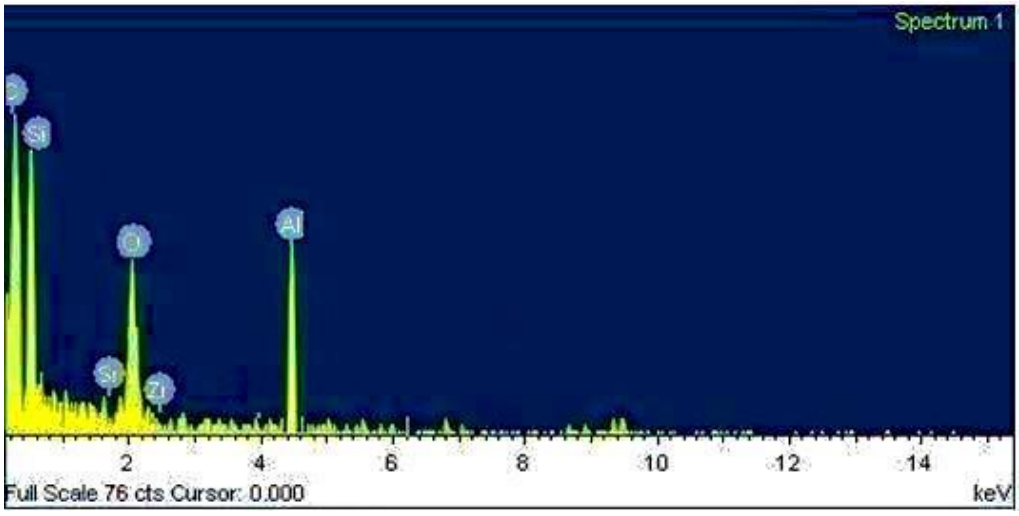

Figure 3.14(c) EDS of 600°C carbonized wood apple shell particulates

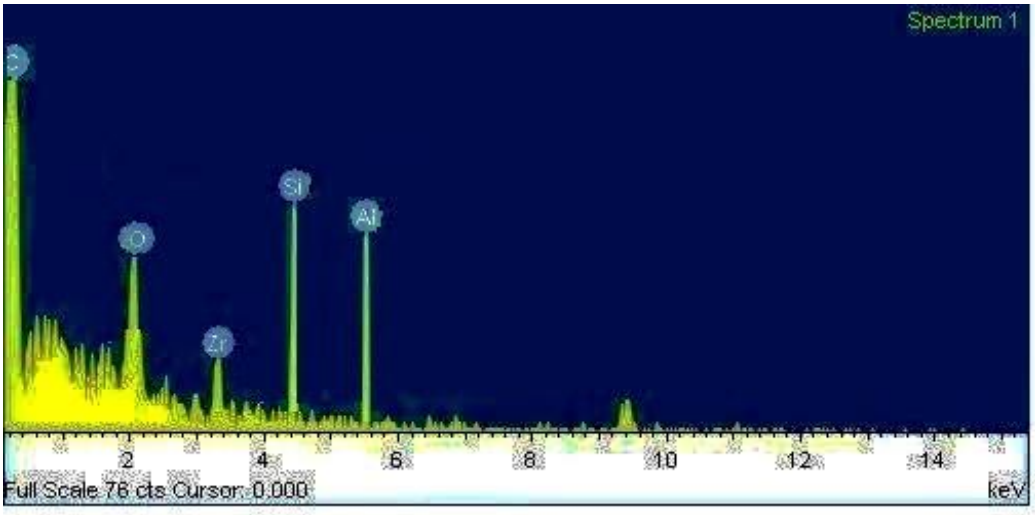

Figure 3.14(d) EDS of 800°C carbonized wood apple shell particulates

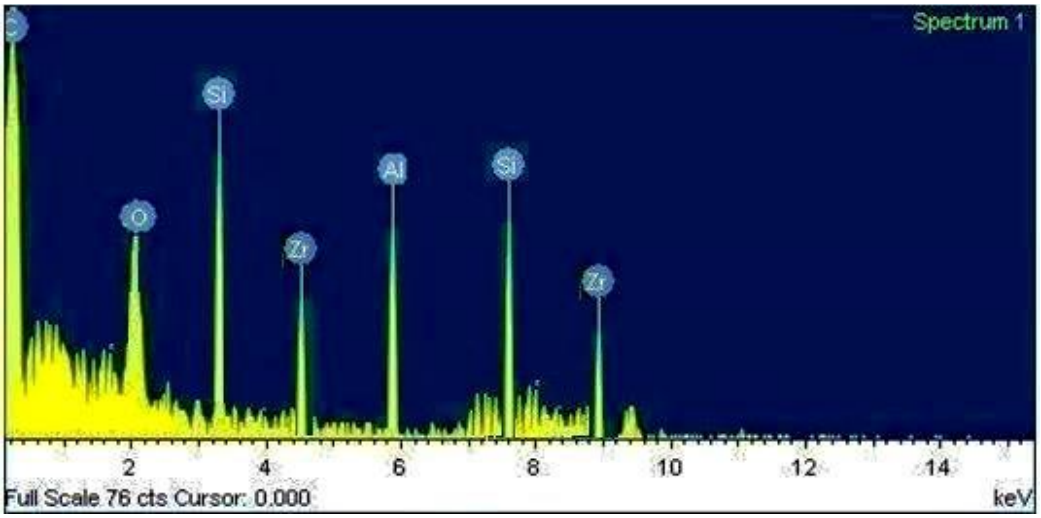

Figure 3.14(e) EDS of activated carbon black wood apple shell particulates

Similarly raw coconut shell particulate consists of mainly carbon, oxygen, silica, and small amount of zirconia and calcium is shown in figure 3.15(a). But these elemental percentages are very less as compared to raw wood apple shell particulate. Here also similar observations are found that carbon content increases at every stage of carbonization process which is shown in figure 3.15(b), 3.15(c), 3.15(d) and 3.15(e). Also the carbon and silicon percentage is more as compared to other non-activated coconut shell particles.

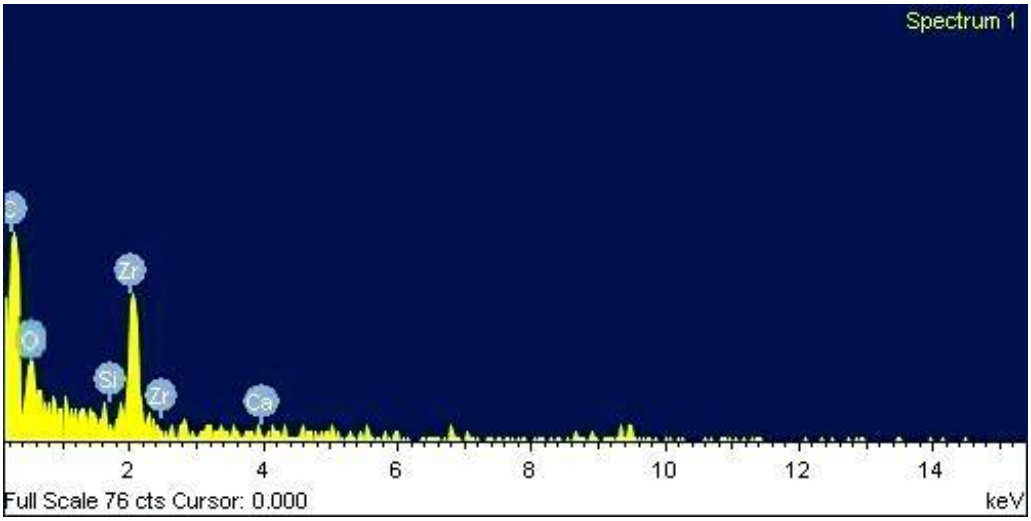

Figure 3.15(a) EDS of raw coconut shell particulates

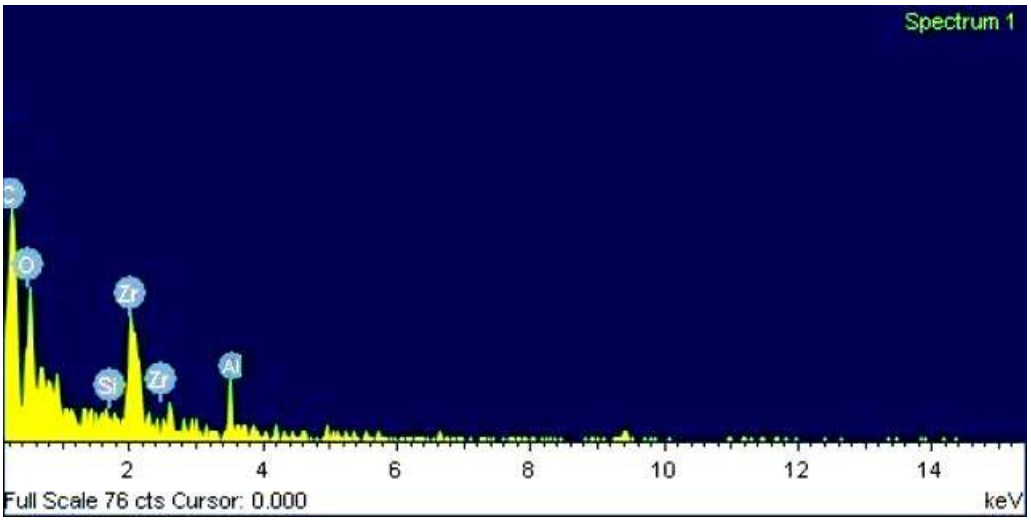

Figure 3.15(b) EDS of 400°C carbonized coconut shell particulates

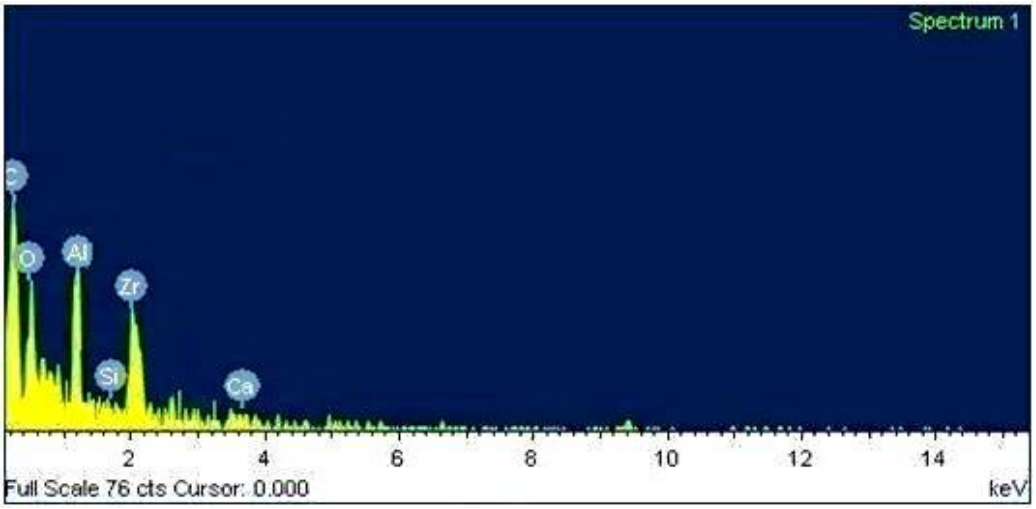

Figure 3.15(c) EDS of 600°C carbonized coconut shell particulates

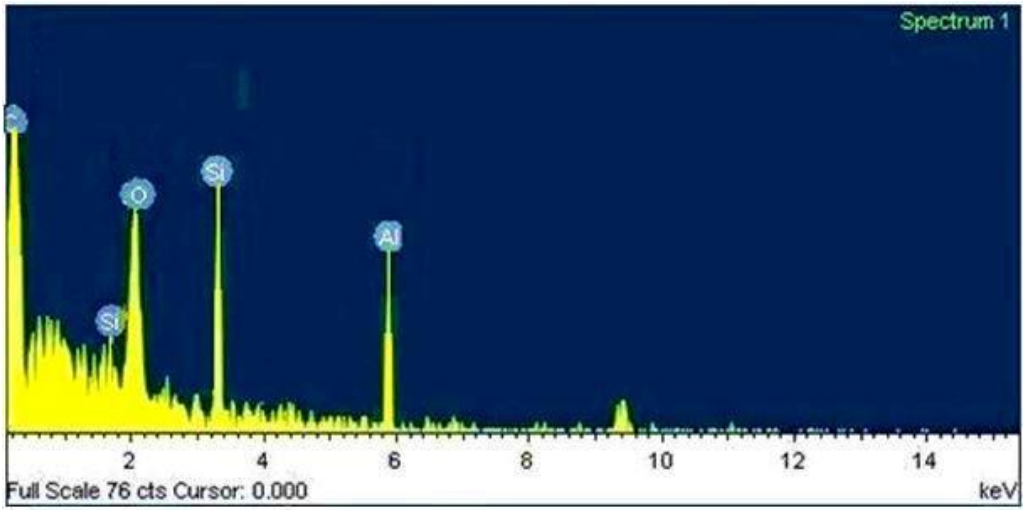

Figure 3.15(d) EDS of 800°C carbonized coconut shell particulates

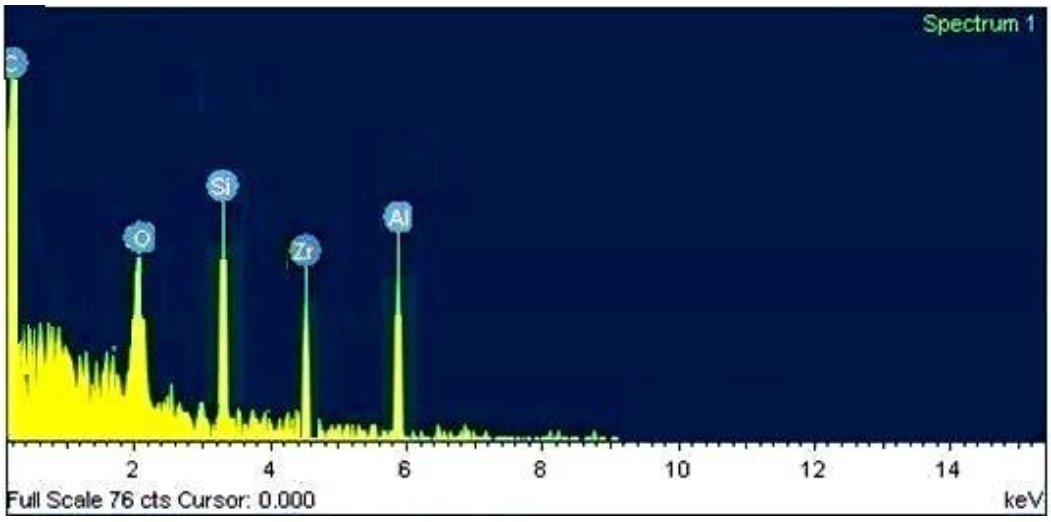

Figure 3.15(e) EDS of activated carbon black coconut shell particulates

Finally activated carbon black particles of wood apple shell and coconut shell contents some hard ceramic particles like SiO_2, Al_2O_3 and zirconia. Hence these particulate can be used as reinforcement in various polymer matrixes.

However the presence of carbon, silicon and other element in both shell particles but the carbon percentage is more in activated wood apple shell particulate as compared to activated coconut shell particulate.

3.5.5 Crystal Structure Transition

The XRD patterns of raw, carbon black and activated carbon black wood apple shell particles have been presented in figures 3.16 (a-e). It is clearly observed from the figure that XRD signals of powder sample contains large amount of noises in it. This behavior confirms the amorphous structure of carbon. As is evident from these figures the sharpness of the peaks of carbon black particles increases as the carbonization temperature increases (400-800°C) as compared to raw particles is shown in figure 3.16(b-d). Correspondingly after activation of raw particles with zinc chloride the sharpness of the peak drastically increases as compared to non-activated particles is shown in figure 3.16(e).

It is observed from figure 3.16(a) that the raw wood apple shell particles at 2θ scale gave peaks at 12.528, 22.560, 34.609, 42.367 and 44.634. Out of these 12.528, 22.560, 34.609 are mainly of the crystalline cellulose and the remaining amorphous areas are due to lignin and hemicelluloses component in shell particles. Phases of these peaks as: Mg_2Si, C, SiO_2, Al_2O_3, MgO, this revealed that this particle has some of the composition of hemicelluloses, cellulose and lignin that has been confirmed by the literature [127].

The XRD patterns of all the wood apple shell particles presents broad profiles (containing only 002 and 100 bands) centered in angular position near to graphite, which indicates hard carbon. This indicates that the wood apple shell carbon black particles contain microcrystalline particles of the order of graphite like planes arranged turbo statically as suggested by Emmerich et al. [128].

The change in (002) and (100) diffraction profiles for carbon black and activated carbon black of wood apple shell particles, prepared at various temperature 400°-800°C (1h soak), with increase in carbonization temperature is shown in figures 3.16(b-d). The relative structural ordering in these carbon black, in relation to their carbonization temperature, was evaluated not only by the most advantageous lattice parameters d_{002} and L_a but also quantitatively by comparing the broadening/sharpening of their (002) and (100) diffractionprofiles. As seen in figures 3.16(b-d) these broad profiles sharpened and some annular shifting of the lines in the direction of graphite characteristic values with increase of carbonization temperature. This result indicates that carbon atoms of carbonized wood apple shell particles are rearranged from disorderly to orderly and the crystalline structure improves remarkably with increasing carbonization temperature as well as reducing the amorphosvity of the particles. Also SiO_2, Al_2O_3, MgO small peaks are present in carbon black particles.

After activation of raw wood apple shell particles with $ZnCl_2$ chemical activating agent at 800°C activation temperature, these two broad peaks 2θ=22° and 43°which corresponds to the peak of graphite [129] is shown in figure 3.16(e). It can be clearly observed from the figure that after activation the two peaks are broad and carbon and silicon dioxide is present in that phase. Similar observations are also found by Kumar et al. [130] in their research work. From the result it is concluded that at every carbonization temperature the two peaks are gradually sharpened and move towards the crystallinity.

The activated carbon samples with broad peaks and absence of sharp peak that revealed predominantly amorphous structure, which is an advantageous property for well-defined porous adsorbents [131]. Broad peaks found at around 22°-24° for all the samples confirm that the samples are non-graphitized and can have high micro porous structure [132]. Also it corresponds to the presence of silica and carbon there by confirming the existence of amorphous SiO_2 in carbon particles. Also the peak intensity of carbon and activated carbon black particulates is gradually increases.

The broad peak at 2θ = 24° corresponds to the presence of silica and thereby confirming the existence of amorphous SiO_2 in activated charcoal. In the entire cases

relative intensity and diffraction peaks of carbon and activated carbon black samples were increased gradually as the carbonization temperature increases.

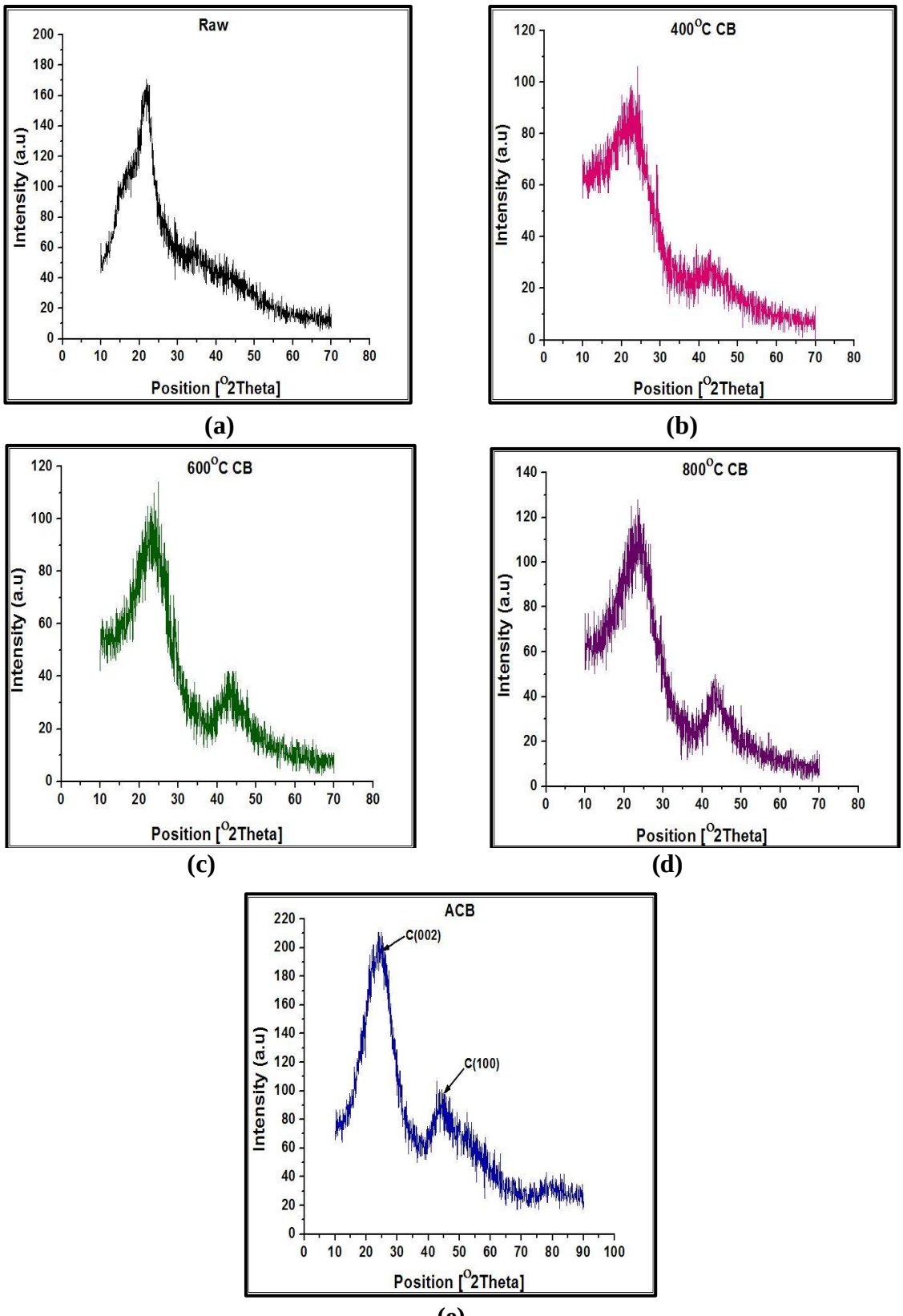

Figure 3.16 XRD analysis of wood apple shell particulates

Similar observations are also found in analysis of coconut shell particles is shown in figure 3.17(a-e). As the carbonization temperature increases the intensity of diffraction peak also increases due to removal of impurities. As the carbonization temperature increases two broad peaks (002) and (100) are observed and slowly sharpen move towards the graphite region. Activated carbon black particles are showing broad and sharp peak than other non-activated particles. Some peaks are indicating to SiO_2 and other small peak indicates to carbon element.

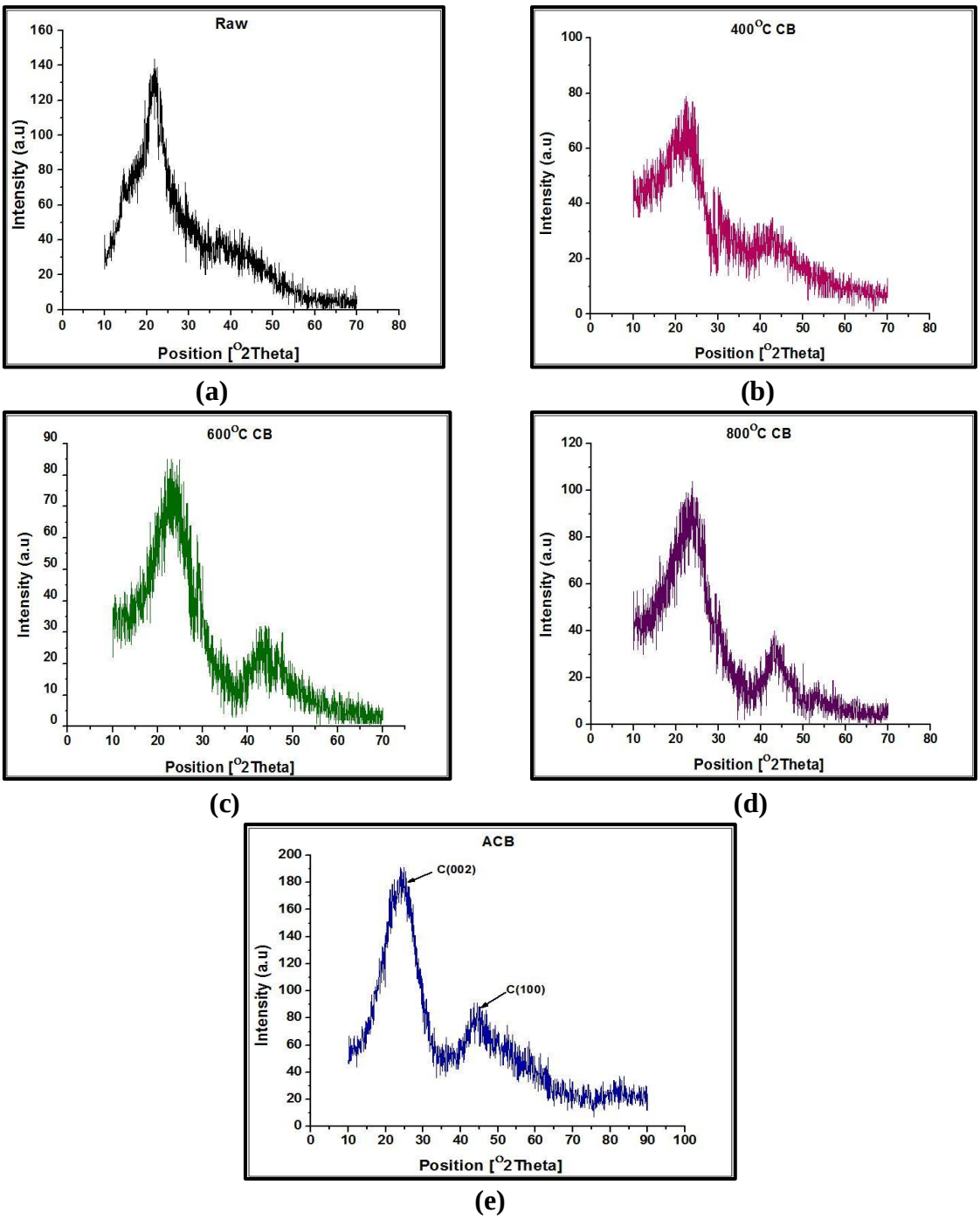

Figure 3.17 XRD analysis of coconut shell particulates

3.5.6 Functional group analysis using FTIR

3.5.6.1 FTIR analysis of Wood apple shell particulates

The drift spectra of raw, carbon black and activated carbon of wood apple particles are shown in figure 3.18 and the surface functionality of particles are given in Table 3.6.

Functional groups presented in the raw particles are more when compared to carbon black particles. New surface functional groups at 3746, 3226, 2945, 2765, 2374, 2116 and 1250cm^{-1} were developed in wood apple shell activated carbon due to chemical activation is shown in figure 3.18.

The main surface functional groups present in the raw wood apple shell were carbonyl groups (such as ketone and quinone), ethers and phenols. As the carbonization temperature increases most of the weak bonds are removed and some new functional group is appeared in both shell particles.

After carbonization, the carbon black displayed the surface functional groups of ketone, quinone aromatic rings. For the activated carbon, the ketone groups are absent due to their thermal instabilities at high temperature. The drift surface of wood apple shell based activated carbon show that both types i.e. acidic and basic surface functional group are present on its surface.

The peaks at 3733, 2916, 3734, 3749 and 3746cm^{-1} is observed for wood apple shell. The peak at about 3700cm^{-1} is due to hydrogen bonded O-H stretching. The hydrophilic tendency of wood apple was reflected in the broad absorption bands, which is related to the –OH groups presented in aliphatic or aromatic alcohol and present in their main components. The peak at around 2850cm^{-1} is due to the C-H asymmetric and symmetric stretching from aliphatic saturated compounds. These two stretching peaks are corresponding to the aliphatic moieties in cellulose and hemicelluloses.

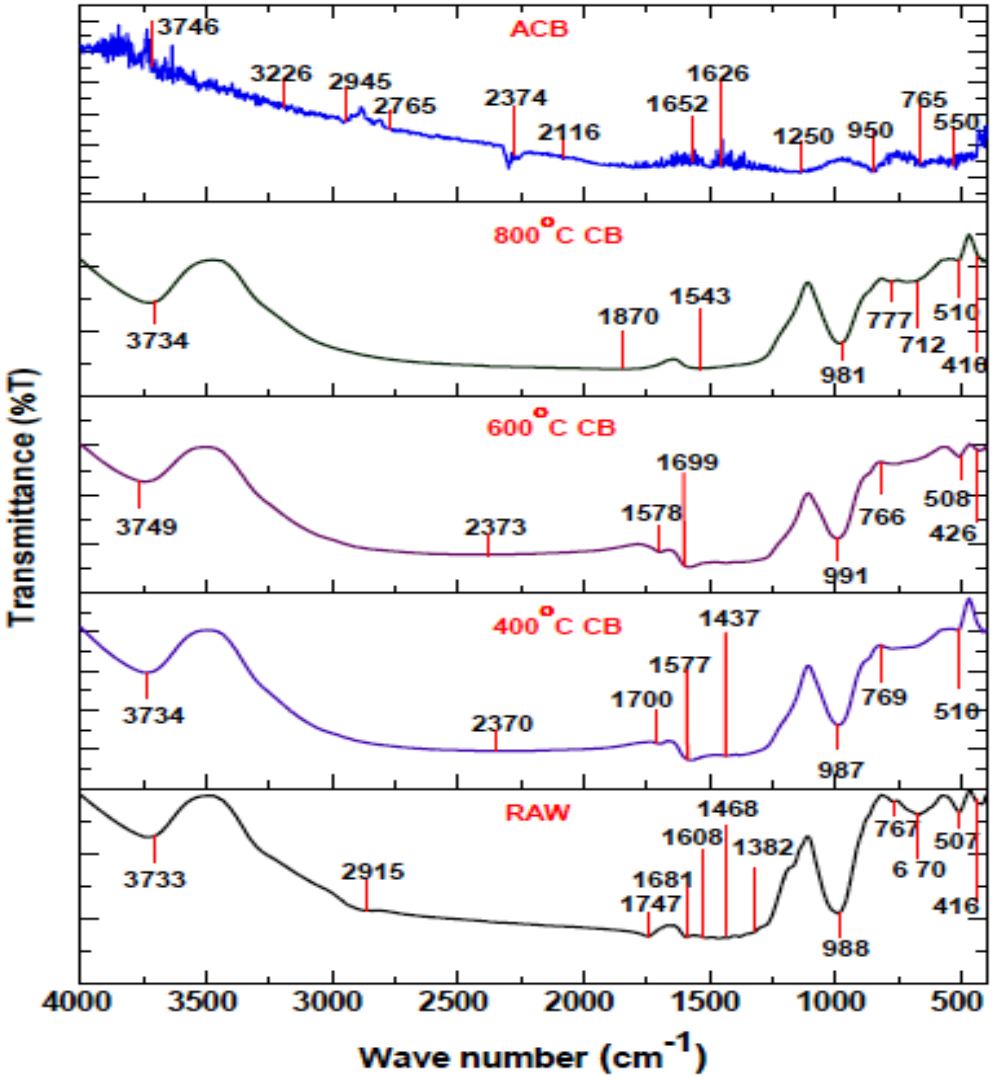

Figure 3.18 FTIR analysis of wood apple shell particulates

Table 3.6 Surface functionality of raw, carbon black and activated carbon of wood apple shell particulates

Wave length (cm^{-1})	Functional Group	Type of Vibration	Intensity	Raw	400°C CB	600°C CB	800C CB	ACB
3733	O-H	stretch,free, H-bonded	strong, sharp	√				
3734	O-H	stretch,free, H-bonded	strong, sharp		√		√	
3749	O-H	stretch, free, H-bonded	strong, sharp			√		
3746	O-H	stretch, free, H-bonded	strong, sharp					√
3226	O-H	stretch, free, H-bonded	strong, broad					√

2916	C-H Asymmetric and symmetric	stretch	medium	√				
2945	C-H	stretch	strong					√
2765	C-H	stretch	medium					√
2370	P-H P-O-H	stretch			√			
2373	P-H P-O-H	stretch				√		
2374	P-H P-O-H	stretch						√
2116	Alkenes -C(triple bond)C-H, -CH_3, CH_2, Si-H	stretch	medium					√
1870	Amide C=O	stretch	strong				√	
1747	Anhydride C=O	stretch	strong	√		√		
1700	Acid C=O	stretch	strong		√			
1699	Amide C=O	stretch	strong			√		
1652	Amide C=O	stretch	strong					√
1626	N-H	bending	medium					√
1591	-C=O, Amide N-H, Aromatics C=C	Stretch, bending	medium-weak, multiple bands	√				
1578	-C=O, Amide N-H, Aromatics C=C	Stretch , bending	medium-weak, multiple bands			√		
1577	-C=O, Amide N-H, Aromatics C=C	Stretch , bending	medium-weak, multiple bands		√			
1543	N=O	asymmetric stretch	medium-weak, multiple bands				√	
1508	Aromatic C=C	stretch	medium-weak, multiple bands	√	√			
1459	-CH_2	stretch	medium	√	√			
1437	Aromatic -C=C-	stretch	medium-weak, multiple bands		√			

1382	-C=H N=O, N-H	Stretch, bending	Variable, strong, two bands	√				
1250	Si-CH_2, C-N, C-O, O-H, N-H	Stretch, bending	strong					√
988	Alkenes =C-H	bending	strong	√				
987	Alkenes =C-H	bending	strong		√			
981	Alkenes =C-H	bending	strong				√	
950	Alkenes =C-H	bending	strong					√
767	Alkyl Halides C–Cl	stretch	strong	√				
765	Alkyl Halides C–Cl	stretch	strong					√
777	C–H "oop", C-C1, N-H	Stretch	Strong, medium				√	
712	=C-H	bending	strong				√	

3.5.6.2 FTIR analysis of Coconut shell particulates

Similar observations are also noticed while analysis is being carried out for coconut shell particles are shown in figure 3.19. The peaks at 3292, 2884, 3734,3733,3720, 3735cm^{-1} for coconut shell were observed is shown in Table 3.7. The hydrophilic tendency was also observed in case of coconut shell. Some functional groups are also exhibited by absorption bands at 3735, 2950, 2755, 2380 and 980cm^{-1} in coconut shell activated carbon particles due to chemical activation of raw particles is presented in Table 3.7.

The presence of sulphur and amino groups on the surface of both wood apple and coconut shell based activated carbon can be attributed to its leguminous plant origin as evident high content of N in elemental analysis. Presence of more nitrogen groups of surface of activated carbon helps in removal of dyes and organic pollutants [133].

In brief, the surface functional groups of the wood apple shell and coconut shell based activated carbon were generally neutral (or slightly acidic), which would explain

the dependence of the adsorptive capacity for both acidic and basic gases on the textural characteristics of the activated carbon.

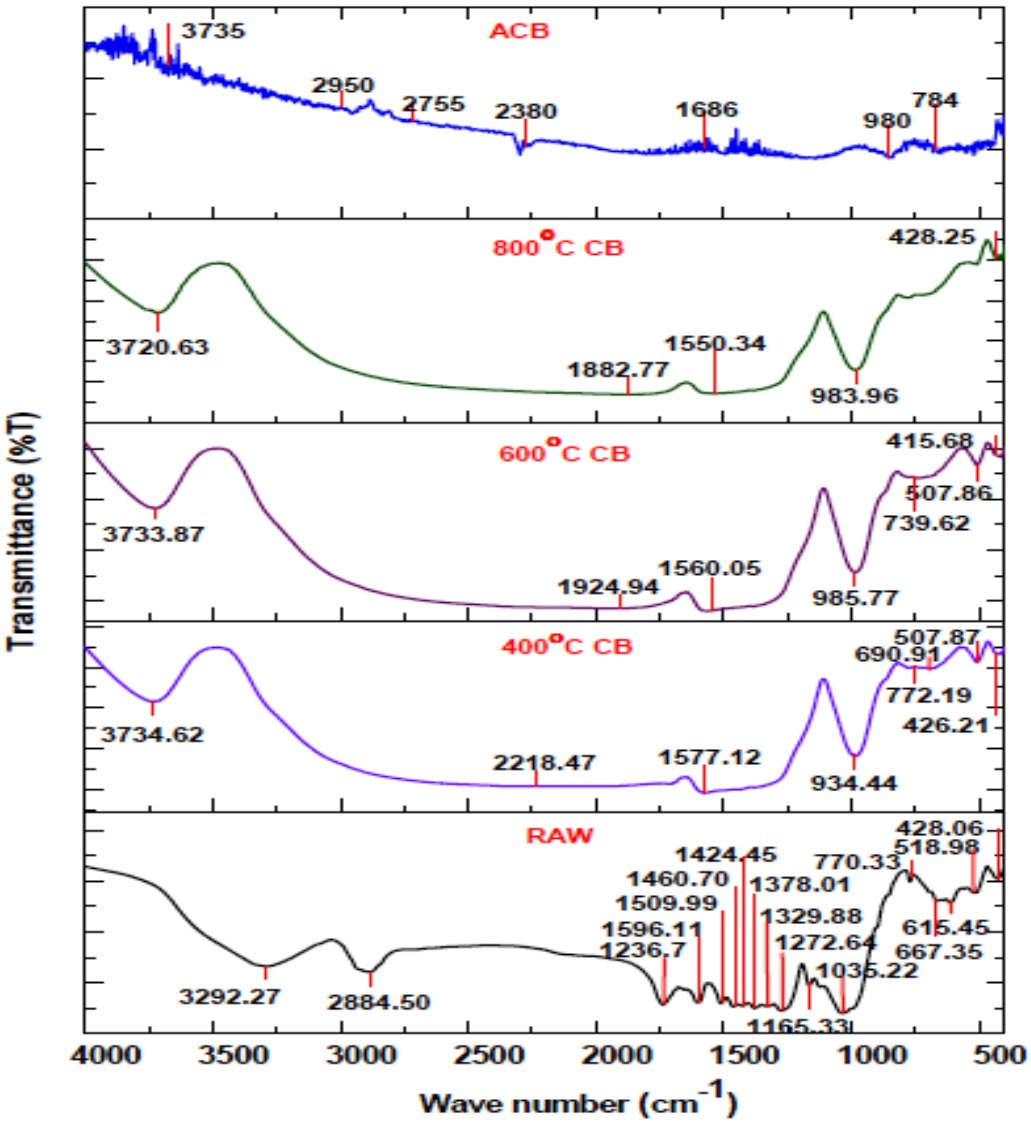

Figure 3.19 FTIR analysis of coconut shell particulates

Table 3.7 Surface functionality of raw, carbon black and activated carbon of coconut shell particulates

Wave length (cm^{-1})	Functional Group	Type of Vibration	Intensity	Raw	400°C CB	600°C CB	800°C CB	ACB
3292	O-H	Stretch, H-bonded	Strong, Broad	√				
3734	O-H	Stretch,free, H-bonded	Strong, Sharp		√			
3733	O-H	Stretch, free,	Strong, Sharp			√		

		H-bonded						
3720	O-H	Stretch, free, H-bonded	Strong, Sharp				√	
3735	O-H	Stretch, free, H-bonded	Strong, Sharp					√
2950	Aromatics C-H	Stretch	Strong					√
2884	Alkenes C-H, asymmetric and symmetric	Stretch	Medium	√				
2755	C-H	Stretch	Medium					√
2380	N-H	Stretch	Medium					√
2218	Nitrile CN	Stretch	Medium		√			
1882	C-O	Stretch	Strong				√	
1686	C=O	Stretch	Strong					√
1596	Aromatics C-C	Stretch	Medium	√				
1509	Aromatics C-C	Stretch	Medium	√				
1577	N-H	Bending	Medium		√			
1506	Aromatics C-C	Stretch	Medium			√		
1550	N-O	Stretch	Strong				√	
1460	Alkenes C-H	Bending	Medium	√				
1424	Aromatics C-C	Stretch	Medium	√				
1378	N-O	Stretch	Strong	√				
1329	Aromatic amines C-N	Stretch	Strong	√				
1272	Easter C-O	Stretch	Strong	√				
1035	Aliphatic amines C-N, C-H, -C-O	Stretch	Medium	√				
934	O-H	Bending	Medium		√			
980	Alkenes =C-H	Bending	Strong					√
983	Alkenes =C-H	Bending	Strong				√	

985	Alkenes =C-H	Bending	Strong			√		
739	Alkenes =C-H	Bending	Strong			√		
770	Alkenes =C-H	Bending	Strong	√				

3.5.7 Thermo Gravimetric Analysis (TGA) of wood apple shell and coconut shell particulates

Thermal analysis is the concept that purely reflects the decomposition reactions that occur at the molecular level of the materials with variation in temperature. For the analysis, around 10-20 milligrams of sample was taken in in an Al_2O_3 crucible at heating rate 5°Cmin^{-1}, from room temperature 30° to 600°C in the present of nitrogen at flow rate of 30ml/min. Thermo-gravimetric weight loss curve was plotted against temperature. The apparatus provides for the continuous measurement of sample weight as a function of temperature (TGA).

Figure 3.20 and 3.21 shows the TGA curve of raw, carbonized and activated carbon of both wood apple and coconut shell. From figures it is clear that initial decrease in weight loss completed below 100°C is due to the moisture loss from the all the material at this temperature.

Next step is the thermal degradation of biomass. In thermal degradation, firstly at 155°-169°C lignin is the first component which decomposes followed by decomposition of hemicellulose which starts from 230°-307°C. After Hemicelluloses decomposition in the final step major weight loss occurred within the temperature range of 323°–392°C as a consequence of the cellulose decomposition.

The same types of thermal behavior were reported by Nunn et al. [121]. They reported that the decomposition of cellulose and lignin took place at a wide temperature range of 200°-400°C and 150°-750°C, respectively. Furthermore the rate of decomposition was slow. Zeriouh et al. [122] reported that the decomposition of hemicellulose, cellulose and lignin occurred at temperature ranges of 180°–240°, 230°–310°, and 300°–400°C, respectively. Researchers already reported that lignin is the first component which decomposes at low temperature (160°-170°C).

For the carbonized material the stages are varied when compared to raw particles the degradation temperature also increases this is due to conversion of lignin in to carbon material. The stages are reduced at the higher carbonization temperature. Due to activation the carbon content are increases hence the carbon has higher thermal resistance this is confirmed by the TGA of activated carbon line.

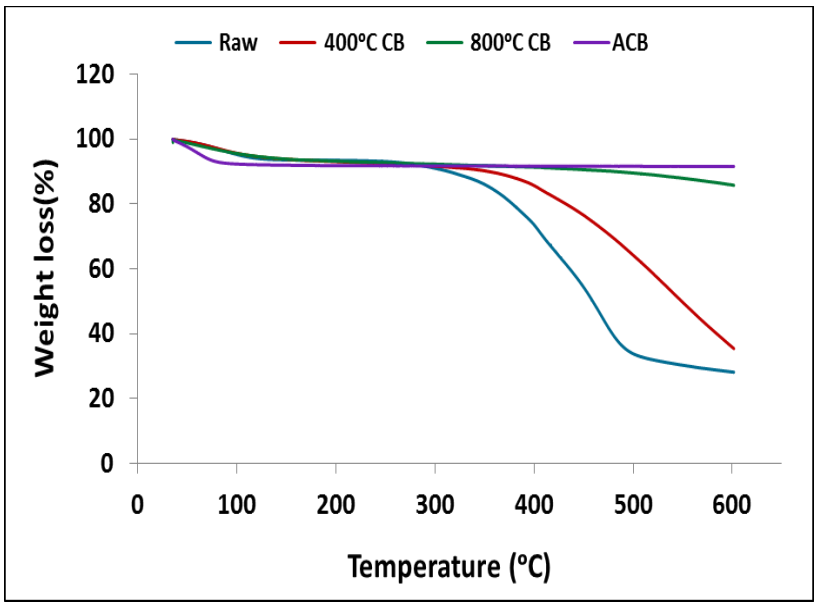

Figure 3.20 TGA of wood apple shell particulates

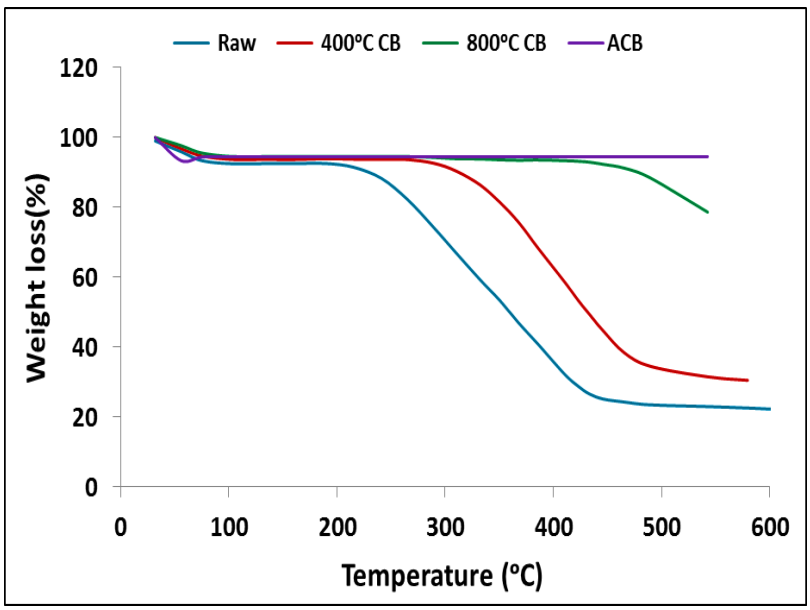

Figure 3.21 TGA of coconut shell particulates

3.5.8 Surface Area Analysis (BET) and Average particle diameter

The BET surface area is one of the parameters that determine the absorption capacity of the activated carbon. Higher surface area implies more availability of surface for adsorption hence better adsorption capacity. The BET surface area and pore volume of both wood apple shell and coconut shell based raw, carbon and activated carbon particles were determined and shown in Table 3.8.

It is clearly observed that from Table 3.8 when the pyrolysis temperature was 400°C, pyrolysis reaction had just commenced, thereby producing very small BET surface area and total volume. This phenomenon was due to the inadequate of heat energy to drive away any substantial amounts of volatiles. As the carbonization temperature increased from 600°C -800°C, increasingly greater volatile matters were released progressively during pyrolysis thereby resulting in the development of some new porosity, and hence BET surface area of the material and total volume (V_{tot}) of the porous increased, while the average diameter of the particle decreased. According to the pyrolysis results, the hemicellulose, cellulose and lignin in wood apple shell would take place dehydrating, linkage breaking off reactions, the structural ordering process of the residual carbon and finally happened polymerization reaction during the carbonization process. With increasing carbonization temperature, polymerization reaction would be deepened, the diameter of sample would be lowered gradually and the micro porous sample would be developed, giving rise to increases in the BET surface area and total volume of micro porosity of carbon black.

For example, the BET surface area of the carbon black obtained from wood apple shell at 800°C was 85.35m^2/g, presenting a rudimentary pore structure. Thus, higher temperature carbon black offers higher potential to produce activated carbon of greater adsorption capacity from wood apple shell.

On the other hand, it was observed that, after chemical activation of raw wood apple shell particles the BET surface area and total volume drastically increases with decreasing of average diameter as compared to the surface area of carbon black particles at various carbonization temperatures and finally enters to nano range. It indicates that more previously inaccessible pore were opened and new pores were

created with the chemical reaction between raw particles and hydrating agent in procession during the activation process.

Similar observation was also found in case of coconut shell particles. As a result, the BET surface area, total volume and average diameter of activated carbon prepared from raw wood apple shell particles were 457.25m^2/g, 0.634cm^3/g and 0.077µm whereas 345.24m^2/g, 0.425cm^3/g and 0.091µm respectively in case of activated carbon prepared from coconut shell particles.

Table 3.8 BET surface area of wood apple and coconut shell particulates

Samples	Precursor					
	Wood apple shell			Coconut shell		
	$S_{f(BET)}$ (m^2/g)	V_{total} (cm^3/g)	$d_{average}$ (µm)	$S_{f(BET)}$ (m^2/g)	V_{total} (cm^3/g)	$d_{average}$ (µm)
Raw	2.42	0.003	2.321	1.16	0.001	3.193
400°C CB	5.60	0.005	1.488	3.52	0.002	2.104
600°C CB	11.14	0.009	0.962	9.23	0.007	1.048
800°C CB	85.35	0.051	0.227	44.28	0.046	0.323
ACB (800°C)	457.25	0.634	0.077	345.24	0.425	0.091

3.5.9 Morphological Characteristics

Scanning Electron Microscopy (SEM) technique was employed to observe the surface physical morphology of wood apple shell and coconut shell-derived carbon black and activated carbon black. Figure 3.22(a-j) shows the SEM micrographs of the raw, carbon black and activated carbon prepared from wood apple shell particles under different conditions. It also gives information about the changes induced by carbonization and activation of raw wood apple shell particles.

It also can be seen from figure 3.22(a) that the surface of the raw wood apple shell was dense and planar and also no porous found on the surface. At higher magnification micron particles are clearly observed on the surface is shown in figure 3.22(b).

For the carbon black pyrolyzed at 400°C of raw wood apple shell particles with a retention time 1h, the micrograph showed some porous on the surface is shows in figure 3.22(c). Initially some porous structure is developed because of removal of volatile mater from the raw particles. Also at 13000x magnifications there are small porous structure has clearly observed in the surface of 400°C carbon black particles is shown in figure 3.22(d).

As the carbonization temperature increases from 400-600°C, the diameter of the carbon black particles are smaller is shown in figure 3.22(e). Also the micros porous are gradually increasing in the surface of 600°C carbon black particles. Considerably the area of the developed porous structure has been increased is shown in figure 3.22(f).

The micrograph of the carbon black at 800°C for 1h (figure 3.22 (g)) shows that there were many pores over the surface, forming a system of advanced pore structures. Due to this well-developed pores, the carbon black possessed high BET surface area and adsorptive capacity. It is because of the reduction of more volatile matter during 800°C carbonization lead to the development of pores on the surface of the carbon black particles. At this temperature the area of the porous structure has also been increased which is proven by the BET analysis. One interesting thing is that within the porous structure some particles are found in nano range is shown in figure 3.22(h) at 50000x higher magnifications. After every stage of carbonization the area of the porous structure in the surface are wider than the size of the existing pores.

After activation of raw wood apple shell a particle, the external surface is chemically activated by $ZnCl_2$ is rich with cavities. There are numerous micropores with regular size are developed in the surface which is clearly observed from the figure 3.22(i) as well as the area of the pores are significantly increases as compared to other carbon and non-carbon particles. The clearly porous structure of the $ZnCl_2$ activated carbon resulted from the evaporation of $ZnCl_2$ during carbonization, leaving the empty space previously occupied by the $ZnCl_2$. Due to the effect of activation at 800°C more number of nano particles are shown on the surface because at higher temperature the diameter of the particles is reduced and comes under nano range which is clearly observed from figure 3.22(j) at 170000x higher magnifications.

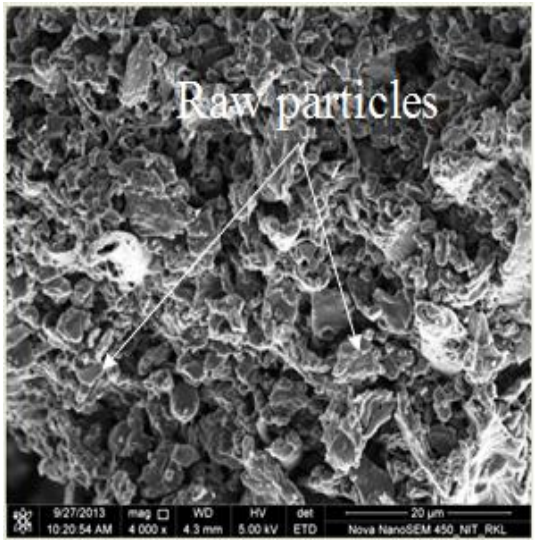
Raw particles

(a)

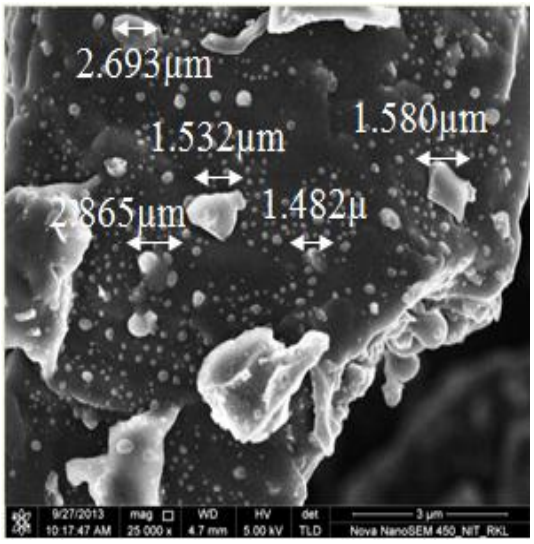
2.693µm
1.532µm
1.580µm
2.865µm
1.482µ

(b)

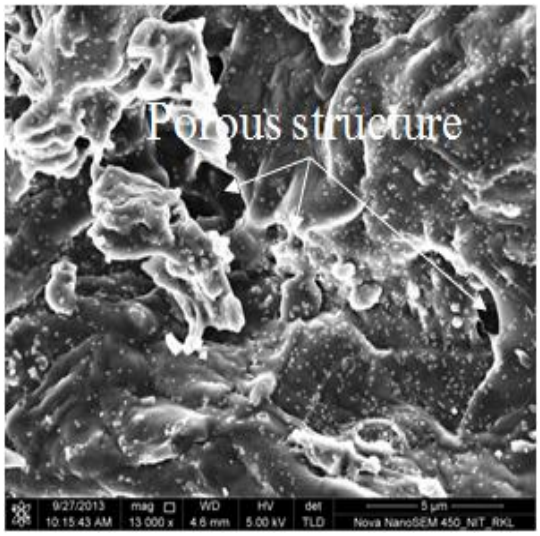
Porous structure

(c)

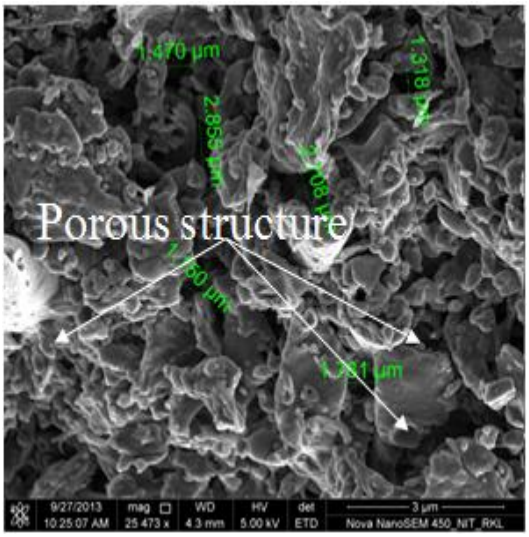
1.470 µm
1.318 µm
2.858 µm
Porous structure
1.781 µm

(d)

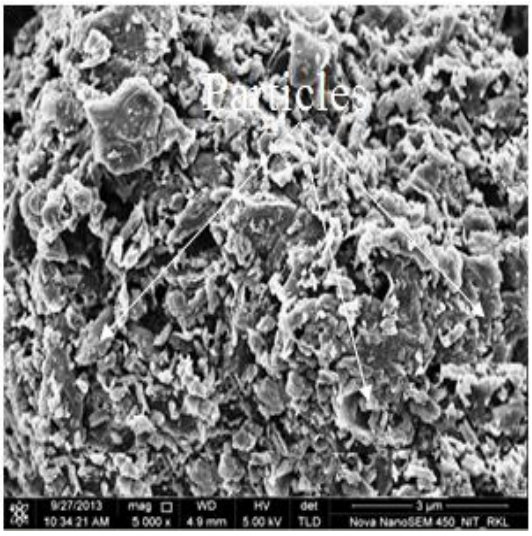
Particles

(e)


Porous structure

(f)

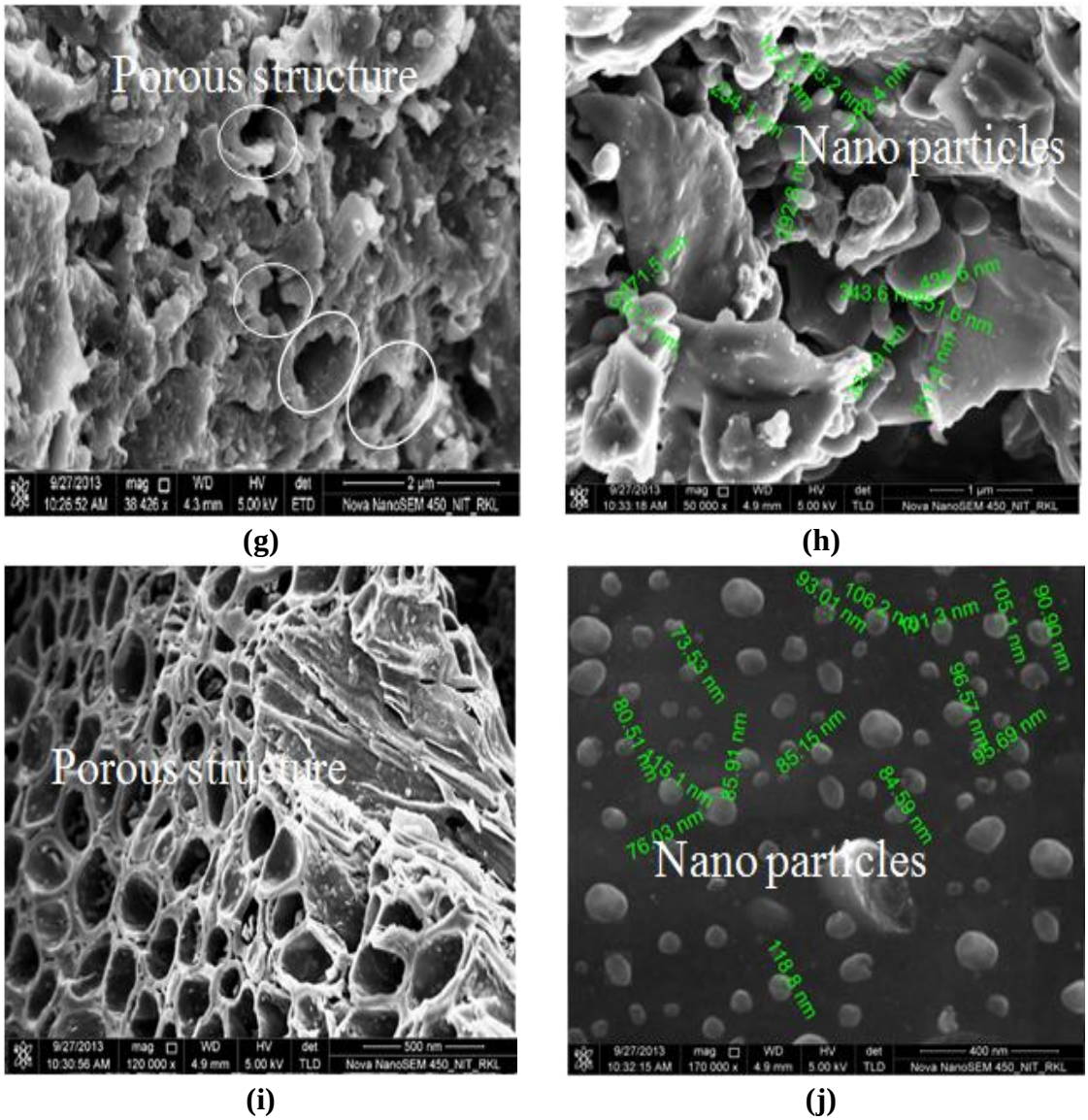

(g) **(h)**

(i) **(j)**

Figure 3.22 SEM images of raw, carbon black and activated carbon particulates of wood apple shell

(a, b) Raw wood apple shell particulates,

(c, d) Carbonized wood apple shell particulates at 400°C,

(e, f) Carbonized wood apple shell particulates at 600°C,

(g, h) Carbonized wood apple shell particulates at 800°C,

(i, j) Activated wood apple shell particulates at 800°C

In the raw coconut shell particles there are no porous found on the surface is shown in figure 3.23 (a). At higher magnification micron particles are clearly observed from the surface is shown in figure 2.23(b). Figure 3.23(c) shows the some raw coconut shell particles on the surface but after pyrolysis at 400°C, some porous are

developed on the surface due to removal of volatile mater from the coconut shell particles is shown in figure 3.23(d).

At 600°C carbonization temperature the diameter of the particles slightly reduces which is clearly observed from figure 3.23(e) and also some micron particles are observed with higher magnifications in figure 3.23(f) with some newly developed pores on the surface.At 800°C carbonization temperature micron particles are converted into nano particles is shown in figure 3.23(g) and also porous structure are developed on the surface of the carbon black particles is shown in figure 3.23(h).

After activation of raw coconut shell particles, the external surface are chemically activated by $ZnCl_2$ is rich with cavities. There are numerous micropores with regular size are developed in the surface which is clearly observed from the figure 3.23(i) as well as the area of the pores are significantly increases. The clearly porous structure of the $ZnCl_2$ activated carbon resulted from the evaporation of $ZnCl_2$ during carbonization, leaving the empty space previously occupied by the $ZnCl_2$. Due to the effect of activation at 800°C more number of nano particles are formed within the pores is clearly observed at 170000x higher magnifications is shown in figure 3.23(j).

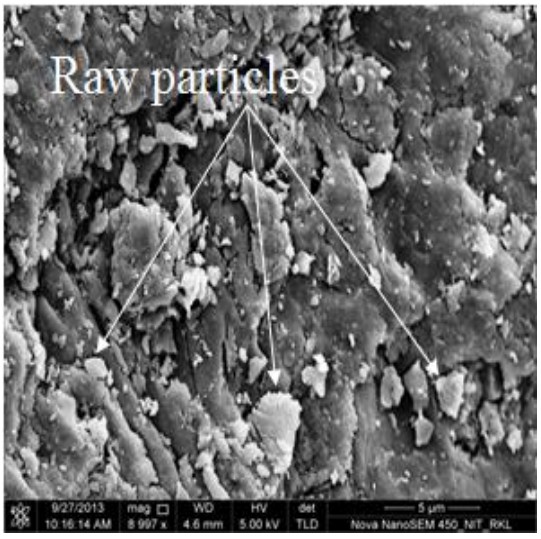

(a)

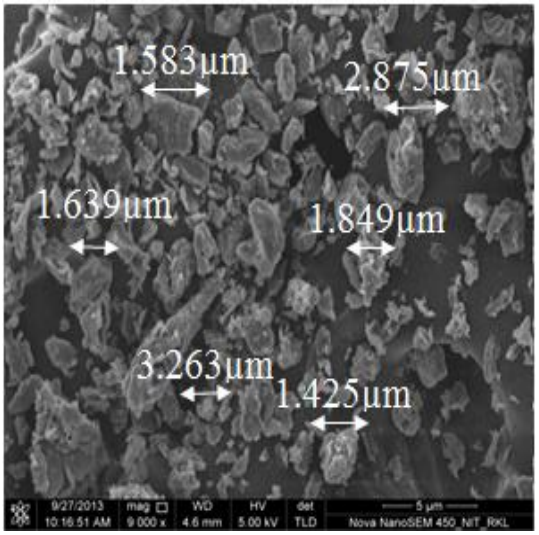

(b)

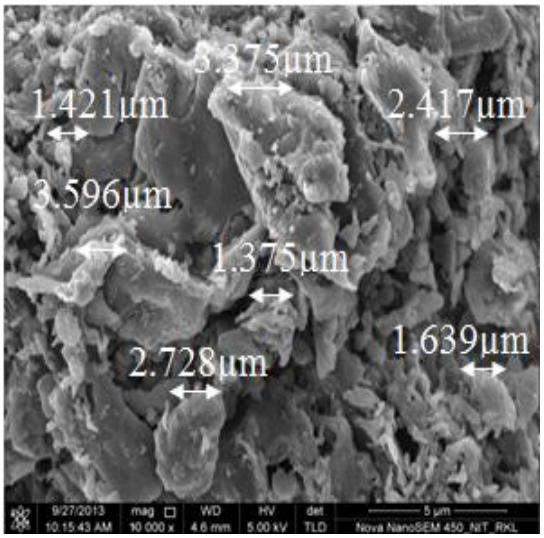
1.421µm
3.375µm
2.417µm
3.596µm
1.375µm
1.639µm
2.728µm

(c)

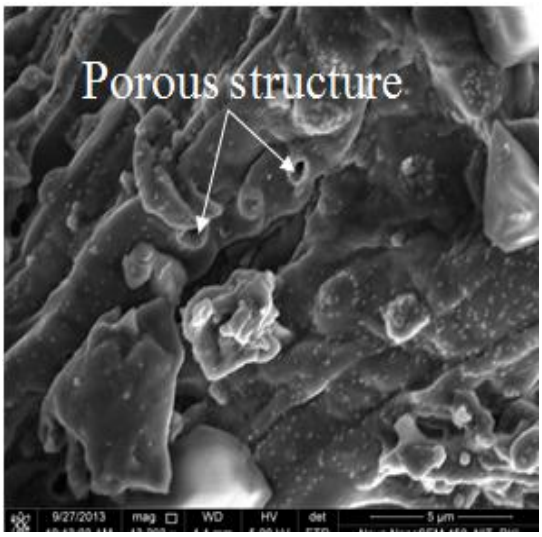
Porous structure

(d)

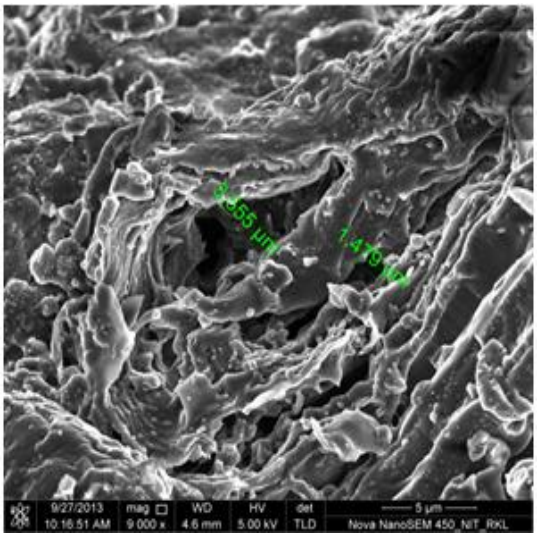

(e)

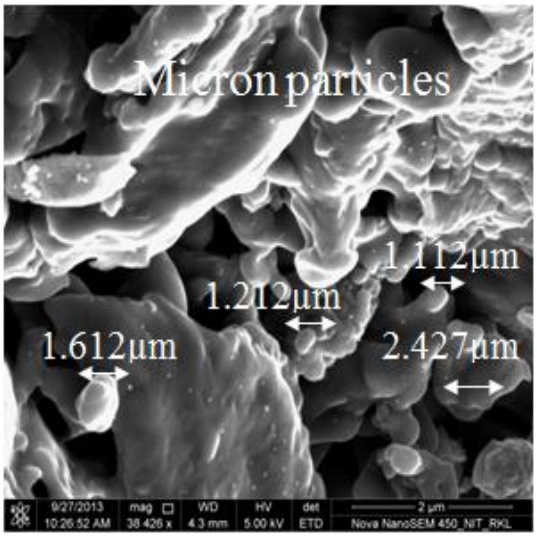
Micron particles
1.112µm
1.212µm
1.612µm
2.427µm

(f)

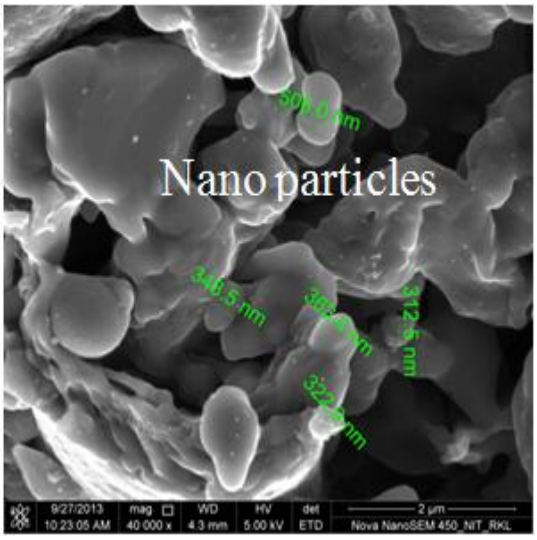
Nano particles

(g)

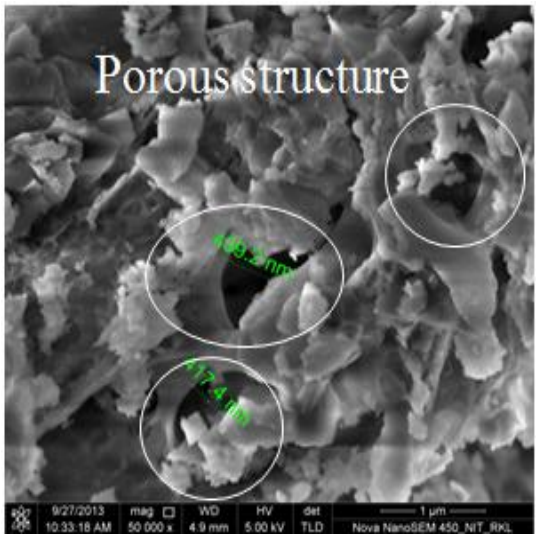
Porous structure

(h)

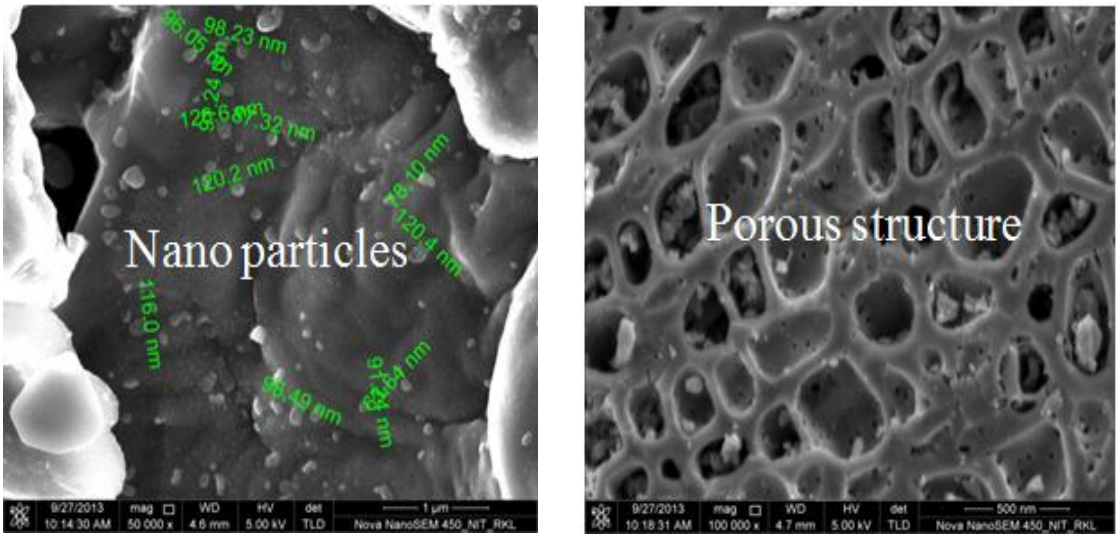

(i) **(j)**

Figure 3.23 SEM images of raw, carbon black and activated carbon particulates of coconut shell

(a, b) Raw coconut shell particulates,

(c, d) Carbonized coconut shell particulates at 400°C,

(e, f) Carbonized coconut shell particulates at 600°C,

(g, h) Carbonized coconut shell particulates at 800°C,

(i, j) Activated coconut shell particulates at 800°C

3.6 CONCLUSION

1. From the experimental result of chemical composition, it is found that raw wood apple shell particles have higher cellulose and lignin content than raw coconut shell particles. Thus it is likely to produce activated carbon with higher microporosity compared to that of coconut shell based activated carbon and provides a basis for further study.
2. From proximate analysis result, it is observed that the fixed carbon percentage of raw wood apple shell particles increases from 19.11% to 94.5% than coconut shell particles after activating with chemical activating agent at 800°C activated temperature.
3. However, ultimate analysis highlights that both particles has negligible sulfur and low nitrogen content with high carbon and oxygen contents. The highest 88.94% carbon is obtained for activated wood apple shell particulate as

compared to activated coconut shell particles. Correspondingly oxygen, hydrogen and nitrogen are also lower than activated coconut shell particles.

4. XRD studies reveals that the main constituents of wood apple and coconut shell carbon based was predominantly graphite and amorphous carbon.
5. The surface functional groups of the wood apple shell and coconut shell based activated carbon were generally neutral (or slightly acidic), which would explain the dependence of the adsorptive capacity for both acidic and basic gases on the textural characteristics of the activated carbon.
6. TGA curve of raw, carbonized and activated carbon of both wood apple and coconut shell particles shows that initial decrease in weight loss completed below 100°C is due to the moisture loss from the all the material at this temperature. Due to activation, in both cases the carbon content are increases hence the carbon has higher thermal resistance; this is confirmed by the TGA of activated carbon line.
7. The carbonization temperatures had great effects on the pore development of the carbon black prepared. With increasing of carbonization temperatures, more volatiles were released and more micropores were formed which increases the BET surface area of the particles and total volume of the pore as well as reduced the diameter of the particles. The results showed that activated wood apple shell particles comprise highest surface area as compared to coconut shell particles. High carbon content value is desired to achieve high BET surface area.
8. Scanning electron microscope images gives a view about the pores present on the surface of raw, carbon black and activated carbon particles of both wood apple shell and coconut shell. From it is inferred that, there was no pore visible on the surface of raw material, but there were clearly visible pores in case of activated carbon. In SEM analysis also it is clearly shown the particle size of the filler and the average particle size of the raw wood apple shell are 2 microns and the activated carbon from wood apple is 85nano meters. Whereas for coconut shell, it is almost 2.5 and activated carbon is 100 nano meters approximately is shown in figure 3.22 and 3.23.

Chapter 4

Mechanical Characterization of raw, carbon and activated carbon filled composite

4.1 INTRODUCTION

The use of natural fibers as filler of plastics is rapidly increasing; as it significantly increases the mechanical properties while lowers the cost of the remaining composite significantly. Use of natural fiber is environment friendly unlike inorganic fillers. Material cost savings, coupled with superior properties; are benefits that are not likely to be ignored by the plastics industry for use in the automotive, building, appliances decking, profiles, door/window frames and other applications.

In the present context natural fibers have the potential not only to reduce CO_2 emission but also save non-renewable resources by substituting glass fiber in plastic composites. Though glass fibers have been extensively used in aerospace, transportation and in process industries, they have several drawbacks. Besides high energy consumption during manufacturing, these fibers also create health hazards. Glass fibers composites are non-recyclable and difficult to dispose of.

On the other hand composites made from natural fiber are environment friendly alternative to glass fiber. The distinct advantages of natural fiber are low weight, low price, better crash absorbance and sound insulation properties.

A key feature of fiber composites that makes them so promising as engineering materials is the opportunity to tailor the material properties through the control of fiber and matrix combinations and the selection of processing techniques. In principle, an infinite range of composite types exists, from randomly oriented chopped fiber-based materials at the lowproperty end to continuous, unidirectional fiber composites at the high-performance end.A judicious selection of matrix and the reinforcing phase can lead to a composite with a combination of strength and modulus comparable to or even better than those of conventional metallic materials [134]. The physical and mechanical characteristics can further be modified by adding a solid filler phase to the matrix body during the composite preparation. It has been observed that by incorporating filler particles into fiber-reinforced composites, synergistic effects may be achieved in the form of higher modulus and reduced material cost, yet accompanied with decreased strength and impact toughness [135, 136]. Garcia et al. [137, 138] suggested this kind of multi-phase composite technique for improving the matrix-dominated properties of

continuous fiber-reinforced composites. In this technique, a supplementary reinforcement such as particulates, whiskers, or micro-fibers is added to the matrix prior to resin impregnation. Jang et al. [139, 140] found a significant improvement in impact energy of hybrid composites incorporating either particulates or ceramic whiskers. Hard particulate fillers consisting of ceramic or metal particles and fiber fillers made of glass are being used these days to dramatically improve the wear resistance of composites, even up to three orders of magnitude [141].

The improved performance of polymers and their composites in industrial and structural applications by the addition of filler materials has shown great promise and so has lately been a subject of considerable interest. Various kinds of polymers and polymer matrix composites reinforced with metal particles have a wide range of industrial applications such as in heaters, electrodes [142] and composites with thermal durability at high temperature [143]. These engineering composites are desired due to their low density, high corrosion resistance, ease of fabrication, and low cost [144–146]. Similarly, ceramic filled polymer composites have been the subject of extensive research in the last two decades. The inclusion of inorganic fillers into polymers for commercial applications is primarily aimed at the cost reduction and stiffness improvement [147, 148]. Along with fiber reinforced composites, the composites made with particulate fillers have been found to perform well in many real-operational conditions.

The mechanical and physical properties of biofiber vary considerably depending on the strength, stiffness of fiber composite, physical, chemical, composition of material, type of raw fibers or particulates, and growth environment. Mechanical properties [149] of plant fibers are much lower when compared to those of the most widely used competing reinforcing glass fibers. Because of their low density the specific properties (property-to-density ratio), strength, and stiffness of plant fibers are comparable to the values of glass fibers [150].

In studying bio filled polymer composites, the factors that have to consider are good adhesion between filler and matrix, high modulus, low stress, low moisture absorption, high durability, and long life time [151, 152].

Popaet al. [153] emphasized that the interface between the filler or reinforcing material and the polymeric matrix is essential in polymeric composites. The interface strengthened the mechanical resistance of composites, and it is where the concentration of mechanical stress occurs as a result of the differences between properties of the matrix and the filler or reinforcing agent.

Rampe et al. [154] studied structural and chemical composition of coconut shell carbon which is prepared at 873 and 1023 K carbonization temperatures with polyvinyl alcohol (PVA). The products were then analyzed by TG-DTA, SEM-EDS, FTIR and XRD. The result showed that the products were in uniform and spherical particle sizes of micrometer dimensions. Product content of C element was 97.44% (wt) and it possesses semi-crystalline structure.

Epoxy resin [22] is a widely used polymer matrix for advanced composites where good stiffness, dimensional stability and chemical resistance are required [45]. However, the mechanical properties of this polymer matrix, such as the strength, modulus and toughness of the epoxy resins may not be sufficient for some end-use applications. It is therefore desirable to modify the polymer matrix to achieve such purposes. The addition of fillers to polymer matrix is a fast and cheap method to modify the properties of the base materials [155]. Addition of various fillers with different shapes, particle size and different sources into the epoxy matrix may result indifferent microstructures and have different effects on the properties of the polymer composites [156]. Literatures survey reveals various attempts made to develop epoxy composites modified with various fillers (such as silica, carbon black, Al_2O_3, $CaSiO_3$, etc.) in other to improve the performance of this matrix. For example, Xing and Li [157] investigated the effect of silica particle size on the wear behavior of epoxy composites at low levels of filler content. In that study, it was proved that the smaller sized particles seemed to be more effective in improving the wear resistance. Particle diameters used were 120 and 510 nm. The wear rate of the composites was reduced dramatically by adding a small amount (i.e. 0.5–4.0 wt.%) of either type of silica filler (120 and 510 nm in diameter, respectively.

Wetzel et al. [158] prepared an epoxy composite by adding Al_2O_3 and conventional $CaSiO_3$ micro-particles, and found that nano-Al_2O_3 and conventional

$CaSiO_3$ had synergistic effects on increasing mechanical properties and wear resistance. Recently, conductive polymer composites obtained by filling polymer matrices with various carbon blacks were reported [159–161]. The potentials of using carbon black filled composites as electrodes for electric double layer capacitors in various electronics application were reported. Particulate fillers of which carbon black is a notable example are widely used as reinforcing filler in polymer industries [14]. These fillers are added to polymers to achieve desirable and enhance the products service qualities. Commercially available carbon blacks are obtained from thermal cracking of natural gas and furnace black produce by incomplete combustion of oil feed stocks [17]. This carbon black is relatively expensive due to its dependence on dwindling supply of crude oil. It is therefore essential to develop viable alternative source of fillers from renewable resources such as agricultural wastes. Bamboo stem, oil palm empty fruit bunches and coconut shells are carbonaceous in nature and rich in organic materials. This biomass can be converted into carbon black thereby reducing unwanted, low-value agricultural residues and underutilized crop into useful, high-value materials.

This chapter presents the mechanical properties of the both wood apple and coconut shell particulate polymer composite reinforcing with three various filler such as raw, carbon black and activated carbon black, which is prepared from two natural waste fibers such as wood apple shell and coconut shell. Details of processing of these composites and the tests conducted on them have been described in the subsequent chapter. The results of various mechanical characterization tests are reported here. This includes evaluation of tensile strength, flexuralstrengthand micro-hardness has been studied and discussed. The interpretation of the results and the comparison among various composite samples are also presented.

4.2 RAW MATERIALS

Raw materials used in this experimental work are listed below:

i. Natural fiber
   - Wood apple shell
   - Coconut shell

ii. Epoxy resin (LY 556)

iii. Hardener (HY 951)

4.2.1 Biomass materials

The details of the wood apple and coconut shell were available in chapter 3 art 3.2

4.2.2 Epoxy resin and Hardener

Epoxy resins are relatively low molecular weight pre-polymers capable of being processed under a variety of conditions. Two important advantages of these over unsaturated polyester resins are: first, they can be partially cured and stored in that state, and second they exhibit low shrinkage during cure. However, the viscosity of conventional epoxy resins is higher and they are more expensive compared to polyester resins. It possesses outstanding mechanical and thermal properties such as high modulus and tensile strength, low creep, high glass transition temperature, high thermal stability, good moisture resistance, outstanding adhesion to a variety of substrates and good electrical properties. Approximately 45% of the total amount of epoxy resins produced is used in protective coatings while the remaining is used in structural applications such as laminates and composites, tooling, molding, casting, construction, adhesives, etc.Therefore it is widely used in composite industry.

The type of epoxy resin used in the present investigation is Araldite LY-556 which chemically belongs to epoxide family. Epoxy resins are characterized by the presence of a three-membered ring containing two carbons and an oxygen (epoxy group or epoxide or oxirane ring). Epoxy is the first liquid reaction product of bisphenol-A with excess of epichlorohydrin and this resin is known as Diglycidyl-Ether of Bisphenol-A (DGEBA). DGEBA is used extensively in industry due to its high fluidity, processing ease, and good physical properties of the cured of resin. Epoxy resin having density 1.2 g/cm^3, equivalent weight and viscosity is 182-192(gr/eq) and 11000-14000 MPa.s at 25°C.

The curing agent was clear epoxy hardener HY-951 [NN0 (2-amineethylethane-1, 2- diamin)] is also used with epoxy resin with an amine value of 260–284 (mg KOH gm^{-1}). Both the epoxy resign and curing agent were obtained from supplier Ciba-Geigy of India Ltd.

4.3 FABRICATION OF COMPOSITES

The various composites were prepared by hand layup technique with raw, carbon black and activated carbon particles as reinforcement in polymer composites using fourdifferentcompositions (5, 10, 15 and 20wt%) which are shown in Table 4.1.

Table 4.1 Weight percentage of filler and matrix

Composites				
Si No	**Wood apple shell particulates (WAS)**		**Coconut shell particulates (CS)**	
01	Raw	5 wt%+Epoxy	Raw	5 wt%+Epoxy
		10 wt%+Epoxy		10 wt%+Epoxy
		15 wt%+Epoxy		15 wt%+Epoxy
		20 wt%+Epoxy		20 wt%+Epoxy
02	400°C CB	5 wt%+Epoxy	400°C CB	5 wt%+Epoxy
		10 wt%+Epoxy		10 wt%+Epoxy
		15 wt%+Epoxy		15 wt%+Epoxy
		20 wt%+Epoxy		20 wt%+Epoxy
03	600°C CB	5 wt%+Epoxy	600°C CB	5 wt%+Epoxy
		10 wt%+Epoxy		10 wt%+Epoxy
		15 wt%+Epoxy		15 wt%+Epoxy
		20 wt%+Epoxy		20 wt%+Epoxy
04	800°C CB	5 wt%+Epoxy	800°C CB	5 wt%+Epoxy
		10 wt%+Epoxy		10 wt%+Epoxy
		15 wt%+Epoxy		15 wt%+Epoxy
		20 wt%+Epoxy		20 wt%+Epoxy
05	ACB (800°C)	5 wt%+Epoxy	ACB(800°C)	5 wt%+Epoxy
		10 wt%+Epoxy		10 wt%+Epoxy
		15 wt%+Epoxy		15 wt%+Epoxy
		20 wt%+Epoxy		20 wt%+Epoxy
*CB- Carbon Black *ACB- Activated Carbon Black				

The methods of preparation of specimen are as follows:

- ✓ A wooden mold of (150×60×5) mm^3 is used for manufacturing the composite. For quick and easy removal of the composite a mold release sheet is placed on the bottom of the wooden mold.

- ✓ The mold release spray is also applied to the inner surface of the mold wall to facilitate easy removal of the composite specimen.

- ✓ A calculated amount of epoxy resin and hardener (ratio of 10:1 by weight) was thoroughly mixed in a container for 2–5min at room temperature (25°C).

- ✓ The required amount of fillers (raw, carbon black and activated carbon) as the case may be was then added to the mixture.Before adding the fillers they were dried in an oven for 24h for removal of moisture if any presented with them.

- ✓ A mechanical stirrer was then used to make a homogenous mixture of epoxy, hardener and the filler. The mixture was then poured in to the prepared mold. A roller was used to roll over the mixture for even distribution and any air bubbles present in the mixture was also removed by this rolling.

- ✓ After 2 to 5min of rolling a mold release sheet was placed on the top of the mold. Before the reaction starts and mixture gets hardened a wooden board of required size was placed on the top of the mold and was loaded from the top with dead weights.

- ✓ The mold was kept with the load in that position for 24h. Due to application of load some polymer may squeeze out from the mold. Care was taken during pouring for this squeezing out of the mix to get a uniform thickness specimen.

- ✓ When the composite was hardened it was removed from the molds and cut with a diamond cutter according to ASTM standard D3039-76 for tensile specimen and D2344-84 for flexural specimen for further analysis and studies. For accuracy five specimens were prepared and tested for each analysis.

Figure 4.1 (a-d)) illustrates the mold used to construct the composite and photograph of the composite slab with specimens cut for mechanical tests.

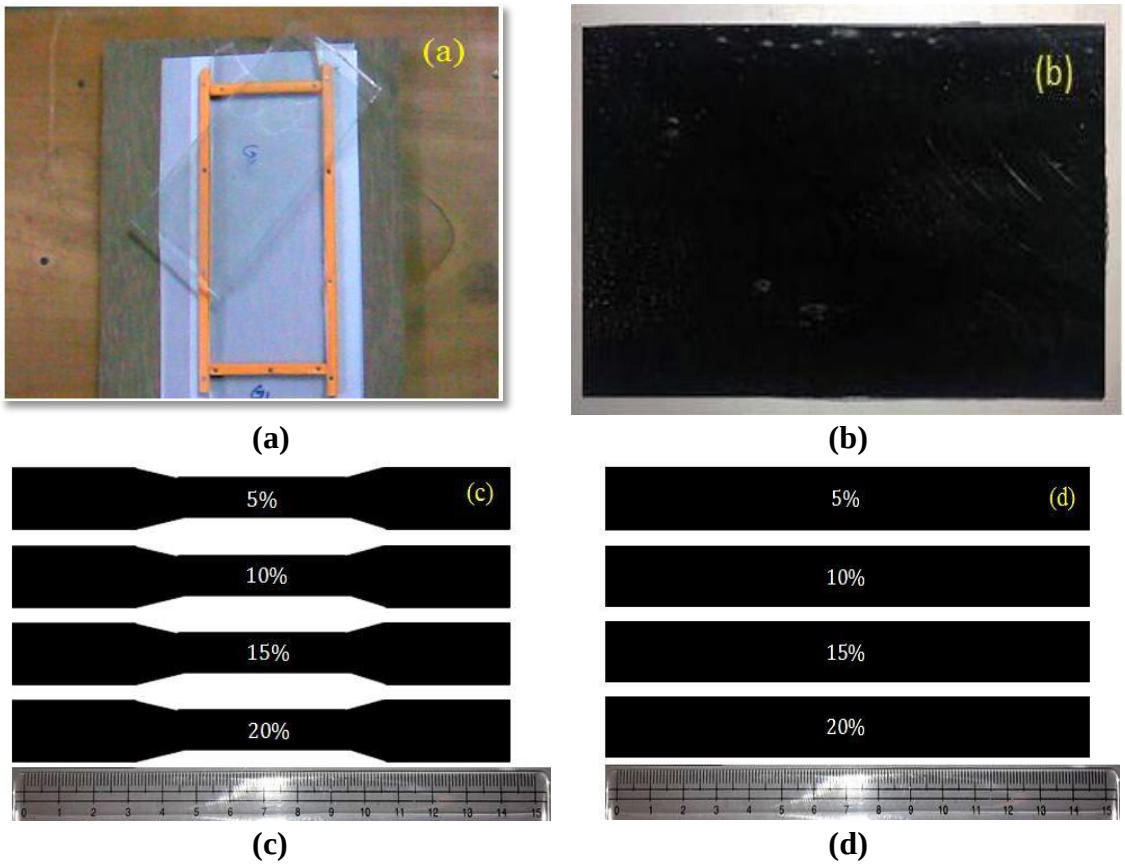

Figure 4.1(a) Mold used for composite preparation **(b)** Photograph of composite slab **(c)** Specimen for Tensile test and **(d)** Flexural Test

4.4 CHARACTERIZATION OF THE COMPOSITES

4.4.1 Density and Void fraction

The composite mainly consist of fiber, matrix and particulate filler. The theoretical density of the composite in terms of weight fraction can be calculated using modified form of Agarwal and Broutman equation [162] to the following form.

$$\rho_{ct} = \frac{1}{\left(W_f/\rho_f\right)+\left(W_m/\rho_m\right)+\left(W_p/\rho_p\right)} \tag{4.1}$$

Where 'W' and 'ρ' represent the weight fraction and density respectively. The suffix 'f', 'm', 'p'and 'ct' stand for the fiber, matrix, particulate filler material and theoretical density of composite respectively.

The actual density of the (ρ_{ca}) composite however can be determined experimentally by water immersion technique.

The volume fraction of voids (V_v) in the composite is calculated by the following equation 4.2:

$$V_v = \frac{\rho_{ct} - \rho_{ca}}{\rho_{ct}} \tag{4.2}$$

Where' ρ 'represent the density of the composite. The suffix '*ct*' and '*ca*' stand for the theoretical and actual density of the composite materials. The actual density of raw, carbon black and activated carbon of wood apple shell particulate found to be 1.068gm/cc, 0.72gm/cc, 0.56gm/cc, 0.32gm/cc and 0.14gm/cc respectively. Following the same principle the actual density of raw, carbon black and activated carbon of coconut shell particulate found to be 1.68gm/cc, 0.81gm/cc, 0.62gm/cc, 0.42gm/cc and 0.19gm/cc respectively. The theoretical and actual densities of all fabricated composite samples along with the corresponding volume fraction of void are presented in Table 4.2 and 4.3.

4.4.2 Tensile property characterization

The tension test is generally performed on flat specimens. The most commonly used specimen geometries are the dog-bone specimen (Figure 4.2) and straight-sided specimen with end tabs. During the test, a uniaxial load is applied through both the ends of the specimen. The test method as per ASTM D 3039-76 standard has been used and the length of the test specimen for the purpose used is 125 mm. The tensile test is performed in a universal testing machine UTM H10KS. The tests were performed with a cross head speed of 5mm/min. For each test composite of five samples were tested and average value was taken for analysis. Figure 4.3 (a, b) shows the machine used for the test and the sample in loading condition. The results obtained from the tests are presented in Table 4.4 and Table 4.5. Few tested samples are also shown in figure 4.3 (c).

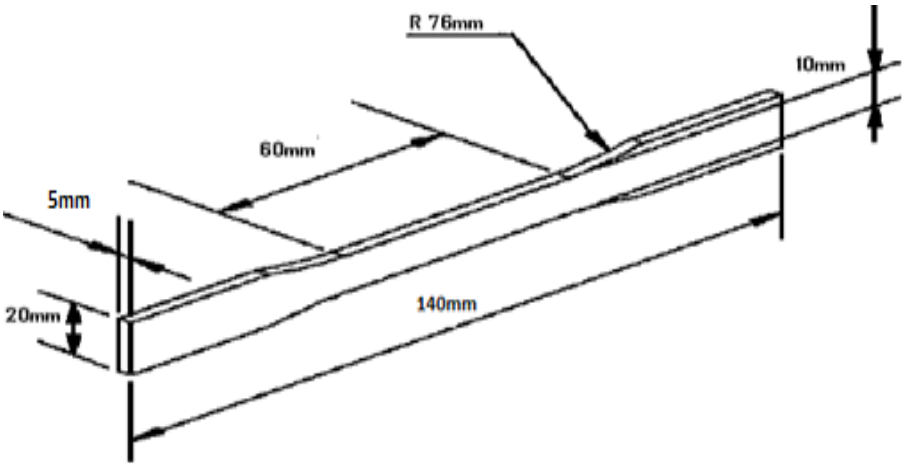

Figure 4.2 Tensile specimen

(a) **(b)** **(c)**

Figure 4.3 Photograph of **(a)** UTM H10KS testing machine **(b)** Sample in loading condition **(c)** Tested samples

4.4.3 Flexural property characterization

Flexural strength is the ability of the composite material to withstand bending forces applied perpendicular to its longitudinal axis. Flexural test was conducted on an UTM H10KS machine in accordance with ASTM D2344-84. Specimens of 150mm length and 20mm wide were cut and were loaded in three points bending with a recommended span to depth ratio of 16:1 as shown in figure 4.4(a). Figure 4.4(b) shows the sample in loading condition with the machine and 4.4(c) shows some of the

fractured samples for the test. The span of 70mm and a cross head speed used for the flexural tests (three point bending). The machine is designed to elongate the specimen at a constant rate, and to continuously and simultaneously measure the instantaneous applied load and the resulting elongations using an extensometer.

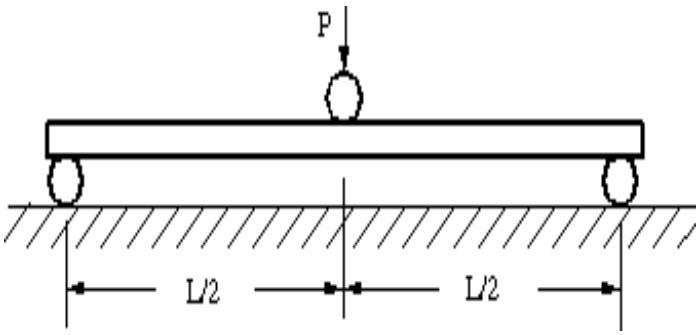

(a)

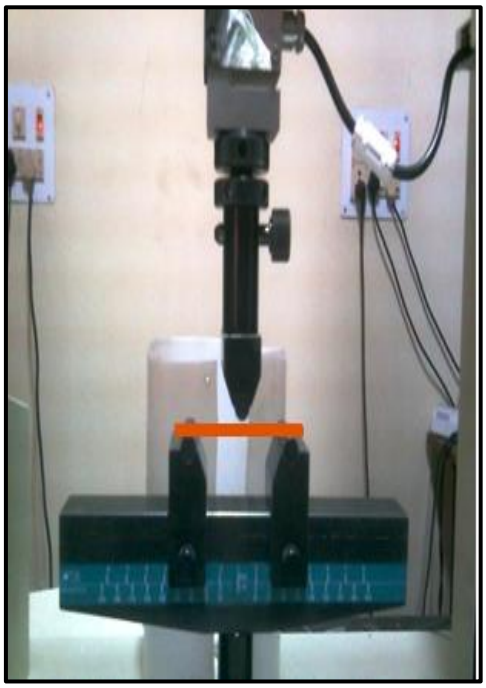

(b)

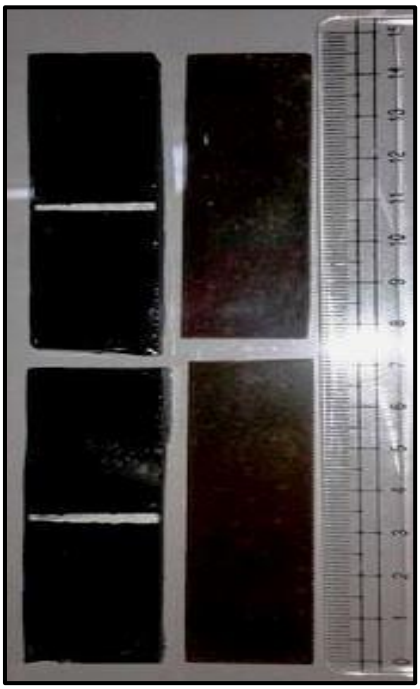

(c)

Figure 4.4 Photograph of **(a)** Flexural specimen **(b)** Sample in loading position **(c)** Fractured samples

The flexural stress in a three point bending test is found out by using the following equation.

$$\sigma_{max} = \frac{(3P_{max}L)}{(bh^2)} \tag{4.3}$$

Where 'P_{max}' indicates maximum load at failure (N), 'L'is the span length (mm), 'b' is the width of specimen (mm) and 'h' is the thickness of specimen (mm) respectively. The flexural modulus is calculated from the slope of the initial portion of the load-deflection curve which is found out by using the equation.

$$E = \frac{(mL^3)}{(4bh^3)} \tag{4.4}$$

Where 'm' is the initial slope of the load deflection curve for each composite, five specimens are tested and average result is obtained.

4.4.4 Micro Hardness test

The hardness property of the samples produced was determined using a Vickers hardness tester. A diamond indenter in the form of a right pyramid witha square base and an angle 136° between opposite faces is forcedin to the material under a load of 5N. The hardness tester is semi-automatic in which the specimen surface isbrought close to indenter, the preset load is applied forsome definite time and load is removed automatically. The loads are slowly applied to avoid error due to inertia effects. The time of load application and load duration can be controlled. Vickers hardness number is directly obtained from the test machine and also it can be calculated using the following equation are presented in Table 4.4 and Table 4.5.

$$H_v = 0.1891\frac{P}{d^2} \text{ and} \tag{4.5}$$

$$d = \left(\frac{H+V}{2}\right)$$

Where 'P' is the applied load (N), 'd' is the diagonal of square impression (mm), 'H' is the horizontal length (mm) and 'V'is the vertical length (mm).

4.5 RESULTS AND DISCUSSION

4.5.1 Effect of Filler Content on Density and Void Fraction of polymer composite

To define the properties of the composites one of the most important property is density. In composites, density generally depends upon the relative proportion of the matrix and the reinforcing materials [163]. Rule of mixture [164] is one such simplest and widely used model for determining the theoretical densities of polymer composites. The result of the void content in the composites for various types of filler varies with their weight fraction in the composite.

As shown in Table 4.2 that the percentage of voids in unfilled epoxy is higher than filled composites. Absence of filler is the main cause of voids in neat epoxy. When filled with filler up to 15wt% the void content decreases. Beyond 15wt% the void content slightly increases. Decrease in void content is due to the good packing characterization whereas increase in void content beyond 15wt% is due to the decrease in volume fraction of matrix material. It is also observed that density of the raw wood apple shell particulate composites decreases with increasing the filler content as compared to neat polymer. This is due to the lower density of filler material with different weight fraction. The composite with 20wt% of filler shows maximum void content. This may be happened due to improper mixing of highest weight fraction of filler with the matrix. It is also observed that the density of the carbon black particulate polymer composites for all weight fraction of particulate are less as compared to raw particulate polymer composite. This is the effect of the carbonization which lowers down the density of the taw shell particulate composite. This has happened because of removal of volatile substances through carbonization process.

Correspondingly in activated wood apple shell composite the density is extremely lower as compared to raw and carbon black filler composites. It is because of due to activating agent most of the volatile substance is removed at 800°C activation temp and create some porous on the surface of the particles.

The void content is the cause for the difference between the values of actual density and theoretically calculated one. The voids significantly affect some of the mechanical properties and even the performance of composites at the place of use. The knowledge of void content is very much essential for estimation of the quality of the composites. It is desirable that a good composite should have fewer voids. However, presence of voids is unavoidable while making composite particularly through hand-lay-up route.

Table 4.3 shows slightly difference result for coconut shell particulate polymer composite. As the filler loading increases density of the raw coconut shell particulate composite increases compared to neat polymer. This is because of the density of the raw coconut filler is higher i.e. 1.68gm/cc.

However after carbonization the composite density found to decrease in composition to raw polymer composite. This is because after carbonization the density of the coconut shell particulate decreases. Still lower density is achieved for activated carbon black filled composite. This is the result of the activation process that brings down the density of the activating particles in composition to raw and carbon black particulates.

High void content usually mean lower fatigue resistance, greater susceptibility to water penetration and weathering [164]. In the present case the volume fraction of void are reasonable small (1.5%) and it can be attributed that the fabricated composites are good enough to be used for further testing.

4.5.2 Effect of Filler Content on Tensile properties of Wood apple shell particulate composite

Effect of various filler content such as raw, carbon black and activated carbon black particles prepared from wood apple shell on tensile strength of the composites is depicted in figure 4.5. It is observed from the plot that the tensile strength of the composites found to increases with increase in the filler content. However with filler content of 15wt% (raw) the tensile strength found to be 45.67MPa compared to neat epoxy strength of 20.13MPa. Thereafter with higher filler content it decreases. A net gain of 55.922% increases in the tensile strength is achieved with filler content.

The tensile strength of the composites filed with carbon black prepared from wood apple shell particles at three carbonization temperature (400°C, 600°C and 800°C) were also carried out. It is found that carbon black particle enhances the strength of the neat polymer composite. Wood apple shell carbon black composite reinforced with carbon black particulate prepared at 800°C with 10wt% filler gives optimum strength of 58.91MPa as recorded from the experiment shown in Table 4.4

Addition of activated carbon black particulates with neat epoxy shows highest tensile strength compared to other non-activated filler composites. 10wt% activated carbon black composite gives superior strength as compared to other non-activated composite. This is almost about 200.64% more strength compared to strength of neat epoxy. This might have happened removal of volatile substances, formation of porous structures and increase in carbon content which forms some ceramic carbide (SiC, ZrC etc.) at the time of carbonization process followed by activation. Formation of these hard ceramic particles increases the strength of the resulted composites. Beyond 10wt% of filler content decrease in strength might be due to poor filler matrix interaction.

Figure 4.6 shows the plot of tensile modulus of wood apple shell particulate composite. It is clearly observed that the tensile modulus of the raw, carbon black and activated carbon black of wood apple shell filled epoxy composite follow the similar trend as observed in the tensile strength. Among all the composites, the highest modulus of 2.631GPa is observed for composites filled with 10wt% activated carbon black particulates. The modulus of the material increases as the carbonization temperature increases and it is found to be maximum for activated carbon composites.

Similar observation is also reported by Imanah and Okieimen [165] while they prepared cocoa pod powder and carbonized cocoa pod powder and used as filler in compounding natural rubber. From their results it is clearly observed that the strength of the carbonized cocoa pod powder increases as filler loading increases. Joseph et al. [166] studied the influence of interfacial adhesion on the mechanical and fractured behaviour of short sisal fiber reinforced polymer composites of several thermoset resin matrices with respect to fiber length and fiber loading. It is clearly observed from their results that the strength of the composite increases up to certain limit and then decreases with further increase in fiber loading. At high filler loading, it is more

difficult for the polymer to penetrate into the smaller gaps between the fillers and matrix, leading to poor wetting, and hence, a reduction in the stress transfer efficiency across the filler-resin interface.

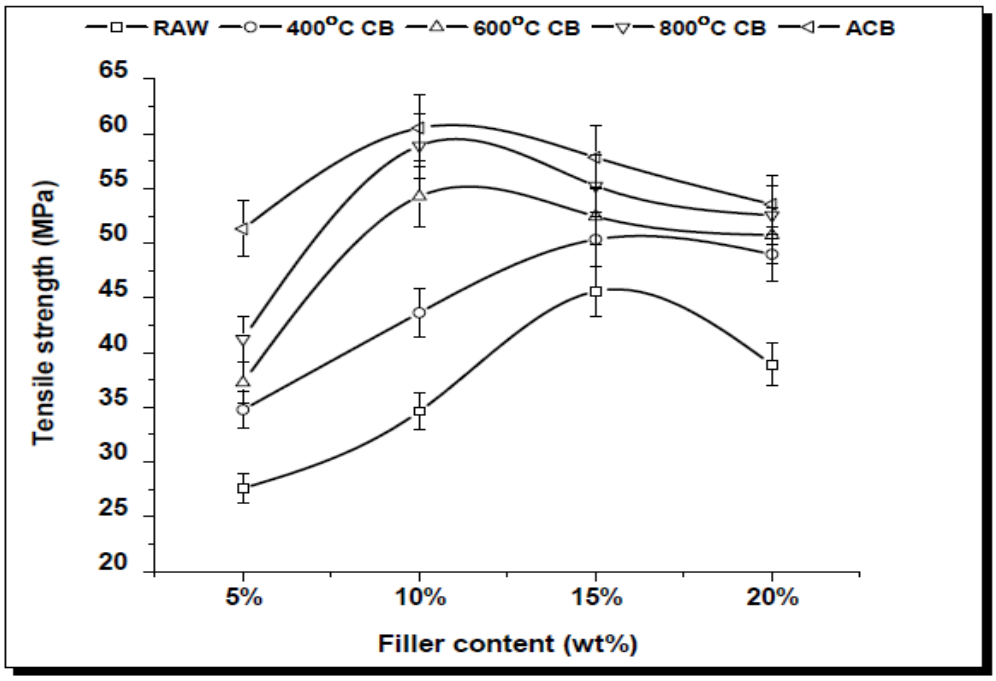

Figure 4.5 Effect of filler content on tensile strength of wood apple shell particulate polymer composite

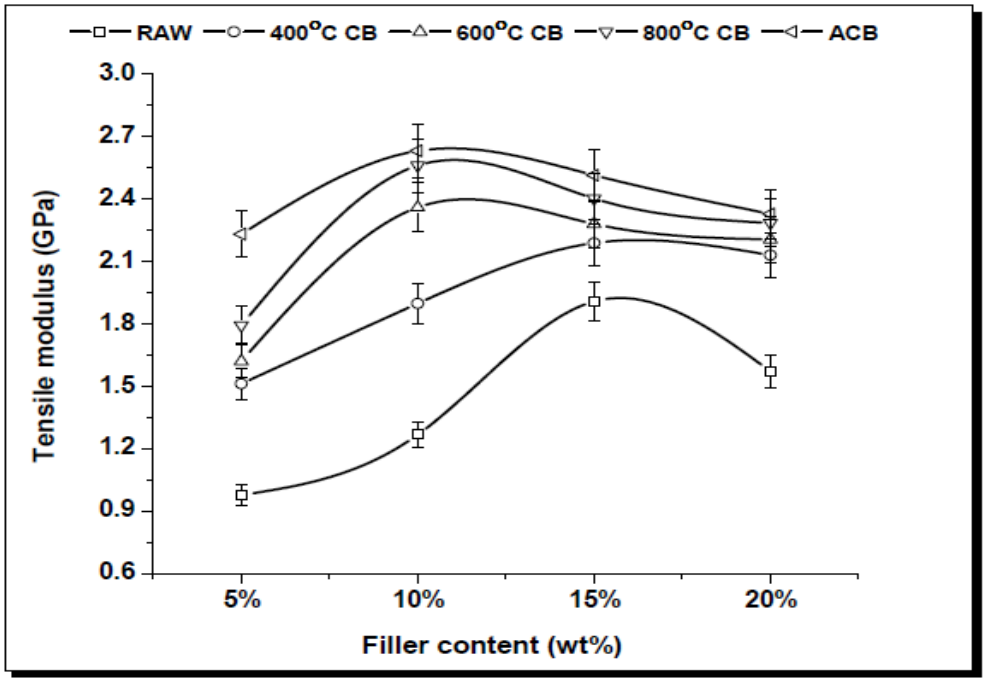

Figure 4.6 Effect of filler content on tensile modulus of wood apple shell particulate polymer composite

4.5.3 Effect of Filler Content on Tensile properties of Coconut shell particulate composite

The influence of filler content on tensile strength and modulus of coconut shell particulate composites are shown in figures 4.7 and 4.8, respectively. Form the figure 4.7 and 4.8 it is clearly observed that tensile strength and modulus of the coconut shell particulate composite increases with increase in filler content. From the result, it is observed that the tensile strength of raw coconut shell particulate composite shows highest strength (43.23MPa) at 20wt%. But when raw coconut shell particulate were carbonized at different carbonization temperature (400°C, 600°C and 800°C) it is found that tensile strength increases for all carbonization temperature with less filler content (i.e) with 15wt%. However with carbonization temperature 800°C highest tensile strength was observed with 10wt% of filler content. The trend achieved for tensile strength and modulus is raw<400°C<600°C<800°C. When the tensile strength and modulus is tested with activated carbon black filled composites it is found that both the values are higher and with only 10wt% of filler content. The possible regionbehind this might be the stiffness of the filler. The filler in this has higher stiffness than matrix material.

As filler content increases, the possibility of filler-matrix interaction also increased which leads to a favorable condition of stresstransfer from the matrix to the filler. This eventually increases the stiffness of the coconut shell particulate composite [167].

4.5.4 Effect of Filler Content on Flexural properties of Wood apple shell particulate composite

Figure 4.9 shows the flexural strength of wood apple shell particulate composite for raw, carbon black (400°C,600°C and 800°C) and activated carbon black.

Flexural strength indicates ability of material to withstand bending forces applied perpendicularly to its longitudinal axis. In the present investigation a maximum flexural strength of 93.745MPa was observed for 5wt% activated carbon black wood apple shell composite, which shows an improvement of nearly 120.11% over the neat epoxy (42.59MPa). It is also seen that carbon black which is prepared at various

carbonization temperatures (400°C, 600°C and 800°C) used as reinforcement significantly improves the flexural strength of the polymer composite than raw wood apple shell particulate composite. It is also found that with increase in the carbonization temperature the strength increases, on the other hand the weight fraction of filler also decreases (from 15wt% to 10wt%). Highest strength was achieved with activated carbon black with still lesser filler loading (i.e) 5wt%. This is the result of the increase in carbon content in the filler material [168].

Similar trend were observed with flexural modulus of the wood apple shell particulate filled polymer composite which is shown in figure 4.10. Flexural modulus of 2.844GPa was recorded for the composite filled with 15wt% activated carbon black particulate than other non-activated polymer composites.

Increasing of modulus has significance to the stiffness properties of activated carbon black composites. The relative stiffness of a material [169] is indicated by its modulus.Incorporation of activated carbon black particles improved the stiffness of the polymer matrix, since the flexural modulus of the composites increased as filler loading was increased

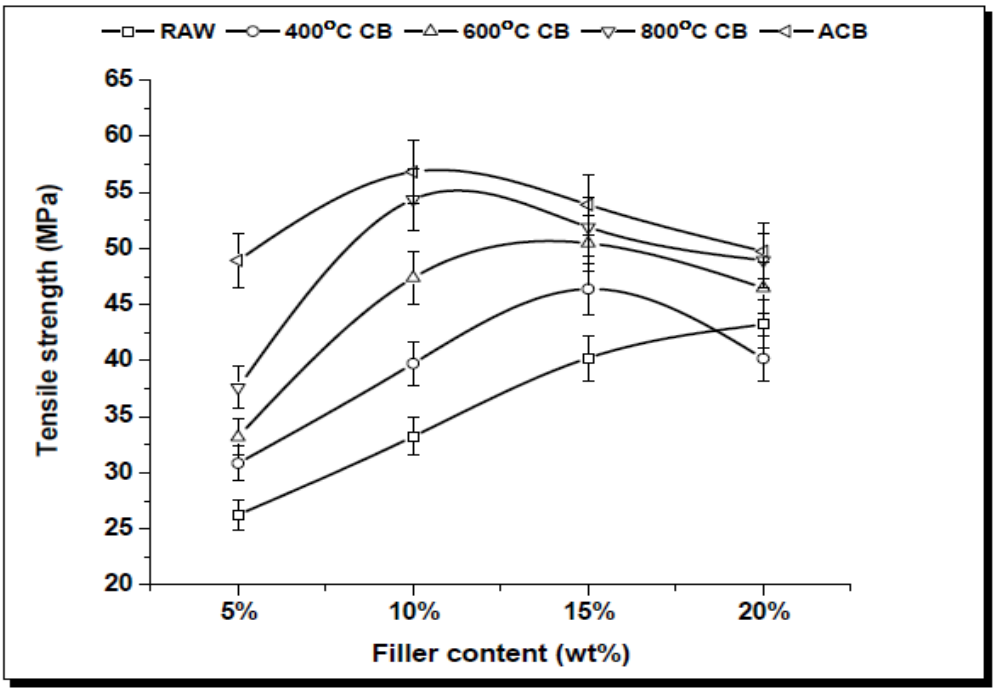

Figure 4.7 Effect of filler content on tensile strength of coconut shell particulate polymer composite

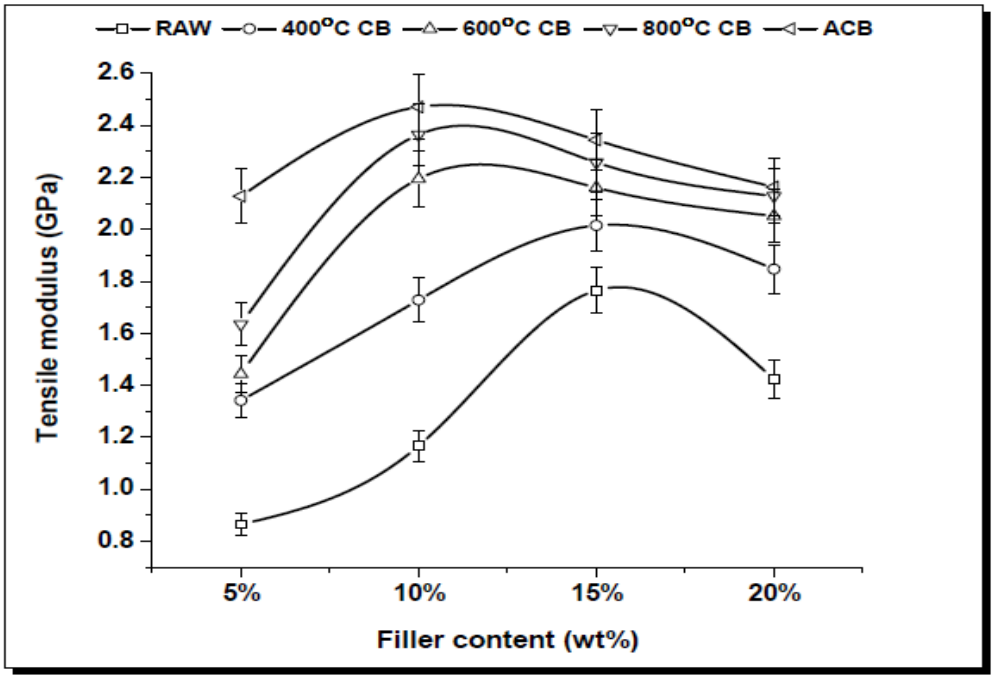

Figure 4.8 Effect of filler content on tensile modulus of coconut shell particulate polymer composite

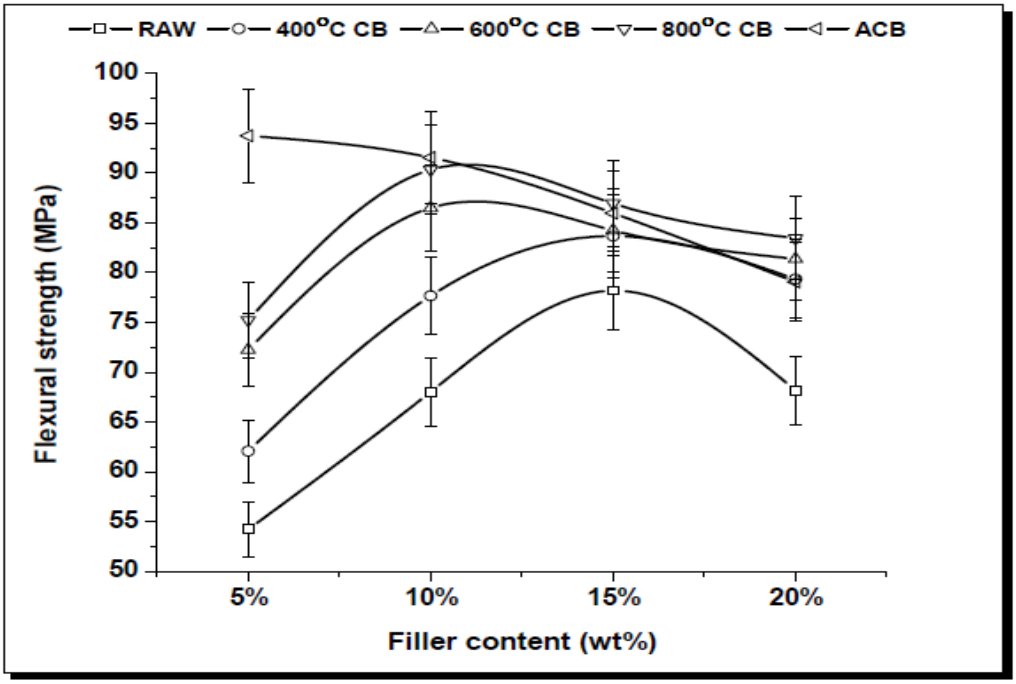

Figure 4.9 Effect of filler content on flexural strength of wood apple shell particulate polymer composite

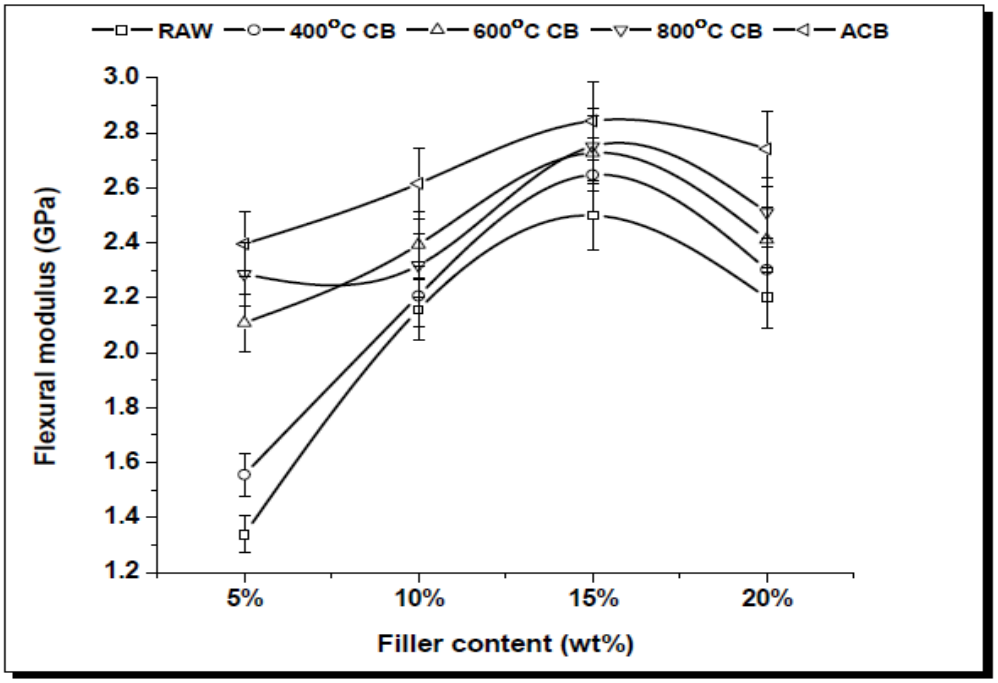

Figure 4.10 Effect of filler content on flexural modulus of wood apple shell particulate polymer composite

4.5.5 Effect of Filler Content on Flexural properties of Coconut shell particulate composite

The effect of weight fraction of filler on flexural strength and modulus of coconut shell particulate polymer composite reinforced with raw, carbon black and activated carbon black filler are shown in figure 4.11 and 4.12 respectively. From figure 4.11 It is observed that the flexural strength of all particulate reinforced composites (i.e. raw, carbon black and activated carbon black) considered in the present study increases with weight fraction of filler in the order of raw, carbon black (i.e. 400°C, 600°C and 800°C) and activated carbon black.

The maximum strength is observed for the composite prepared with the 10wt% reinforced activated carbon particulate composite. The strength of the composites increases as the filler percentage increases up to 10wt% beyond that the strength of composite decreases. This is due to lighter density of activated carbon black particulate, which leads to improper mixing of resin and particulate during fabrication process.

Also because of this improper mixing the distribution of particulates are not uniform throughout the matrix. This in turn reduces the stress transfer from matrix to filler and sometimes leads to poor bonding particulate and matrix. Same type of observation was also reported by Ismail et al. [170] and Yao and Li [171] in their investigation.

Generally the addition of filler content increases the modulus in all composites. The flexural modulus of coconut shell particulate composites at different filler loading is shown figure 4.12. As the coconut shell particulates (raw, carbon black and activated carbon black) content increases in the neat epoxy, the modulus of the composite increases. The flexural modulus shows steady increase with the content of filler materials up to 15wt% in all the composites. The activated carbon black composite of 15wt% shows maximum modulus. At higher filler loading (20wt %) the strength shows decreasing trend. As pointed out by Nam-Jeong Lee and Jyongsik Jang [41] this type of behavior might have happened due to crack formation of crack or poor filler-matrix adhesion.

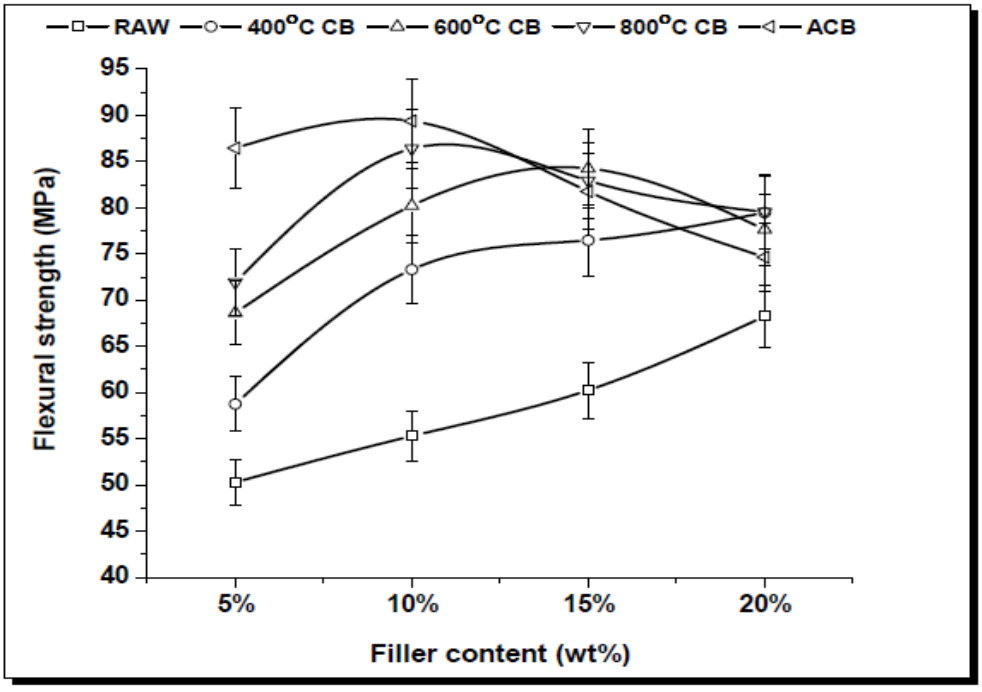

Figure 4.11 Effect of filler content on flexural strength of coconut shell particulate polymer composite

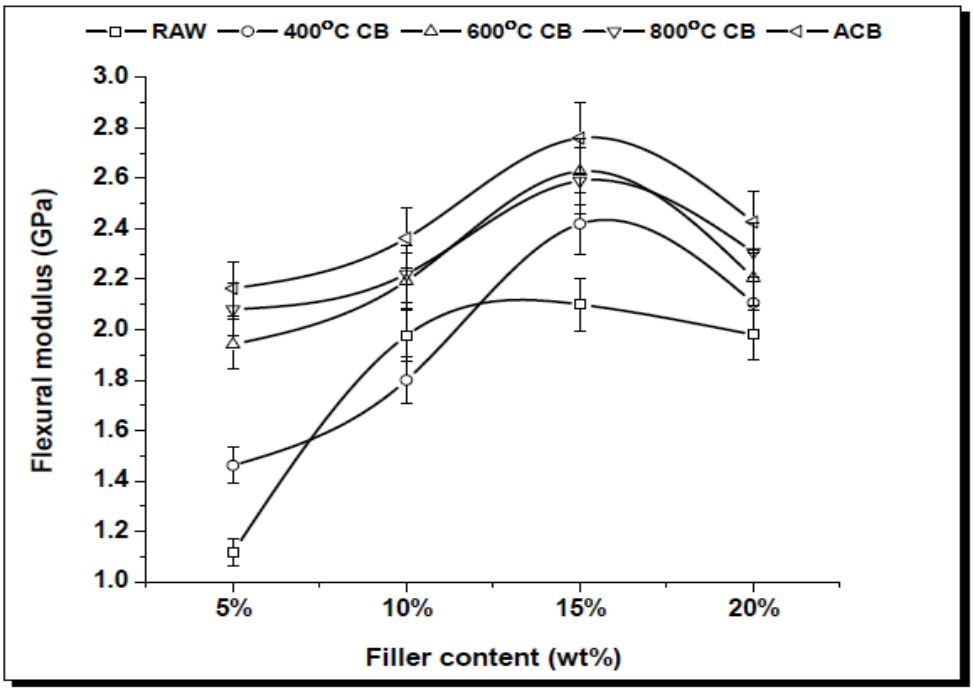

Figure 4.12 Effect of filler content on flexural modulus of coconut shell particulate polymer composite

4.5.6 Comparison between Wood apple shell and Coconut shell particulate composite

To compare the strength and modulus of carbonization material obtained from two natural fillers (wood apple and coconut) filled composite the obtained results have been plotted a comparison graph are drawn for the optimum results in raw, carbonized (800°C) and activated.

From both the figures 4.13 and 4.14 it is clear that the strength and modulus of neat epoxy increases with addition of filler material. It is observed from the plot that both tensile strength and modulus of the composites filled with wood apple shell particulate are higher whether it is raw, carbonized or activated carbon in comparison to coconut shell particles with 10wt% of filler reinforcement.

An increase in 66.74% of strength in tensile and 77.87% in modulus with epoxy and 6.09% in tensile strength and 6.081% in tensile modulus is achieved with in comparison to activated coconut shell particulate composite in wood apple shell composite.

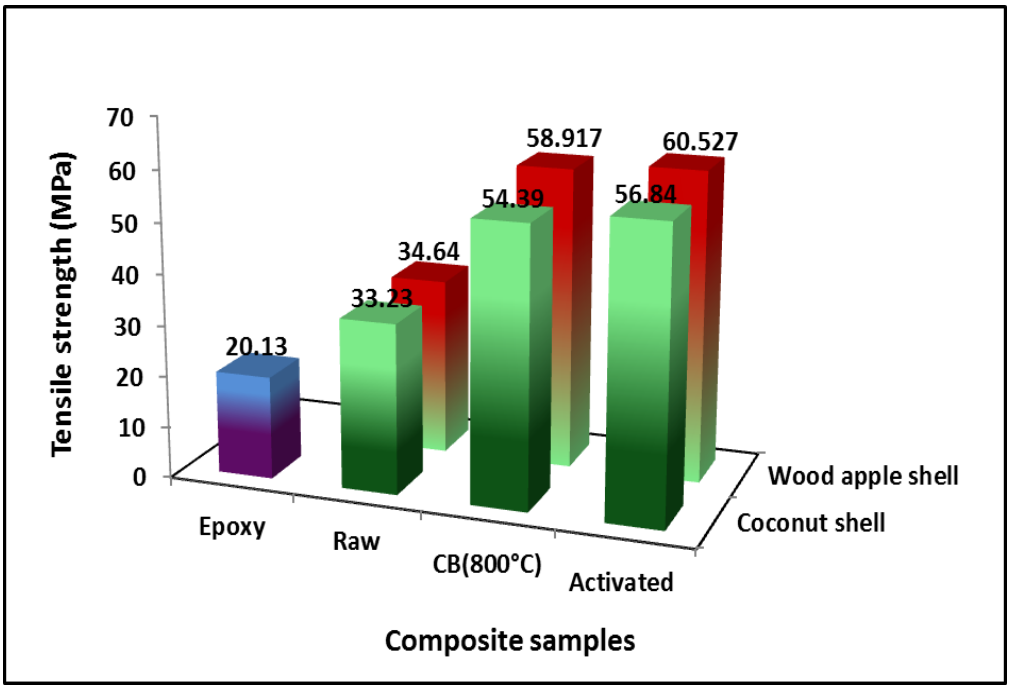

Figure 4.13 Effect of 10wt% filler content on tensile strength of polymer composites

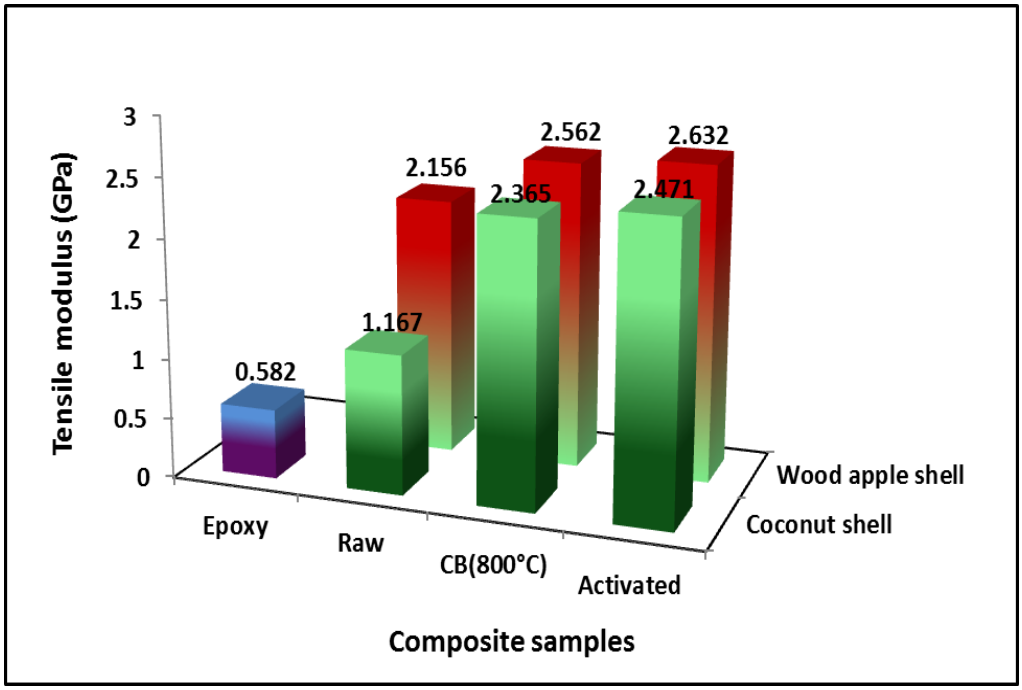

Figure 4.14 Effect of 10wt% filler content on tensile modulus of polymer composite

Comparative plots are also drawn for the 5wt% and 15wt% reinforced raw, carbonized (800°C) and activated carbon for both fillers are shown in figure 4.15 and 4.16. It is observed that 50.74% increase in flexural strength and 73.54% in flexural modulus is achieved for activated coconut shell particulate composite compared to neat

epoxy. When we compared the strength and modulus with wood apple shell it is found that an increase of 54.567% in flexural strength and 74.26% in flexural modulus is achieved for activated filled composite.

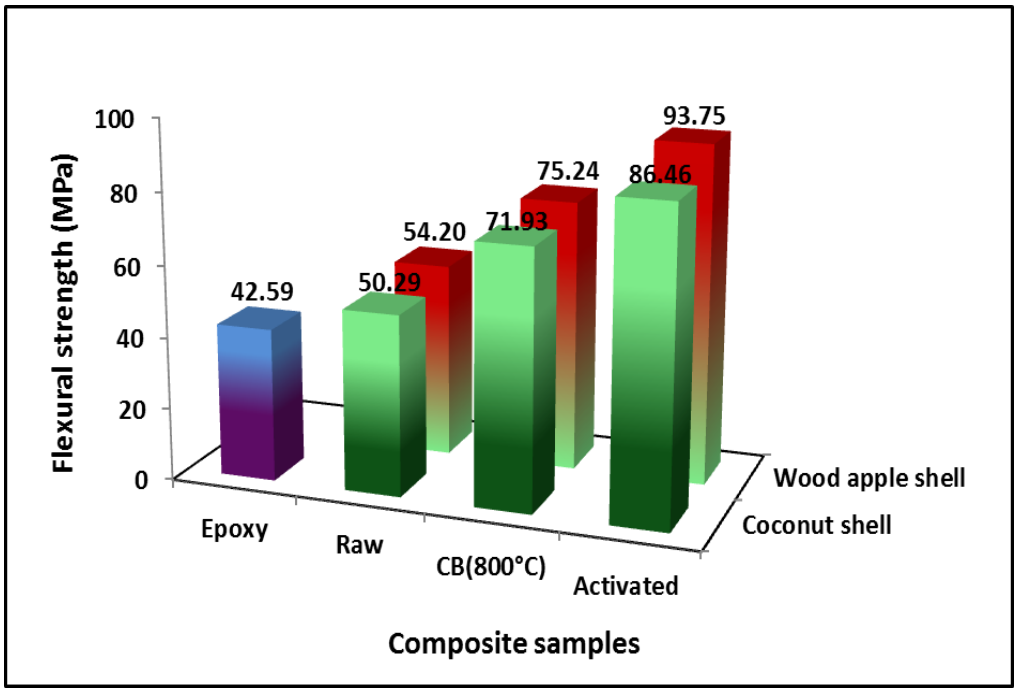

Figure 4.15 Effect of 5wt% filler content on flexural strength of polymer composite

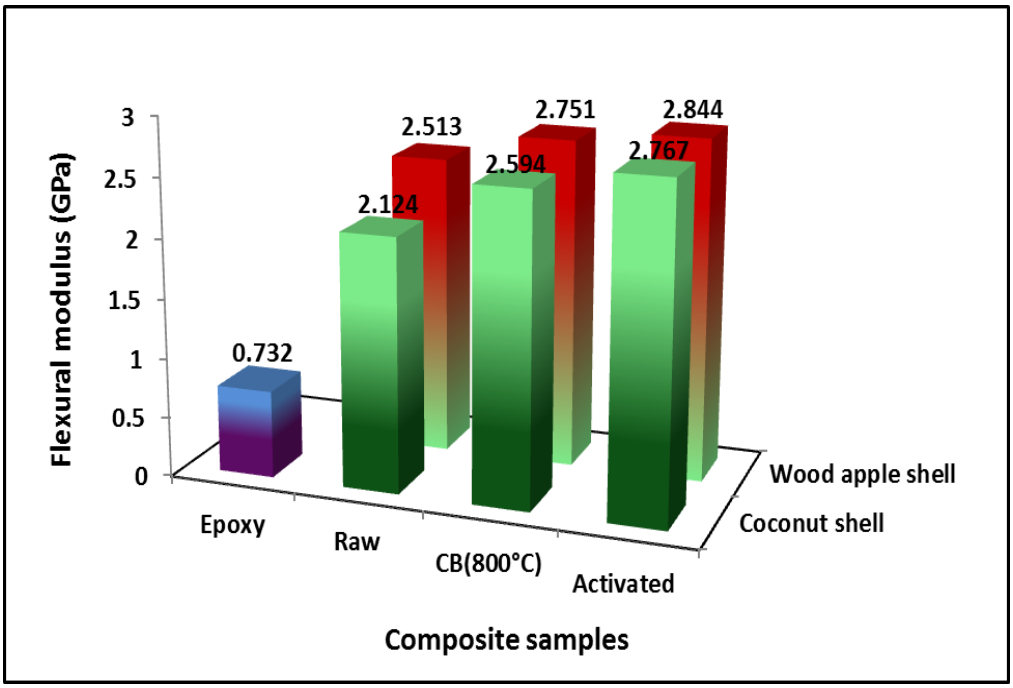

Figure 4.16 Effect of 15wt% filler content on flexural modulus of polymer composite

Hence it can be concluded here that superior mechanical properties can be obtained with carbonized and activated carbon particulate composite. Among the two lignocellulosic materials, under study wood apple shell particulate composite gives superior strength and modulus than coconut shell particulate composite.

4.5.7 Effect of filler content on Micro Hardness of Wood apple shell and Coconut shell particulate composite

The effect of filler content on the micro-hardness of wood apple and coconut particulate reinforced composites are shown in Table 4.5 and 4.6. From the results it is clearly observed that the hardness of the composites increases as the filler percentage increases and also with increase in carbonization temperature. Higher hardness values are observed for the activated carbon reinforced composites for both the lignocellulosic fillers.

4.5.8 Morphological Studies of Tensile tested specimens

4.5.8.1 Morphological studies of Tensile tested wood apple shell specimens

SEM micrographs of the fracture surfaces of the raw, carbonized and activated filler reinforced composites of wood apple and coconut for tensile strength specimen are shown in figure 4.17(a-h). Figure 4.17(a) shows the SEM image of neat epoxy. It is seen that due to application of tensile load direct facture occurs without any cracks formation on the surface of the specimen. Some voids are seen on the surface but no cracks are being developed due to these voids.

Figure 4.17(b) shows the micrograph o the 15wt% of raw wood apple shell composite. From the figure it is clear that due to tensile load the matrix along with particles are stretched and overlapped with other surface.20wt% raw filler composite is shown in figure 4.17(c) it is observed that due to higher filler content micro voids are formed. Probably theses micro voids decrease the strength of the composites at higher filler loading. This validates the lower value tensile strength obtained with 20wt% filler composites. When composite with 10wt% carbon black (800°C) reinforced wood apple shell composites (figure 4.17(d)) it is observed that due to tensile load compression of particulates fillers took place in the lateral direction. This compression took place due

to porous structure formed in the fillers which is responsible for increase in the strength.

From the figure 4.17(e) (activated carbon reinforced composite) it is clearly observed there is no evidence of crack formation or chipping out of particulates is available on the surface of the specimen under test. However evidence of ceramic particles on the surface indicates the effect of strain caused by the applied stress. Though the ceramic particles are coming out to the surface still they are found in fact within the matrix as a result the increases in strength is achieved.

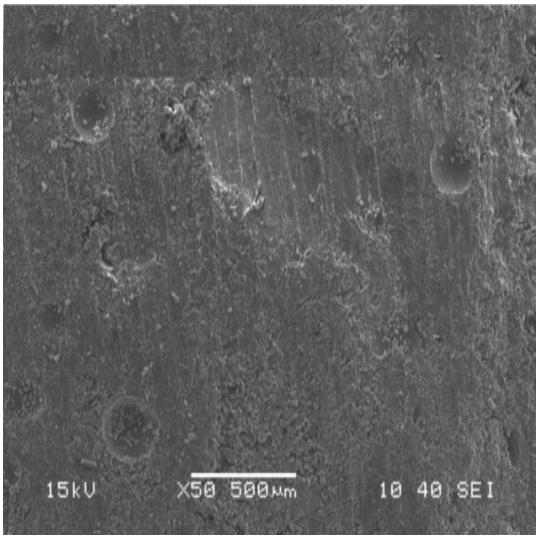

(a)

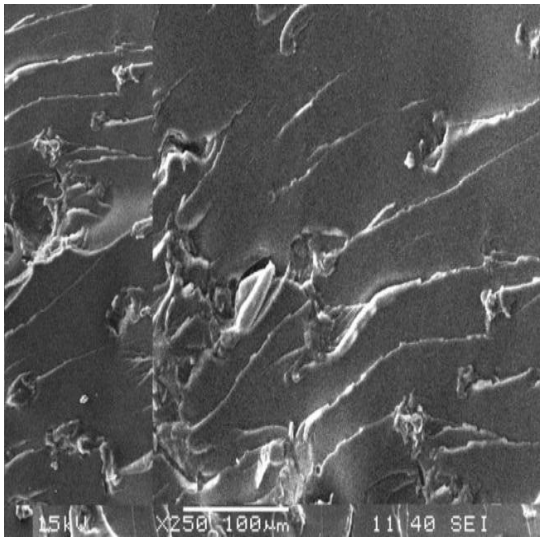

(b)

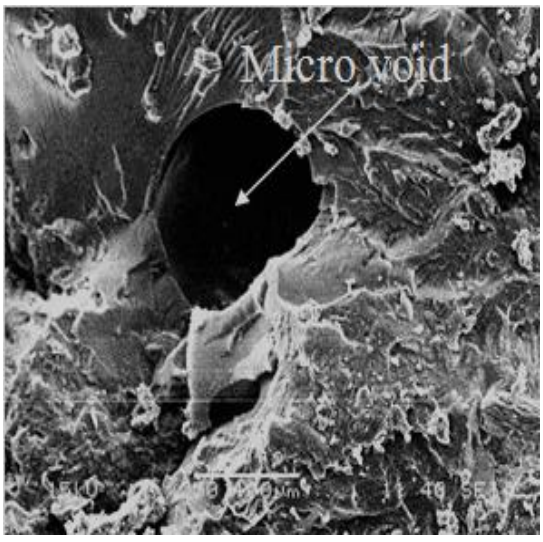

(c)

(d)

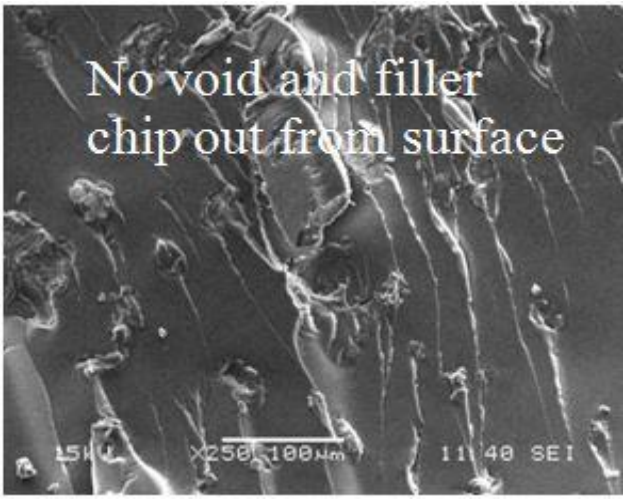

(e)

Figure 4.17 (a-e) SEM micrographs of wood apple shell tensile tested composite

(a) Epoxy composite

(b) 15wt% raw WAS composite

(c) 20wt% raw WAS composite

(d) 10wt% carbon black (800°C) WAS composite

(e) 10wt% activated WAS composite

4.5.8.2 Morphological studies of Tensile tested coconut shell specimens

The SEM image of 20wt% raw coconut shell filler composites is shown in figure 4.17(a). There is no sigh of voids on the surface still slipping of surface took place. This might have occurred due to formation of internal cracks which are not visible on the surface. Figure 4.17(b) which shows the morphology of the specimen for 10wt% carbon black (800°C) reinforced composite derived from coconut shell. Even after application of tensile load the surface found to be smooth. There are no cracks or void found on the surface. Some carbon particles that chipped out are available on the surface. This is the reason the tensile strength for the specimen is found to be higher than raw composites. Similar type of observations is also made with activated composite with higher surface texture (figure 4.17(c)). Probably the distribution, interfacial bonding is better with activated carbon black particles. Hence more strength is achieved with this.

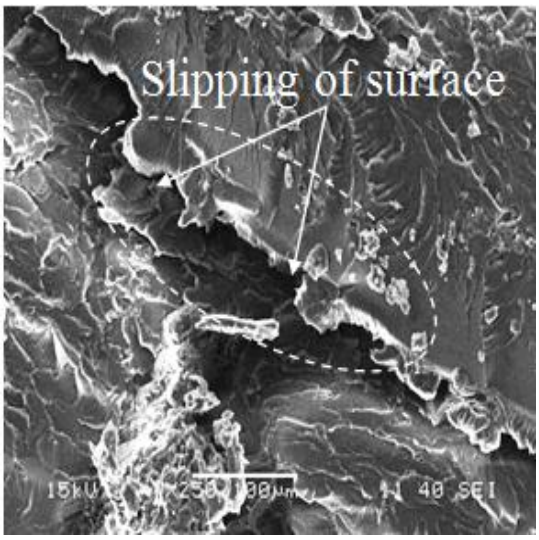

(a)

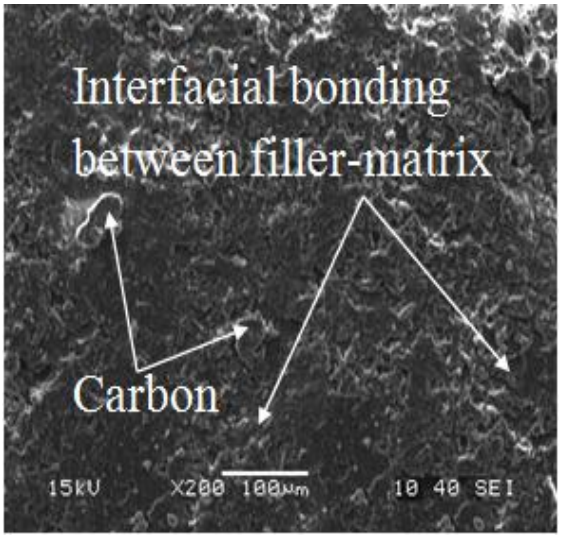

(b)

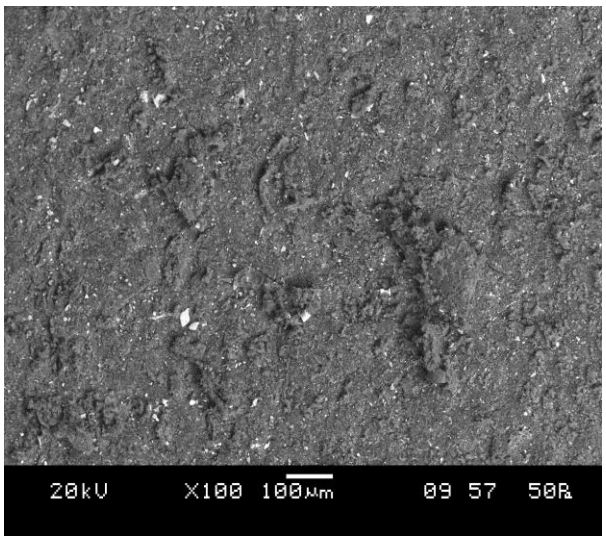

(c)

Figure 4.18 (a-c) SEM micrographs of coconut shell tensile tested composite

(a) 20wt% raw coconut shell composite

(**b)** 10wt% carbon black (800°C) coconut shell composite

(c) 10wt% activated coconut shell composite

4.6 CONCLUSION

1. Effect of carbonization and activation on tensile and flexural properties of wood apple and coconut shell reinforced epoxy composites was studied with different filler loading. It is observed from the results that strength and hardness of the polymer composite was greatly influenced by carbonization and activation.

2. Due to activation of the particulates the strength of the composite is increased and also reduces the void content in the composites.

3. Comparing the results of flexural strength and tensile strength of all particulate composites (raw carbon black and activated carbon black) of wood apple and coconut shell, it is found that wood apple shell particulates composite gives highest strength, modulus and hardness compared with other activated and non-activated particulates composite.

4. The morphological study confirms that the strength of the composites increases due to incorporation of activation particulates.

Table 4.2 Actual and theoretical densities of wood apple shell particulate composites

Composite samples	Filler (wt%)	Theoretical Density (gm/cc)	Actual Density (gm/cc)	Void Fraction (%)
Epoxy	0	1.20	1.18	1.666
Raw	5	1.192	1.179	1.067
	10	1.185	1.175	0.83
	15	1.178	1.172	0.48
	20	1.171	1.162	0.773
400°C CB	5	1.161	1.156	0.455
	10	1.125	1.121	0.355
	15	1.09	1.087	0.293
	20	1.058	1.05	0.833
600°C CB	5	1.135	1.128	0.558
	10	1.076	1.072	0.457
	15	1.024	1.021	0.33
	20	0.976	0.97	0.615
800°C CB	5	1.054	1.048	0.6
	10	0.941	0.935	0.559
	15	0.849	0.845	0.439
	20	0.774	0.769	0.659
ACB (800°C)	5	0.87	0.864	0.649
	10	0.682	0.679	0.561
	15	0.561	0.559	0.495
	20	0.477	0.474	0.662

Table 4.3 Actual and theoretical densities of coconut shell particulate composites

Composite samples	Filler (wt%)	Theoretical Density (gm/cc)	Actual Density (gm/cc)	Void Fraction (%)
Epoxy	0	1.2	1.18	1.666
Raw	5	1.217	1.20	1.067
	10	1.235	1.229	0.494
	15	1.253	1.249	0.365
	20	1.272	1.269	0.282
400°C CB	5	1.171	1.164	0.648
	10	1.144	1.138	0.515
	15	1.119	1.114	0.40
	20	1.094	1.091	0.311
600°C CB	5	1.146	1.139	0.611
	10	1.097	1.091	0.537
	15	1.052	1.047	0.493
	20	1.01	1.004	0.588
800°C CB	5	1.098	1.091	0.559
	10	1.012	1.007	0.479
	15	0.938	0.933	0.584
	20	0.875	0.869	0.68
ACB(800°C)	5	0.948	0.943	0.478
	10	0.783	0.779	0.458
	15	0.667	0.664	0.509
	20	0.581	0.577	0.641

Table 4.4 Mechanical properties of wood apple shell particulate composites

Composite samples	Filler (wt%)	Tensile Strength (MPa)	Flexural Strength (MPa)	Tensile Modulus (GPa)	Flexural Modulus (GPa)	Hardness (Hv)
Epoxy	0	20.13	42.59	0.58	0.73	19.42
Raw	5	27.6	54.2	0.97	1.33	23.58
	10	34.64	68.02	1.26	2.15	25.3
	15	45.6	78.19	1.90	2.50	24.55
	20	38.88	68.16	1.57	2.20	23.6
400°C CB	5	34.77	62.06	1.51	1.55	23.92
	10	43.64	77.67	1.89	2.20	25.9
	15	50.34	83.67	2.18	2.64	26.5
	20	48.98	79.34	2.12	2.30	25.3
600°C CB	5	37.26	72.24	1.62	2.10	24.26
	10	54.27	86.49	2.35	2.39	26.1
	15	52.45	84.24	2.28	2.72	26.9
	20	50.73	81.37	2.2	2.41	27.3
800°C CB	5	41.23	75.23	1.79	2.28	24.85
	10	58.91	90.34	2.56	2.31	26.5
	15	55.25	86.95	2.40	2.75	27.2
	20	55.56	83.45	2.28	2.51	27.5
ACB (800°C)	5	51.31	93.74	2.23	2.39	25.96
	10	60.52	91.56	2.63	2.61	27.21
	15	57.84	85.98	2.51	2.84	27.98
	20	53.54	79.06	2.32	2.74	28.93

Table 4.5 Mechanical properties of coconut shell particulate composites

Composite samples	Filler (wt%)	Tensile Strength (MPa)	Flexural Strength (MPa)	Tensile Modulus (GPa)	Flexural Modulus (GPa)	Hardness (Hv)
Epoxy	0	20.13	42.59	0.58	0.73	19.42
Raw	5	26.25	50.29	0.86	1.16	20.75
	10	33.23	55.28	1.16	1.97	23.19
	15	40.23	60.25	1.76	2.10	22.18
	20	43.23	68.25	1.42	1.98	21.64
400°C CB	5	30.84	58.75	1.34	1.46	24.14
	10	39.74	73.31	1.72	1.79	24.86
	15	46.39	76.46	2.01	2.41	23.84
	20	40.18	79.48	1.84	2.10	21.47
600°C CB	5	33.19	68.62	1.44	1.94	21.98
	10	47.39	80.23	2.19	2.19	25.19
	15	50.48	84.26	2.16	2.62	24.89
	20	46.49	77.64	2.05	2.20	23.39
800°C CB	5	37.59	71.93	1.63	2.08	22.35
	10	54.39	86.39	2.36	2.22	26.13
	15	51.92	82.94	2.25	2.62	25.92
	20	48.95	79.53	2.12	2.30	24.13
ACB (800°C)	5	48.94	86.46	2.12	2.16	23.53
	10	56.84	89.39	2.47	2.36	26.82
	15	53.91	81.76	2.34	2.64	27.13
	20	49.75	74.64	2.16	2.42	27.48

Chapter 5

Solid particle Erosion studies of particulate composite (raw)

5.1 INTRODUCTION

Tribology deals with relative motion of surfaces which comprises friction, wear of materials, scratching and rubbing. Further a sophistic definition portrays tribology as a science and technology of surfaces, in contact and relative motion, as well as support of activities that should diminishes the costs resulting from friction and wear [173,174]. Economic consequences of materials' wear are clearly described in the Rabinowicz book 4 – quoting a report to the British Government of 1966 when the word 'tribology' was used for the first time [175]. Increasing applications of polymeric materials require knowledge of their tribological properties – different from much better understood tribological properties of metals and ceramics [176]. A significant part of tribology deals with the selection of materials and surface processing inasmuch as they affect wear [174].

Wear is a kind of loss of materials to a solid surface which occur due to relative motion of substance with respect to another substance. Formerly wear was defined as damaged to a surface. The most common form of that damage is loss or displacement of material and volume can be used as a measure of wear-volume of material removed or volume of material displaced. For scientific purposes this is frequently the measure used to quantify wear. In many studies, particularly material investigations, mass loss is frequently the measure used instead of volume. This is done because of the relative ease of performing a weight loss measurement. However there are some problems in using mass as primary measure of wear.

Wear causes a huge annual expenditure by industry and consumers. Most of this is replacing or repairing equipment that has worn to the extent that it no longer performs a useful function. In most of the agricultural industries 40% of the machine components replaced on equipment failed through wear. Estimates of direct cost of wear to industrial nations vary from 1% to 4% of GNP and it is estimated that 10% of all energy generated by man is dissipated in various friction processes. This direct cost includes replacements of wear part, an increase in the work load and time, loss of productivity, as well as loss of energy and the increased environmental liability, are material troubles in daily work and business.

In 1960s a systematic exertions in wear research had instigated in the industrial nations. Thus the magnitude of losses caused to mankind (which can be expressed in percentage points of GDP) makes it absolutely necessary to study ways to minimize it. Thus minimizing wear, affects the economics of production in a major way. Even though in the twenty-first century there are still wear problems present in industrial applications. This actually reveals the complexity of the wear phenomenon [177].

There are different types of wear such as abrasive, adhesive, fatigue and erosive wear, for polymer composite erosive wear is particularly interesting. In addition, composites acquire a significant place when it comes to operating in a dusty environment where resistance to erosion becomes an important aspect.

Solid particle erosion is a general term used to define the mechanical degradation (wear) of any material subjected to a stream of erodent particles impinging on its surface which results from solid particles moving at various velocities and impingement angles striking the surface of a material is one of the most encountered types of wear and has recently been a subject of a number of researches [178-180]. The effect of particle erosion on structural and engineering components has been recognized for a long time [181]. Damage caused by erosion has been reported in several industries for a wide range of situations.

Most recently polymers are combining with the various natural fibers and fillers and finding increased application such as aerospace, pipe line carrying sand slurries, water turbines, helicopter rotor blades, pump impeller blades, high speed vehicles and aircrafts, water turbines, aircraft engine blades, missile components, canopies, radomes, wind screens and outer space applications etc. In such applications, one important characteristic is the erosion behavior as these parts operate very often in dusty environments [182–185] because of their outstanding specific mechanical and tribological properties by Guadagnoa et al. [186] and McIntyre et al. [187]. Also, there have been various reports of applications of polymers and their composites in erosive wear situations in the literature [184,188-189]. Hence, study on the erosive wear behavior of such composites is important. Some studies have been emphasized that the erosive wear behavior of polymer based natural fiber composite is not intrinsic behavior and it strongly depend on many processing parameters such as operating

parameters, characteristics of polymermartial, physical and interfacial adhesion properties of fiber, additives and contact condition.

5.2 MECHANISM OF EROSIVE WEAR

Barkoula and Karger-Kocsis [190] presented in 2002 a review article on the solid particle erosion of polymers and polymericcomposites focusing on the dominating mechanisms, the most discussed influencing parameters and the different trends observedin the literature. A detailed analysis was given on the effect of experimental conditions (erodent velocity, erodent characteristics, erodent flux rate) and target material characteristics (morphological-, thermal-, thermo mechanical-, and mechanical properties) on the erosive response of polymers and polymermatrix composites.

Erosive wear involves several wear mechanisms which are largely controlled by the various parameters such as particlematerial, the angle of impingement, the impact velocity, and the particle size. Figure 5.1 summarizes the most important ones. All have important effects on erosive wear; this effect tends to show variations depending upon whether the material tested are ductile, semi ductile or brittle.

According to Bitter [191], erosion is a material damage caused by the attack of particles entrained in a fluid system impacting the surface at high speed. Hutchings [192] defines it as an abrasive wear process in which the repeated impact of small particles entrained in a moving fluid against a surface result in the removal of material from the surface. Erosion due to the impact of solid particles can either be constructive (material removal desirable) or destructive (material removal undesirable), and therefore, it can be desirable to either minimize or maximize erosion, depending on the application. The constructive applications include sand blasting, high-speed water-jet cutting, blast stripping of paint from aircraft and automobiles, blasting to remove the adhesive flash from bonded parts, erosive drilling of hard materials. Whereas the solid particle erosion is destructive in industrial applications such as erosion of machine parts, surface degradation of steam turbine blades, erosion of pipelines carrying slurries and particle erosion in fluidized bed combustion systems. In most erosion processes, target material removal typically occurs as the result of a large number of impacts of irregular angular particles, usually carried in pressurized fluid streams.

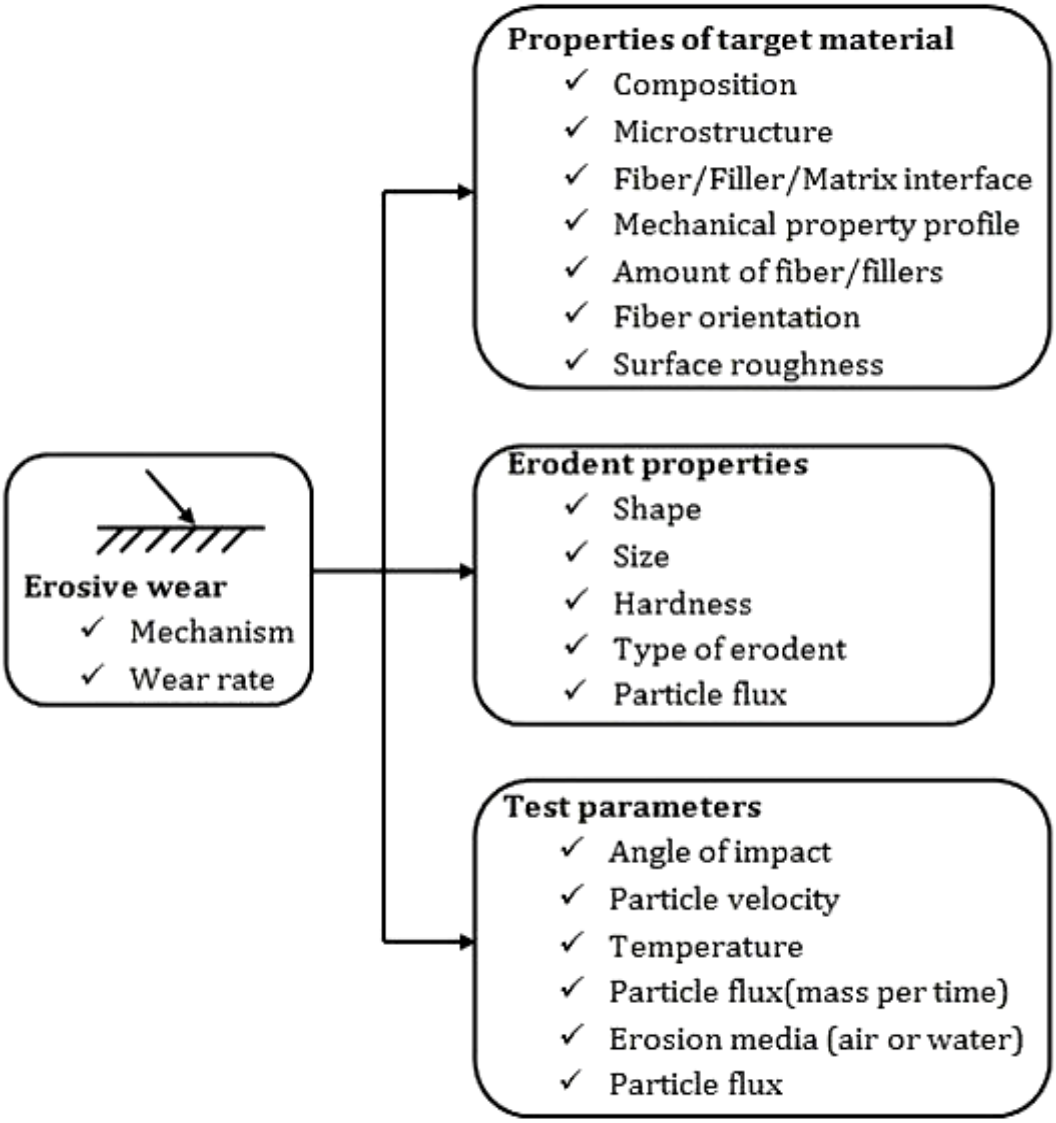

Figure 5.1 Influence of material, erodent and test parameters on erosive wear performance of polymers and their composites

It is generally recognized that erosive wear is a characteristic of a system and is influenced by many parameters. Laboratory scale investigation if designed properly allows careful control of the tribo system whereby the effects of different variables on wear behavior of PMC scan be isolated and determined. The data generated through such investigation under controlled conditions may help in correct interpretation of the results. General factors influencing erosion test are given in Table 5.1. E is the mass removed divided by the mass of particles [184].

Table 5.1 General factors influencing erosion [184]

Eroded surface properties Hardness	Ductile: ***E*** is inversely proportional to the Vickers hardness Brittle: very little correlation
Stress level	Ductile: little effect on ***E*** Brittle: more effect on ***E***
Surface finish	Rougher surfaces raise ***E*** (this is a transient initial effect)
Eroding particle properties Size	Ductile: no effect for particle diameters ≥ 100 pm; lower ***E*** for particle diameters ≤ 100 /Jrn Brittle: ductile behavior for particle diameters ≥10 /μm
Shape	Angular particles produce more wear
Hardness	Harder particles produce more wear (they also tend to be more angular)
Flow and environmental conditions Angle of impingement	Ductile: maximum erosion at about 20” Brittle: maximum erosion at about 90”
Particle velocity	Ductile: $E \alpha U_0^{2-3}$ Brittle: $E \alpha U_0^{3-5}$
Particle flux (mass per time)	Generally small effect on ***E***
Temperature	Less effect than predicted from corresponding change in hardness (for temperatures less than half the melting point in Kelvins)

5.2.1 Influence of Impact angle (α) on Erosive wear rate

Among the various parameters, Impact angle is one of the most important parameters for the erosion behavior of composite materials. Dependence of erosion rate on the impact angle is largely determined by the nature of the target material and other operating conditions. The impact angle is usually defined as the angle between the trajectory of the eroding particles and the sample surface. Impact can range from 0° to 90°.

At zero impact angle there is negligible wear because the eroding particles do not impact the surface, although even at relatively small impact angles of about 20°, severe wear may occur if the particles are hard and the surface is soft. If erosion rate goes through a maximum at intermediate impact angles, typically in the range 15°<α<30°, it is concluded that the ‘**ductile mode of erosive wear**’ prevails. Ductile material erosion wear involves the removal of material by plastic deformation.

Conversely if the maximum erosion rate occurs at high impact angles i.e. α=90°, then the behavior of the material is purely '**brittle mode**' is assumed. Brittle erosion involving the removal of material by fracture processes. It is generally seen that reinforced composites have been found to exhibit **semi-ductile behaviour** with the maximum erosion rate at intermediate angles, i.e. 45°< α< 60°. The relationship between the wear rate and impact angle for ductile and brittle materials is shown in figure 5.2.

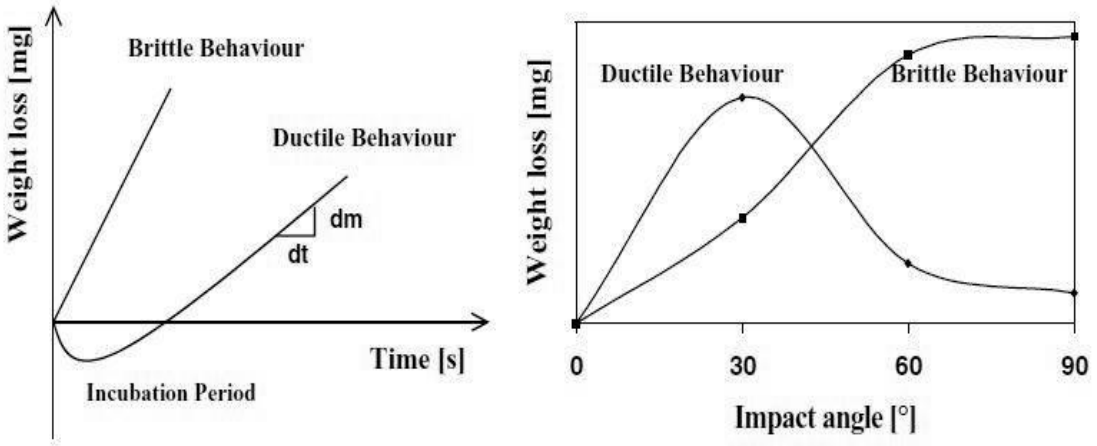

Figure 5.2 Schematic representation of the effect of impact angle on wear rates ofductile and brittle materials [190]

5.2.2 Influence of Impact velocity (υ) on Erosive wear rate

The velocity (υ) of the erosive particle has very strong effect on the wear process. If the velocity is very low then stresses at impact are insufficient for plastic deformation to occur and wear proceeds by surface fatigue [193]. When the velocity is increased it is possible for the eroded material to deform plastically. In this case, wear is caused by repetitive plastic deformation. At brittle wear response, wear proceeds by sub surface cracking. At very high particle velocities melting of the impacted surface may even occur.

From medium to high velocity, once steady state conditions have reached erosion rate (E_r) can be expressed as a simple power function of impact velocity (v) [193] equation:

$$E_r = kv^n \tag{5.1}$$

Where'*k*' is an empirical constant of proportionality includes the effect of all the other variables. The value of '*n*'and '*k*'are found by least-square fitting of the data points in plots which represent the erosion rate dependence on impact velocity by using the power law. The characteristics of the erodent and that of the target material determine the value of the exponent '*n*'. It has been stated that '*n*' varies in the range of 2–3 for polymeric materials behaving in a ductile manner, while for polymer composites behaving in brittle fashion the value of '*n*' is in the range of 3–5 [184]. The fitting parameters are summarized in Table 5.17 and Table 5.18.

5.3 SOLID PARTICLE EROSION WEAR OF POLYMER COMPOSITE

The most important factors influencing the erosion rate of the polymer composite materials can be summarized under four categories; (i) The properties of the target materials (matrix material properties and morphology, reinforcement type, amount and orientation, interface properties between the matrices and reinforcements, etc.), (ii) Environment and testing conditions (temperature, chemical interaction of erodent with the target), (iii) Operating parameters (angle of impingement, impinging velocity, particle flux–mass per unit time, etc.) and (iv) The properties of the erodent (size, shape, type, hardness, etc.) [194,173]. Thus it seems that the erosion resistance of the material can be evaluated after investigating the combination of above parameters.

Numerous research works have been carried out to evaluate the resistance of various polymers such as nylon, epoxy, polypropylene, bismileimide etc.and their composite using various natural filler for the tribological application. In recent years some work has been done on natural fiber like Oil palm [195], Jute [196], Betelnut [197] and Bamboo [198]. Chin and Yousif [199] attempted to use kenaf fibers reinforced epoxy composite for bearing application. In all these work it is stated that, the wear resistance of polymeric composites can be improved when natural fiber is used as a reinforcing material.

Patnaik et al. [200] presented a review articles on solid particle erosion behaviour of fiber and particulate filled polymer composites. Various predictions

models have been proposed to describe the erosion rate with their suitable applications on real life conditions.

Arjula et al. [201] evaluated erosion efficiency (η) of polymers and polymeric composites by collecting the available data from the literature pertaining to solid particle erosion under normal impact conditions. The result indicates the influence of hardness of various polymers and polymer composites on their erosion resistance.Mohanty et al. [202] studied solid particle erosion behavior of short date palm leaf (DPL) fiber reinforced polyvinyl alcohol (PVA) composite using silica sand particles (200 ± 50 μm) as an erodent at different impingement angles (15°–90°) and impact velocities (48–109m/s).The neat PVA shows maximum erosion rate at 30° impingement angle whereas PVA/DPL composites exhibit maximum erosion rate at 45° impingement angle irrespective of fiber loading showing semi ductile behavior.

Mishra and Acharya [203], Deo and Acharya [204] reported the tribo potential of sugarcane, lantana camaran and bamboo fiber reinforcement in thermoset polymers for enhancing erosive wear resistance. In their studies it is concluded that fiber volume fraction has a significant influence on the erosion rate.

As new developments are still under way to explore innovative fields for tribo-application of natural fiber base materials, in this chapter an attempt has been made to study the potential of using wood apple shell and coconut shell particulate epoxy base composite for tribological applications. As an initial investigation in the present work the influence of impact velocity, impact angle and particulate loading on erosive wear has been carried out and results of these investigations are presented in the subsequent sections.

5.4 EXPERIMENT

5.4.1 Preparation of the test specimens

Preparation of the test specimens were carried out as per the procedure discussed in chapter-4, Art-4.3. Specimens of dimension 25×25×5 mm^3 were cut from the composite slabs. Adequate care has been taken to keep the thickness constant (5mm) for all the samples.

5.4.2 Measurement of impact velocity of erodent particles: Double disc method

The most commonly used method for measuring impact velocity of the erodent particle is the double disc method developed by Ives and Ruff [205]. It consists of a pair of metal disc mounted on a common shaft and the stream of erodent particles is arranged to strike the upper disc, which has a thin radial slit cut in it. The exit particles from nozzle impinge on the upper disc with some of the particles passing through the slit, which eventually erode a mark on lower disc. Two erosion exposures are made, one with stationary disc and other with rotating disc at known rpm. These exposures give rise to erosion marks A and B on the lower disc (Figure 5.3). Measurement of the angular displacement between these marks gives a measure of the flight time of the particles as they cross the space between the discs. The particle velocity can be found by using the following equation.

$$v = \frac{L}{t} = \frac{Lv360°}{\theta} \tag{5.2}$$

Where 'L' is separation of two discs, 't' is time in second, 'v' is rotation speed of disc per second and 'θ' is angular displacement between the marks. The above equation can also be expressed as

$$v = \frac{2\pi rvL}{S} \tag{5.3}$$

Where 'r' is radius from the disc center and 'S' is linear separation of two marks. The details of impact velocity calibration at various pressures are given in Table 5.2.

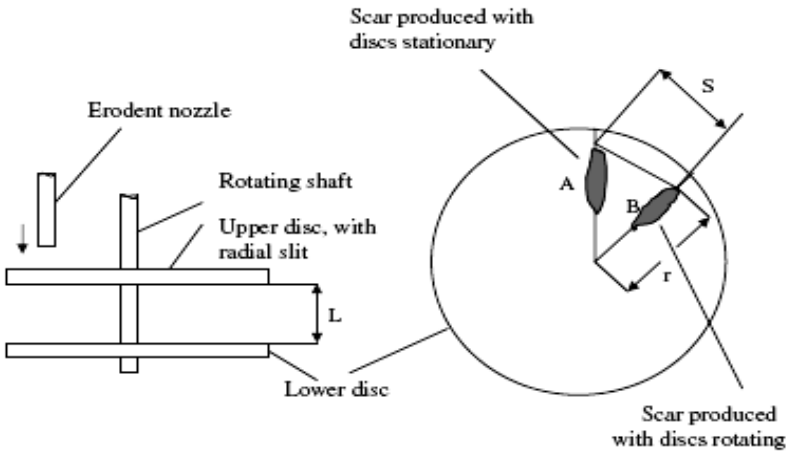

Figure 5.3 Schematic diagram of methodology used for velocity calibration

Table 5.2 Impact velocity calibration at various pressures

Pressure (bar)	Speed of rotating disc(rpm)	Angle θ (°)	Velocity (m/s)	Avg. impact velocity(m/s)
1 bar	2000	7.0	42.85	47.25
		6.5	46.15	
		6.0	50.00	
		6.0	50.00	
2 bar	2000	4.0	75.00	69.16
		4.5	66.67	
		4.0	75.00	
		5.0	60.00	
3 bar	2000	4.5	66.67	81.845
		4.0	75.00	
		3.5	85.71	
		3.0	100.00	

5.4.3 Erosion Wear Test Set-Up

The wear test is conducted on erosion wear test apparatus designed according to the ASTM G76-95 standard test method. The test evaluates the wear characteristics of the developed wood apple and coconut shell particulates composite. The schematic of air jet erosion test rig is shown in figure 5.4(a). The details of the erosion test parameters for the experiment conducted are given in Table 5.3. The weight loss is recorded for subsequent calculation of erosion rate is shown in Table 5.4 to 5.12 for neat polymer, wood apple shell and coconut shell particulate composite.

The photograph of solid particle erosion test apparatus used for the present investigation is shown in figure 5.4(b). The rig consists of an air compressor, a particle feeder, an air particle mixingand accelerating chamber. Dry compressed air is mixed with angular silica sand (200±50µm size) abrasive particles, which are fed at a constant rate from a conveyor belt in to the mixing chamber and then accelerated by passing the mixture through a tungsten carbide (WC) converging nozzle of 3mm diameter. These accelerated particles impact the specimen, which can be held at various angles (30°, 45°, 60° and 90°) with respect to the impacting particles using an adjustable sample holder. Required pressure can be adjusted with the pressure regulator fitted with the machine.

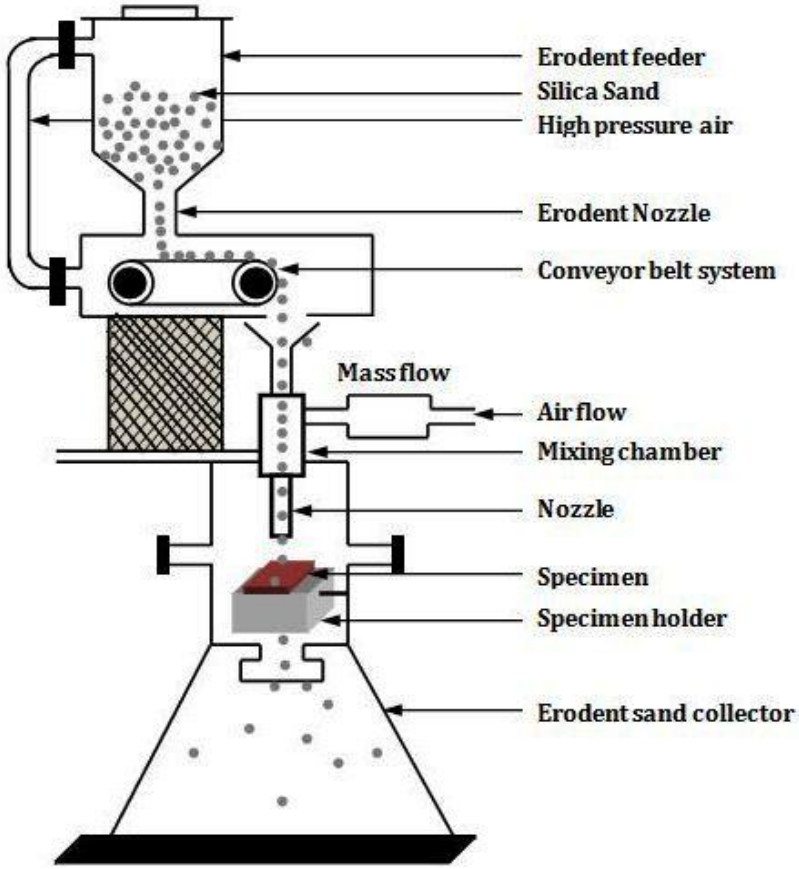

(a)

1. **Sand hopper**
2. **Conveyor belt system for sand flow**
3. **Pressure transducer**
4. **Particle-air mixing chamber**
5. **Nozzle**
6. **X-Y and h axes assembly**
7. **Sample holder**

(b)

Figure 5.4 (a) Schematic of air jet erosion test Rig **(b)** Photograph of the Solid Particle Erosion Test Set up

The condition under which the erosion test has been carried out is given in Table 5.3. A standard test procedure is employed for each erosion test. The sample were cleaned with petroleum ether and weighted to an accuracy of 0.001g using Pan electronic machine (Contach Mach) before and after each erosion test. The test samples after loaded in the test rig with desired angle of impingement were eroded for 10min and weighted to determine the weight loss (W_m). The erosion rate (E_r) is then calculated by using the following equation.

$$E_r = \frac{W_m}{W_e} \tag{5.4}$$

Where 'W_m' is the mass loss of test sample (gm) which can be found out from the difference in weight of the samples prior and after each test and 'W_e' is the mass of the erodent particles (gm) striking the target sample for 10min (i.e.) the testing time. This procedure has been repeated until the erosion rate attains a constant steady-state value.

Table 5.3 Operating parameters for the erosion test

Test parameters	
Erodent	*Silica sand*
Erodent size (μm)	200±50
Erodent shape	Angular
Hardness of silica particles (HV)	1420±50
Impingement angle (α°)	30, 45, 60 and 90
Impact velocity (m/s)	48, 70 and 82
Erodent feed rate (gm/min)	2±0.02
Test temperature(°C)	RT
Nozzle to sample distance (mm)	10

5.4.4 Erosion efficiency

G. Sundararajan et al. [206] proposed a term erosion efficiency 'η' to identify the brittle and ductile erosion response of various polymeric materials. It is defined as the fraction of the volume that is actually removed as erosion debris out of that which is displaced. Then 'η' is given as

$$\eta = \frac{2 \times E_r \times H_\upsilon}{\rho \times \upsilon^2} \tag{5.5}$$

Where 'E_r' is the actual erosion rate (kg/kg), 'H_v' is the hardness of eroding materials (MPa), 'ρ' is the density of the eroding material (kg/m^3) and'υ'is the impact velocity (m/s) of erodent. For calculating erosion efficiency, the Vickers hardness (H_v) values were converted to projected area hardness values (in mega Pascal) by multiplying with the factor 9.807.

The magnitude of 'η' can be used to characterize the nature and mechanism of erosion. For example, ideal micro-ploughing involving just the displacement of the material from the crater without any fracture (and hence no erosion) has zero efficiency (η=0). In contrast, if the material removal is by ideal micro-cutting, 'η' is unity (η=1.0 or 100%). If erosion occurs by lip or platelet formation and their fracture by repeated impact, as is usually the case in ductile materials, the magnitude of η will be very low, i.e. $\eta \leq 100\%$. In the case of brittle materials, erosion occurs usually by spall and removal of large chunks of materials resulting from the interlinking of lateral or radial cracks and thus η can be expected to be even greater than 100% [200].

The values of erosion efficiencies of composites under this study are calculated using equation 5.5 and are listed in Table-5.13 and Table-5.14 for both wood apple and coconut shell particulate composite along with their hardness values and operating conditions. Based on these results various graphs were plotted and presented in the subsequent sections for discussions.

5.5 RESULTS AND DISCUSSION

5.5.1 Effect of Impact Angle (α) on Erosion Rate of Wood apple shell and Coconut shell particulate composite

The effect of impact angle on erosion rate of wood apple shell epoxy composite is studied at various impact velocities such as 48, 70 and 82m/s are shown in figure 5.5 to 5.7 respectively. It is evident from the figure that impact angle has significant influence on erosion rate. From the figure it is clearly observed that to neat epoxy composite shows maximum erosion rate ($E_{r\ max}$) takes place at 90° impact angle.

Whereas after adding raw wood apple shell particulates with epoxy, the peak erosion rate for the composites shifted from 90° to 45° impact angle irrespective of filler loading and with different velocity of impact. Minimum erosion rate ($E_{r\ min}$) is obtained at an impact angle of 30° for all composite under all velocity of impact. As mentioned earlier (art 5.2.1) impact angle is one of the most important parameter for classifying the erosion behavior of any material. From this investigation it is seen that pure epoxy shows maximum erosion at 90° indicates its brittle nature. With different weight fraction of filler loading maximum erosion for the filled composites with epoxy changes from 90° to 45°. This change in impact angle for the composite responds to solid particle impact neither behavior in a purely ductile nor in a purely brittle nature. This behavior can be termed as semi ductile in nature.

While working with coconut shell particulate (raw) composite, this composite also shows similar behavior as wood apple shell particulate composite showing semi ductile nature. These results are shown in figure 5.8 to 5.10.

It is also observed from these plots that 10wt% of particulate filler for both wood apple shell and coconut shell shows minimum wear in composite to other weight fraction of particulate (5, 15 and 20wt%) . in addition it is found that erosion resistance of wood apple shell particulate composite is higher than coconut shell particulate composite.

5.5.2 Effect of Impact velocity (v) on Erosion Rate of Wood apple shell and Coconut shell particulate composite

The variation of steady state erosion rate of all composites with impact velocity at different impact angles are shown in the form of histogram in figure 5.11 to 5.14. It is seen that the speed at which the erosion particles impacted on the surface of the samples has very strong effect on the wear process.

It is observed from the plots that there is no significant variation in the wear rate at low impact velocities (48m/s). However for the increase in the velocity to 70 and 82m/s it is found that erosion rate increase to higher values. This might have happened due to creation of severe plastic deformation on the composite surface at

higher velocities. Same type of behavior was repeated by Rout et al. [207], while working with Rice husk filled composite.

The similar observations were also found in coconut shell particulate composites which are shown in figure 5.15 to 5.18. Minimum erosion rate was also observed 10wt% coconut and wood apple shell particulate composite with all impact velocities.

As mentioned earlier (art 5.2.2) influence of impact velocity (υ) on Erosive wear rate is one of the most important parameter for classifying the erosion behavior of any material. Figure 5.19 to 5.26 illustrates the variation of erosion rate with impact velocity at different impingement angle for neat epoxy, wood apple and coconut shell particulate composites. The least-square fits to data point were obtained by using power law and the values of 'n' and 'k' are summarized in Table-5.15 and 5.16. From, the figures 5.19 to 5.22 the velocity exponents found for 30°, 45°, 60° and 90° impingement angles are in the range of 2.023-3.474, 2.263-2.623, 2.642-3.554 and 1.895-2.561 respectively for the wood apple shell reinforced epoxy composites whereas from the figure 5.23 to 5.26 the velocity exponents found for 30°, 45°, 60° and 90° impingement angles are in the range of 2.192-2.38, 1.893-1.988, 1.744-2.079 and 1.762-2.125 respectively for the coconut shell reinforced epoxy composites. The velocity exponents at various impingement angles found arein good agreement with finding of Harsha et al. [208].

As mentioned earlier (art 5.4.4) erosion efficiency is also one of the important parameter for classifying the erosion behavior of any material. The erosion efficiency of the wood apple and the coconut shell composites are listed in Table 5.13 and 5.14. According to the categorization made by Roy et al. [209], it has been observed that the erosion efficiencies of epoxy varies from 1.579-3.923 whereas for wood apple shell 5, 10, 15 and 20wt% reinforced epoxy composite varies from 0.976-2.473, 0.590-1.676, 0.657-1.782 and 0.827-1.962 respectively and 0.948-2.650, 0.886-2.249, 1.036-2.948 and 1.084-2.918 for the coconut shell composites at different impact velocities and with different impact angles. Further it is noticed that the erosion efficiency of all tested sample slightly decreases with increase in impact velocity. Similar observations are also reported by Srivastava et al. [210] for glass fiber epoxy composite. Thus it can be conclude that the erosion efficiency is not exclusively a material property but also

depends on other operational variables such as impact velocity and impingement angle. From the values obtained it is clearly observed that for 10wt% wood apple and coconut shell epoxy composites the erosion efficiency is less when compared to neat epoxy and other weight percentages (5, 15 and 20 wt%) filler composites. This lower erosion efficiency of the composites indicates better erosion resistance in comparison to neat epoxy composite and other filled composites.

5.5.3 Comparison between Wood apple shell and Coconut shell particulate composite

A comparative analysis for wear behavior of both lignocellulosic (wood apple shell and coconut shell) polymer composites is shown in the form of histograms in figure 5.27at 48m/s impact velocity. From the results is clearly observed that 10wt% wood apple shell particulate composite shows minimum wear properties compared to coconut shell particulate composite as well as maximum wear is occurring at 45° impact angle which indicates the semi ductility nature of the composite. All other velocities shows similar trend, therefore they are not shown here.

5.6 MORPHOLOGICAL ANALYSIS OF ERODED SURFACE

Figure 5.28 (a), (b) shows the surface morphology of 5 and 10wt% filled composite. Severe damage on the surface of both the composites is clearly visible. However damage caused to 10wt% filler is less of no crater formation is visible on the surface with increase of filler content (15 and 20wt %). Figure 5.28(c) and (d) instead of surface damage, crater is being formed on the surface. The size of the crater on 20wt% filler seems to be very higher depth in comparison to 15wt% filler. This indicates higher erosion with 15 and 20wt% filler content. This might have happened due to higher weight percentage of filler which leads to poor wettability with the epoxy resin. The morphological features also matching with the experimental results. Figure 5.28(e) shows the micrograph of the wood apple shell composite at 90° impact angle. Due to normal impact of the erodent particles crater has been formed eroding the matrix material which is visible on the micrograph. Though formation of crater is there but filler materials are not chipped out from the composite. They are still intact with the

composite. This is the indication of good bonding between filler and the matrix material which leads to higher erosive strength of the composite.

The morphology of 10wt% of coconut shell particles at 45° and 90° impact angles are shown in figure 5.29(a) and (b). Other impact angles morphology are not shown here because 10wt% with 45° and 90° impact angles give optimum results. Figure 5.29(a) shows that crater has been formed but not so large as compared to Figure 5.29(b) in which the impact angle is 90°. This is because the velocity at which the erodent strikes the target is less as compared to normal impact.

Compared figure 5.29(b) with figure 5.28(e) with same parameter it is seen that for coconut shell particulate composite chipping out of large number of particles took place in comparison to figure 5.28(c) for wood apple shell composite. This might have happened because cellulose content of coconut shell is (30.04wt%) less compared to wood apple shell (39.54wt%) which is responsible for giving strength to the composite. Because of this chipping out of filler particles, erosion wear is found to be less compared to coconut shell keeping all parameter same for the experiment.

5.7 CONCLUSION

Experiments were conducted to study the solid particle erosion of both wood apple and coconut shell particulate reinforced epoxy composites with silica sand as erodent. Polymer composites are experimented at various impingement angles and impact velocities for different filler weight fraction. Based on the studies, the following conclusions are drawn.

1. Study of influence of impingement angle on erosion rate of the composites filled with different weight percentage of filler loading reveals their semi ductile nature with respect to erosive wear. The peak erosion rate is found to be occurring at 45° impingement angle for all the composite samples under various experimental conditions irrespective of filler loading.

2. The present investigation revealed that the erosion resistance of the particulate composites increases with the addition of fillers. For the present case higher erosion strength is achieved with 10wt% raw wood apple shell particulate composite as compared to coconut shell particulate composite.

3. The SEM figure indicates a favorable interfacial bonding between filler and matrix in wood apple shell composite in comparison to coconut shell particulate. Formation of crater and chipping of fiber are the main reasons for erosion for the composites under study.

4. From the experiment it is believed that possible use of these particulate composites can be made in the areas such as pipe lines carrying coal dust, slurries, desert structure, low cost housing, boats/sporting equipment, partition boards, doors and window panels.

Table 5.4 Weight loss and erosion rate of Epoxy composite with respect to impact angle due to erosion for a period of 600 seconds

Impact Velocity (m/s)	Impact Angle (°)	Epoxy	
		Weight loss (g)	Erosion rate×10^{-4} (g/g)
48	30	0.0033	1.65
	45	0.0045	2.24
	60	0.0050	2.50
	90	0.0056	2.80
70	30	0.0048	2.40
	45	0.0059	2.94
	60	0.0064	3.20
	90	0.0072	3.60
82	30	0.0056	2.78
	45	0.0066	3.29
	60	0.0071	3.55
	90	0.0080	4.00

Table 5.5 Weight loss and erosion rate of 5wt% Raw WAS particulate composite with respect to impact angle due to erosion for a period of 600 seconds

Impact Velocity (m/s)	Impact Angle (°)	Raw 5wt%	
		Weight loss (g)	Erosion rate×10^{-4} (g/g)
48	30	0.0020	1.00
	45	0.0030	1.50
	60	0.0020	1.00
	90	0.0020	1.00
70	30	0.0032	1.59
	45	0.0042	2.10
	60	0.0035	1.75
	90	0.0032	1.60
82	30	0.0038	1.89
	45	0.0046	2.30
	60	0.0041	2.03
	90	0.0035	1.73

Table 5.6 Weight loss and erosion rate of 10wt% Raw WAS particulate composite with respect to impact angle due to erosion for a period of 600 seconds

Impact Velocity (m/s)	Impact Angle (°)	Raw 10wt%	
		Weight loss (g)	Erosion rate×10^{-4} (g/g)
48	30	0.0010	0.50
	45	0.0018	0.92
	60	0.0012	0.61
	90	0.0018	0.90
70	30	0.0016	0.80
	45	0.0023	1.17
	60	0.0019	0.95
	90	0.0021	1.05
82	30	0.0019	0.94
	45	0.0028	1.40
	60	0.0024	1.22
	90	0.0022	1.11

Table 5.7 Weight loss and erosion rate of 15wt% Raw WAS particulate composite with respect to impact angle due to erosion for a period of 600 seconds

Impact Velocity (m/s)	Impact Angle (°)	Raw 15wt%	
		Weight loss (g)	Erosion rate×10^{-4} (g/g)
48	30	0.0016	0.81
	45	0.0020	1.00
	60	0.0016	0.80
	90	0.0018	0.91
70	30	0.0020	1.00
	45	0.0031	1.54
	60	0.0028	1.38
	90	0.0022	1.10
82	30	0.0022	1.08
	45	0.0034	1.71
	60	0.0029	1.47
	90	0.0024	1.20

Table 5.8 Weight loss and erosion rate of 20wt% Raw WAS particulate composite with respect to impact angle due to erosion for a period of 600 seconds

Impact Velocity (m/s)	Impact Angle (°)	Raw 20wt%	
		Weight loss (g)	Erosion rate×10^{-4} (g/g)
48	30	0.0018	0.92
	45	0.0022	1.10
	60	0.0019	0.95
	90	0.0019	0.95
70	30	0.0027	1.35
	45	0.0034	1.70
	60	0.0030	1.48
	90	0.0025	1.25
82	30	0.0029	1.43
	45	0.0040	2.00
	60	0.0035	1.74
	90	0.0028	1.40

Table 5.9 Weight loss and erosion rate of 5wt% Raw CS particulate composite with respect to impact angle due to erosion for a period of 600 seconds

Impact Velocity (m/s)	Impact Angle (°)	Raw 5wt%	
		Weight loss (g)	Erosion rate×10^{-4} (g/g)
48	30	0.0026	1.28
	45	0.0036	1.80
	60	0.0030	1.50
	90	0.0028	1.40
70	30	0.0035	1.73
	45	0.0043	2.13
	60	0.0036	1.80
	90	0.0034	1.70
82	30	0.0038	1.90
	45	0.0047	2.35
	60	0.0041	2.07
	90	0.0038	1.88

Table 5.10 Weight loss and erosion rate of 10wt% Raw CS particulate composite withrespect to impact angle due to erosion for a period of 600 seconds

Impact Velocity (m/s)	Impact Angle (°)	Raw 10wt%	
		Weight loss (g)	Erosion rate×10^{-4} (g/g)
48	30	0.0022	1.10
	45	0.0032	1.62
	60	0.0028	1.40
	90	0.0024	1.20
70	30	0.0030	1.50
	45	0.0039	1.94
	60	0.0034	1.70
	90	0.0032	1.60
82	30	0.0032	1.61
	45	0.0040	1.98
	60	0.0036	1.80
	90	0.0033	1.65

Table 5.11 Weight loss and erosion rate of 15wt% Raw CS particulate composite withrespect to impact angle due to erosion for a period of 600 seconds

Impact Velocity (m/s)	Impact Angle (°)	Raw 15wt%	
		Weight loss (g)	Erosion rate×10^{-4} (g/g)
48	30	0.0028	1.40
	45	0.0039	1.95
	60	0.0038	1.90
	90	0.0036	1.80
70	30	0.0038	1.90
	45	0.0074	2.35
	60	0.0042	2.10
	90	0.0040	2.00
82	30	0.0040	2.00
	45	0.0049	2.47
	60	0.0043	2.16
	90	0.0046	2.30

Table 5.12 Weight loss and erosion rate of 20wt% Raw CS particulate composite with respect to impact angle due to erosion for a period of 600 seconds

Impact Velocity (m/s)	Impact Angle (°)	Raw 20wt%	
		Weight loss (g)	Erosion rate×10^{-4} (g/g)
48	30	0.0029	1.45
	45	0.0040	2.01
	60	0.0040	2.00
	90	0.0038	1.90
70	30	0.0043	2.15
	45	0.0050	2.51
	60	0.0046	2.30
	90	0.0042	2.12
82	30	0.0046	2.28
	45	0.0051	2.56
	60	0.0048	2.38
	90	0.0044	2.18

Table 5.13 Erosion efficiency of Raw WAS particulate composite

Impact Velocity (m/s)	Impact Angle (°)	Erosion efficiency (η)				
		Neat Epoxy	Raw 5 wt%	Raw 10 wt%	Raw 15 wt%	Raw 20 wt%
		Hv=MPa 190.452	Hv=MPa 231.249	Hv=MPa 248.117	Hv=MPa 240.762	Hv=MPa 231.445
48	30	2.312	1.649	0.916	1.453	1.591
	45	3.138	2.473	1.676	1.782	1.902
	60	3.503	1.649	1.125	1.426	1.643
	90	3.923	1.649	1.649	1.622	1.643
70	30	1.581	1.047	1.527	0.659	0.889
	45	1.937	1.387	0.767	1.011	1.120
	60	2.108	1.153	0.628	0.909	0.975
	90	2.372	1.054	0.692	0.725	0.827
82	30	1.332	1.065	0.590	0.657	0.844
	45	1.579	1.299	0.877	1.044	1.185
	60	1.704	1.144	0.768	0.897	1.034
	90	1.920	0.976	0.697	0.733	0.829

Table 5.14 Erosion efficiency of Raw CS particulate composites

Impact Velocity (m/s)	Impact Angle (°)	Erosion efficiency (η)				
		Neat Epoxy	**Raw 5wt%**	**Raw 10wt%**	**Raw 15wt%**	**Raw 20wt%**
		Hv=MPa 190.452	**Hv=MPa 203.495**	**Hv=MPa 227.424**	**Hv=MPa 217.519**	**Hv=MPa 212.223**
48	30	2.312	1.884	1.767	2.116	2.105
	45	3.138	2.650	2.602	2.948	2.918
	60	3.503	2.208	2.249	2.872	2.903
	90	3.923	2.061	1.928	2.721	2.758
70	30	1.581	1.197	1.133	1.351	1.468
	45	1.937	1.474	1.465	1.670	1.713
	60	2.108	1.246	1.284	1.493	1.570
	90	2.372	1.177	1.208	1.422	1.447
82	30	1.332	0.958	0.886	1.036	1.134
	45	1.579	1.185	1.090	1.279	1.273
	60	1.704	1.044	0.991	1.119	1.184
	90	1.920	0.948	0.908	1.191	1.084

Table 5.15 Parameters characterizing the velocity dependence of erosion rate of raw wood apple shell particulate composite

Filler content (wt%)	Impact Angle (°)	k	n	R^2
0(Neat epoxy)	30°	4.00E-06	3.4749	0.999
	45°	1.00E-05	3.5184	0.998
	60°	2.00E-05	3.5547	1.000
	90°	2.00E-05	3.566	0.996
5	30°	1.00E-06	2.692	0.999
	45°	6.00E-06	2.3164	0.991
	60°	5.00E-07	2.8484	0.991
	90°	2.00E-06	2.5618	0.974
10	30°	5.00E-07	2.6903	0.998
	45°	5.00E-06	2.2634	0.977
	60°	5.00E-07	2.7644	0.994
	90°	2.00E-05	1.895	0.999
15	30°	1.00E-05	2.0232	0.998
	45°	2.00E-06	2.5262	0.99
	60°	8.00E-07	2.6915	0.961
	90°	1.00E-05	2.014	0.999
20	30°	3.00E-06	2.3533	0.968
	45°	1.00E-06	2.6232	0.999
	60°	1.00E-06	2.6425	0.999
	90°	6.00E-06	2.2264	0.999

Table 5.16 Parameters characterizing the velocity dependence of erosion rate of raw coconut shell particulate composite

Filler content (wt%)	Impact Angle (°)	k	n	R^2
0(Neat epoxy)	30°	4.00E-06	3.4749	0.999
	45°	1.00E-05	3.5184	0.998
	60°	2.00E-05	3.5547	1.000
	90°	2.00E-05	3.566	0.996
5	30°	7.00E-06	2.2487	0.9961
	45°	3.00E-05	1.9885	0.9934
	60°	2.00E-05	2.0799	0.9759
	90°	2.00E-05	2.044	0.9974
10	30°	7.00E-06	2.2315	0.9866
	45°	4.00E-05	1.8935	0.9609
	60°	2.00E-05	1.9775	0.9947
	90°	1.00E-05	2.1252	0.959
15	30°	1.00E-05	2.1921	0.9752
	45°	3.00E-05	1.9511	0.9918
	60°	7.00E-05	1.7442	0.9934
	90°	3.00E-05	1.9252	0.9053
20	30°	5.00E-06	2.3814	0.9707
	45°	3.00E-05	1.9766	0.9532
	60°	6.00E-05	1.8331	0.989
	90°	7.00E-05	1.7628	0.9903

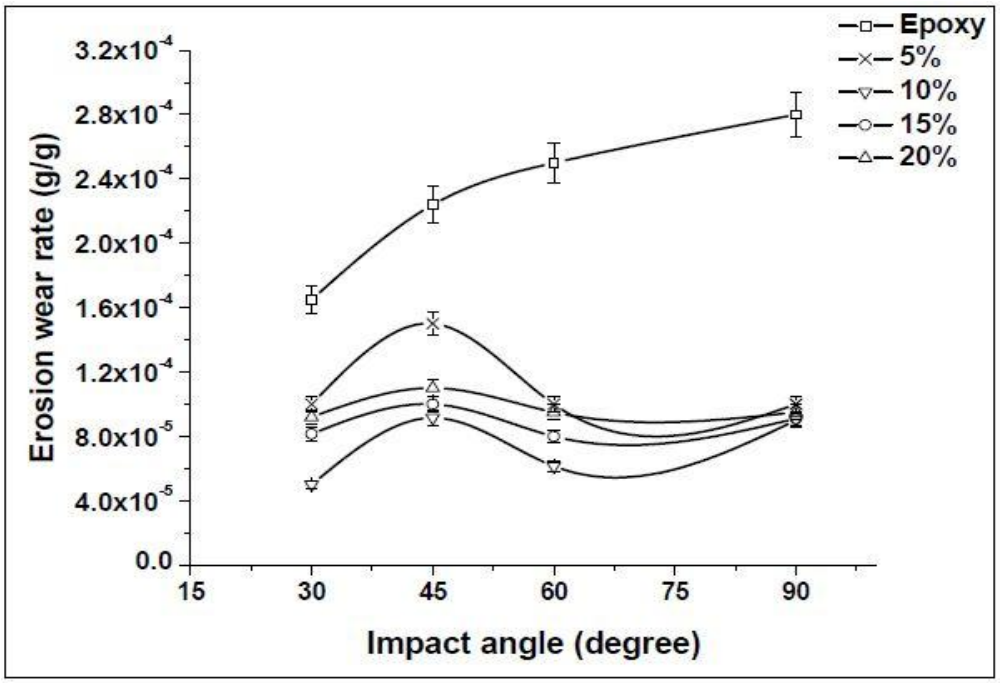

Figure 5.5 Variation of erosion rate with different impact angle of raw wood apple shell particulate composite at impact velocity 48m/s

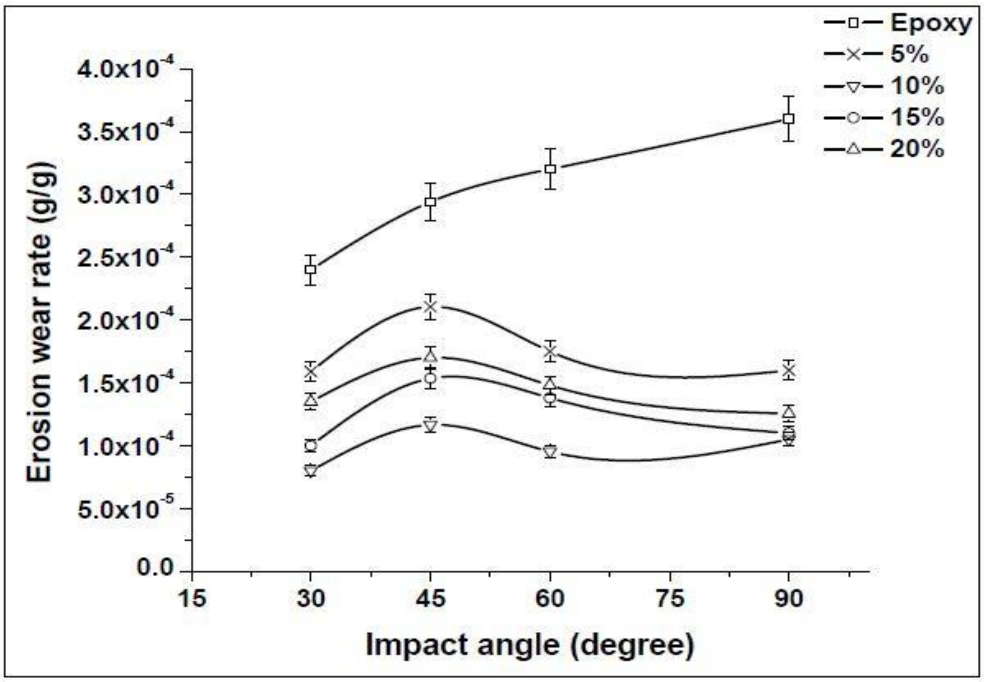

Figure 5.6 Variation of erosion rate with different impact angle of raw wood apple shell particulate composite at impact velocity 70m/s

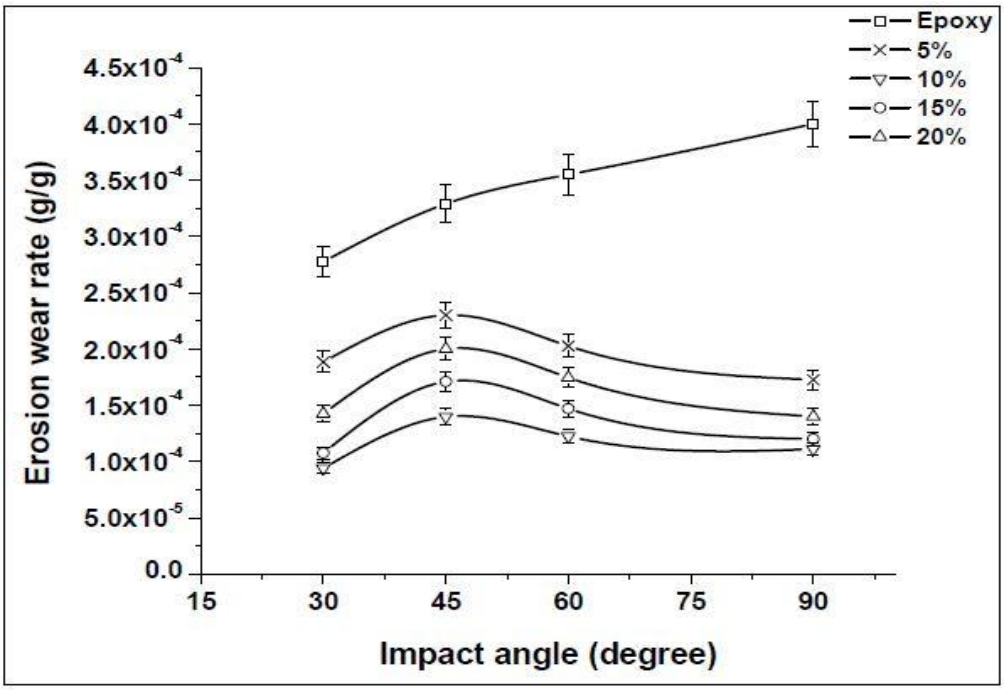

Figure 5.7 Variation of erosion rate with different impact angle of raw wood apple shell particulate compositeat impact velocity 82m/s

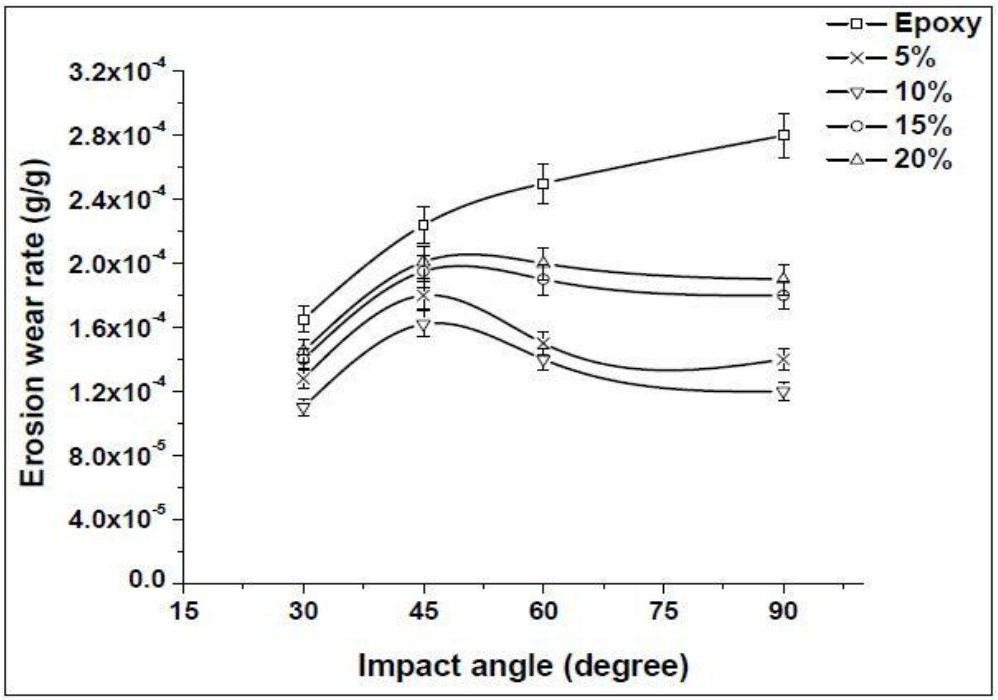

Figure 5.8 Variation of erosion rate with different impact angle of raw coconut shell particulate composite at impact velocity 48m/s

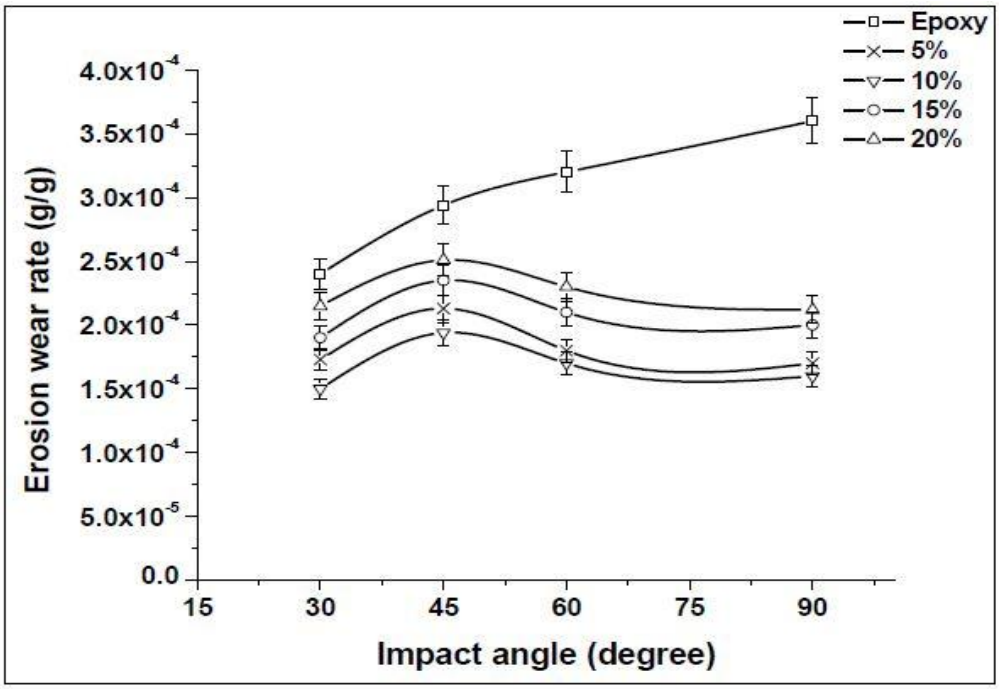

Figure 5.9 Variation of erosion rate with different impact angle of raw coconut shell particulate composite at impact velocity 70m/s

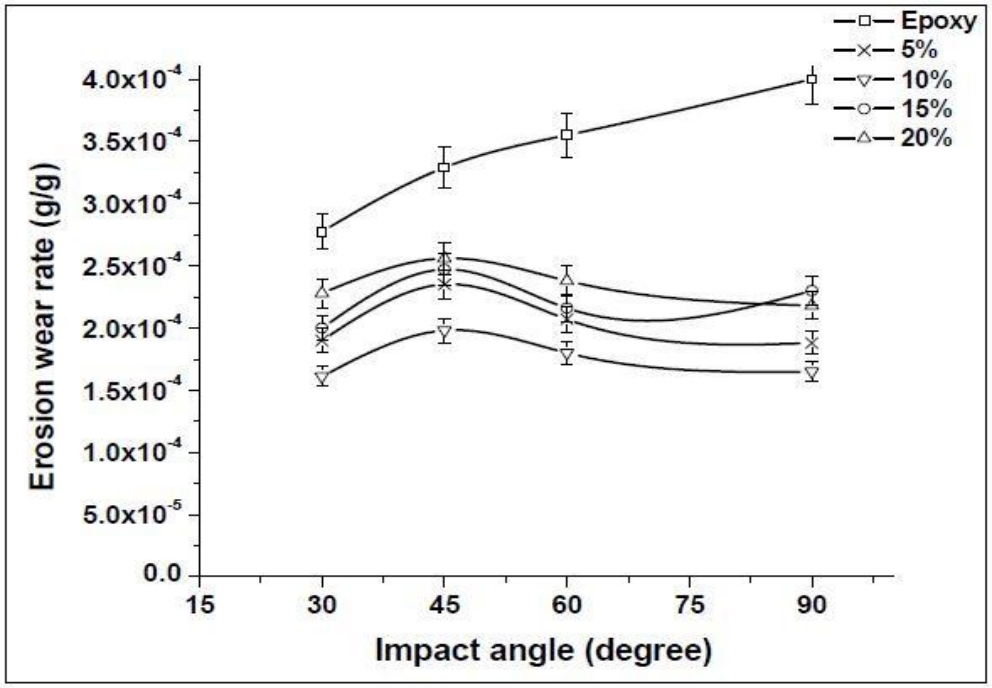

Figure 5.10 Variation of erosion rate with different impact angle of raw coconut shell particulate composite at impact velocity 82m/s

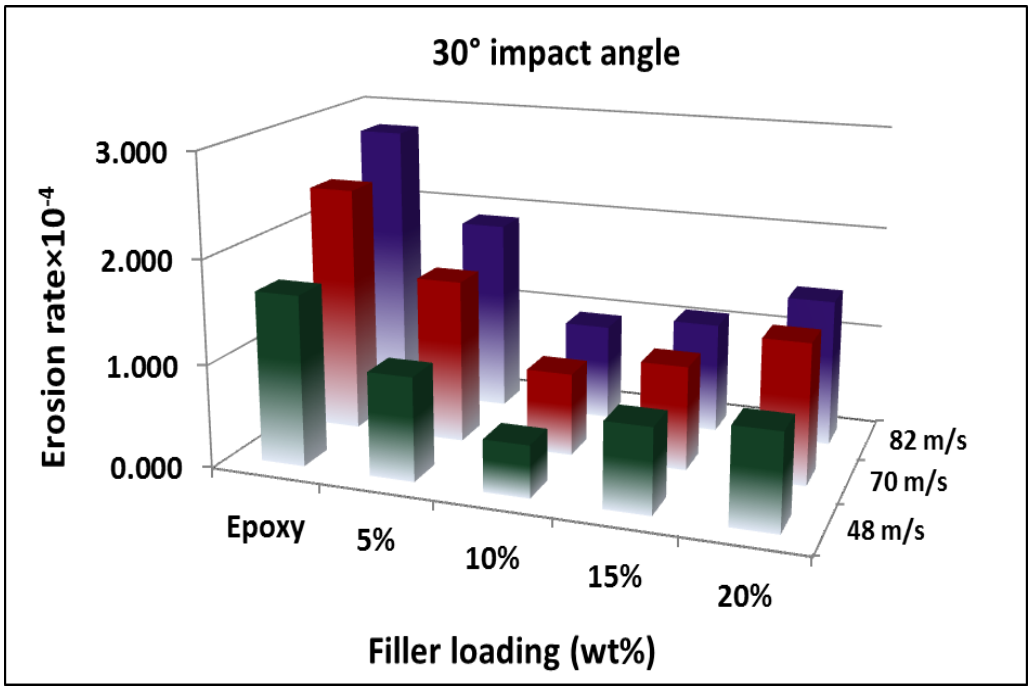

Figure 5.11 Histogram showing the effect of impact velocities on steady state erosive wearrates of raw wood apple shell particulate composite for 30° impact angle

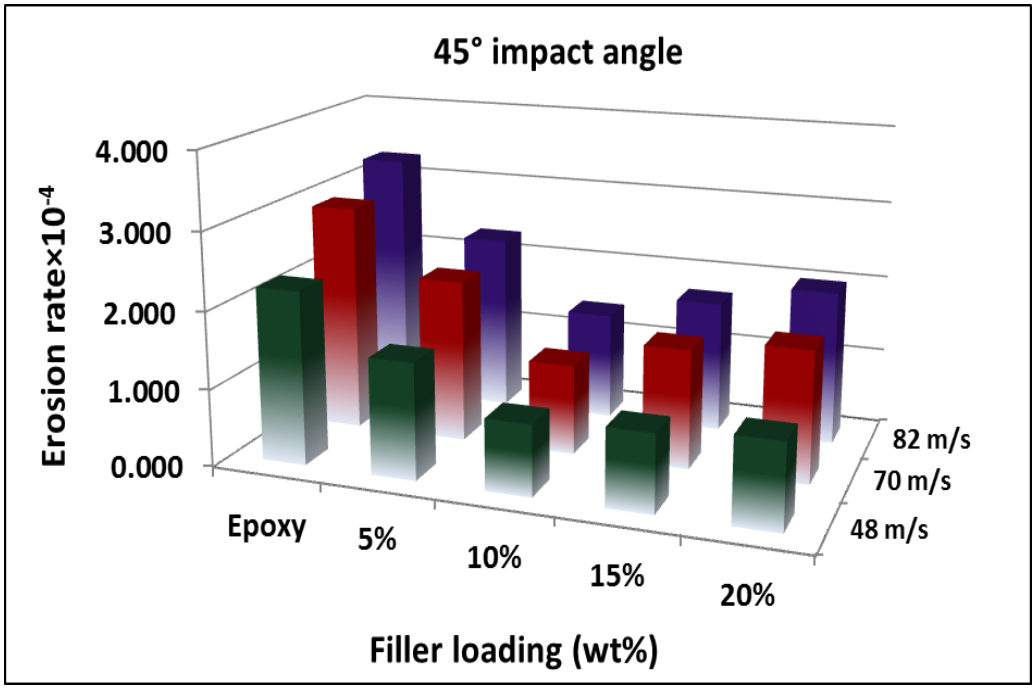

Figure 5.12 Histogram showing the effect of impact velocities on steady state erosive wear rates of raw wood apple shell particulate composite for 45° impact angle

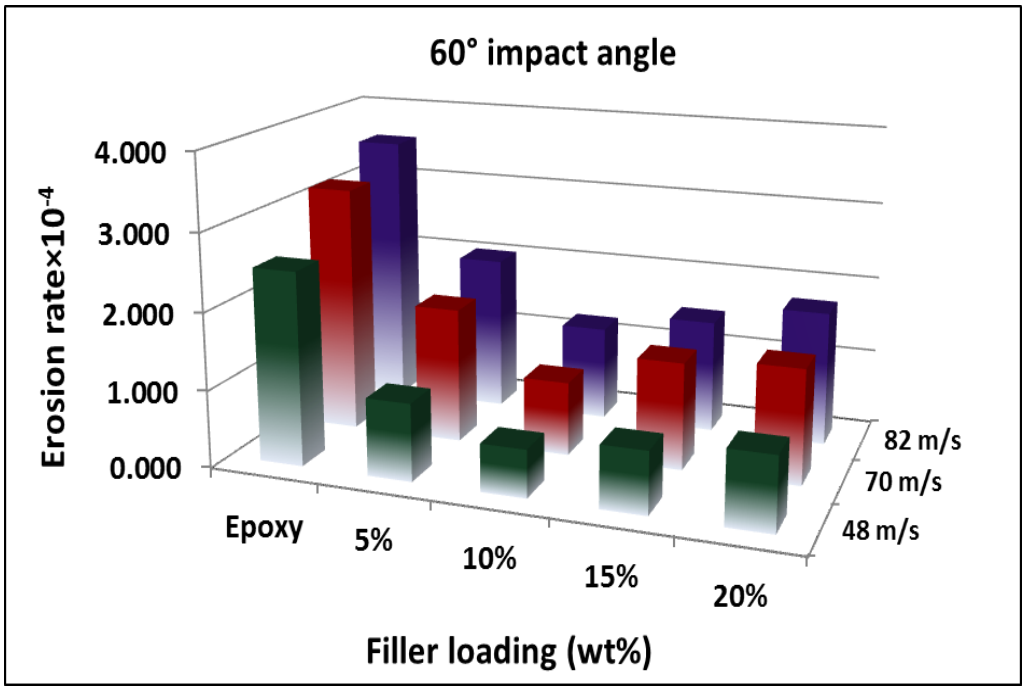

Figure 5.13 Histogram showing the effect of impact velocities on steady state erosive wear rates of raw wood apple shell particulate composite for 60° impact angle

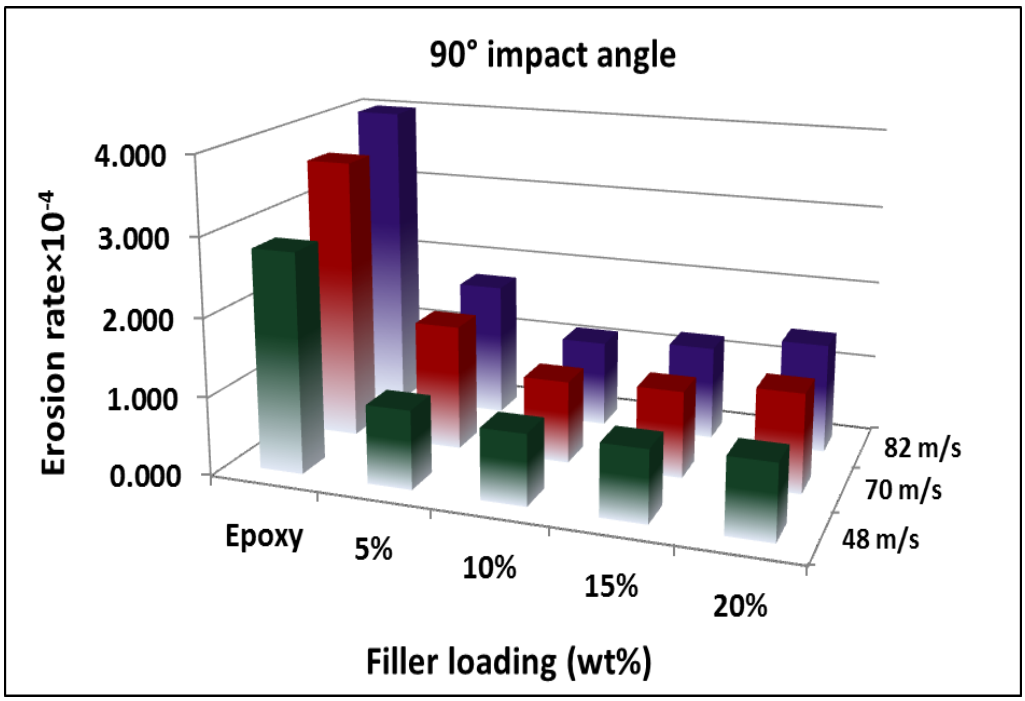

Figure 5.14 Histogram showing the effect of impact velocities on steady state erosive wearrates of raw wood apple shell particulate composite for 90° impact angle

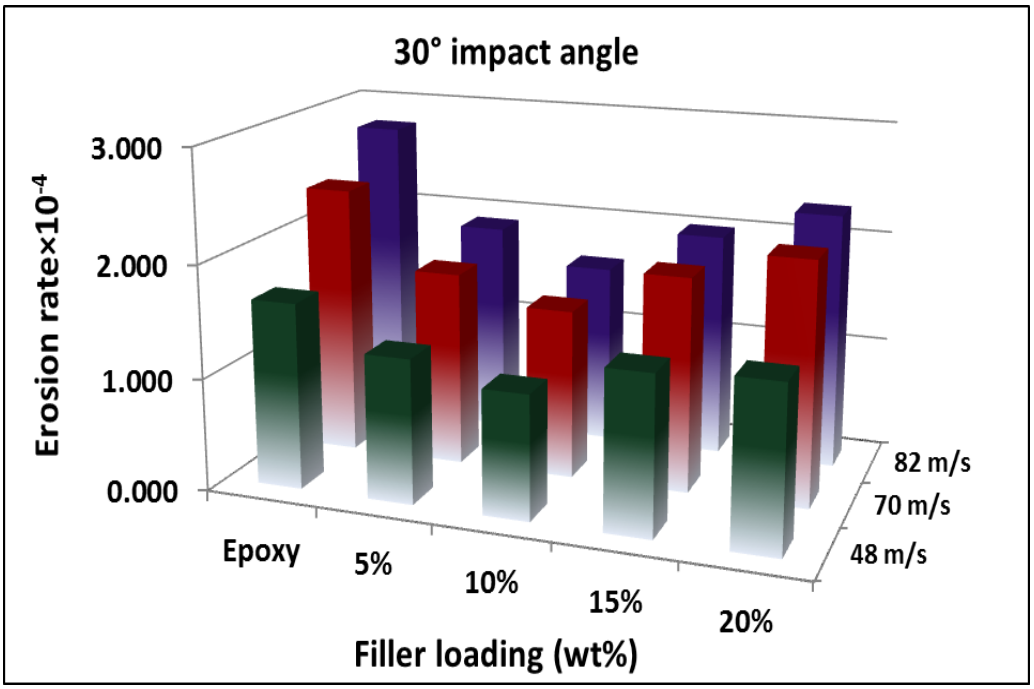

Figure 5.15 Histogram showing the effect of impact velocities on steady state erosive wear rates of raw coconut shell particulate composite for 30° impact angle

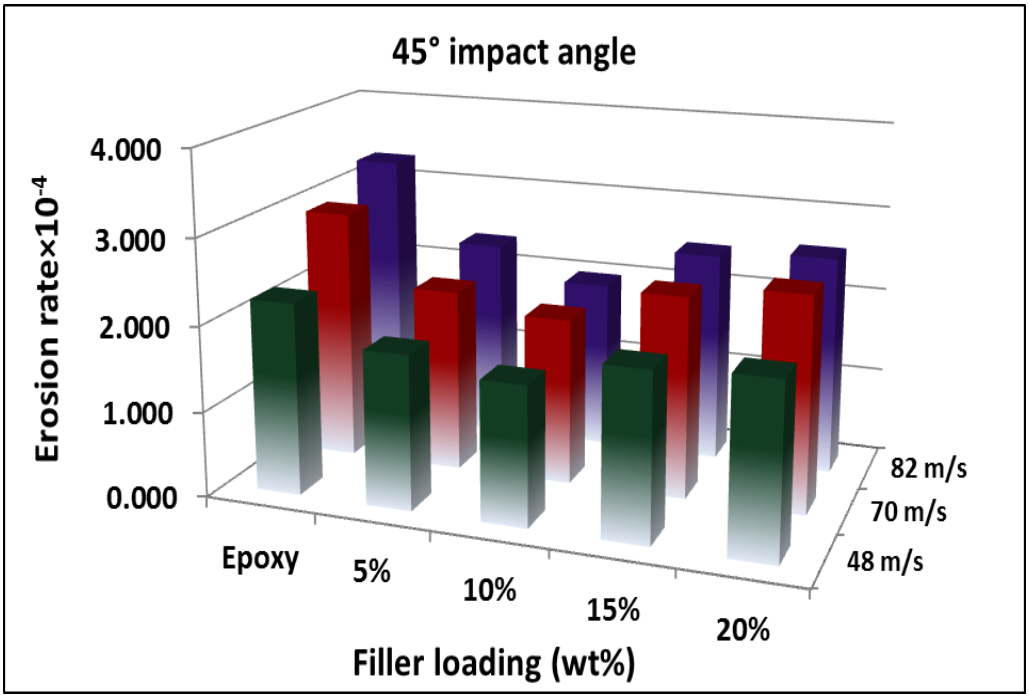

Figure 5.16 Histogram showing the effect of impact velocities on steady state erosive wear rates of raw coconut shell particulate composite for 45° impact angle

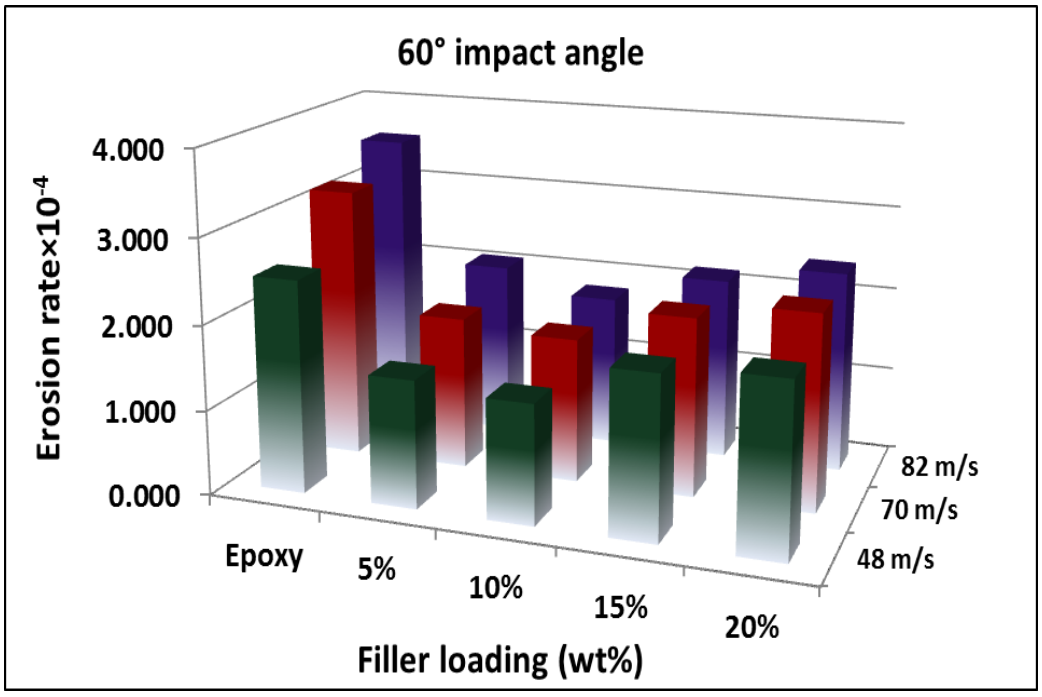

Figure 5.17 Histogram showing the effect of impact velocities on steady state erosive wear rates of raw coconut shell particulate composite for 60° impact angle

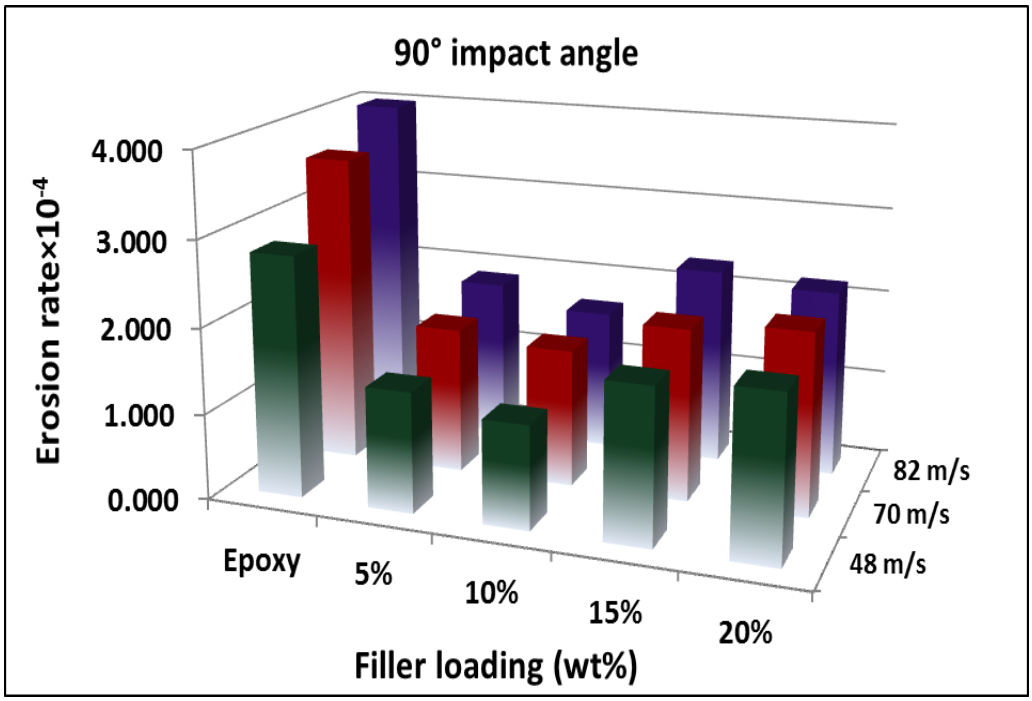

Figure 5.18 Histogram showing the effect of impact velocities on steady state erosive wear rates of raw coconut shell particulate composite for 90° impact angle

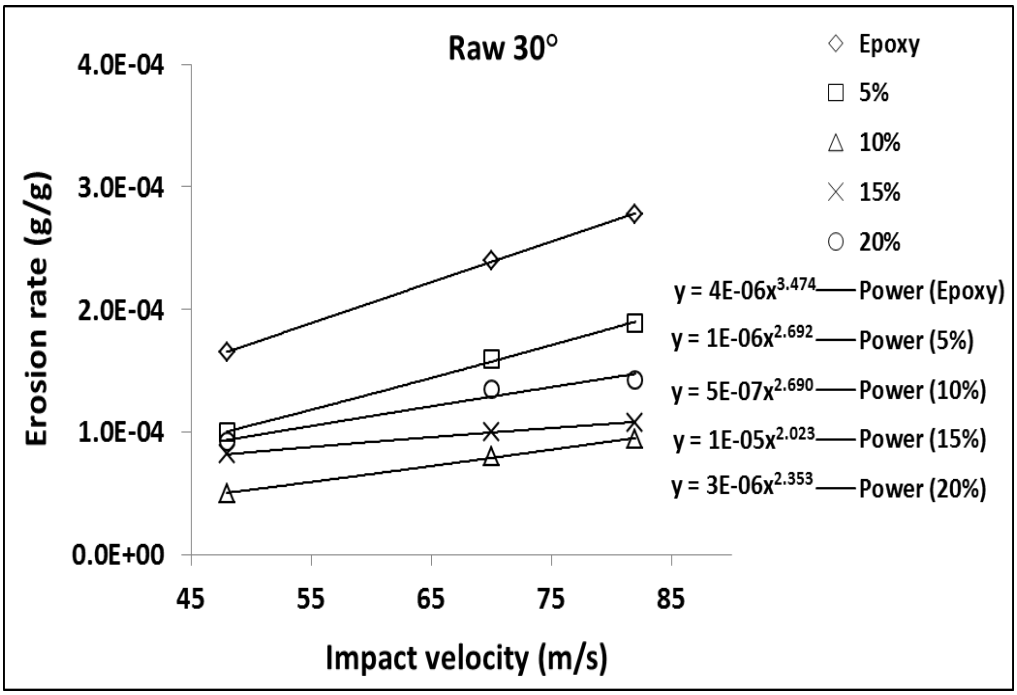

Figure 5.19 Erosion parameter of wood apple shell particulate composite at impact angle 30°

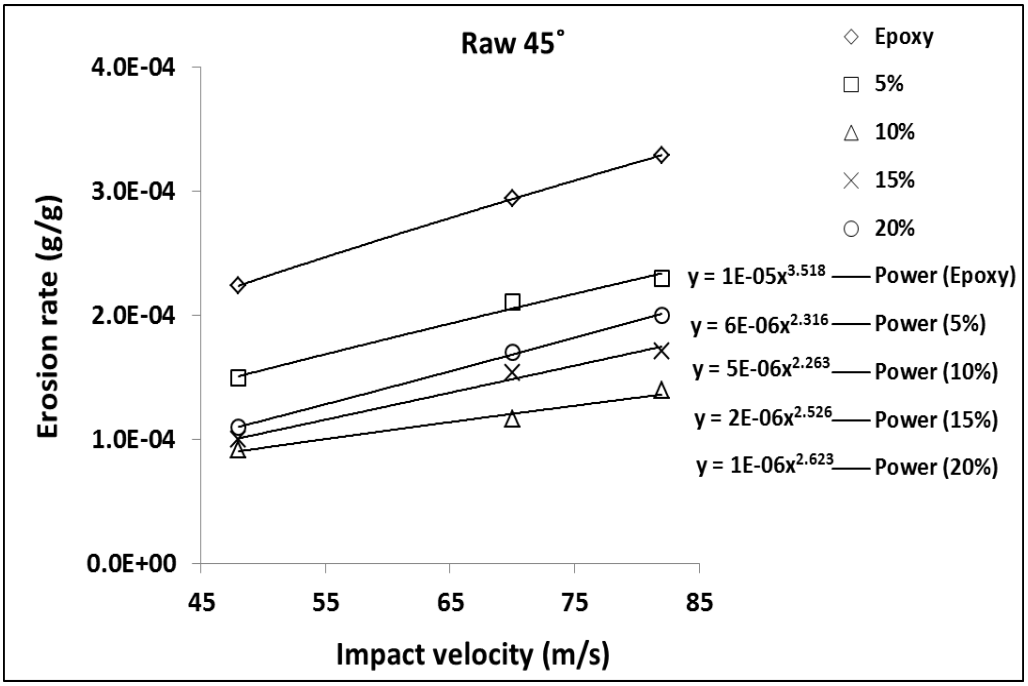

Figure 5.20 Erosion parameter of wood apple shell particulate composite at impact angle 45°

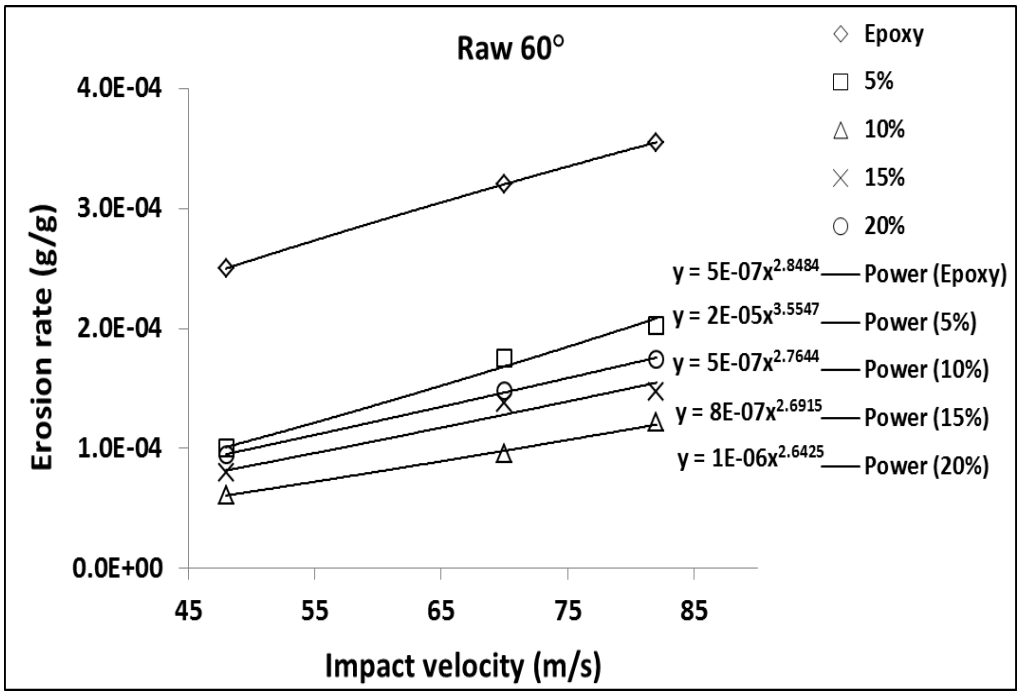

Figure 5.21 Erosion parameter of wood apple shell particulate composite at impact angle 60°

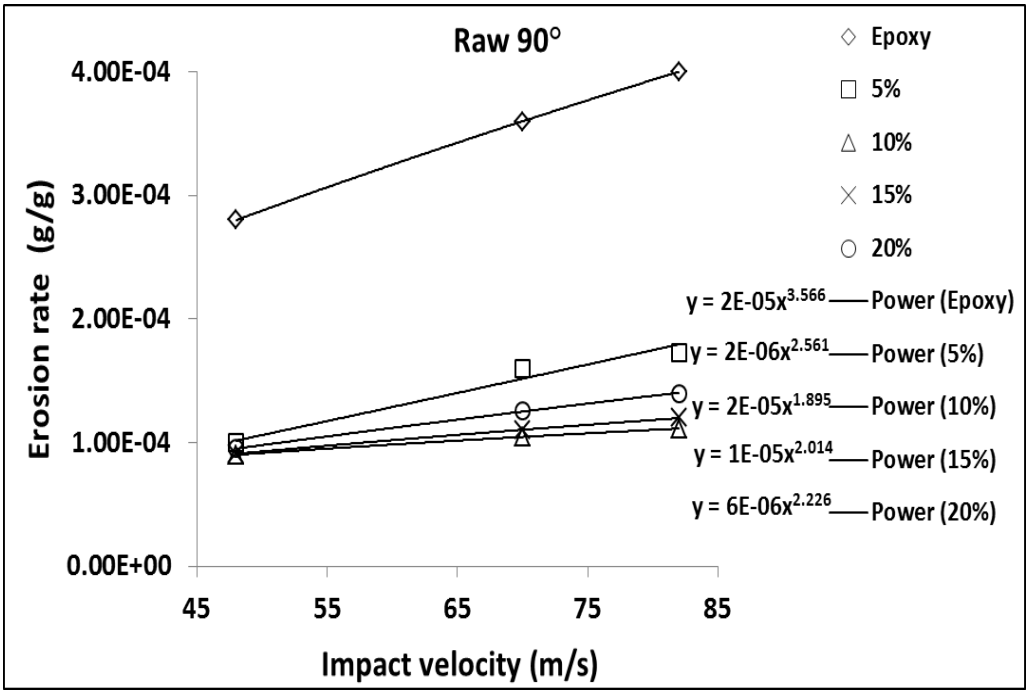

Figure 5.22 Erosion parameter of wood apple shell particulate composite at impact angle 90°

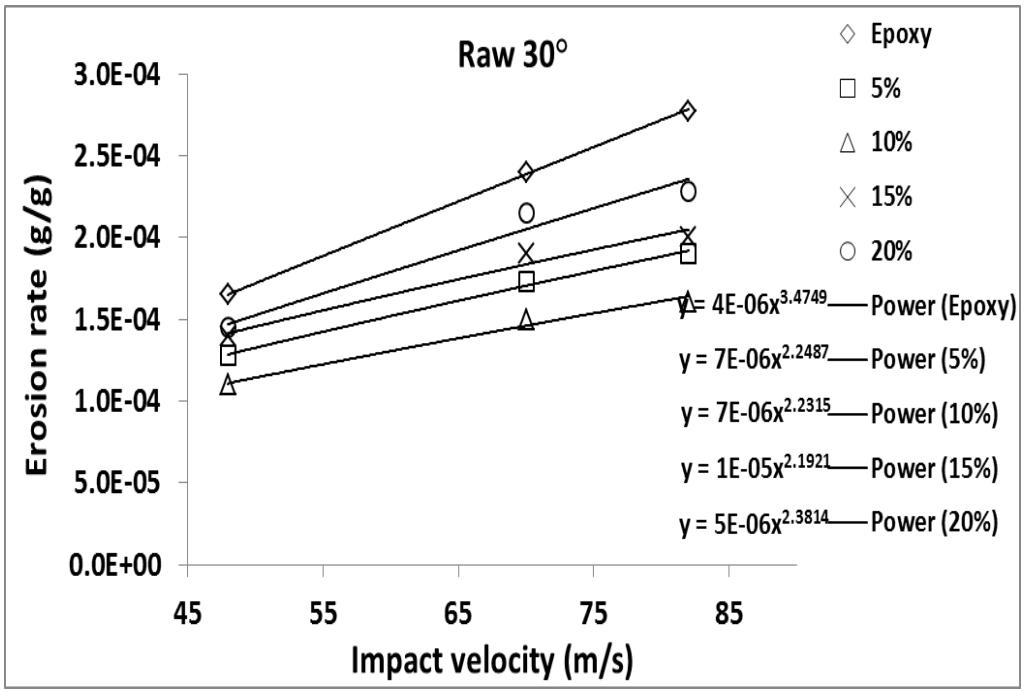

Figure 5.23 Erosion parameter of coconut shell particulate composite at impact angle 30°

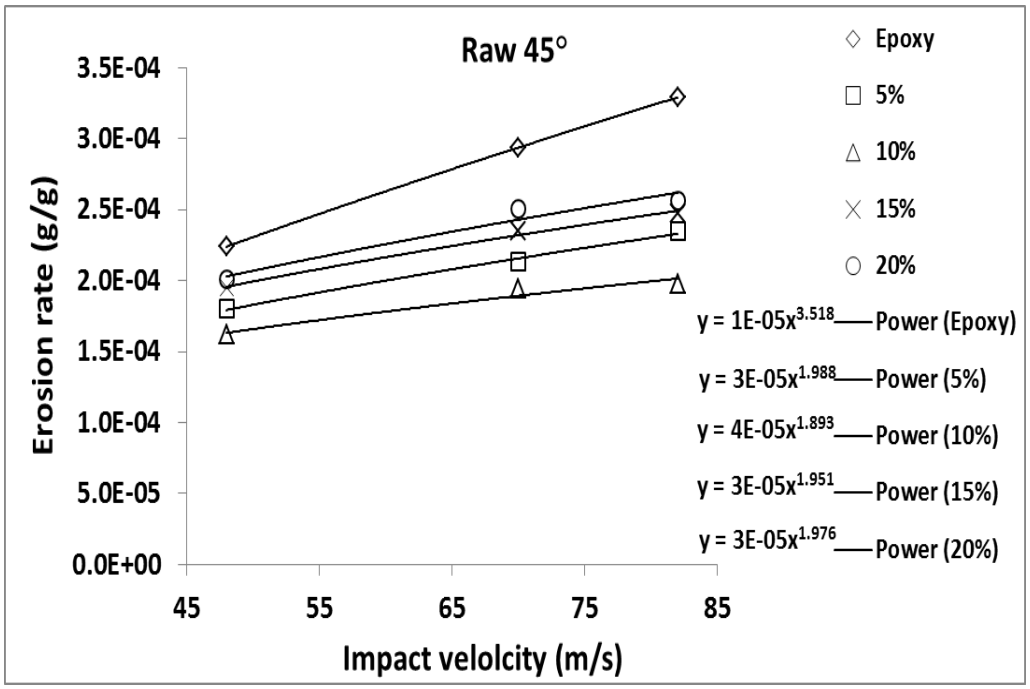

Figure 5.24 Erosion parameter of coconut shell particulate composite at impact angle 45°

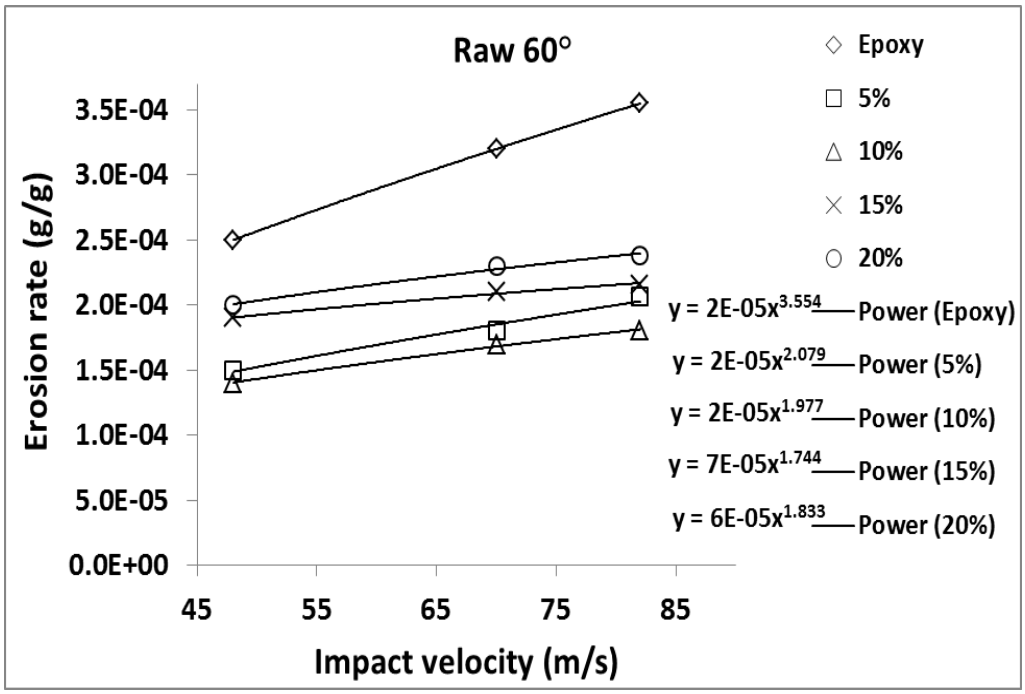

Figure 5.25 Erosion parameter of coconut shell particulate composite at impact angle 60°

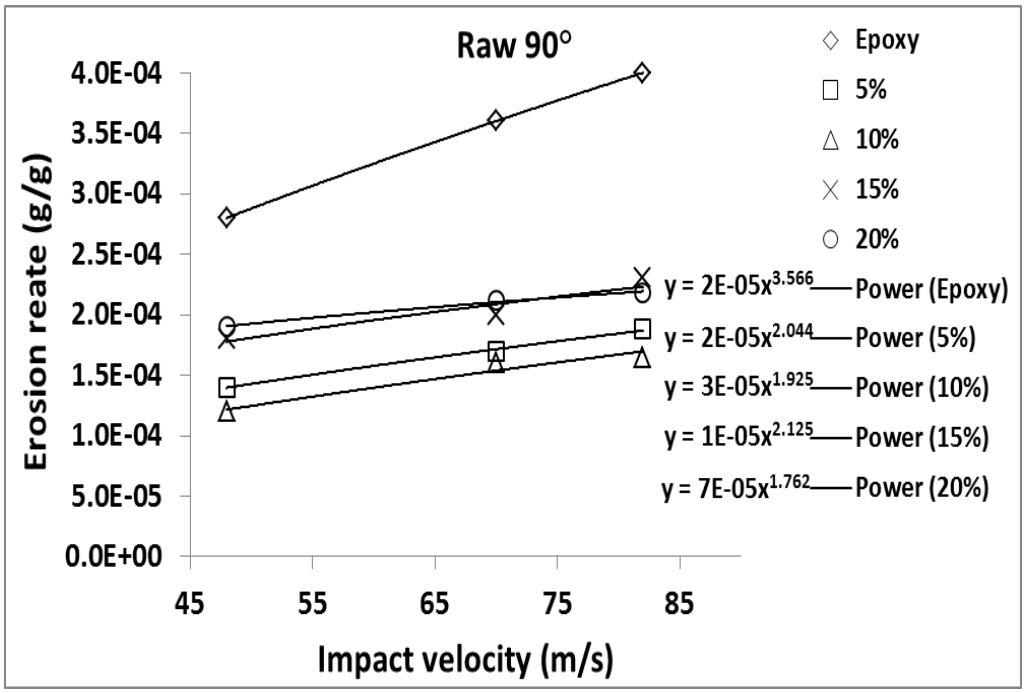

Figure 5.26 Erosion parameter of coconut shell particulate composite at impact angle 90°

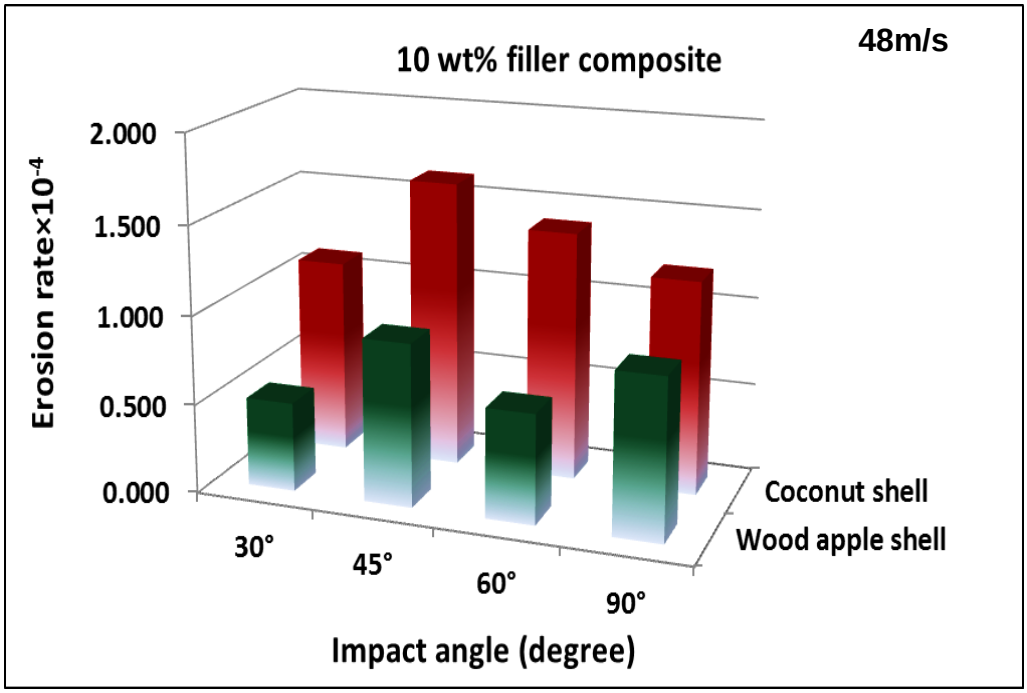

Figure 5.27 Histogram showing the comparison between raw wood apple and coconut shell particulate composite at 48m/s impact velocity with various impact angles

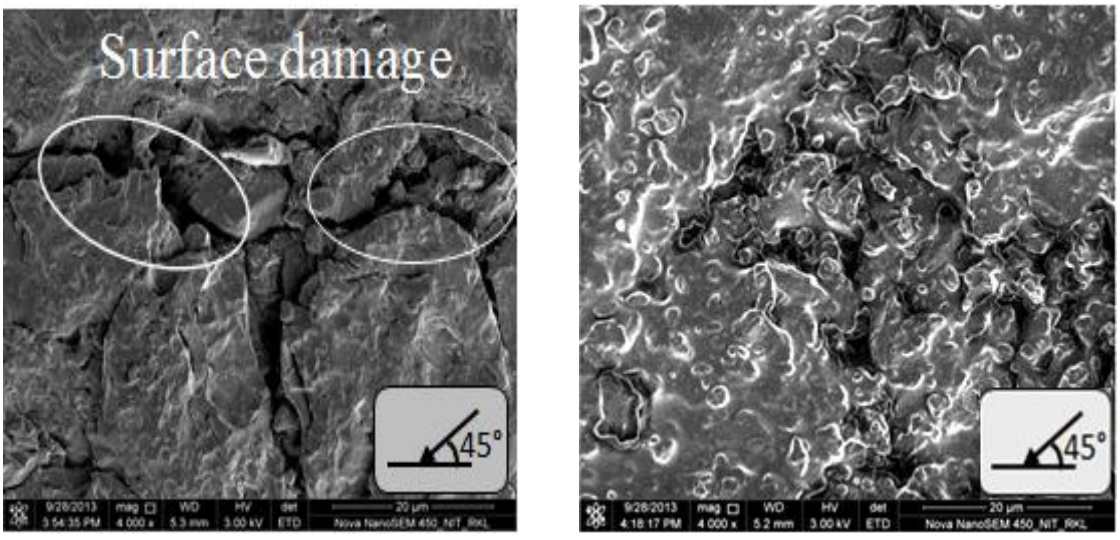

(a) **(b)**

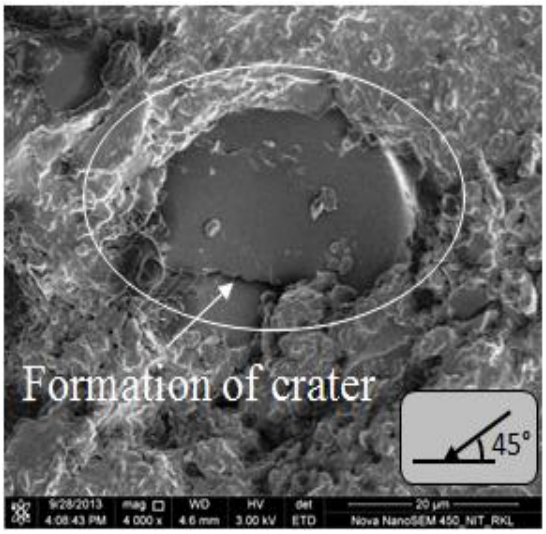

(c)

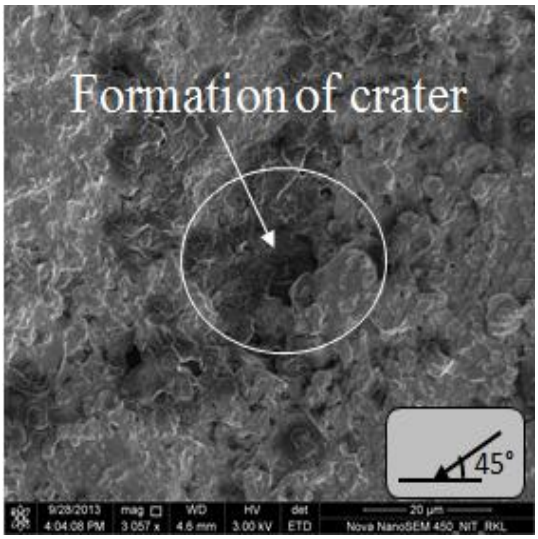

(d)

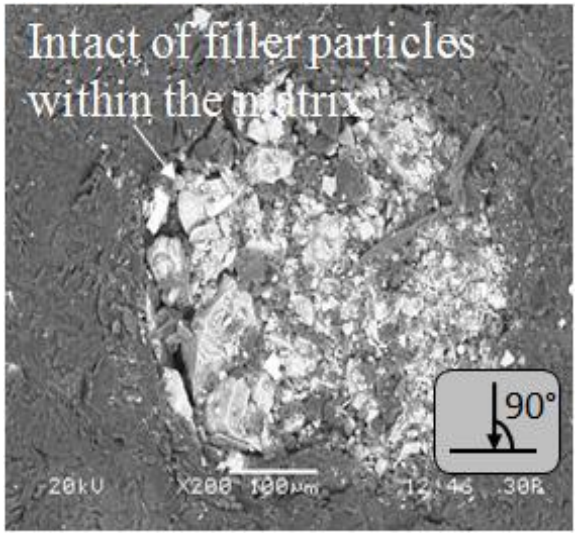

(e)

Figure 5.28 (a-e) SEM images of eroded surface of wood apple shell particulate composite after erosion at different impact angles

(a) 5wt% WAS composite at45° impact angle and impact velocity 48m/s

(b) 10wt% WAS composite at45impact angle and impact velocity 48m/s

(c) 15wt% WAS composite at 45°impact angle and impact velocity 48m/s

(d) 20wt% WAS composite at 45°impact angle and impact velocity 48m/s

(e) 10wt% WAS composite at 90° impact angle and impact velocity48m/s

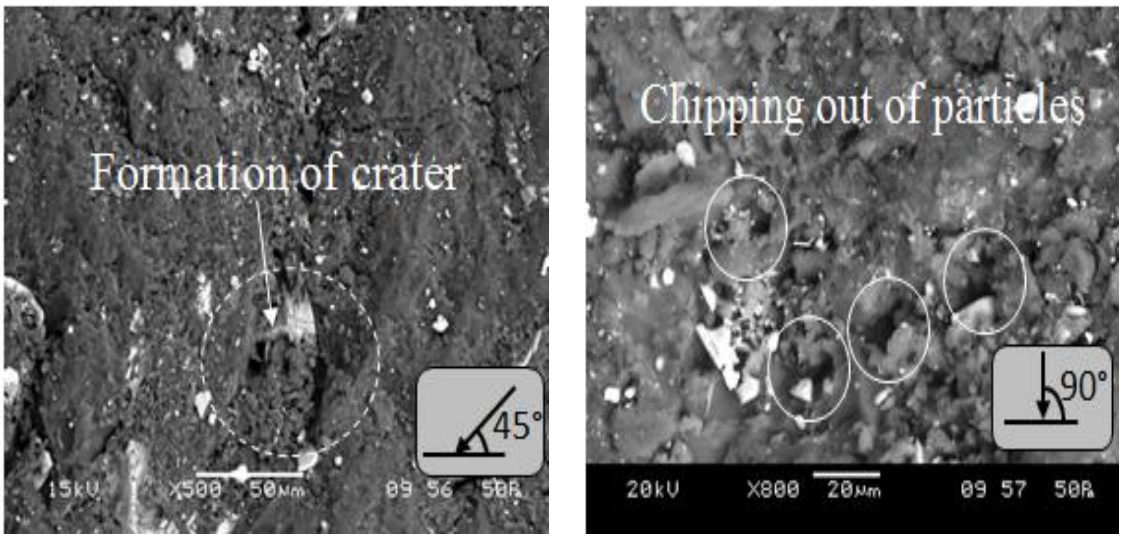

(a) **(b)**

Figure 5.29 (a-b) SEM images of eroded surface of coconut shell particulate composite after erosion

(a) 10wt% coconut shell composites at 45° impact angle and impact velocity 48m/s

(b) 10wt% coconut shell composites at 90° impact angle and impact velocity 48m/s

Chapter 6

Solid particle Erosion studies of Carbon black and Activated carbon black filled epoxy composite

6.1 INTRODUCTION

In the particulate reinforced polymer composites particles acts as load carrying material which increasesthe strength and modulus of the composite. Carbon fibres are carbonaceous material with fibrous shape with diameter of 5 to 10µm. the excellent properties of carbon fibres include high stiffness, light weight, high chemical resistance, high temperature tolerance and low thermal expansion.

Activated carbons, ACs, are well known porous carbonaceous materials which contain a large number of open or accessible micropores and mesopores [211, 212]. The traditional term for activated carbon is activated charcoal [213]. ACs are prepared in particulate form, either as powders (particles size <100µm, average diameter ~ 20µm) or granules (particle size in the range 100µm to several mm) [214]. Activated carbons can be made from nearly all carbon-rich and inexpensive precursors with a low content of inorganic substances: wood [213,215], lignite [216,217], coconut [218-219], peat [220-222], pistachio shell [223], walnut shell [224], saw dust [225], almond shell [226,227], charcoal [228], bituminous coal [229,230], brown coal [231], petroleum coke [232,233], etc.

In business world, cost of processing plays an important role for the use of activated carbon fibre (ACF) in applications. To reduce cost of processing, some emerging studies were performed in making use agricultural by-products in biomass form as raw materials to produce cost effective ACF [234-238]. Such raw materials are ready in fibre shape naturally. Making use of such biomass as ACF materials can solve the waste disposal problem, and at the same time turning waste into wealth.

Carbon black reinforced composites based on high performance thermosetting polymer such as epoxy is gaining an edge over the synthetic fiber due to better mechanical and tribological properties. Recently, conductive polymer composites obtained by filling polymer matrices with various carbon blacks were reported [239–240]. Carbon black is widely used for adsorption of pollutants from gaseous and liquid streams, for recovery of solvents, due to their high adsorptive capacities, porous size and relatively high mechanical strength. It is also used for coating, ink and inkjet application.

The literature is not exhaustive but limited to certain use in commercial and domestic applications of activated carbon. However as per the information of the author the use of ACF in tribological applications is meager.

Harsha et al. [241] discussed about the solid particle erosion behavior of various polyaryletherketones (PAEKs) composites at different impingement angles and impact velocities. The result shows that among various polyaryletherketones composite ketone/ether ratios showed significant influence on erosion behavior.

Tewari et al. [242] discussed about the solid particle erosion behavior of carbon fiber– and glass fiber–epoxy composites at different impingement angles and impact velocities. The result shows that carbon and glass fiber reinforced epoxy composites showed semi ductile erosion behavior, with maximum erosion rate at 60° impingement angle.

Tewari et al [243] evaluated solid particle erosion behavior of unidirectional carbon fiber (CF) reinforced polyetheretherketone (PEEK) compositesat different impingement angles (15–90°) for different fiber orientations (0, 45, and 90°).they have the opinion that the fiber orientations had a significant influence on erosion rate and unidirectional CF reinforced PEEK composites showed semi-ductile erosion behavior, with maximum erosion rate at 60° impingement angle.

Rattan et al. [244] developed Polyetherimide (PEI) composite reinforced with plain weave carbon fabric (CF) and characterized their physical and mechanical properties. From their resultsit was confirmed thatCarbon fabric (40% by volume) reinforced PEI composite fabricated using the impregnation technique exhibited improved mechanical properties compared to neat PEI. PEI and its composite though neither are ductile materials, exhibited erosion peaks at low angles of impingement (15° and 30°, respectively), which is generally seen in the case of ductile materials.

From the above discussion it is found that though carbon fiber applications in tribological area are available but no work on carbon black filler obtained from biomass for different tribological application are carried out till date.

Hence in the present work an attempt has been made to study the effect of carbon and activated carbon black filled composites obtained from different biomass such as wood apple shell and coconut shell on the solid particle erosion behaviour.

6.2 MATERIALS AND METHOD

6.2.1 Raw Materials Used

Raw materials used in the present experiment are:

1. Carbon and Activated carbon black of Wood apple shell and Coconut shell particles obtained at 400°C, 600°C, 800°Ccarbonization temperature and activated temp (800°C)
2. Epoxy resin and Hardener

6.2.1.1 Wood apple shell (WAS)

The details of the wood apple shell and its chemical constituents used for the present investigation are explained in chapter 3 art 3.2.1.

6.2.1.2 Coconut shell (CS)

The details of the coconut shell and its chemical constituents used for the present investigation are explained in chapter 3 art 3.2.2.

6.2.1.3 Methods of Carbonization and Activation

The details of the method for carbonized and activated carbon particles are explained in chapter 3 art 3.3.2 and 3.3.3.

6.2.1.4 Epoxy resin and Hardener

The details of the epoxy resin and hardener used for the present investigation are same as explained in chapter 4 art 4.2.2.

6.3 METHODS

6.3.1 Preparation of Composites

Preparation of the polymer composite with the filler addition is same as explained in chapter 4 art.4.3. The preparation of the test samples are carried out as per the procedure explained in chapter 4 art. 4.3. Specimens of dimensions 25×25×5mm^3 were cut from the slab produced and were used for erosion test.

6.3.2 Test apparatus & Experiment

The erosion test apparatus for the present case is one which is used earlier. The details of the test apparatus, procedure and the conditions under which the test has been carried out is same for this investigation also and has been discussed in details in chapter 5,art-5.7.3.

The experimental results of the weight loss and erosion efficiency for carbon and activated carbon black fillers addition with epoxy of both carbon and activated particulate composite with different impact angle and impact velocities are tabulated and presented in Table 6.1 to 6.40.

6.4 RESULTS AND DISCUSSION

Based on the tabulated results various graphs were plotted and presented in figure-6.1 to 6.16 for carbon and activated carbon fillersreinforced epoxy composite.

6.4.1 Effect of Impact angle (α) on erosion rate of Carbon and Activated carbon of Wood apple shell and Coconut shell particulate composites

Figure 6.1 to 6.4 illustrate the erosion wear rate of carbon black (400°C, 600°C and 800°C) and activated carbon black (800°C) reinforced epoxy composite as a function of impact angle (30°, 45°, 60° and 90°) under different impact velocities (48m/s, 70m/s and 82m/s).

In chapter 5 it was observed that neat epoxy composite exhibits brittle behavior and this brittle behavior changes from brittle to semi ductile nature due to addition of

raw particulates fillers in neat epoxy. In the present investigation it is found that that erosion wear properties were greatly influenced with the incorporation of carbon black and activated carbon black particles. From figure 6.1 it is seen that after addition of carbon black (400°C) particles with neat epoxy the peak erosion occur at 60° impact angle. Hence the nature of the carbon black composite which shows earlier semi ductile nature with raw wood apple shell (Figure 5.5) filled composite changes from semi ductile to semi brittle and minimum erosion rate is found with 10wt% particulate filled composite. Figure 6.2 and 6.3 are the plots of erosion rate for carbon black filled composites obtained at 600 and 800°C. It is interesting to note here that the behavior of the composite with these filler changes from semi brittle to brittle (i.e.) peak erosion takes place at 90°. Also minimum wear rate found with 20wt% of filler obtained at 800°C.

After addition of activated carbon black particles with neat epoxy the material loss reduced significantly as compared to other carbon black composites as well as maximum erosion rate occurs at 90°C impact angle which indicates brittle nature of the activated carbon black compositeis shown in figure 6.4.

The reduction in material loss in this particulate filled polymer composite is due to the presence of hard ceramic particles such as silicon carbide, zirconia and alumina in the filler material obtained with the increase in carbonization temperature. Presence of these ceramic particles increases thehardness. Also the KE associated with the erodent during impact is very well absorbed by the composite.

From figure 6.5 it is found that maximum ($E_{r\,max}$) occurs at 45° impact angle of carbon black (400°C) filled particulate composites which indicates the semi ductility nature of the composite and is similar to the nature shown by of the raw coconut shell particulate filled composite.Material loss is also found to decrease drastically compared to raw and neat epoxy composite. After addition of carbon black particulates obtained at 600°C with neat epoxy the behavior of the composite changes to semi brittle because maximum erosion occurs at 60° impact angle. It is also found minimum for 10wt% carbon black filled composite in composition to other which is shown in figure 6.6. With addition of carbon black obtained at 800°C the behavior of the composite again changed from semi brittle to pure brittle nature which is shown in figure 6.7.

The behavior of activated carbon black coconut shell composites is shown in figure 6.8 which follows the similar trend as figure 6.7 but material loss is reduced compared to other carbon black composites. Minimum wear is also found with 10wt% activated carbon black composite.

Though the behavior of the composite is same as pure epoxy and filled composite with carbon black and activated carbon, the interesting point with the filled composites are material loss significantly reduced from raw>carbon black obtained at 400°C>600°C>800°C>activated carbon black (800°C). This is the result of the presence of hard ceramic particles at these temperatures.

Due to chemical activation, surface area and adsorption capacity of the filler materials increases. As surface area increases the particle size decreases. Due to small particle size the dispersion of the particles in epoxy increases. Increase in the porous structure enhances the adsorption of epoxy with the particles and creates favorable interfacial bonding between the fillers and polymer. This is the reason that leads to high erosion resistance.

6.4.2 Effect of Impact velocity (v) on erosion rate of carbon and activated carbon of Wood apple shell and Coconut shell particulate composite

The effect of impact velocity of particle on erosion rate is also studied, and the results are presented in figure 6.9 to 6.12. It is evident from the figures that at low impact velocity 48m/s, there is not much variation in erosion rate. However, with further increase in impact velocity, the erosion rate increases significantly. This might have happen because at higher impact velocity, the erosion mainly occurs due to plastic deformation due to which amount of material removed is more. From the graphs it is seen thatwith increase in impact velocity from 48 to 82m/s there is a gradual increase in erosion rate when there is an increase in impact angle (i.e.) from 30° to 90°. This is because at a particular impact angle tangential component of the velocityand at 90° is maximum.

Effects of impact velocity on steady state erosive wear of coconut shell polymer composite is shown in figure 6.13 to 6.16. It is observed that coconut shell particulate

composites also showed similar type of behavior shown by wood apple shell particulate composites.

As mentioned earlier (art 5.2.2) influence of impact velocity (υ) on Erosive wear rate is one of the most important parameter for classifying the erosion behavior of any material. Figure 6.17 to 6.24 illustrates the variation of erosion rate with impact velocity at different impingement angle for activated carbon of wood apple and coconut shell particulate composites. The least-square fits to data point were obtained by using power law and the values of 'n' and 'k' are summarized in Table-6.41and 6.42. From, the figure 6.17 to 6.20 the velocity exponents found for 30°, 45°, 60° and 90° impingement angles are in the range of 2.934-4.442, 2.555-3.126, 2.328-3.898 and 2.027-2.949 respectively for the activated carbon black (wood apple shell) reinforced epoxy composites whereas from the figure 5.23 to 5.26 the velocity exponents found for 30°, 45°, 60° and 90° impingement angles are in the range of 3.884-5.205, 3.620-3.805, 2.438-3.231 and 2.430-3.284 respectively for the activated carbon black (coconut shell) reinforced epoxy composites.

As mentioned earlier (art 5.4.4) erosion efficiency is also one of the important parameter for classifying the erosion behavior of any material. The erosion efficiency of the wood apple and the coconut shell composites are listed in Table 6.17-6.20 and 6.37-6.40. The efficient ranges of the different composites 400°C,600°C,800°C and activated 800°C of both wood apple and coconut are 0.334-1.947, 0.052-1.180, 0.078-1.147, 0.064-1.115,(wood apple) 0.787-3.097, 0.314-1.995, 0.265-1.317 and 0.205-1.289(coconut) respectively.

It has been observed that the erosion efficiencies are decreasing as the carbonization temperature increasing. Further it is noticed that the erosion efficiency of activated carbon reinforced composites is very less when compared to carbonized carbon reinforced composite. From the values obtained it is clearly observed that carbon and activated carbon of wood apple is less when compared to coconut shell. This lower erosion efficiency indicates a better erosion resistance.

6.4.3 Comparison of both lignocellulosic polymer composites

A comparative analysis for wear properties of both wood apple and coconut shell activated polymer composite is shown in form of histogram in figure 6.25. Among all the carbon and activated carbon black composite, optimum result is found for 20wt% activated carbon black filled wood apple shell polymer composite exhibiting minimum wear. Hence a comparison has been shown here for both wood apple and coconut shell particulates composite at 48m/s velocity with 20wt% filler. All other velocity shows similar trend, therefore they are not shown here.

6.5 SEM ANALYSIS

In order to account for differences in the wear rates, scanning electron microscopy (SEM) was utilized to determine the mode of material removal and the benefits of impregnation or graphitization. Figure 6.26 shows the erodent surface of wood apple shell composite (20wt %) reinforced with 800°C activated carbon black particles. Due to the impact of hard silica sand particles on the surface of the composites at 45° impact angle grove formations on the surface are found to be less. Some minor surface cracks are visible.

Figure 6.27 shows the SEM image of 20wt% (activated) wood apple shell composite. It is clearly observed that due to impact of hard silica sand particles (90°) on the surface small grooves are formed on the entire surface. Same surface at higher magnification (figure 6.28) shows the detachment of particles from each other but no sign of chipping out of particles are found.

Figure 6.29is for the surface eroded at 90° impact angle for coconut shell particulate (activated carbon). Compared to the figure 6.27 which is for wood apple shell here the formation of grooves are larger and deeper. The same surface at higher magnification indicates (figure 6.30) that deeper groove formation is due to removal of particles from the surface. Due to repetitive impact of erodent, the particles are being chipped out leading to higher erosion for coconut shell particulates. Cracks that are formed on particle to particle surface area being enlarged and look like continuous crack lines.

6.6 CONCLUSION

Experiments were conducted to study the solid particle erosion behaviour of carbon and activated carbon black of wood apple and coconut shell particulate reinforced epoxy composites with silica sand as erodent. Developed compositeswere tested for their erosion resistance at various impingement angles and impact velocities for different filler weight fraction. Based on the studies, the following conclusions are drawn.

1. Among two carbon black (obtained at 800°C) polymer composite, under study (i.e.) wood apple shell and coconut shell. Wood apple shell polymer composite showed minimum wear(i.e.) erosion strength of composites reinforced with wood apple shell carbon black obtained at carbonization temperature of 800C is found to be higher in comparison to coconut shell carbon black.

2. Both carbon black reinforced epoxy composites exhibit brittle behaviour as maximum erosion takes place at 90° impact angle.

3. When reinforced with activated carbon black particles for both wood apple shell and coconut shell shows higher erosion resistance than composites reinforced with carbon black obtained from wood apple shell and coconut shell.

4. Hardness of carbon black polymer composite for both the cases increases with increase in carbonization temperature. For activation carbon filler composites higher hardness values are observed compared to carbon black composite.

5. From SEM analysis it is observed that material removal takes place due to less adherence strength between particles rather than chipping out of particles from the materials.

Table 6.1 Weight loss and erosion rate of 5wt% 400°C CB WAS particulate composites with respect to impact angle due to erosion for a period of 600 seconds

Impact Velocity (m/s)	Impact Angle (°)	5wt% 400°C CB	
		Weight loss (g)	Erosion rate×10^{-4} (g/g)
48	30	0.0012	0.62
	45	0.0018	0.88
	60	0.0023	1.13
	90	0.0015	0.75
70	30	0.0019	0.94
	45	0.0026	1.30
	60	0.0033	1.65
	90	0.0026	1.30
82	30	0.0024	1.21
	45	0.0030	1.50
	60	0.0039	1.94
	90	0.0028	1.42

Table 6.2 Weight loss and erosion rate of 10wt% 400°C CB WAS particulate composites with respect to impact angle due to erosion for a period of 600 seconds

Impact Velocity (m/s)	Impact Angle (°)	10wt% 400°C CB	
		Weight loss (g)	Erosion rate×10^{-4} (g/g)
48	30	0.0003	0.17
	45	0.0006	0.29
	60	0.0010	0.50
	90	0.0004	0.22
70	30	0.0012	0.60
	45	0.0016	0.82
	60	0.0018	0.92
	90	0.0012	0.61
82	30	0.0015	0.77
	45	0.0020	1.01
	60	0.0024	1.20
	90	0.0017	0.86

Table 6.3 Weight loss and erosion rate of 15wt% 400°C CB WAS particulate composites with respect to impact angle due to erosion for a period of 600 seconds

Impact Velocity (m/s)	Impact Angle (°)	15wt% 400°C CB	
		Weight loss (g)	Erosion rate×10^{-4} (g/g)
48	30	0.0005	0.25
	45	0.0007	0.37
	60	0.0012	0.62
	90	0.0008	0.40
70	30	0.0014	0.70
	45	0.0018	0.88
	60	0.0023	1.15
	90	0.0016	0.81
82	30	0.0018	0.89
	45	0.0023	1.13
	60	0.0029	1.43
	90	0.0020	1.01

Table 6.4 Weight loss and erosion rate of 20wt% 400°C CB WAS particulate composites with respect to impact angle due to erosion for a period of 600 seconds

Impact Velocity (m/s)	Impact Angle (°)	20wt% 400°C CB	
		Weight loss (g)	Erosion rate×10^{-4} (g/g)
48	30	0.0006	0.31
	45	0.0011	0.53
	60	0.0018	0.88
	90	0.0010	0.48
70	30	0.0017	0.83
	45	0.0021	1.05
	60	0.0028	1.40
	90	0.0020	1.00
82	30	0.0021	1.03
	45	0.0027	1.33
	60	0.0033	1.64
	90	0.0024	1.20

Table 6.5 Weight loss and erosion rate of 5wt% 600°C CB WAS particulate composites with respect to impact angle due to erosion for a period of 600 seconds

Impact Velocity (m/s)	Impact Angle (°)	5wt% 600°C CB	
		Weight loss (g)	Erosion rate×10^{-4} (g/g)
48	30	0.0005	0.23
	45	0.0005	0.25
	60	0.0010	0.48
	90	0.0012	0.62
70	30	0.0007	0.33
	45	0.0007	0.35
	60	0.0012	0.58
	90	0.0014	0.72
82	30	0.0008	0.40
	45	0.0008	0.39
	60	0.0012	0.60
	90	0.0016	0.80

Table 6.6 Weight loss and erosion rate of 10wt% 600°C CB WAS particulate composites with respect to impact angle due to erosion for a period of 600 seconds

Impact Velocity (m/s)	Impact Angle (°)	10wt% 600°C CB	
		Weight loss (g)	Erosion rate×10^{-4} (g/g)
48	30	0.0003	0.15
	45	0.0004	0.22
	60	0.0008	0.38
	90	0.0010	0.57
70	30	0.0007	0.35
	45	0.0006	0.32
	60	0.0008	0.38
	90	0.0013	0.67
82	30	0.0007	0.36
	45	0.0007	0.34
	60	0.0008	0.40
	90	0.0014	0.69

Table 6.7 Weight loss and erosion rate of 15wt% 600°C CB WAS particulate composites with respect to impact angle due to erosion for a period of 600 seconds

Impact Velocity (m/s)	Impact Angle (°)	15wt% 600°C CB	
		Weight loss (g)	Erosion rate×10^{-4} (g/g)
48	30	0.0002	0.11
	45	0.0003	0.17
	60	0.0005	0.23
	90	0.0010	0.50
70	30	0.0004	0.21
	45	0.0005	0.27
	60	0.0007	0.33
	90	0.0012	0.60
82	30	0.0005	0.23
	45	0.0006	0.28
	60	0.0007	0.34
	90	0.0012	0.62

Table 6.8 Weight loss and erosion rate of 20wt% 600°C CB WAS particulate composites with respect to impact angle due to erosion for a period of 600 seconds

Impact Velocity (m/s)	Impact Angle (°)	20wt% 600°C CB	
		Weight loss (g)	Erosion rate×10^{-4} (g/g)
48	30	0.0002	0.08
	45	0.0003	0.13
	60	0.0004	0.19
	90	0.0010	0.48
70	30	0.0002	0.08
	45	0.0005	0.23
	60	0.0006	0.29
	90	0.0012	0.58
82	30	0.0002	0.12
	45	0.0004	0.22
	60	0.0005	0.27
	90	0.0012	0.60

Table 6.9 Weight loss and erosion rate of 5wt% 800°C CB WAS particulate composites with respect to impact angle due to erosion for a period of 600 seconds

Impact Velocity (m/s)	Impact Angle (°)	5wt% 800°C CB	
		Weight loss (g)	Erosion rate×10^{-4} (g/g)
48	30	0.0004	0.18
	45	0.0005	0.25
	60	0.0009	0.43
	90	0.0012	0.59
70	30	0.0005	0.24
	45	0.0007	0.33
	60	0.0010	0.51
	90	0.0013	0.67
82	30	0.0005	0.26
	45	0.0007	0.35
	60	0.0011	0.53
	90	0.0014	0.69

Table 6.10 Weight loss and erosion rate of 10wt% 800°C CB WAS particulate composites with respect to impact angle due to erosion for a period of 600 seconds

Impact Velocity (m/s)	Impact Angle (°)	10wt% 800°C CB	
		Weight loss (g)	Erosion rate×10^{-4} (g/g)
48	30	0.0002	0.11
	45	0.0004	0.18
	60	0.0007	0.33
	90	0.0010	0.51
70	30	0.0004	0.21
	45	0.0006	0.29
	60	0.0009	0.45
	90	0.0012	0.59
82	30	0.0005	0.23
	45	0.0006	0.31
	60	0.0009	0.46
	90	0.0012	0.61

Table 6.11 Weight loss and erosion rate of 15wt% 800°C CB WAS particulate composites with respect to impact angle due to erosion for a period of 600 seconds

Impact Velocity (m/s)	Impact Angle (°)	15wt% 800°C CB	
		Weight loss (g)	Erosion rate×10^{-4} (g/g)
48	30	0.0002	0.09
	45	0.0003	0.15
	60	0.0004	0.21
	90	0.0009	0.45
70	30	0.0002	0.12
	45	0.0004	0.18
	60	0.0006	0.332
	90	0.0011	0.55
82	30	0.0003	0.14
	45	0.0004	0.20
	60	0.0007	0.34
	90	0.0011	0.56

Table 6.12 Weight loss and erosion rate of 20wt% 800°C CB WAS particulate composites with respect to impact angle due to erosion for a period of 600 seconds

Impact Velocity (m/s)	Impact Angle (°)	20wt% 800°C CB	
		Weight loss (g)	Erosion rate×10^{-4} (g/g)
48	30	0.0001	0.06
	45	0.0002	0.09
	60	0.0003	0.15
	90	0.0008	0.39
70	30	0.0001	0.06
	45	0.0003	0.15
	60	0.0004	0.21
	90	0.0010	0.49
82	30	0.0002	0.10
	45	0.0003	0.17
	60	0.0005	0.23
	90	0.0010	0.51

Table 6.13 Weight loss and erosion rate of 5wt% ACB WAS particulate composites with respect to impact angle due to erosion for a period of 600 seconds

Impact Velocity (m/s)	Impact Angle (°)	5wt% ACB(800°C)	
		Weight loss (g)	Erosion rate×10^{-4} (g/g)
48	30	0.0002	0.08
	45	0.0003	0.16
	60	0.0006	0.31
	90	0.0009	0.47
70	30	0.0004	0.21
	45	0.0005	0.27
	60	0.0008	0.41
	90	0.0011	0.56
82	30	0.0005	0.26
	45	0.0007	0.35
	60	0.0011	0.53
	90	0.0014	0.69

Table 6.14 Weight loss and erosion rate of 10wt% ACB WAS particulate composites with respect to impact angle due to erosion for a period of 600 seconds

Impact Velocity (m/s)	Impact Angle (°)	10wt% ACB(800°C)	
		Weight loss (g)	Erosion rate×10^{-4} (g/g)
48	30	0.0002	0.08
	45	0.0003	0.13
	60	0.0004	0.20
	90	0.0008	0.41
70	30	0.0003	0.17
	45	0.0004	0.22
	60	0.0007	0.33
	90	0.0010	0.49
82	30	0.0004	0.19
	45	0.0005	0.26
	60	0.0008	0.39
	90	0.0011	0.56

Table 6.15 Weight loss and erosion rate of 15wt% ACB WAS particulate composites with respect to impact angle due to erosion for a period of 600 seconds

Impact Velocity (m/s)	Impact Angle (°)	15wt% ACB(800°C)	
		Weight loss (g)	Erosion rate×10^{-4} (g/g)
48	30	0.0001	0.05
	45	0.0002	0.10
	60	0.0003	0.14
	90	0.0007	0.33
70	30	0.0001	0.07
	45	0.0003	0.14
	60	0.0005	0.24
	90	0.0009	0.44
82	30	0.0002	0.12
	45	0.0004	0.18
	60	0.0006	0.31
	90	0.0010	0.50

Table 6.16 Weight loss and erosion rate of 20wt% ACB WAS particulate composites with respect to impact angle due to erosion for a period of 600 seconds

Impact Velocity (m/s)	Impact Angle (°)	20wt% ACB(800°C)	
		Weight loss (g)	Erosion rate×10^{-4} (g/g)
48	30	0.00002	0.01
	45	0.0001	0.03
	60	0.0001	0.06
	90	0.0004	0.20
70	30	0.0001	0.03
	45	0.0002	0.11
	60	0.0004	0.18
	90	0.0007	0.37
82	30	0.0001	0.06
	45	0.0003	0.13
	60	0.0004	0.20
	90	0.0008	0.42

Table 6.17 Erosion efficiency of 400°C CB WAS particulate epoxy composites

Impact Velocity (m/s)	Impact Angle (°)	Erosion efficiency (η)				
		Neat Epoxy	5wt% 400°C CB	10wt% 400°C CB	15wt% 400°C CB	20wt% 400°C CB
		Hv=MPa 190.452	Hv=MPa 234.583	Hv=MPa 254.001	Hv=MPa 259.963	Hv=MPa 148.117
48	30	2.312	1.082	0.334	0.491	0.621
	45	3.138	1.514	0.587	0.737	1.034
	60	3.503	1.947	0.997	1.229	1.724
	90	3.923	1.298	0.449	0.786	0.936
70	30	1.581	0.617	0.395	0.461	0.550
	45	1.937	0.856	0.537	0.582	0.692
	60	2.108	0.087	0.603	0.758	0.919
	90	2.372	0.856	0.399	0.534	0.659
82	30	1.332	0.719	0.524	0.598	0.695
	45	1.579	0.889	0.689	0.761	0.894
	60	1.704	1.150	0.822	0.963	1.105
	90	1.920	0.839	0.587	0.677	0.810

Table 6.18 Erosion efficiency of 600°C CB WAS particulate epoxy composites

Impact Velocity (m/s)	Impact Angle (°)	Erosion efficiency (η)				
		Neat Epoxy	5wt% 600°C CB	10wt% 600°C CB	15wt% 600°C CB	20wt% 600°C CB
		Hv=MPa 190.452	Hv=MPa 237.918	Hv=MPa 255.963	Hv=MPa 263.808	Hv=MPa 267.731
48	30	2.312	0.407	0.326	0.232	0.161
	45	3.138	0.452	0.475	0.360	0.277
	60	3.503	0.859	0.813	0.463	0.397
	90	3.923	1.180	1.247	1.030	1.033
70	30	1.581	0.214	0.231	0.140	0.052
	45	1.937	0.231	0.210	0.181	0.151
	60	2.108	0.379	0.247	0.214	0.188
	90	2.372	0.478	0.445	0.395	0.384
82	30	1.332	0.247	0.268	0.165	0.089
	45	1.579	0.244	0.252	0.201	0.161
	60	1.704	0.369	0.298	0.237	0.199
	90	1.920	0.494	0.512	0.438	0.442

Table 6.19 Erosion efficiency of 800°C CB WAS particulate epoxy composites

Impact Velocity (m/s)	Impact Angle (°)	Erosion efficiency (η)				
		Neat Epoxy	5wt% 800°C CB	10wt% 800°C CB	15wt% 800°C CB	20wt% 800°C CB
		Hv=MPa 190.452	Hv=MPa 243.704	Hv=MPa 259.886	Hv=MPa 266.75	Hv=MPa 269.693
48	30	2.312	0.361	0.276	0.235	0.155
	45	3.138	0.494	0.449	0.394	0.257
	60	3.503	0.855	0.824	0.541	0.396
	90	3.923	1.147	1.077	1.142	1.069
70	30	1.581	0.226	0.248	0.149	0.078
	45	1.937	0.307	0.341	0.221	0.189
	60	2.108	0.477	0.529	0.387	0.273
	90	2.372	0.628	0.695	0.657	0.631
82	30	1.332	0.178	0.198	0.123	0.094
	45	1.579	0.237	0.265	0.172	0.156
	60	1.704	0.361	0.395	0.299	0.218
	90	1.920	0.471	0.523	0.487	0.478

Table 6.20 Erosion efficiency of ACB (800°C) WAS particulate epoxy composites

Impact Velocity (m/s)	Impact Angle (°)	Erosion efficiency (η)				
		Neat Epoxy	5wt% ACB	10wt% ACB	15wt% ACB	20 wt% ACB
		Hv=MPa 190.452	Hv=MPa 254.59	Hv=MPa 266.848	Hv=MPa 274.4	Hv=MPa 283.717
48	30	2.312	0.193	0.275	0.224	0.064
	45	3.138	0.418	0.441	0.427	0.179
	60	3.503	0.799	0.682	0.609	0.312
	90	3.923	1.115	1.099	1.038	1.035
70	30	1.581	0.256	0.273	0.150	0.076
	45	1.937	0.325	0.352	0.290	0.269
	60	2.108	0.496	0.529	0.479	0.448
	90	2.372	0.679	0.786	0.882	0.910
82	30	1.332	0.213	0.222	0.175	0.112
	45	1.579	0.289	0.303	0.260	0.238
	60	1.704	0.432	0.456	0.451	0.362
	90	1.920	0.556	0.655	0.730	0.752

Table 6.21 Weight loss and erosion rate of 5wt% 400°C CB CS particulate composites with respect to impact angle due to erosion for a period of 600 seconds

Impact Velocity (m/s)	Impact Angle (°)	5wt% 400°C CB	
		Weight loss (g)	Erosion rate×10^{-4} (g/g)
48	30	0.0020	0.83
	45	0.0030	1.80
	60	0.0024	1.50
	90	0.0022	1.40
70	30	0.0026	1.30
	45	0.0030	1.50
	60	0.0035	1.77
	90	0.0030	1.50
82	30	0.0032	1.60
	45	0.0034	1.70
	60	0.0040	1.98
	90	0.0032	1.60

Table 6.22 Weight loss and erosion rate of 10wt% 400°C CB CS particulate composites with respect to impact angle due to erosion for a period of 600 seconds

Impact Velocity (m/s)	Impact Angle (°)	10wt% 400°C CB	
		Weight loss (g)	Erosion rate×10^{-4} (g/g)
48	30	0.0016	1.10
	45	0.0026	1.62
	60	0.0022	1.40
	90	0.0020	1.20
70	30	0.0018	0.90
	45	0.0018	0.92
	60	0.0028	1.40
	90	0.0017	0.83
82	30	0.0028	1.40
	45	0.0030	1.50
	60	0.0034	1.70
	90	0.0030	1.50

Table 6.23 Weight loss and erosion rate of 15wt% 400°C CB CS particulate composites with respect to impact angle due to erosion for a period of 600 seconds

Impact Velocity (m/s)	Impact Angle (°)	15wt% 400°C CB	
		Weight loss (g)	Erosion rate×10^{-4} (g/g)
48	30	0.0024	1.40
	45	0.0034	1.95
	60	0.0030	1.90
	90	0.0028	1.80
70	30	0.0030	1.50
	45	0.0032	1.61
	60	0.0038	1.91
	90	0.0024	1.20
82	30	0.0036	1.80
	45	0.0038	1.90
	60	0.0042	2.10
	90	0.0034	1.70

Table 6.24 Weight loss and erosion rate of 20wt% 400°C CB CS particulate composites with respect to impact angle due to erosion for a period of 600 seconds

Impact Velocity (m/s)	Impact Angle (°)	20wt% 400°C CB	
		Weight loss (g)	Erosion rate×10^{-4} (g/g)
48	30	0.0025	1.45
	45	0.0036	2.01
	60	0.0032	2.00
	90	0.0034	1.90
70	30	0.0035	1.73
	45	0.0037	1.84
	60	0.0042	2.11
	90	0.0034	1.71
82	30	0.0040	2.00
	45	0.0043	2.17
	60	0.0046	2.31
	90	0.0042	2.11

Table 6.25 Weight loss and erosion rate of 5wt% 600°C CB CS particulate composites with respect to impact angle due to erosion for a period of 600 seconds

Impact Velocity (m/s)	Impact Angle (°)	5wt% 600°C CB	
		Weight loss (g)	Erosion rate×10^{-4} (g/g)
48	30	0.0010	0.52
	45	0.0013	0.65
	60	0.0019	0.95
	90	0.0010	0.50
70	30	0.0020	1.00
	45	0.0024	1.20
	60	0.0026	1.30
	90	0.0022	1.10
82	30	0.0028	1.40
	45	0.0030	1.50
	60	0.0036	1.80
	90	0.0028	1.40

Table 6.26 Weight loss and erosion rate of 10wt% 600°C CB CS particulate composites with respect to impact angle due to erosion for a period of 600 seconds

Impact Velocity (m/s)	Impact Angle (°)	10wt% 600°C CB	
		Weight loss (g)	Erosion rate×10^{-4} (g/g)
48	30	0.0003	0.16
	45	0.0005	0.27
	60	0.0008	0.39
	90	0.0004	0.19
70	30	0.0014	0.70
	45	0.0015	0.73
	60	0.0022	1.10
	90	0.0015	0.73
82	30	0.0024	1.20
	45	0.0022	1.10
	60	0.0030	1.50
	90	0.0026	1.30

Table 6.27 Weight loss and erosion rate of 15wt% 600°C CB CS particulate composites with respect to impact angle due to erosion for a period of 600 seconds

Impact Velocity (m/s)	Impact Angle (°)	15wt% 600°C CB	
		Weight loss (g)	Erosion rate×10^{-4} (g/g)
48	30	0.0005	0.24
	45	0.0006	0.31
	60	0.0010	0.49
	90	0.0007	0.33
70	30	0.0024	1.20
	45	0.0026	1.30
	60	0.0030	1.50
	90	0.0020	1.00
82	30	0.0032	1.60
	45	0.0028	1.40
	60	0.0040	2.00
	90	0.0032	1.60

Table 6.28 Weight loss and erosion rate of 20wt% 600°C CB CS particulate composites with respect to impact angle due to erosion for a period of 600 seconds

Impact Velocity (m/s)	Impact Angle (°)	20wt% 600°C CB	
		Weight loss (g)	Erosion rate×10^{-4} (g/g)
48	30	0.0006	0.28
	45	0.0010	0.48
	60	0.0015	0.76
	90	0.0008	0.40
70	30	0.0028	1.40
	45	0.0030	1.51
	60	0.0034	1.71
	90	0.0022	0.10
82	30	0.0036	1.80
	45	0.0034	1.70
	60	0.0042	2.10
	90	0.0038	1.90

Table 6.29 Weight loss and erosion rate of 5 wt% 800°C CB CS particulate composites with respect to impact angle due to erosion for a period of 600 seconds

Impact Velocity (m/s)	Impact Angle (°)	5wt% 800°C CB	
		Weight loss (g)	Erosion rate×10^{-4} (g/g)
48	30	0.0008	0.42
	45	0.0011	0.54
	60	0.0013	0.65
	90	0.0017	0.87
70	30	0.0020	0.98
	45	0.0020	1.00
	60	0.0018	0.91
	90	0.0022	1.08
82	30	0.0026	1.30
	45	0.0024	1.20
	60	0.0022	1.10
	90	0.0027	1.35

Table 6.30 Weight loss and erosion rate of 10wt% 800°C CB CS particulate composites with respect to impact angle due to erosion for a period of 600 seconds

Impact Velocity (m/s)	Impact Angle (°)	10wt% 800°C CB	
		Weight loss (g)	Erosion rate×10^{-4} (g/g)
48	30	0.0002	0.12
	45	0.0004	0.22
	60	0.0006	0.32
	90	0.0011	0.53
70	30	0.0012	0.60
	45	0.0010	0.50
	60	0.0012	0.58
	90	0.0013	0.67
82	30	0.0018	0.90
	45	0.0014	0.70
	60	0.0015	0.73
	90	0.0020	1.00

Table 6.31 Weight loss and erosion rate of 15wt% 800°C CB CS particulate composites with respect to impact angle due to erosion for a period of 600 seconds

Impact Velocity (m/s)	Impact Angle (°)	15wt% 800°C CB	
		Weight loss (g)	Erosion rate×10^{-4} (g/g)
48	30	0.0004	0.20
	45	0.0005	0.27
	60	0.0008	0.41
	90	0.0009	0.46
70	30	0.0014	0.70
	45	0.0016	0.80
	60	0.0014	0.70
	90	0.0018	0.90
82	30	0.0016	0.80
	45	0.0018	0.90
	60	0.0016	0.80
	90	0.0024	1.20

Table 6.32 Weight loss and erosion rate of 20wt% 800°C CB CS particulate composites with respect to impact angle due to erosion for a period of 600 seconds

Impact Velocity (m/s)	Impact Angle (°)	20wt% 800°C CB	
		Weight loss (g)	Erosion rate×10^{-4} (g/g)
48	30	0.0004	0.22
	45	0.0009	0.43
	60	0.0010	0.52
	90	0.0017	0.85
70	30	0.0020	1.00
	45	0.0017	0.85
	60	0.0017	0.84
	90	0.0020	1.00
82	30	0.0020	1.00
	45	0.0022	1.10
	60	0.0018	0.90
	90	0.0029	1.43

Table 6.33 Weight loss and erosion rate of 5wt% ACB CS particulate composites with respect to impact angle due to erosion for a period of 600 seconds

Impact Velocity (m/s)	Impact Angle (°)	5wt% ACB(800°C)	
		Weight loss (g)	Erosion rate×10^{-4} (g/g)
48	30	0.0006	0.32
	45	0.0006	0.32
	60	0.0010	0.51
	90	0.0014	0.71
70	30	0.0018	0.90
	45	0.0016	0.80
	60	0.0016	0.81
	90	0.0020	1.00
82	30	0.0022	1.10
	45	0.0020	1.00
	60	0.0018	0.90
	90	0.0024	1.20

Table 6.34 Weight loss and erosion rate of 10wt% ACB CS particulate composites with respect to impact angle due to erosion for a period of 600 seconds

Impact Velocity (m/s)	Impact Angle (°)	10wt% ACB(800°C)	
		Weight loss (g)	Erosion rate×10^{-4} (g/g)
48	30	0.0001	0.07
	45	0.0003	0.13
	60	0.0004	0.21
	90	0.0009	0.47
70	30	0.0006	0.30
	45	0.0006	0.30
	60	0.0008	0.41
	90	0.0012	0.60
82	30	0.0010	0.50
	45	0.0008	0.40
	60	0.0011	0.53
	90	0.0016	0.80

Table 6.35 Weight loss and erosion rate of 15wt% ACB CS particulate composites with respect to impact angle due to erosion for a period of 600 seconds

Impact Velocity (m/s)	Impact Angle (°)	15wt% ACB(800°C)	
		Weight loss (g)	Erosion rate×10^{-4} (g/g)
48	30	0.0002	0.11
	45	0.0004	0.21
	60	0.0007	0.36
	90	0.0008	0.39
70	30	0.0010	0.50
	45	0.0010	0.50
	60	0.0010	0.50
	90	0.0016	0.80
82	30	0.0012	0.60
	45	0.0014	0.70
	60	0.0012	0.60
	90	0.0020	1.00

Table 6.36 Weight loss and erosion rate of 20wt% ACB CS particulate composites with respect to impact angle due to erosion for a period of 600 seconds

Impact Velocity (m/s)	Impact Angle (°)	20wt% ACB(800°C)	
		Weight loss (g)	Erosion rate×10^{-4} (g/g)
48	30	0.0004	0.20
	45	0.0004	0.22
	60	0.0006	0.32
	90	0.0013	0.65
70	30	0.0012	0.60
	45	0.0013	0.67
	60	0.0012	0.62
	90	0.0018	0.90
82	30	0.0018	0.90
	45	0.0014	0.70
	60	0.0016	0.80
	90	0.0022	1.10

Table 6.37 Erosion efficiency of 400°C CB CS particulate epoxy composites

Impact Velocity (m/s)	Impact Angle (°)	Erosion efficiency (η)				
		Neat Epoxy	5wt% 400°C CB	10 wt% 400°C CB	15wt% 400°C CB	20 wt% 400°C CB
		Hv=MPa 190.452	Hv=MPa 236.741	Hv=MPa 243.802	Hv=MPa 233.799	Hv=MPa 210.556
48	30	2.312	1.761	1.487	2.186	2.094
	45	3.138	2.648	2.454	3.097	3.015
	60	3.503	2.118	2.045	2.732	2.680
	90	3.923	1.942	1.859	2.550	2.848
70	30	1.581	1.079	0.787	1.285	1.363
	45	1.937	1.245	0.805	1.379	1.449
	60	2.108	1.469	1.224	1.636	1.662
	90	2.372	1.245	0.727	1.028	1.347
82	30	1.332	0.968	0.892	1.124	1.148
	45	1.579	1.028	0.956	1.186	1.246
	60	1.704	1.198	1.083	1.311	1.326
	90	1.920	0.968	0.956	1.061	1.211

Table 6.38 Erosion efficiency of 600°C CB CS particulate epoxy composites

Impact Velocity (m/s)	Impact Angle (°)	Erosion efficiency (η)				
		Neat Epoxy	5wt% 600°C CB	10wt% 600°C CB	15wt% 600°C CB	20wt% 600°C CB
		Hv=MPa 190.452	Hv=MPa 215.558	Hv=MPa 247.038	Hv=MPa 244.096	Hv=MPa 229.386
48	30	2.312	0.854	0.314	0.486	0.555
	45	3.138	1.071	0.533	0.629	0.952
	60	3.503	1.562	0.767	0.992	1.503
	90	3.923	0.821	0.377	0.668	0.795
70	30	1.581	0.772	0.647	1.142	1.306
	45	1.937	0.927	0.677	1.237	1.408
	60	2.108	1.004	1.017	1.427	1.995
	90	2.372	0.850	0.676	0.952	1.026
82	30	1.332	0.788	0.808	1.110	1.223
	45	1.579	0.844	0.741	0.971	1.155
	60	1.704	1.013	1.010	1.387	1.427
	90	1.920	0.788	0.876	1.110	1.291

Table 6.39 Erosion efficiency of 800°C CB CS particulate epoxy composites

Impact Velocity (m/s)	Impact Angle (°)	Erosion efficiency (η)				
		Neat Epoxy	5wt% 800°C CB	10wt% 800°C CB	15wt% 800°C CB	20wt% 800°C CB
		Hv=MPa 190.452	Hv=MPa 219.186	Hv=MPa 256.257	Hv=MPa 254.197	Hv=MPa 236.643
48	30	2.312	0.732	0.265	0.473	0.520
	45	3.138	0.945	0.488	0.641	1.016
	60	3.503	1.135	0.707	0.970	1.224
	90	3.923	1.317	1.175	1.088	1.012
70	30	1.581	0.804	0.623	0.778	1.111
	45	1.937	0.820	0.519	0.890	0.945
	60	2.108	0.742	0.602	0.778	0.934
	90	2.372	0.886	0.697	1.001	1.111
82	30	1.332	0.777	0.681	0.648	0.810
	45	1.579	0.717	0.530	0.729	0.891
	60	1.704	0.657	0.553	0.648	0.729
	90	1.920	0.807	0.757	0.972	1.158

Table 6.40 Erosion efficiency of ACB (800°C) CS particulate epoxy composites

Impact Velocity (m/s)	Impact Angle (°)	Erosion efficiency (η)				
		Neat Epoxy	5wt% ACB	10wt% ACB	15wt% ACB	20wt% ACB
		Hv=MPa 190.452	Hv=MPa 230.759	Hv=MPa 263.024	Hv=MPa 266.064	Hv=MPa 269.496
48	30	2.312	0.680	0.205	0.383	0.811
	45	3.138	0.684	0.381	0.730	0.892
	60	3.503	1.085	0.615	1.252	1.289
	90	3.923	1.108	1.178	1.157	1.239
70	30	1.581	0.899	0.413	0.818	1.144
	45	1.937	0.799	0.413	0.818	1.277
	60	2.108	0.804	0.565	0.818	1.182
	90	2.372	0.999	0.827	1.108	1.216
82	30	1.332	0.801	0.502	0.715	1.250
	45	1.579	0.728	0.402	0.834	0.972
	60	1.704	0.655	0.532	0.715	1.111
	90	1.920	0.873	0.803	1.192	1.228

Table 6.41 Parameters characterizing the velocity dependence of erosion rate of activated wood apple shell particulate composite

Filler content (wt%)	Impact Angle (°)	k	n	R^2
0(Neat epoxy)	30°	4.00E-06	3.4749	0.999
	45°	1.00E-05	3.5184	0.998
	60°	2.00E-05	3.5547	1
	90°	2.00E-05	3.566	0.996
5	30°	1.00E-09	3.781	0.965
	45°	1.00E-07	2.816	0.999
	60°	1.00E+00	2.328	0.989
	90°	6.00E-06	2.027	0.9858
10	30°	1.00E-08	3.175	0.9705
	45°	8.00E-08	2.817	0.9965
	60°	2.00E-07	2.761	0.9976
	90°	5.00E-06	2.062	0.9779
15	30°	2.00E-08	2.934	0.9064
	45°	2.00E-07	2.555	0.9951
	60°	6.00E-08	2.924	0.9982
	90°	1.00E-06	2.304	1
20	30°	1.00E-11	4.442	0.9785
	45°	1.00E-10	3.126	0.9749
	60°	6.00E-10	3.898	0.9545
	90°	7.00E-08	2.949	0.982

Table 6.42 Parameters characterizing the velocity dependence of erosion rate of activated coconut shell particulate composite

Filler content (wt%)	Impact Angle (°)	k	n	R^2
0(Neat epoxy)	30°	4.00E-06	3.4749	0.999
	45°	1.00E-05	3.5184	0.998
	60°	2.00E-05	3.5547	1
	90°	2.00E-05	3.566	0.996
5	30°	3.00E-09	3.8849	0.9806
	45°	7.00E-09	3.67	0.9891
	60°	8.00E-07	2.5838	0.9891
	90°	2.00E-06	2.4669	0.9967
10	30°	4.00E-12	5.2052	0.9985
	45°	4.00E-09	3.6202	0.9982
	60°	3.00E-08	3.2368	0.9996
	90°	1.00E-06	2.4302	0.9241
15	30°	3.00E-11	4.8217	0.963
	45°	3.00E-09	3.7575	0.9997
	60°	9.00E-07	2.4387	0.9954
	90°	4.00E-08	3.2849	0.996
20	30°	4.00E-10	4.3274	0.9992
	45°	3.00E-09	3.8052	0.9348
	60°	4.00E-08	3.2313	0.9996
	90°	2.00E-06	2.4575	0.9906

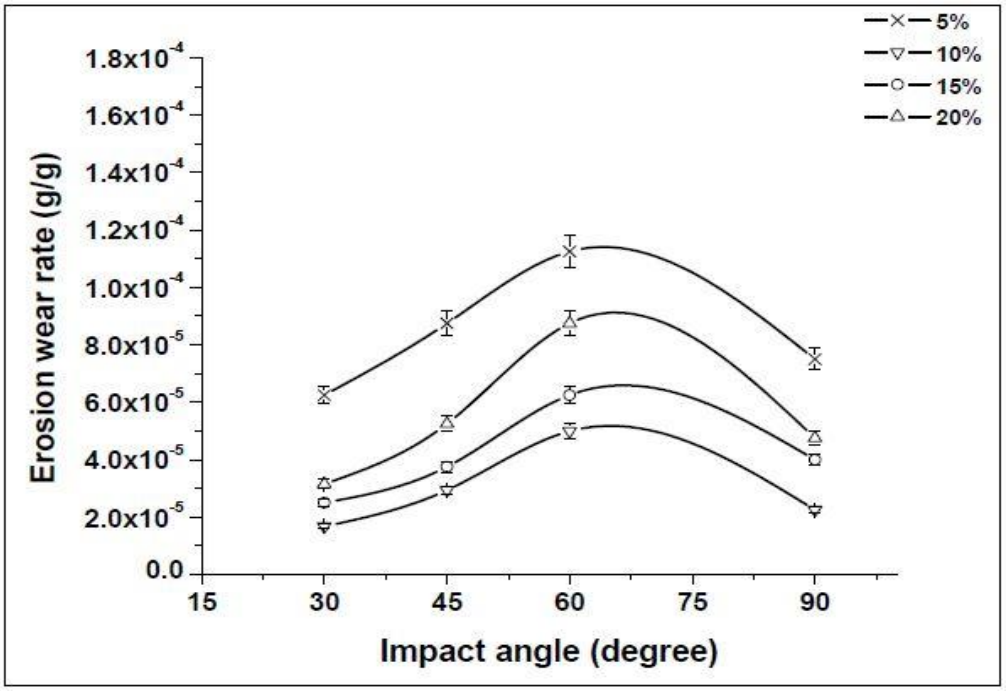

Figure 6.1 Variation of erosion rate with different impact angle at impact velocity 48m/s of 400°C carbon black wood apple shell particulate composite

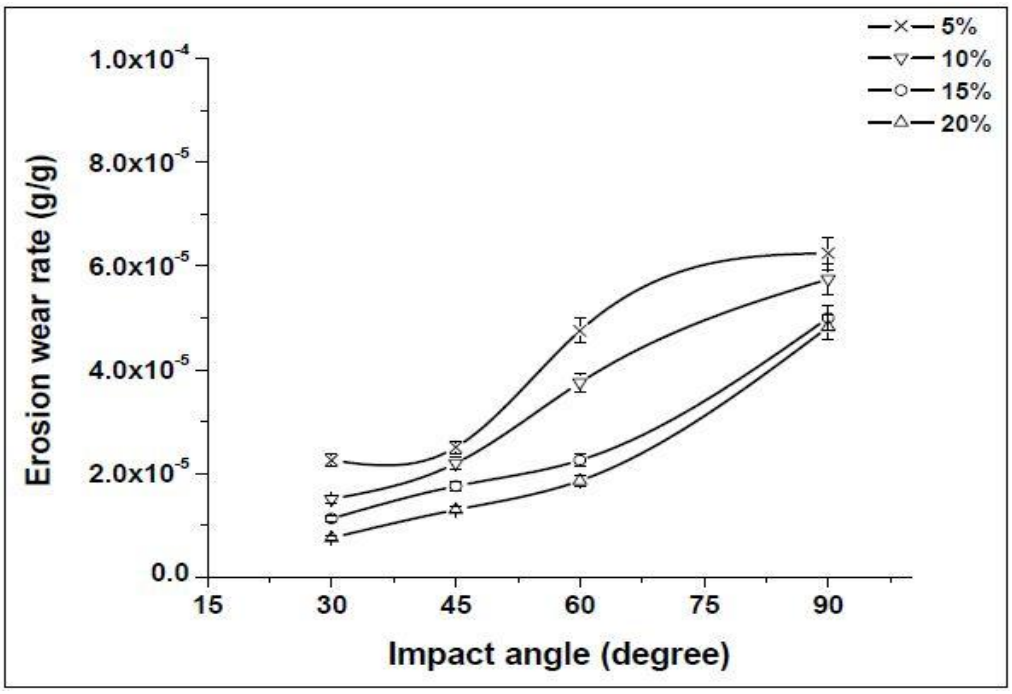

Figure 6.2 Variation of erosion rate with different impact angle at impact velocity 48m/s of 600°C carbon black wood apple shell particulate composite

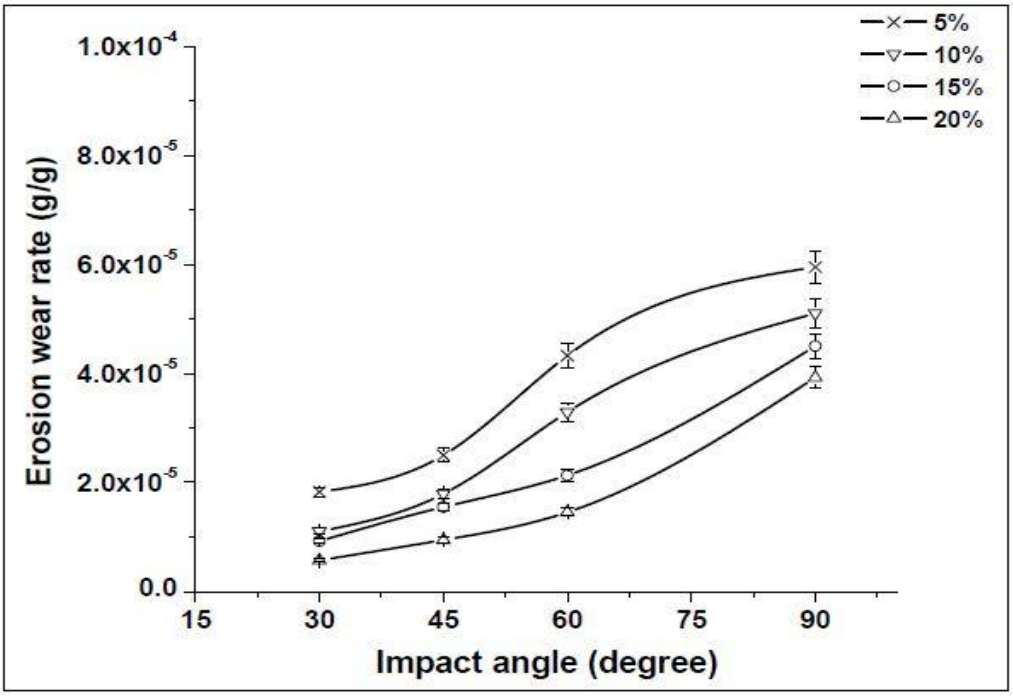

Figure 6.3 Variation of erosion rate with different impact angle at impact velocity 48m/sof 800°C carbon black wood apple shell particulate composite

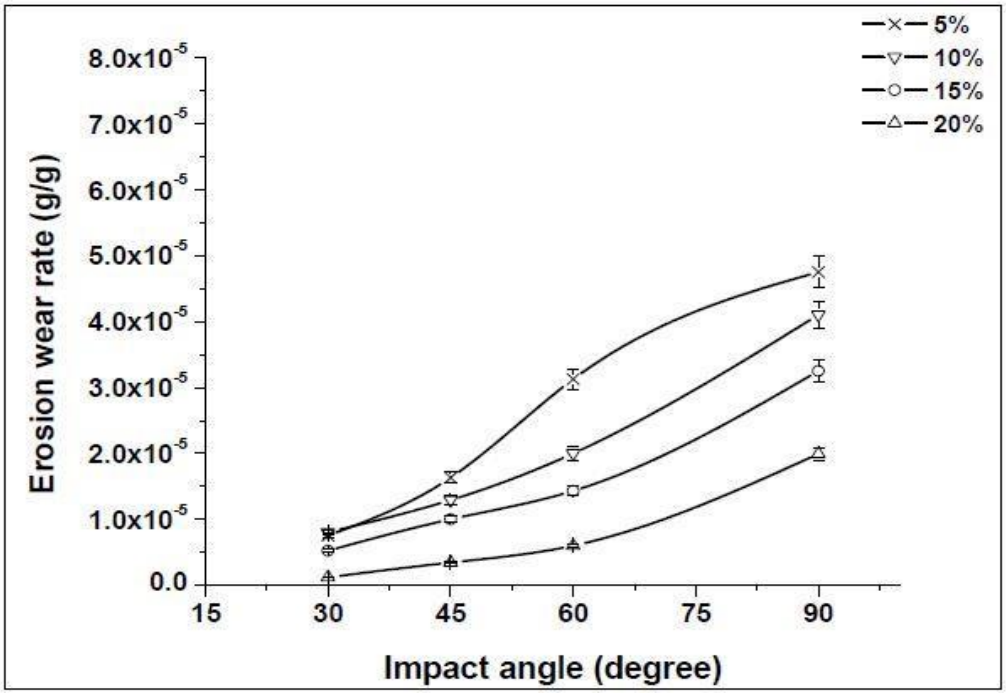

Figure 6.4 Variation of erosion rate with different impact angle at impact velocity 48m/s of activated carbon black wood apple shell particulate composite

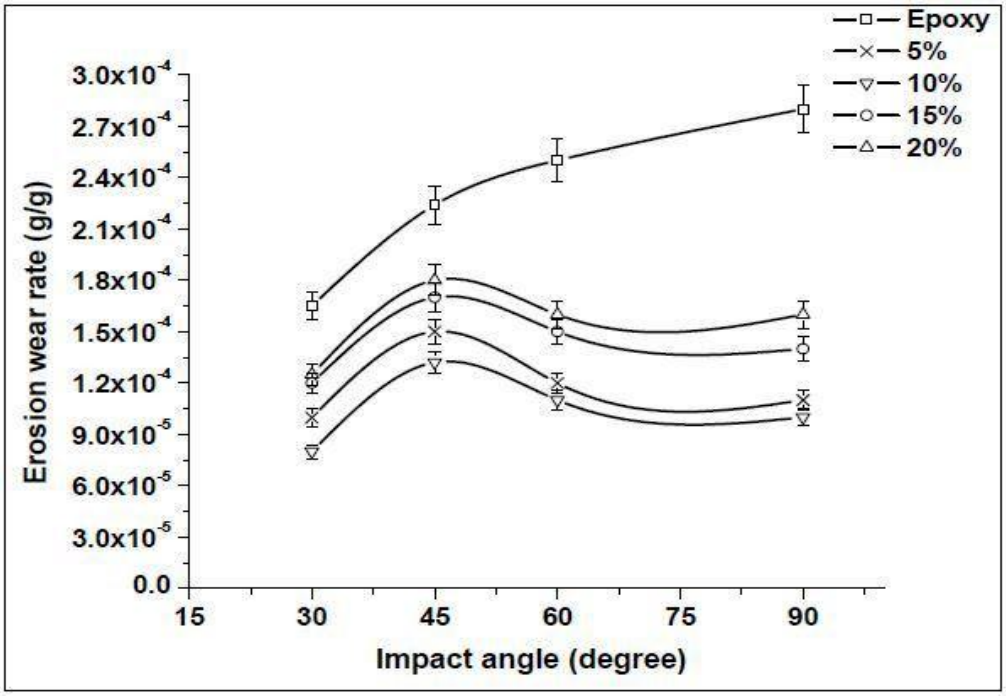

Figure 6.5 Variation of erosion rate with different impact angle at impact velocity 48 m/s of 400°C carbon black coconut shell particulate composite

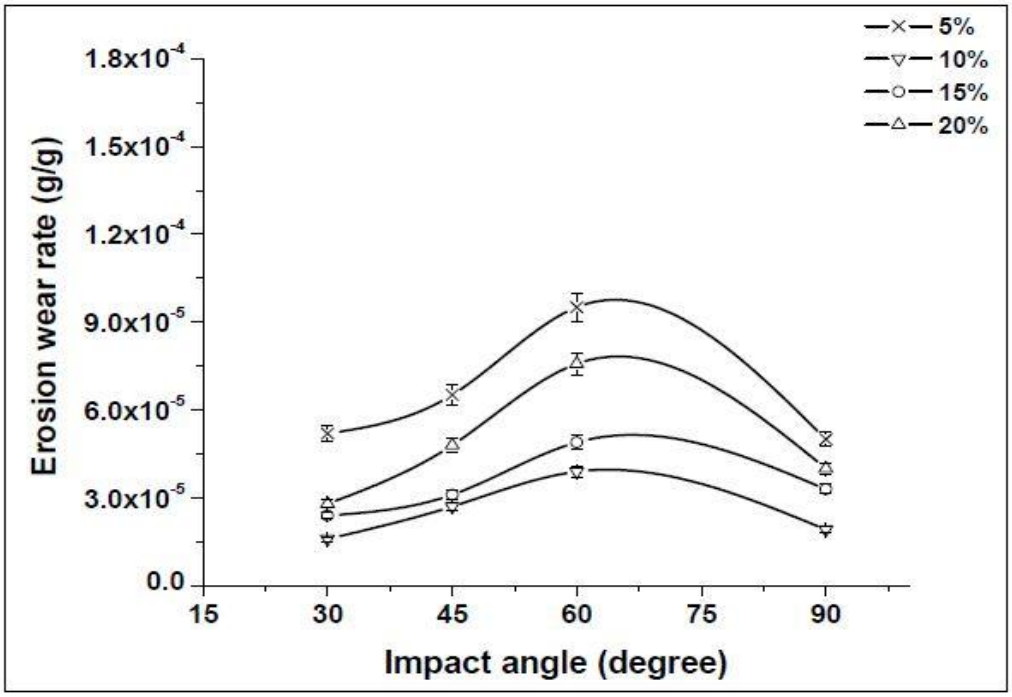

Figure 6.6 Variation of erosion rate with different impact angle at impact velocity 48m/s of 600°C carbon black coconut shell particulate composite

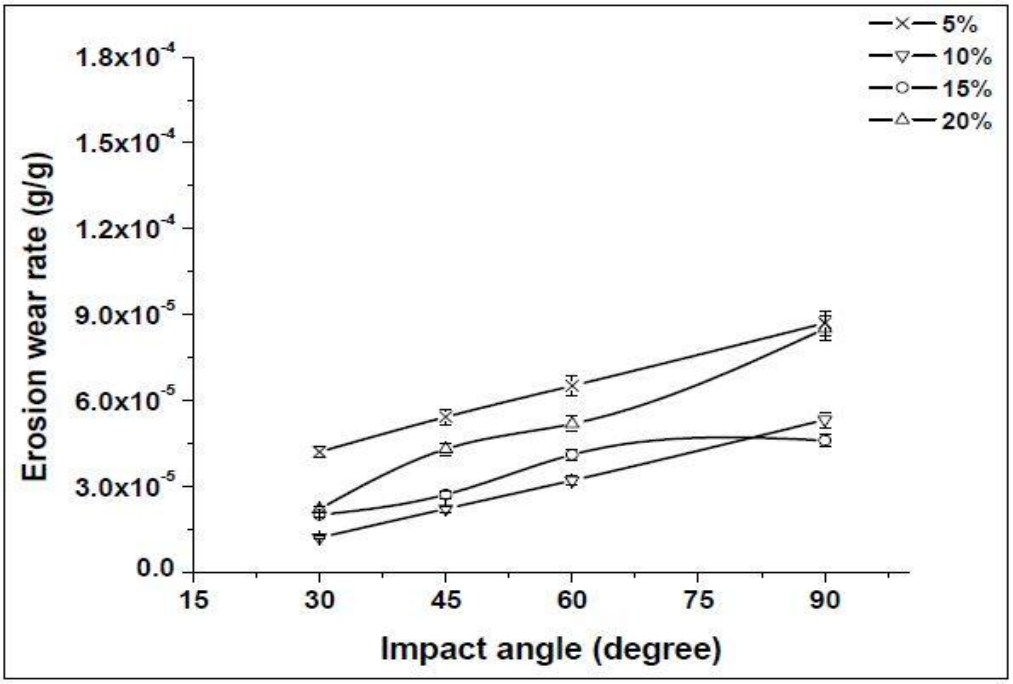

Figure 6.7 Variation of erosion rate with different impact angle at impact velocity 48m/s of 800°C carbon black coconut shell particulate composite

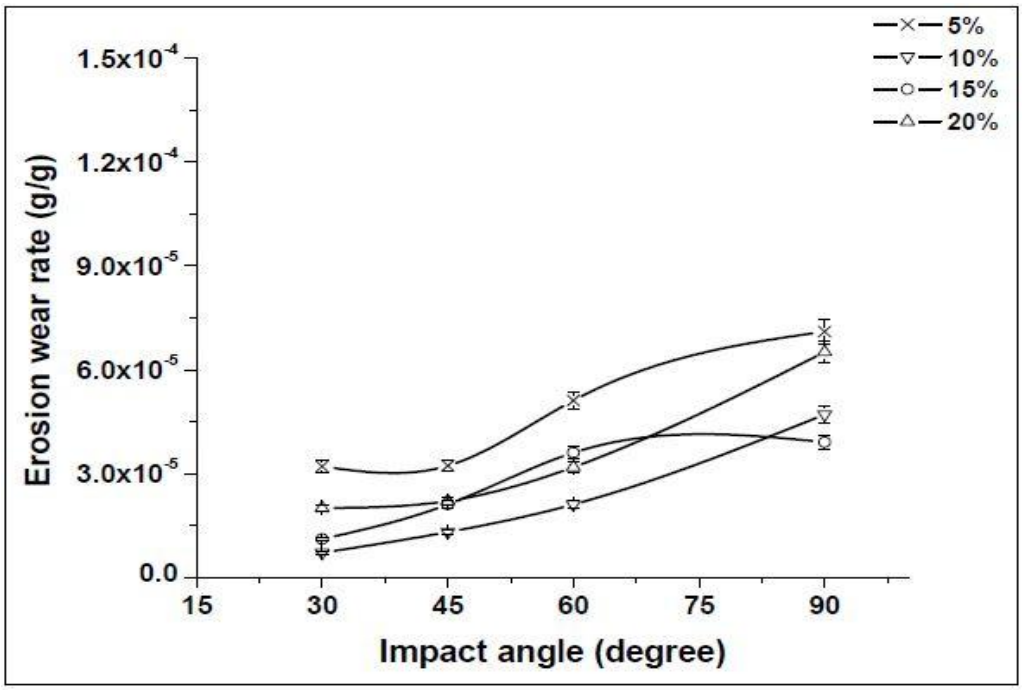

Figure 6.8 Variation of erosion rate with different impact angle at impact velocity 48m/s of activated carbon black coconut shell particulate composite

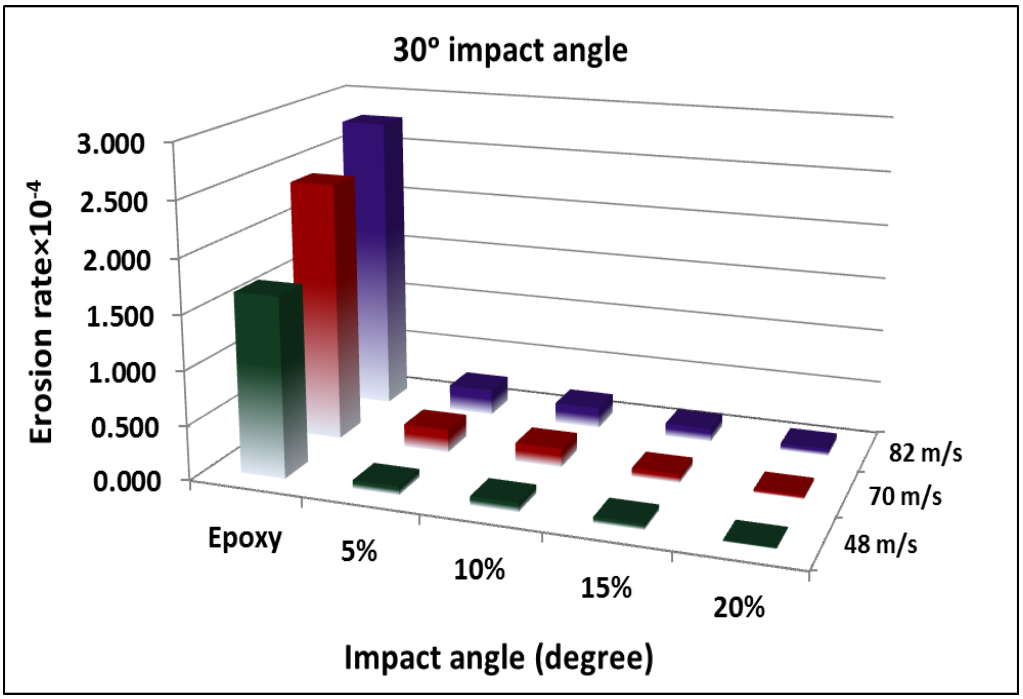

Figure 6.9 Histogram showing the effect of impact velocities on steady state erosive wear rate of activated wood apple shell particulate composite

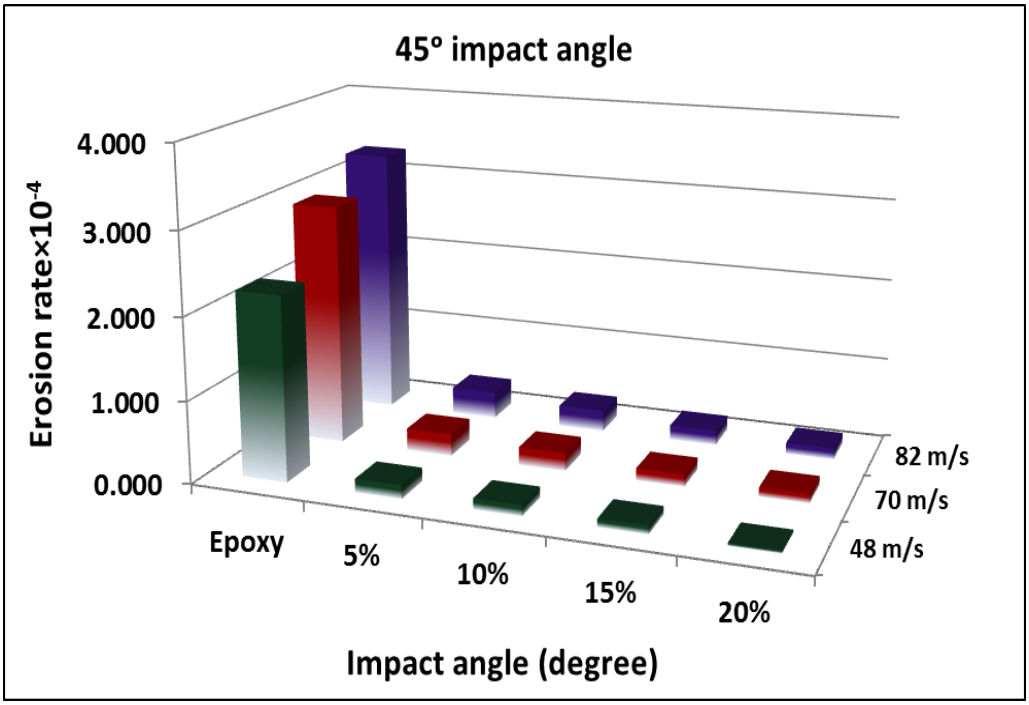

Figure 6.10 Histogram showing the effect of impact velocities on steady state erosive wear rate of activated wood apple shell particulate composite

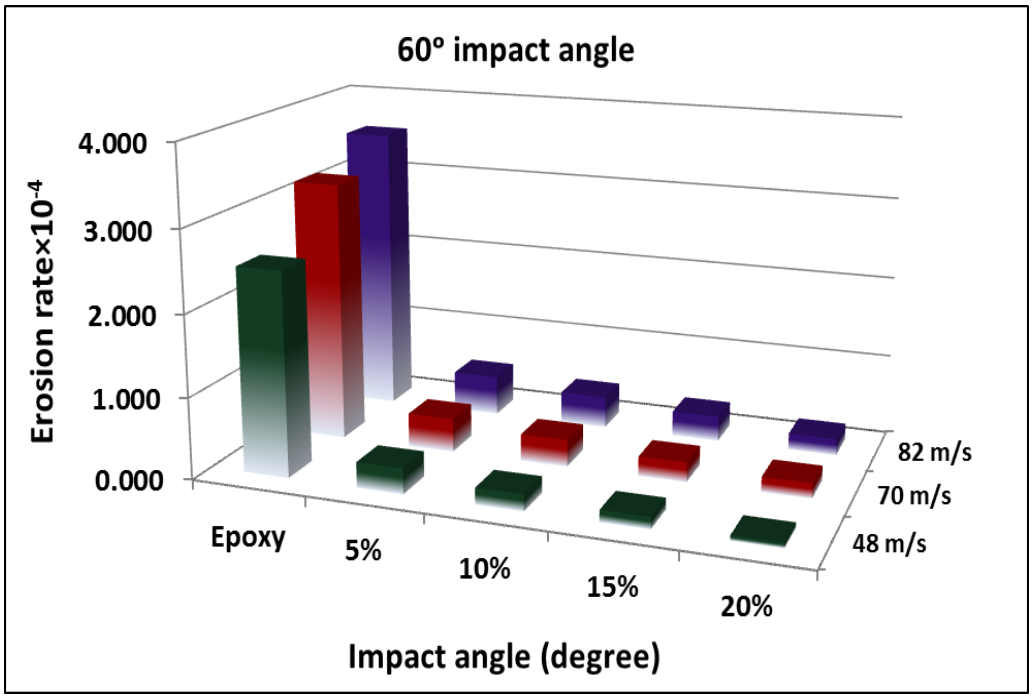

Figure 6.11 Histogram showing the effect of impact velocities on steady state erosive wear rate of activated wood apple shell particulate composite

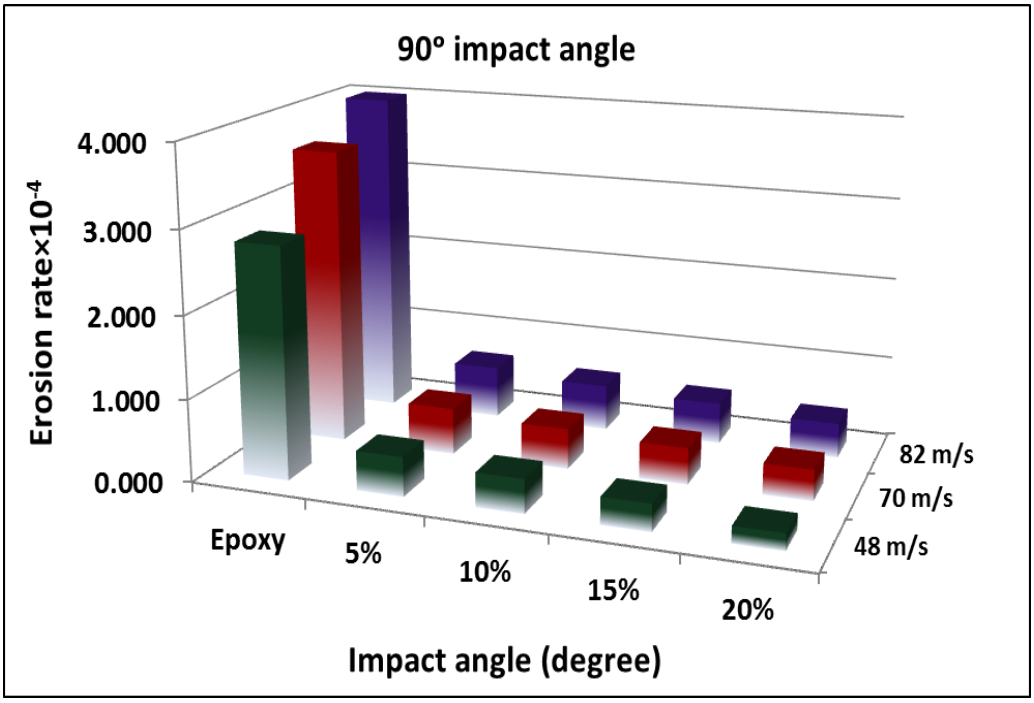

Figure 6.12 Histogram showing the effect of impact velocities on steady state erosive wear rate of activated wood apple shell particulate composite

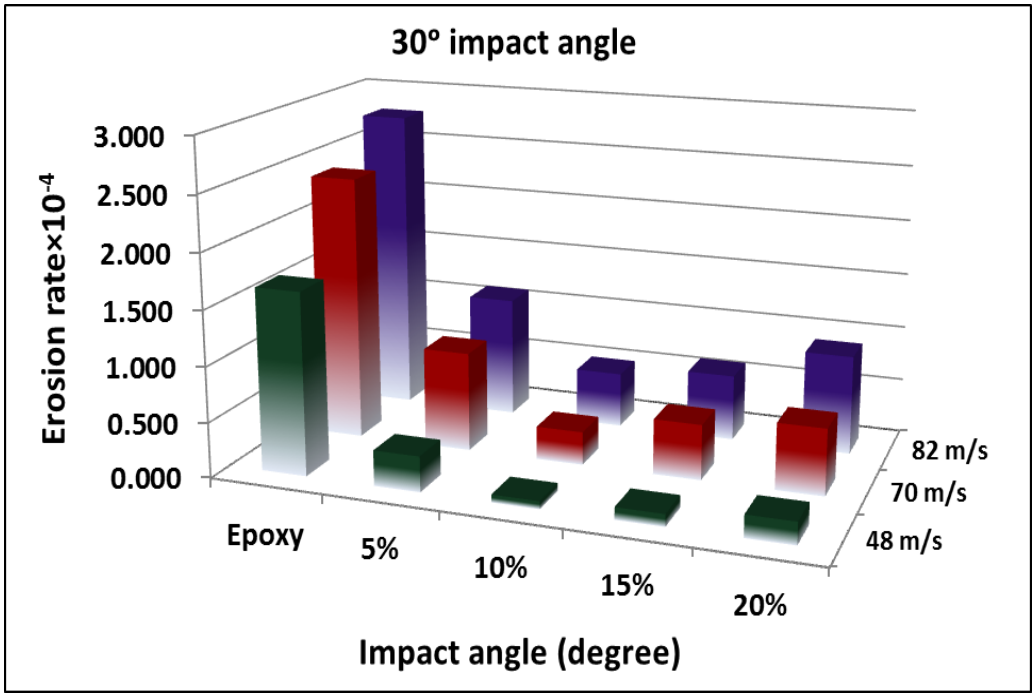

Figure 6.13 Histogram showing the effect of impact velocities on steady state erosive wear rate of activated coconut shell particulate composite

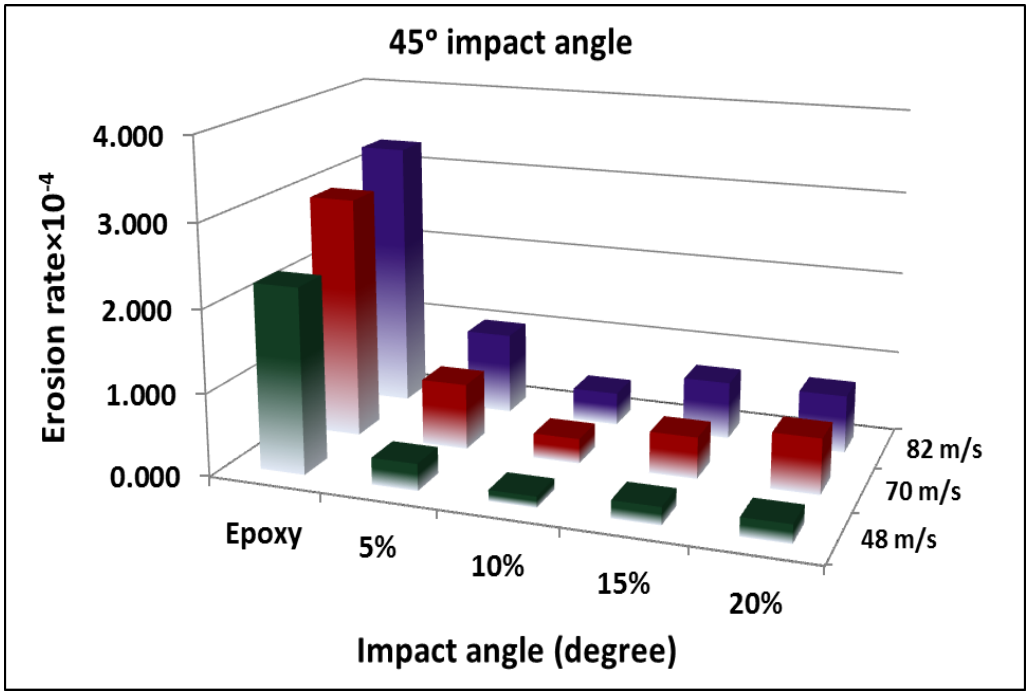

Figure 6.14 Histogram showing the effect of impact velocities on steady state erosive wear rate of activated coconut shell particulate composite

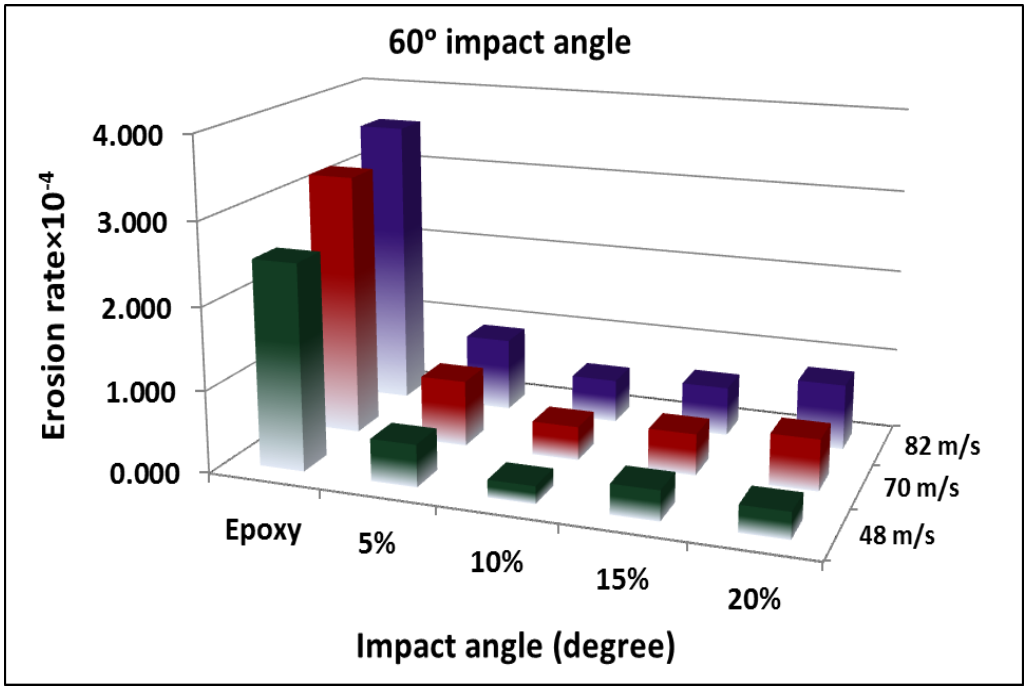

Figure 6.15 Histogram showing the effect of impact velocities on steady state erosive wear rate of activated coconut shell particulate composite

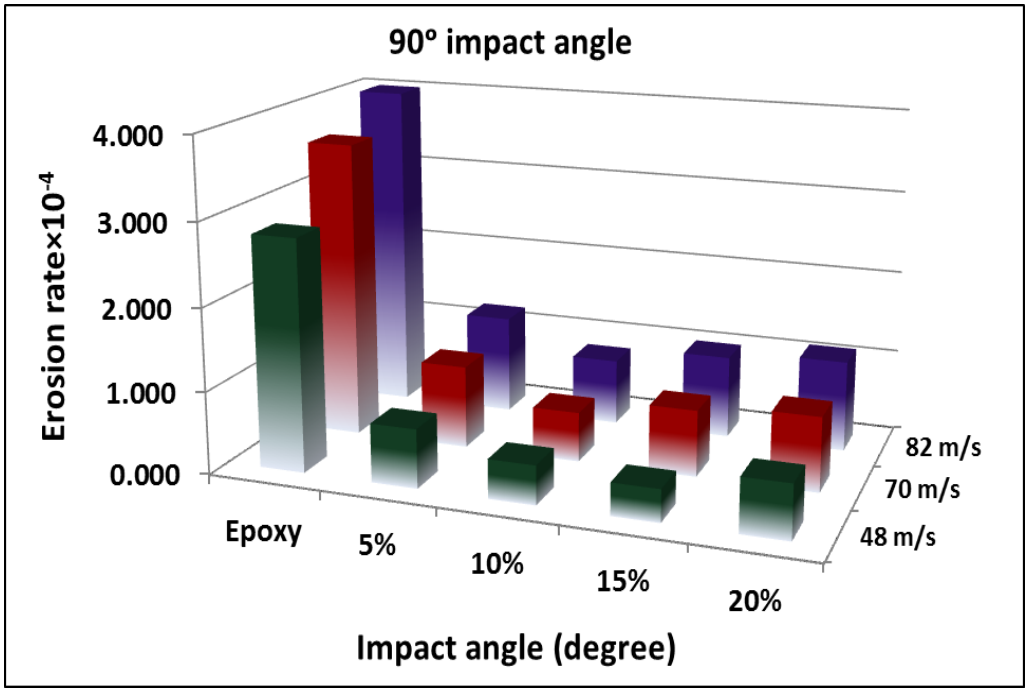

Figure 6.16 Histogram showing the effect of impact velocities on steady state erosive wear rate of activated coconut shell particulate composite

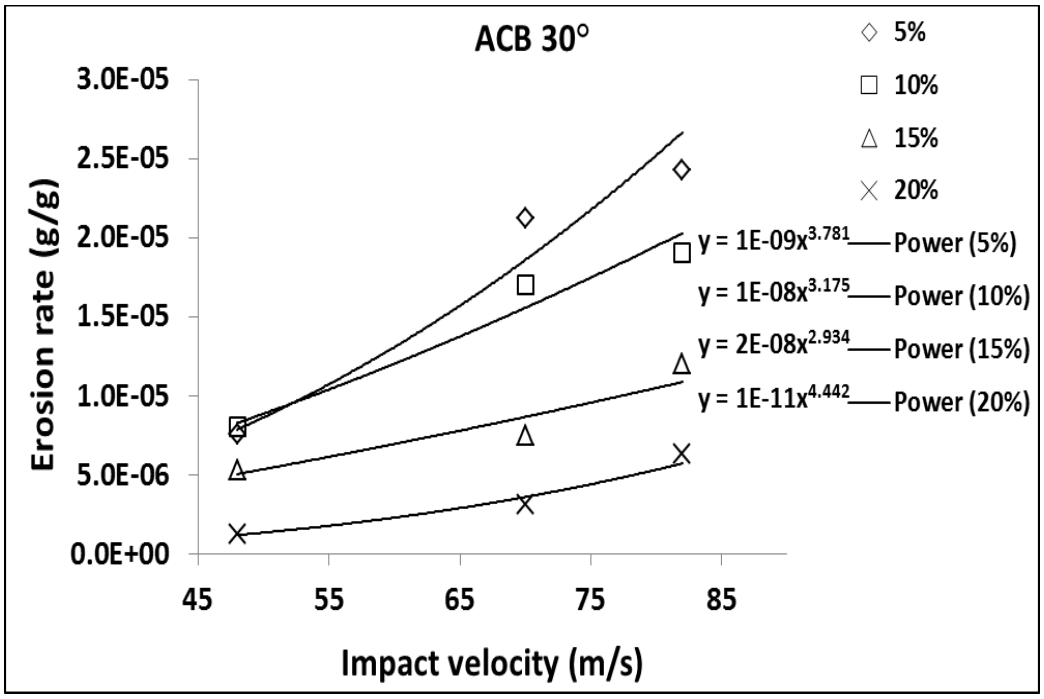

Figure 6.17 Erosion parameter of activated wood apple shell particulate composite at impact angle 30°

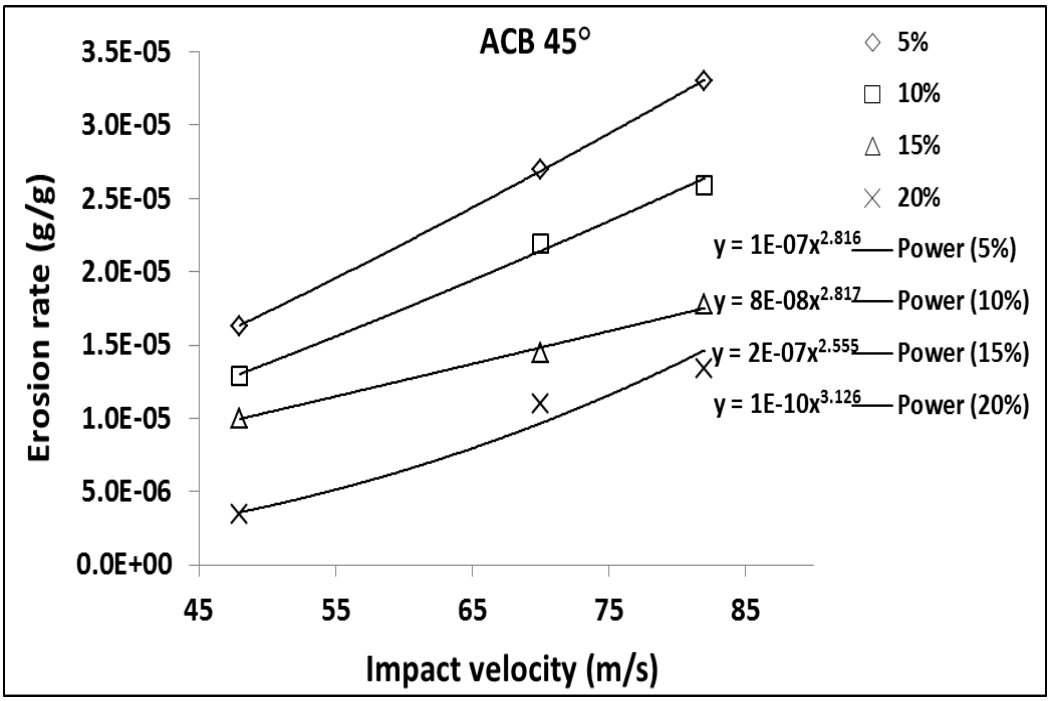

Figure 6.18 Erosion parameter of activated wood apple shell particulate composite at impact angle 45°

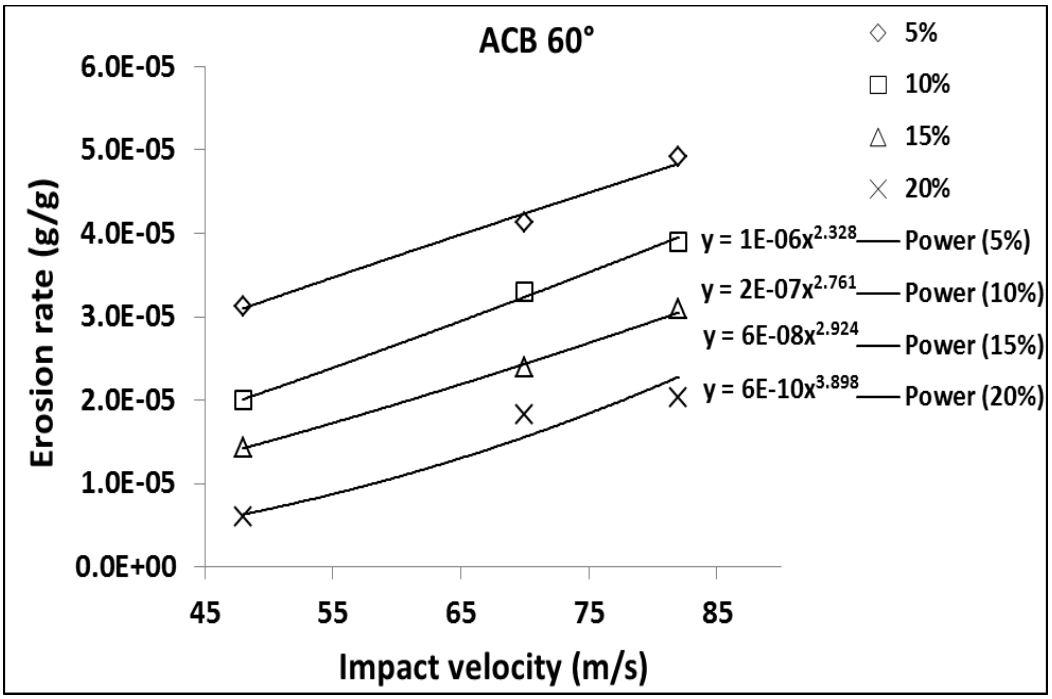

Figure 6.19 Erosion parameter of activated wood apple shell particulate composite at impact angle 60°

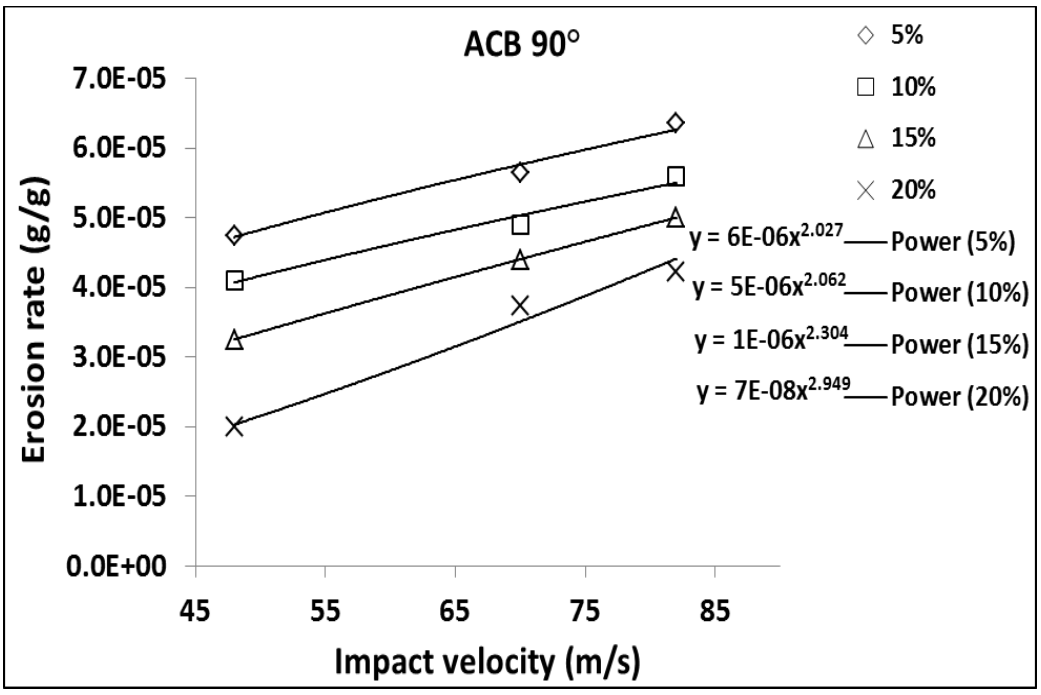

Figure 6.20 Erosion parameter of activated wood apple shell particulate composite at impact angle 90°

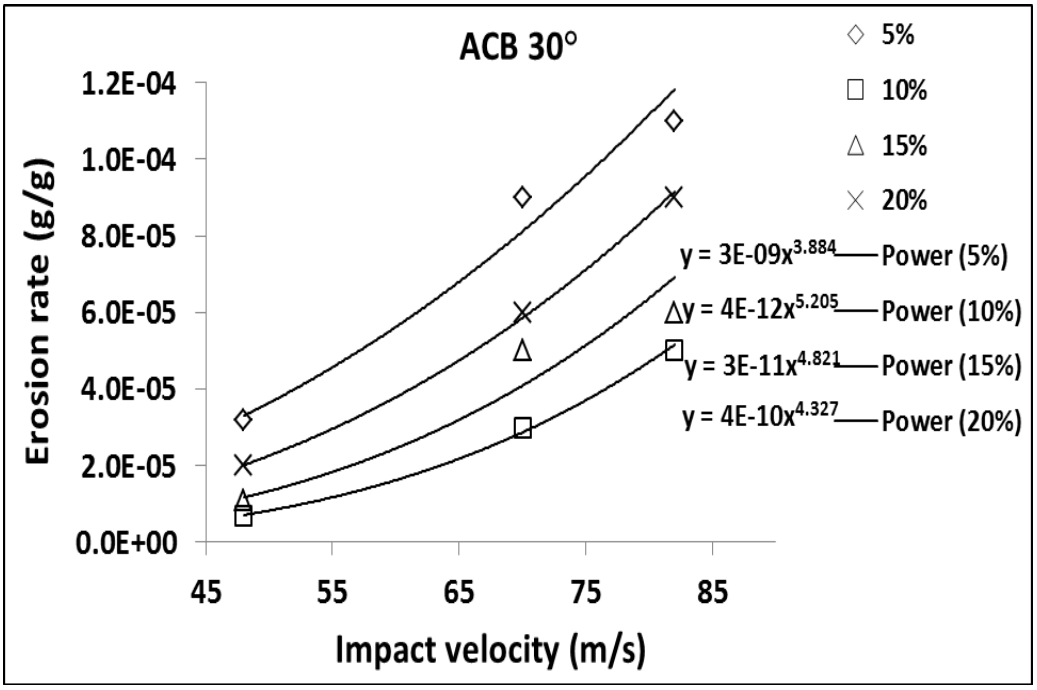

Figure 6.21 Erosion parameter of activated coconut shell particulate composite at impact angle 30°

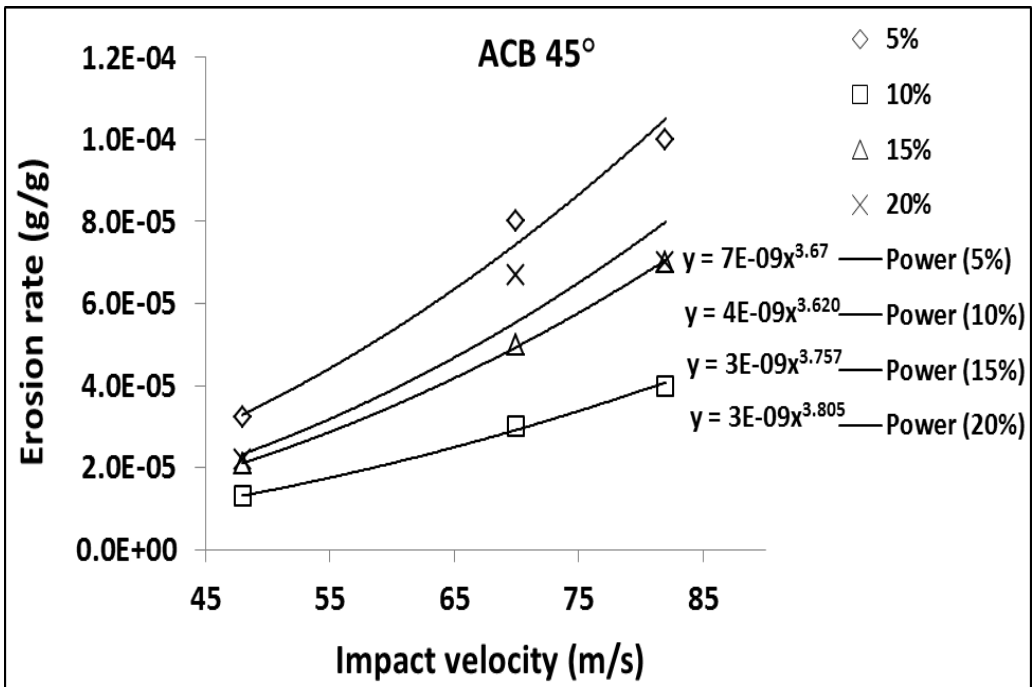

Figure 6.22 Erosion parameter of activated coconut shell particulate composite at impact angle 45°

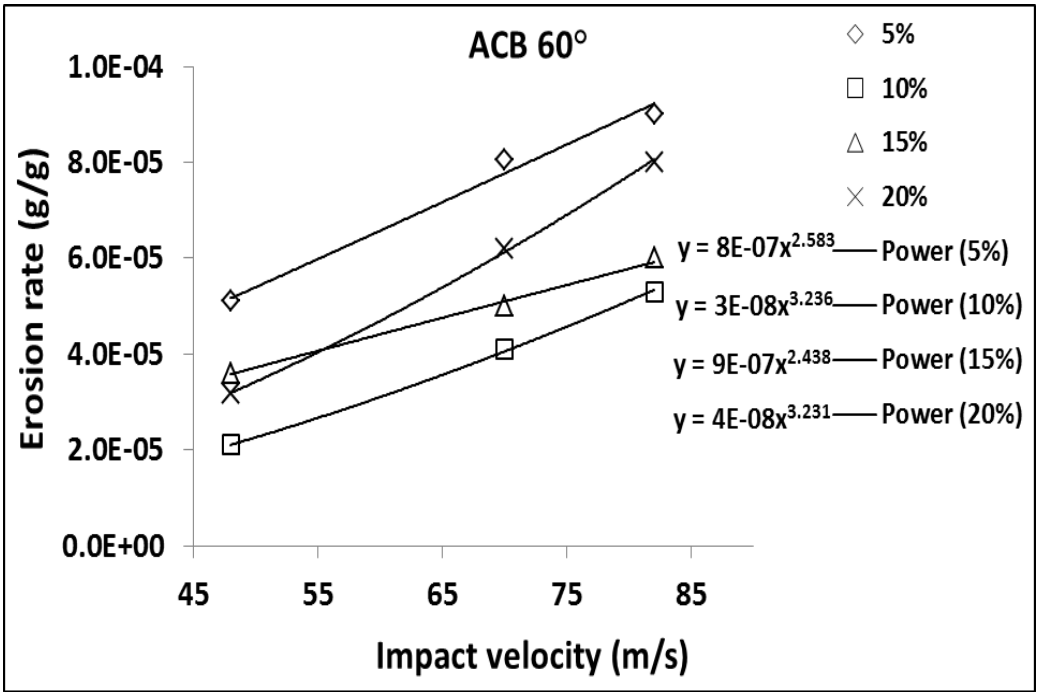

Figure 6.23 Erosion parameter of activated coconut shell particulate composite at impact angle 60°

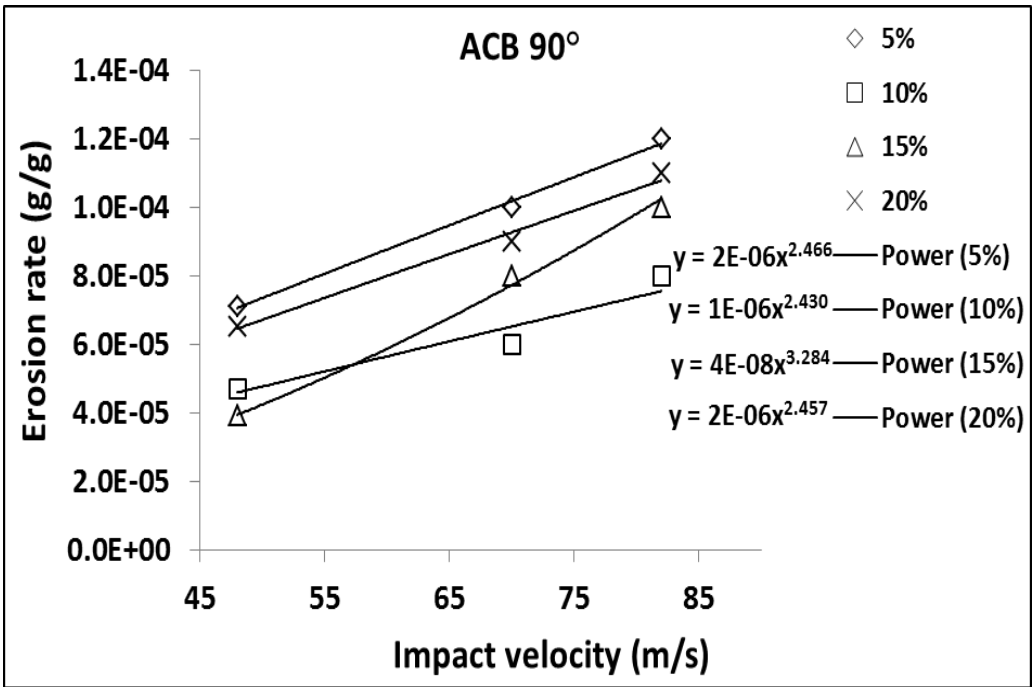

Figure 6.24 Erosion parameter of activated coconut shell particulate composite at impact angle 90°

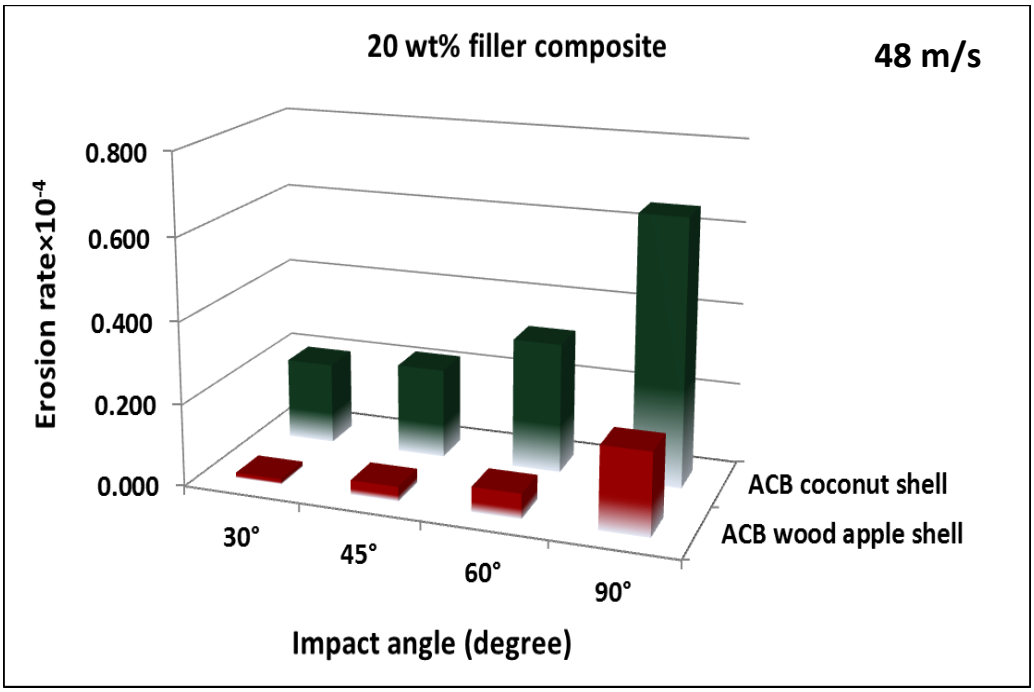

Figure 6.25 Histogram showing the comparison between activated wood apple and coconut shell particulate composites at impact velocity 48m/s with various impact angles

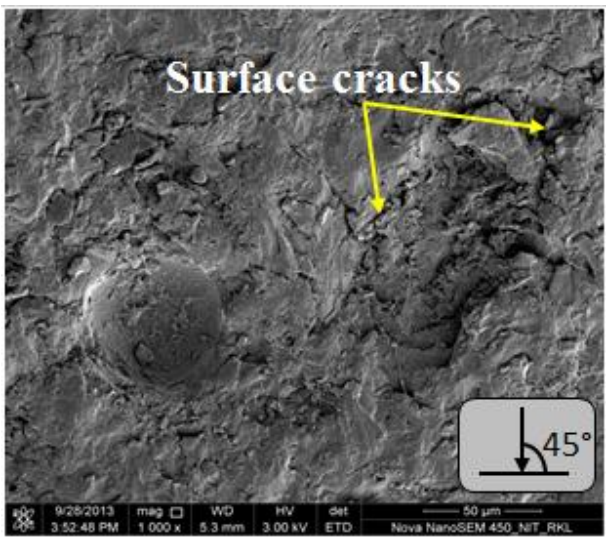

Figure 6.26 Micrographs of the 20wt% of activated carbon black (800°C) wood apple shell particulate reinforced epoxy composite eroded at 45°

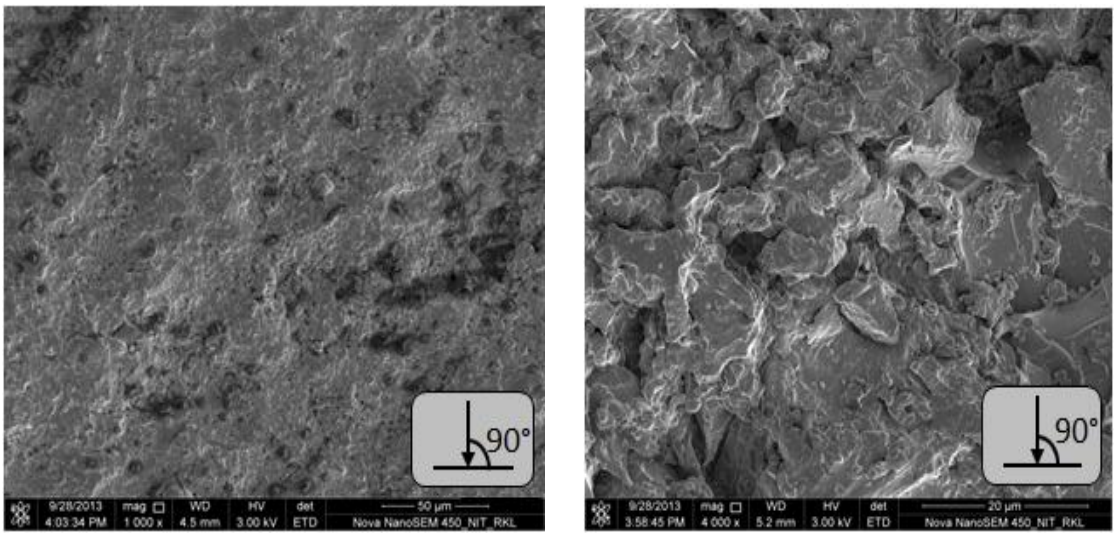

(a) **(b)**

Figure 6.27 Micrographs of the 20wt% of activated carbon black (800°C) wood apple shell particulate reinforced epoxy composite eroded at 90° **(a)** lower magnification **(b)** higher magnification

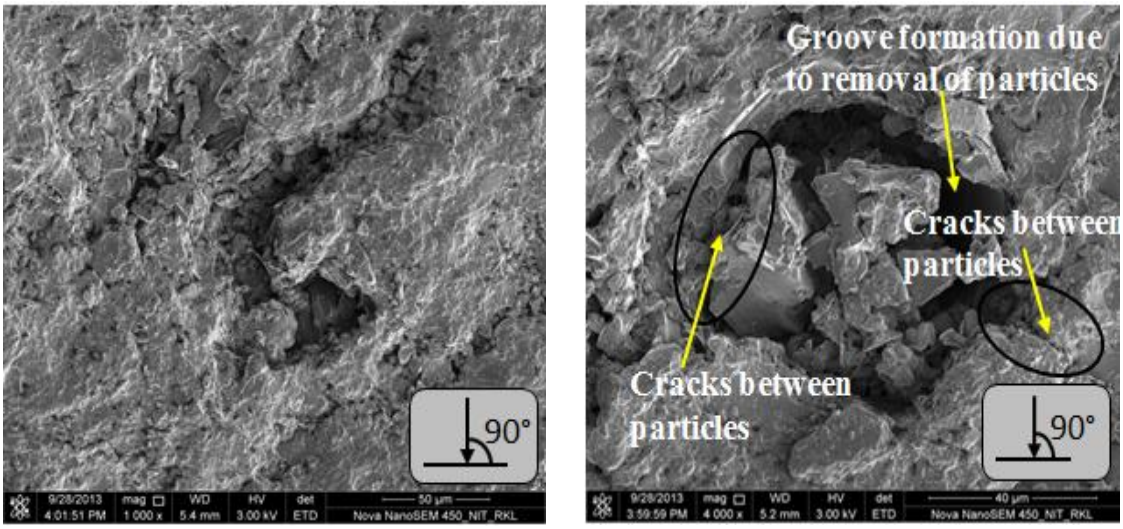

(a) **(b)**

Figure 6.28 Micrographs of the 20wt% of activated carbon black (800°C) coconut shell particulate reinforced epoxy composite eroded at 90°° **(a)** lower magnification **(b)** higher magnification

Chapter 7

Conclusion and Scope for Future Work

7.1 CONCLUSION

The conclusions drawn from the present investigations are as follows.

1. A new class of epoxy based composites reinforced with carbon black and activated carbon black with wood apple shell and coconut shell fillers have been fabricated successfully in the laboratory for the development of value added products.
2. Both carbon black and activation of carbon black with wood apple and coconut shell were successfully fabricated in the laboratory by pyrolysis process.
3. Effect of carbonization temperature and activation temperature increases the tensile, flexural properties of the particulate composite for different weight percentages.
4. The erosion resistance of the polymers increases with as the filler addition increases and also as the carbonization temperature increases. The best result was achieved for only activated carbon reinforced filled epoxy composites.
5. The raw wood apple shell and coconut shell filler composites shows a semi ductile behavior to solid particle erosion since the maximum erosion occurs at 45° impact angle.
6. As the carbonization temperature increases the material nature is changing to semi ductile to semi brittle and brittle behaviour since the maximum erosion occurs at 90° impact angel.
7. The erosion efficiency of the activated carbon reinforced composite shows lesser when compared to other raw and carbonized fillers. This lower erosion efficiency of composite indicates a better erosion resistance.
8. The morphologies of the eroded surfaces of raw wood apple and coconut shell filler reinforced composites suggest that overall erosion damage of the composite is mainly due to formation of crater and chipping of fiber.
9. The fracture surface study with carbon black and activation carbon black indicates that due to higher surface area and porus formation in particles the interfacial bonding is high, which in turn improves the erosion resistance of the composite.

7.2 RECOMMENDATION FOR FURTHER RESEARCH

1. In the present investigation we have used wood apple and coconut shell to prepare a carbon and activated carbon fillers. However there may be other natural fibers which also contain carbon as major constituents can be used for preparation of carbon black.
2. Hand-lay-up technique is used to fabricate the composite in the present work. However there exists other manufacturing process for polymer matrix composite. They could be tried and analyzed, so that a final conclusion can be drawn there from. However the results provided in this thesis can act as a base for the utilization of carbon black obtained from natural fibers.
3. In this work we have used $ZnCl_2$ as activation agent other chemical reagents and higher carbonization temperature more than 800°C could be tried.
4. In the erosion test sand particle of 200±50 microns only have been used. This work can be further extended to other particle size and types of particle like glass bead etc, to study the effect of particle size and type of particles on wear behavior of the composite.

Chapter 8

Miscellaneous

REFERENCES

1. Olivier, J. G. (2012). Trends in global CO_2 emissions: 2012 Report (p. 40). Hague: PBL Netherlands Environmental Assessment Agency.
2. Haita, C. (2012). The State of Compliance in the Kyoto Protocol. International Center for Climate Governance, 1-6.
3. Climate Modelling Forum, I. (2009). INDIA'S GHG Emissions Profile: Results of Five Climate Modelling Studies. Ministry of Environment and Forests.
4. http://www.thehindubusinessline.com/opinion/article 2726531.ece
5. Guoyi, H., Marie, O., Karl, H., & David, L. (2012). China's carbon emission trading: An overview of current development.
6. Pierson, H. O. (2012). Handbook of carbon, graphite, diamonds and fullerenes: processing, properties and applications. William Andrew.
7. Burchell, T. D. (Ed.). (1999). Carbon materials for advanced technologies. Elsevier.
8. Manocha, S. M. (2003). Porous carbons. Sadhana, 28(1-2), 335-348.
9. He, Y., & Zhang, G. L. (2009). Historical record of black carbon in urban soils and its environmental implications. Environmental pollution, 157(10), 2684-2688.
10. Ismail, H., & Suryadiansyah, S. (2004). Effects of Filler Loading on Properties of Polypropylene–Natural Rubber–Recycle Rubber Powder (PP–NR–RRP) Composites. Journal of reinforced plastics and composites, 23(6), 639-650.
11. Li, H. Y., Chen, H. Z., Xu, W. J., Yuan, F., Wang, J. R., & Wang, M. (2005). Polymer-encapsulated hydrophilic carbon black nanoparticles free from aggregation. Colloids and Surfaces A: Physicochemical and Engineering Aspects, 254(1), 173-178.
12. Jakab, E., & Omastova, M. (2005). Thermal decomposition of polyolefin/carbon black composites. Journal of analytical and applied pyrolysis, 74(1), 204-214.
13. Tan, J. S., & Ani, F. N. (2004). Carbon molecular sieves produced from oil palm shell for air separation. Separation and purification technology, 35(1), 47-54.
14. Zhang, W., Zhang, X., Liang, M., & Lu, C. (2008). Mechanochemical preparation of surface-acetylated cellulose powder to enhance mechanical properties of cellulose-filler-reinforced NR vulcanizates. Composites Science and Technology, 68(12), 2479-2484.

15. Khalil, H. A., Noriman, N. Z., Ahmad, M. N., Ratnam, M. M., & Fuaad, N. N. (2007). Polyester composites filled carbon black and activated carbon from bamboo (Gigantochloa scortechinii): Physical and mechanical properties. Journal of reinforced plastics and composites, 26(3), 305-320.
16. Degrange, J-M., Marc Thomine, Ph Kapsa, Jean-Marc Pelletier, Laurent Chazeau, G. Vigier, G. Dudragne, and L. Guerbe. (2005). Influence of viscoelasticity on the tribological behaviour of carbon black filled nitrile rubber (NBR) for lip seal application. Wear, 259(1), 684-692.
17. He, Y., & Zhang, G. L. (2009). Historical record of black carbon in urban soils and its environmental implications. Environmental pollution, 157(10), 2684-2688.
18. Saxena, R. C., Adhikari, D. K., & Goyal, H. B. (2009). Biomass-based energy fuel through biochemical routes: a review. Renewable and Sustainable Energy Reviews, 13(1), 167-178.
19. Karthikeyan, S., Sivakumar, P., & Palanisamy, P. N. (2008). Novel activated carbons from agricultural wastes and their characterization. Journal of Chemistry, 5(2), 409-426.
20. Mattson, J. S., & Mark, H. B. (1971). Activated carbon: surface chemistry and adsorption from solution. M. Dekker.
21. Hutchings, I. M. (1992). Tribology: friction and wear of engineering materials.
22. Khalil, H. A., Firoozian, P., Bakare, I. O., Akil, H. M., & Noor, A. M. (2010). Exploring biomass based carbon black as filler in epoxy composites: Flexural and thermal properties. Materials & Design, 31(7), 3419-3425.
23. Ojha, S., Acharya, S. K., & Raghavendra, G. (2015). Mechanical properties of natural carbon black reinforced polymer composites. Journal of Applied Polymer Science, 132(1).
24. Parshetti, G. K., Hoekman, S. K., & Balasubramanian, R. (2013). Chemical, structural and combustion characteristics of carbonaceous products obtained by hydrothermal carbonization of palm empty fruit bunch. Bioresource technology, 135, 683-689.
25. Alagumuthu, G., & Rajan, M. (2010). Equilibrium and kinetics of adsorption of fluoride onto zirconium impregnated cashew nut shell carbon. Chemical Engineering Journal, 158(3), 451-457.

26. Baccar, R., Bouzid, J., Feki, M., & Montiel, A. (2009). Preparation of activated carbon from Tunisian olive-waste cakes and its application for adsorption of heavy metal ions. Journal of Hazardous Materials, 162(2), 1522-1529.

27. Bello-Huitle, V., Atenco-Fernández, P., & Reyes-Mazzoco, R. (2010). Adsorption studies of methylene blue and phenol onto pecan and castile nutshells prepared by chemical activation. Revista Mexicana de Ingenieria Quimica, 9(3), 313-322.

28. Castro, J. B., Bonelli, P. R., Cerrella, E. G., & Cukierman, A. L. (2000). Phosphoric acid activation of agricultural residues and bagasse from sugar cane: influence of the experimental conditions on adsorption characteristics of activated carbons. Industrial & engineering chemistry research, 39(11), 4166-4172.

29. Demirbas, E., Dizge, N., Sulak, M. T., & Kobya, M. (2009). Adsorption kinetics and equilibrium of copper from aqueous solutions using hazelnut shell activated carbon. Chemical Engineering Journal, 148(2), 480-487.

30. Satyanarayana, K. G., Guimaraes, J. L., & Wypych, F. E. R. N. A. N. D. O. (2007). Studies on lignocellulosic fibers of Brazil. Part I: Source, production, morphology, properties and applications. Composites Part A: Applied Science and Manufacturing, 38(7), 1694-1709.

31. Mohamed, A. R., Mohammadi, M., & Darzi, G. N. (2010). Preparation of carbon molecular sieve from lignocellulosic biomass: A review. Renewable and Sustainable Energy Reviews, 14(6), 1591-1599.

32. Silvestre-Albero, A., Goncalvez, M., Itoh, T., Kaneko, K., Endo, M., Thommes, M., Rodríguez-Reinoso, F. & Silvestre-Albero, J. (2012). Well-defined mesoporosity on lignocellulosic-derived activated carbons. Carbon, 50(1), 66-72.

33. Dufresne, A. (2010). Polymer nanocomposites from biological sources. Encyclopedia of nanoscience and nanotechnology, 21, 219-250.

34. Heux, L., Dinand, E., & Vignon, M. R. (1999). Structural aspects in ultrathin cellulose micro fibrils followed by 13 C CP-MAS NMR. Carbohydrate Polymers, 40(2), 115-124.

35. Brannvall, E. (2007). Aspects on strength delivery and higher utilisation of the strength potential of softwood kraft pulp fibres (Doctoral dissertation, PhD dissertation, KTH Royal Institute of Technology, Stockholm, Sweden).

36. John, M. J., & Thomas, S. (2008). Bio fibres and bio composites. Carbohydrate polymers, 71(3), 343-364.
37. Scriven, E. F. V., Tomey, J. E., & Murugan, R. (1996). Kirk-Othmer Encyclopedia of Chemical Technology, Vol. 20.
38. Thygesen, A., Thomsen, A. B., Daniel, G., & Lilholt, H. (2007). Comparison of composites made from fungal defibrated hemp with composites of traditional hemp yarn. Industrial Crops and Products, 25(2), 147-159.
39. Joseph, S., Peacocke, C., Lehmann, J., & Munroe, P. (2009). Developing a biochar classification and test methods. Biochar for Environmental Management–Science and Technology, 107-126.
40. Kruk, M., Dufour, B., Celer, E. B., Kowalewski, T., Jaroniec, M., & Matyjaszewski, K. (2005). Synthesis of mesoporous carbons using ordered and disordered mesoporous silica templates and polyacrylonitrile as carbon precursor. The Journal of Physical Chemistry B, 109(19), 9216-9225.
41. Lu, A. H., & Zheng, J. T. (2001). Study of microstructure of high-surface-area polyacrylonitrile activated carbon fibers. Journal of colloid and interface science, 236(2), 369-374.
42. Hayashi, J. I., Kazehaya, A., Muroyama, K., & Watkinson, A. P. (2000). Preparation of activated carbon from lignin by chemical activation. Carbon, 38(13), 1873-1878.
43. Sentorun-Shalaby, C., Ucak-Astarlioglu, M. G., Artok, L., & Sarici, C. (2006). Preparation and characterization of activated carbons by one-step steam pyrolysis/activation from apricot stones. Microporous and mesoporous materials, 88(1), 126-134.
44. Ioannidou, O., & Zabaniotou, A. (2007). Agricultural residues as precursors for activated carbon production—a review. Renewable and Sustainable Energy Reviews, 11(9), 1966-2005.
45. Li, W., Zhang, L. B., Peng, J. H., Li, N., & Zhu, X. Y. (2008). Preparation of high surface area activated carbons from tobacco stems with K_2CO_3 activation using microwave radiation. Industrial crops and products, 27(3), 341-347.
46. Zhang, T., Walawender, W. P., Fan, L. T., Fan, M., Daugaard, D., & Brown, R. C. (2004). Preparation of activated carbon from forest and agricultural residues through CO_2 activation. Chemical Engineering Journal, 105(1), 53-59.

47. Kopac, T., & Toprak, A. (2007). Preparation of activated carbons from Zonguldak region coals by physical and chemical activations for hydrogen sorption. International Journal of Hydrogen Energy, 32(18), 5005-5014.
48. Bouchelta, C., Medjram, M. S., Bertrand, O., & Bellat, J. P. (2008). Preparation and characterization of activated carbon from date stones by physical activation with steam. Journal of Analytical and Applied Pyrolysis, 82(1), 70-77.
49. Williams, P. T., & Reed, A. R. (2006). Development of activated carbon pore structure via physical and chemical activation of biomass fibre waste. Biomass and bioenergy, 30(2), 144-152.
50. Ucar, S., Erdem, M., Tay, T., & Karagoz, S. (2009). Preparation and characterization of activated carbon produced from pomegranate seeds by $ZnCl_2$ activation. Applied Surface Science, 255(21), 8890-8896.
51. Weitkamp, J., Sing, K. S. W., & Schuth, F. (Eds.). (2002). Handbook of porous solids. Wiley-Vch.
52. San Miguel, G., Fowler, G. D., & Sollars, C. J. (2003). A study of the characteristics of activated carbons produced by steam and carbon dioxide activation of waste tyre rubber. Carbon, 41(5), 1009-1016.
53. Haimour, N. M., & Emeish, S. (2006). Utilization of date stones for production of activated carbon using phosphoric acid. Waste Management, 26(6), 651-660.
54. Franklin, R. E. (1951, October). Crystallite growth in graphitizing and non-graphitizing carbons. In Proceedings of the Royal Society of London A: Mathematical, Physical and Engineering Sciences (Vol. 209, No. 1097, pp. 196-218). The Royal Society.
55. Smísek, M., & Cerny, S. (1970). Active carbon: manufacture, properties and applications (Vol. 12). Elsevier Publishing Company.
56. Standard Test Method for Carbon Black – Morphological Characterization of Carbon Black Using Electron Microscopy" , ASTM International method D 3849 – 04, November 2004
57. Brunauer, S., Emmett, P. H., & Teller, E. (1938). Adsorption of gases in multimolecular layers. Journal of the American chemical society, 60(2), 309-319.
58. Gregg, S. J., Sing, K. S. W., & Salzberg, H. W. (1967). Adsorption surface area and porosity. Journal of the Electrochemical Society, 114(11), 279C-279C.

59. Lastoskie, C., Gubbins, K. E., & Quirke, N. (1993). Pore size distribution analysis of microporous carbons: a density functional theory approach. The journal of physical chemistry, 97(18), 4786-4796

60. Hummel, D. (1962). Identification and analysis of surface-active agents by infrared and chemical methods (Vol. 1). Interscience Publishers.

61. Standard Test Method for Carbon Black – Total and External Surface Area by Nitrogen Adsorption", ASTM International method D 6556 – 04, November 2004

62. Standard Test Method for Carbon Black – Oil Absorption Number (OAN)" , ASTM International method D 2414 – 05, February 2005

63. Okieimen F. E. &Imanah J. E. (2003).The characterization of agricultural waste product as filler in NR formulations. Nigeria journal of polymer science and technology; 3. (1), 178-240

64. Igwe, I. O., & Ejim, A. A. (2011). Studies on mechanical and end-use properties of natural rubber filled with snail shell powder. Materials Sciences and Applications, 2(07), 801.

65. Adeosun, B. F. (2000). Mechanical and Rheological Properties of Natural Rubber Composites Reinforced with Agricultural Waste. Nigerian Journal of Polymer Science and Technology, 1, 58-62.

66. Lopattananon, N., Panawarangkul, K., Sahakaro, K., & Ellis, B. (2006). Performance of pineapple leaf fibre–natural rubber composites: the effect of fiber surface treatments. Journal of Applied Polymer Science, 102(2), 1974-1984.

67. Ismail, H., Mega, L., & Khalil, H. P. S. A. (2001). Effect of a silane coupling agent on the properties of white rice husk ash–polypropylene/natural rubber composites. Polymer International, 50(5), 606-611.

68. Aguele, F. O., Madufor, C. I., & Adekunle, K. F. (2014). Comparative Study of Physical Properties of Polymer Composites Reinforced with Uncarbonised and Carbonised Coir. Open Journal of Polymer Chemistry, 4(03), 73.

69. Onyeagoro, G. N. (2012). Cure characteristics and physico-mechanical properties of carbonized bamboo fibre filled natural rubber vulcanizates. International Journal of Modern Engineering Research (IJMER), 2(6), 4683-4690.

70. Hwang, L. L., Chen, J. C., & Wey, M. Y. (2013). The properties and filtration efficiency of activated carbon polymer composite membranes for the removal of humic acid. Desalination, 313, 166-175.

71. Ugbesia, S. O., Ekebafe, L. O., & Ayo, M. D. (2011). Effect of carbonization temperature of filler on the tensile properties of natural rubber compounds filled with cassava (Manihot esculenta) peel carbon. Pacific Journal of Science and Technology, 12(1), 339-343.

72. Imoisili, P. E., Ukoba, K. O., Adejugbe, I. T., Adgidzi, D., & Olusunle, S. O. O. (2013). Mechanical properties of rice husk/carbon black hybrid natural rubber composite. Chemistry and Materials Research, 3(8), 12-16.

73. Olowoyo, D. N., & Orere, E. E. (2012). Preparation and Characterization of Activated Carbon Made From Palm-Kernel Shell, Coconut Shell, Groundnut Shell and Obeche Wood (Investigation of Apparent Density, Total Ash Content, Moisture Content, Particle Size Distribution Parameters. International Journal of Research in Chemistry and Environment, 7, 32-35.

74. Ismail, A., Sudrajat, H., & Jumbianti, D. (2010). Activated carbon from durian seed by h_3po_4 activation: preparation and pore structure characterization. Indonesian Journal of Chemistry, 10(1), 36-40.

75. Azevedo, D. C., Araujo, J. C. S., Bastos-Neto, M., Torres, A. E. B., Jaguaribe, E. F., & Cavalcante, C. L. (2007). Microporous activated carbon prepared from coconut shells using chemical activation with zinc chloride. Microporous and Mesoporous Materials, 100(1), 361-364.

76. Gomez-de-Salazar, C., Sepulveda-Escribano, A., & Rodrıguez-Reinoso, F. (2000). Preparation of carbon molecular sieves by controlled oxidation treatments. Carbon, 38(13), 1889-1892.

77. Hayashi, J. I., Horikawa, T., Takeda, I., Muroyama, K., & Ani, F. N. (2002). Preparing activated carbon from various nutshells by chemical activation with K_2CO_3. Carbon, 40(13), 2381-2386.

78. Olivares-Marin, M., Fernandez-González, C., Macías-García, A., & Gómez-Serrano, V. (2006). Preparation of activated carbon from cherry stones by chemical activation with $ZnCl_2$. Applied Surface Science, 252(17), 5967-5971.

79. Adinata, D., Daud, W. M. A. W., & Aroua, M. K. (2007). Production of carbon molecular sieves from palm shell based activated carbon by pore sizes

modification with benzene for methane selective separation. Fuel processing technology, 88(6), 599-605.

80. Li, W., Yang, K., Peng, J., Zhang, L., Guo, S., & Xia, H. (2008). Effects of carbonization temperatures on characteristics of porosity in coconut shell chars and activated carbons derived from carbonized coconut shell chars. Industrial Crops and Products, 28(2), 190-198.
81. Chandra, T. C., Mirna, M. M., Sunarso, J., Sudaryanto, Y., & Ismadji, S. (2009). Activated carbon from durian shell: Preparation and characterization. Journal of the Taiwan Institute of Chemical Engineers, 40(4), 457-462.
82. Guo, S., Peng, J., Li, W., Yang, K., Zhang, L., Zhang, S., & Xia, H. (2009). Effects of CO_2 activation on porous structures of coconut shell-based activated carbons. Applied Surface Science, 255(20), 8443-8449.
83. Ahmad, R., & Kumar, R. (2010). Adsorptive removal of Congo red dye from aqueous solution using Bael shell carbon. Applied Surface Science, 257(5), 1628-1633.
84. AlwanNasifJassim, Lina Kareem Amlah, Dhafer FazaAli, Aseel Tami AbdAljabar. (2012). Preparation and Characterization of Activated Carbon from Iraqi Apricot Stones. Canadian Journal on Chemical Engineering & Technology, 3(3).
85. Gottipati, R., & Mishra, S. (2013). Preparation of microporous activated carbon from Aegle marmelos fruit shell by KOH activation. The Canadian Journal of Chemical Engineering, 91(7), 1215-1222.
86. El-Sayed, G. O., Yehia, M. M., & Asaad, A. A. (2014). Assessment of activated carbon prepared from corncob by chemical activation with phosphoric acid. Water Resources and Industry, 7, 66-75.
87. Yavuz, R., Akyildiz, H., Karatepe, N., & Çetinkaya, E. (2010). Influence of preparation conditions on porous structures of olive stone activated by H_3PO_4. Fuel Processing Technology, 91(1), 80-87.
88. Bhushan, B., & Gupta, B. K. (1995). Micromechanical characterization of Ni-P coated aluminium-magnesium, glass, and glass-ceramic substrates and finished magnetic thin-film rigid disks. Advances in Information Storage Systems, 6, 193-208.
89. Archard, J. (1953). Contact and rubbing of flat surfaces. Journal of applied physics, 24(8), 981-988.

90. Bhansali, K. J. (1980). Wear coefficients of hard-surfacing materials. Wear control handbook (eds) MB Peterson and WO Winer (New York: ASME) pp, 373-383.

91. Archard, J. F., & Hirst, W. (1957, January). An examination of a mild wear process. In Proceedings of the Royal Society of London A: Mathematical, Physical and Engineering Sciences (Vol. 238, No. 1215, pp. 515-528). The Royal Society.

92. Hokkirigawa, K. (1997). Wear maps of ceramics. Ceramics Japan, 32, 19-25.

93. Holm, R. (1946), Electric Contact, Almquist and Wiksells, Stockholm, Section 40.

94. Lancaster, J. K. (1978). Wear mechanisms of metals and polymers. Transactions of the Institute of Metal Finishing, 56(4), 145-153.

95. Rabinowicz, E. (1980). Wear coefficients-metals. Wear Control Handbook, 475-506.

96. Lim, S. C., & Ashby, M. F. (1987). Overview no. 55 wear-mechanism maps. Acta metallurgica, 35(1), 1-24.

97. Hokkirigawa, K., & Kato, K. (1988). An experimental and theoretical investigation of ploughing, cutting and wedge formation during abrasive wear. Tribology International, 21(1), 51-57.

98. Burwell, J. T. (1957). Survey of possible wear mechanisms. Wear, 1(2), 119-141.

99. Stokes, J. (2008). Theory and application of the high velocity oxy-fuel (HVOF), Thermal spray process. Dublin City University. ISBN 1-87232-753-2, ISSN 1649-8232.

100. Benedict, G. H. (1968). Correlation of Disk Machines and Gear Tests. Lubrication Engineering, 24(12), 591.

101. Yahagi, Y., & Mizutani, Y. (1984). Corrosive wear of steel in gasoline-ethanol-water mixtures. Wear, 97(1), 17-25.

102. Yahagi, Y., Nagasawa, Y., Hotta, S., & Mizutani, Y. (1986). Corrosive wear of cast iron under reciprocating lubrication (No. 861599). SAE Technical Paper.

103. Rengstorff, G. W., Miyoshi, K., & Buckley, D. H. (1986). Interaction of sulphuric acid corrosion and mechanical wear of iron. ASLE transactions, 29(1), 43-51.

104. Harmsen, P. F. H., Huijgen, W., Bermudez, L., & Bakker, R. (2010). Literature review of physical and chemical pre-treatment processes for lignocellulosic biomass.

105. Raju, G. U., & Kumarappa, S. (2011). Experimental study on mechanical properties of groundnut shell particle-reinforced epoxy composites. Journal of Reinforced Plastics and Composites, 30(12), 1029-1037.

106. Jacob, M., Thomas, S., & Varughese, K. T. (2004). Mechanical properties of sisal/oil palm hybrid fibre reinforced natural rubber composites. Composites Science and Technology, 64(7), 955-965.

107. Swamy, R. P., Kumar, G. M., Vrushabhendrappa, Y., & Joseph, V. (2004). Study of areca-reinforced phenol formaldehyde composites. Journal of reinforced plastics and composites, 23(13), 1373-1382.

108. Raveendran, K., Ganesh, A., & Khilar, K. C. (1995). Influence of mineral matter on biomass pyrolysis characteristics. Fuel, 74(12), 1812-1822.

109. Lu, J. Z., Wu, Q., Negulescu, I. I., & Chen, Y. (2006). The influences of fibre feature and polymer melt index on mechanical properties of sugarcane fiber/polymer composites. Journal of applied polymer science, 102(6), 5607-5619.

110. Mohanty, A. K., Misra, M., & Hinrichsen, G. (2000). Bio fibres, biodegradable polymers and bio composites: an overview. Macromolecular materials and Engineering, 276(1), 1-24.

111. Singh, U., Kochhar, A., & Boora, R. (2012). Proximate composition, available carbohydrates, Dietary Fibres and Anti-Nutritional factors in Bael (Aegle marmelos L.) Leaf, Pulp and Seed Powder. International Journal of Scientific and Research Publications.

112. Anusha, G. (2011). The removal of iron from wastewater using wood apple shell as adsorbent. In Second International Conference on Environmental Science and Technology IPCBEE (Vol. 6).

113. Anandkumar, J., & Mandal, B. (2009). Removal of Cr (VI) from aqueous solution using Bael fruit (Aegle marmelos correa) shell as an adsorbent. Journal of hazardous materials, 168(2), 633-640.

114. Heschel, W., & Klose, E. (1995). On the suitability of agricultural by-products for the manufacture of granular activated carbon. Fuel, 74(12), 1786-1791.

115. Kirubakaran, C. J., Krishnaiah, K., & Seshadri, S. K. (1991). Experimental study of the production of activated carbon from coconut shells in a fluidized bed reactor. Industrial & engineering chemistry research, 30(11), 2411-2416.

116. Su, W., Zhou, L., & Zhou, Y. (2003). Preparation of microporous activated carbon from coconut shells without activating agents. Carbon, 41(4), 861-863.

117. Samantrai, S. P., Raghavendra, G., & Acharya, S. K. (2014). Effect of carbonization temperature and fibre content on the abrasive wear of rice husk char reinforced epoxy composite. Proceedings of the Institution of Mechanical Engineers, Part J: Journal of Engineering Tribology, 228(4), 463-469.

118. Fu, S. Y., Feng, X. Q., Lauke, B., & Mai, Y. W. (2008). Effects of particle size, particle/matrix interface adhesion and particle loading on mechanical properties of particulate–polymer composites. Composites Part B: Engineering, 39(6), 933-961.

119. Demirbas, A. (2004). Combustion characteristics of different biomass fuels. Progress in energy and combustion science, 30(2), 219-230.

120. Khalil, R. A., Meszaros, E., Gronli, M. G., Varhegyi, G., Mohai, I., Marosvolgyi, B., & Hustad, J. E. (2008). Thermal analysis of energy crops: Part I: The applicability of a macro-thermobalance for biomass studies. Journal of Analytical and Applied Pyrolysis, 81(1), 52-59.

121. Nunn, T. R., Howard, J. B., Longwell, J. P., & Peters, W. A. (1985). Product compositions and kinetics in the rapid pyrolysis of sweet gum hard wood. Industrial & Engineering Chemistry Process Design and Development, 24(3), 836-844.

122. Zeriouh, A., & Belkbir, L. (1995). Thermal decomposition of a Moroccan wood under a nitrogen atmosphere. Thermochimica acta, 258, 243-248.

123. Fisher, T., Hajaligol, M., Waymack, B., Kellog, D., 2002. Pyrolysis behavior and kinetics of biomass derived materials. J. Anal. Appl. Pyrolysis 62, 331–349.

124. Bowen, P. (2002). Particle size distribution measurement from millimeters to nanometers and from rods to platelets. Journal of Dispersion Science and Technology, 23(5), 631-662.

125. Agarwal, B. D., Broutman, L. J., & Chandrashekhara, K. (2006). Analysis and performance of fiber composites. John Wiley & Sons.

126. Sarki, J., Hassan, S. B., Aigbodion, V. S., & Oghenevweta, J. E. (2011). Potential of using coconut shell particle fillers in eco-composite materials. Journal of alloys and compounds, 509(5), 2381-2385.

127. Park, S., Baker, J. O., Himmel, M. E., Parilla, P. A., & Johnson, D. K. (2010). Research cellulose crystallinity index: measurement techniques and their impact on interpreting cellulase performance. Biotechnol Biofuels, 3(10).

128. Emmerich, F. G., De Sousa, J. C., Torriani, I. L., & Luengo, C. A. (1987). Applications of a granular model and percolation theory to the electrical resistivity of heat treated endocarp of babassu nut. Carbon, 25(3), 417-424.

129. Lua, A. C., & Yang, T. (2004). Effect of activation temperature on the textural and chemical properties of potassium hydroxide activated carbon prepared from pistachio-nut shell. Journal of colloid and interface science, 274(2), 594-601.

130. Kumar, M., & Gupta, R. C. (1994). Influence of carbonization conditions and wood species on carbon dioxide reactivity of resultant wood char powder. Fuel processing technology, 38(3), 223-233.

131. Tongpoothorn, W., Sriuttha, M., Homchan, P., Chanthai, S., & Ruangviriyachai, C. (2011). Preparation of activated carbon derived from Jatropha curcas fruit shell by simple thermo-chemical activation and characterization of their physico-chemical properties. Chemical Engineering Research and Design, 89(3), 335-340.

132. Zhao, J., Yang, L., Li, F., Yu, R., & Jin, C. (2009). Structural evolution in the graphitization process of activated carbon by high-pressure sintering. Carbon, 47(3), 744-751.

133. Malik, R., Ramteke, D. S., & Wate, S. R. (2006). Physico-chemical and surface characterization of adsorbent prepared from groundnut shell by $ZnCl_2$ activation and its ability to absorb colour. Indian journal of chemical Technology, 13(4), 319.

134. Jang, B. Z. (1994). Advanced polymer composites: principles and applications.ASM International, Materials Park, OH 44073-0002, USA, 1994. 305.

135. Pukanszky, B. (1995). Particulate filled polypropylene: structure and properties. In Polypropylene structure, blends and composites (pp. 1-70). Springer Netherlands.

136. Acosta, J. L., Morales, E., Ojeda, M. C., & Linares, A. (1986). Effect of addition of sepiolite on the mechanical properties of glass fibre reinforced polypropylene. Die Angewandte Makromolekulare Chemie, 138(1), 103-110.

137. Garcia, R., Evans, R. E., & Palmer, R. J. (1987). Structural property improvements through hybridized composites. Toughened Composites, ASTM STP, 937, 397-412.

138. Garcia, R. (1983). Methods of Improving the Matrix Dominated Performance of Composite Structures: A Technical Review (No. NADC-83058-60). Naval Air Development Centre Warminster Pa Aircraft and Crew Systems Technology Directorate.

139. Jang, B. Z., & Lin, T. L. (1989). Mechanical Behavior of Hybrid Composites Containing both Short and Continuous Fibers. In Annual Technical Conf. ANTEC (Vol. 35, pp. 1552-1557).

140. Liau, J. Y., Jang, B. Z., Hwang, L. R. and Wilcox, R. C. (1988). Toughening Composites by Matrix. Modification, Plastics Engineering, 44: 33–37.

141. Sawyer, W. G., Freudenberg, K. D., Bhimaraj, P., & Schadler, L. S. (2003). A study on the friction and wear behaviour of PTFE filled with alumina nanoparticles. Wear, 254(5), 573-580.

142. Kim, J. I., Kang, P. H., & Nho, Y. C. (2004). Positive temperature coefficient behavior of polymer composites having a high melting temperature. Journal of Applied Polymer Science, 92(1), 394-401.

143. Nikkeshi, S., Kudo, M., & Masuko, T. (1998). Dynamic viscoelastic properties and thermal properties of Ni powder–epoxy resin composites. Journal of Applied Polymer Science, 69(13), 2593-2598.

144. Zhu, K., & Schmauder, S. (2003). Prediction of the failure properties of short fiber reinforced composites with metal and polymer matrix. Computational Materials Science, 28(3), 743-748.

145. Rusu, M., Sofian, N., & Rusu, D. (2001). Mechanical and thermal properties of zinc powder filled high density polyethylene composites. Polymer Testing, 20(4), 409-417.

146. Tavman, I. H. (1997). Thermal and mechanical properties of copper powder filled poly (ethylene) composites. Powder Technology, 91(1), 63-67.

147. Rothon, R. N. (1997). Mineral Fillers in Thermoplastics: Filler Manufacture. Journal of Adhesion, 64, 87–109.

148. Rothon, R. N. (1999). Effects of Particulate Fillers on Flame Retardant Properties of Composites. Advanced Polymer Science, 139, 67–107.

149. Wambua, P., Ivens, J., & Verpoest, I. (2003). Natural fibres: can they replace glass in fibre reinforced plastics? Composites science and technology, 63(9), 1259-1264.

150. Rabinowicz, E. (1995). Friction and wear of materials. New York, John Wiley and Sons.

151. Hsu, D. T., Kim, H. K., Shi, F. G., Tong, H. Y., Chungpaiboonpatana, S., Davidson, C., & Adams, J. M. (2000). Curing kinetics and optimal cure schedules for under fill materials. Microelectronics journal, 31(4), 271-275.

152. Fu, S. Y., Feng, X. Q., Lauke, B., & Mai, Y. W. (2008). Effects of particle size, particle/matrix interface adhesion and particle loading on mechanical properties of particulate–polymer composites. Composites Part B: Engineering, 39(6), 933-961.

153. Popa, M., Arnautu, M., & Davydov, Y. (2002). The interface in polymer matrix composites. Handbook of Polymer Blends and Composites. AK Kulshreshtha and C. Vasile, Eds., Rapra Techno, UK.

154. Rampe, M. J., Setiaji, B., Trisunaryanti, W., & Triyono, T. (2011). Fabrication and characterization of carbon composite from coconut shell carbon. Indonesian Journal of Chemistry, 11(2), 124-130.

155. Rashid, E. S. A., Ariffin, K., Kooi, C. C., & Akil, H. M. (2009). Preparation and properties of POSS/epoxy composites for electronic packaging applications. Materials & Design, 30(1), 1-8.

156. Jia, Q. M., Zheng, M., Xu, C. Z., & Chen, H. X. (2006). The mechanical properties and tribological behaviour of epoxy resin composites modified by different shape nanofillers. Polymers for advanced technologies, 17(3), 168-173.

157. Xing, X. S., & Li, R. K. Y. (2004). Wear behaviour of epoxy matrix composites filled with uniform sized sub-micron spherical silica particles. Wear, 256(1), 21-26

158. Wetzel, B., Haupert, F., & Zhang, M. Q. (2003). Epoxy nanocomposites with high mechanical and tribological performance. Composites Science and Technology, 63(14), 2055-2067.

159. Krzesinska, M., Zachariasz, J., & Lachowski, A. I. (2008). Eco-composite developed using biomorphous stiff skeleton of carbonised yucca and furfuryl alcohol as filler. Journal of Materials Science, 43(17), 5763-5771.

160. Dandekar, M. S., Arabale, G., & Vijayamohanan, K. (2005). Preparation and characterization of composite electrodes of coconut-shell-based activated carbon and hydrous ruthenium oxide for supercapacitors. Journal of power sources, 141(1), 198-203.

161. Kim, Y. J., Lee, B. J., Suezaki, H., Chino, T., Abe, Y., Yanagiura, T., & Endo, M. (2006). Preparation and characterization of bamboo-based activated carbons as electrode materials for electric double layer capacitors. Carbon, 44(8), 1592-1595.

162. Agarwal, B. D., Broutman, L. J., & Chandrashekhara, K. (2006). Analysis and performance of fiber composites. John Wiley & Sons.

163. Sudheer, M., Subbaya, K. M., Jawali, D., & Bhat, T. (2012). Mechanical Properties of Potassium Titanate Whisker Reinforced Epoxy Resin Composites. Journal of Minerals and Materials Characterization and Engineering, 11(02), 193.

164. Mallick, P. K. (2007). Fibre-reinforced composites: materials, manufacturing, and design. CRC press.

165. Imanah, J. E., & Okieimen, F. E. (2003). Rheological and mechanical properties of natural rubber reinforced with agricultural by-product. Journal of applied polymer science, 90(13), 3718-3722.

166. Joseph, K., Varghese, S., Kalaprasad, G., Thomas, S., Prasannakumari, L., Koshy, P., & Pavithran, C. (1996). Influence of interfacial adhesion on the mechanical properties and fracture behaviour of short sisal fibre reinforced polymer composites. European Polymer Journal, 32(10), 1243-1250.

167. Pothan, L. A., Thomas, S., & Groeninckx, G. (2006). The role of fibre/matrix interactions on the dynamic mechanical properties of chemically modified banana fibre/polyester composites. Composites Part A: Applied Science and Manufacturing, 37(9), 1260-1269.

168. Ojha, S., Acharya, S. K., & Raghavendra, G. (2014). A novel approach to utilize waste carbon as reinforcement in thermoset composite. Proceedings of the Institution of Mechanical Engineers, Part E: Journal of Process Mechanical Engineering, 0954408914547118.

169. Ibrahim, M. S., Sapuan, S. M., & Faieza, A. A. Mechanical and Thermal Properties of Composites From Unsaturated Polyester Filled With Oil Palm Ash. Journal of Mechanical Engineering and Sciences, 2, 133-147.

170. Ismail, H., Edyham, M. R., & Wirjosentono, B. (2002). Bamboo fibre filled natural rubber composites: the effects of filler loading and bonding agent. Polymer testing, 21(2), 139-144.

171. Yao W and Li Z. Flexural behaviour of bamboo-fibre reinforced mortar laminates. Cement and Concrete Research 2003; 33(1): 15–19.

172. Lee, N. J., & Jang, J. (1999). The effect of fibre content on the mechanical properties of glass fibre mat/polypropylene composites. Composites Part A: Applied Science and Manufacturing, 30(6), 815-822.

173. Bhushan, B. (2013). Principles and applications of tribology. John Wiley & Sons.

174. Ivusic, V. (1998). Hrvatsko drustvo za materijale i tribologiju.

175. Rabinowicz, E. (1965). Friction and wear of materials.

176. Brostow, W., Deborde, J. L., Jaclewicz, M., & Olszynski, P. (2003). Tribology with emphasis on polymers: friction, scratch resistance and wear. Journal of Materials Education, 25(4/6), 119-132.

177. Kivikyto-Reponen, P. (2006). Correlation of material characteristics and wear of powder metallurgical metal matrix composites. Helsinki University of Technology.

178. Biswas, S., Satapathy, A., & Patnaik, A. (2009). Erosion wear behaviour of polymer composites: a review. Journal of Reinforced Plastics and Composites.

179. Drensky, G., Hamed, A., Tabakoff, W., & Abot, J. (2011). Experimental investigation of polymer matrix reinforced composite erosion characteristics.Wear, 270(3), 146-151.

180. Mahapatra, S. S., & Patnaik, A. (2009). Study on mechanical and erosion wear behavior of hybrid composites using Taguchi experimental design. Materials & Design, 30(8), 2791-2801.

181. Wahl H, Hartenstein F. (1946). Strahlverschleiss, rankhscheVerlagshandlung, Stuttgart

182. T.H. Tsiang. (1986). Journal of Composite Technology and Research 8(4) 154.

183. Tilly, G. P., & Sage, W. (1970). The interaction of particle and material behaviour in erosion processes. Wear, 16(6), 447-465.

184. Pool, K. V., Dharan, C. K. H., & Finnie, I. (1986). Erosive wear of composite materials. Wear, 107(1), 1-12.

185. Smeltzer, C. E., Gulden, M. E., & Compton, W. A. (1970). Mechanisms of metal removal by impacting dust particles. Journal of Fluids Engineering, 92(3), 639-652.

186. Guadagnoa, L., Vertuccioa, L., Sorrentinoa, A., Raimondoa, M., Naddeoa, C., Vittoriaa,V., (2009). Mechanical and barrier properties of epoxy resin filled with multi-walled carbon nanotubes. Carbon, 47(10), 2419-2430.

187. McIntyre, S., Kaltzakorta, I., Liggat, J. J., Pethrick, R. A., & Rhoney, I. (2005). Influence of the epoxy structure on the physical properties of epoxy resin nanocomposites. Industrial & engineering chemistry research, 44(23), 8573-8579

188. Kulkarni, S. M. (2001). Influence of matrix modification on the solid particle erosion of glass/epoxy composites. Polymers & polymer composites, 9(1), 25-30.

189. Aglan, H. A., & Chenock, T. A. (1993). Erosion damage features of polyimide thermoset composites. SAMPE quarterly, 24(2), 41-47.

190. Barkoula, N. M., & Karger-Kocsis, J. (2002). Review processes and influencing parameters of the solid particle erosion of polymers and their composites.Journal of materials science, 37(18), 3807-3820.

191. Bitter, J. G. A. (1963). A study of erosion phenomena: Part II. Wear, 6(3), 169-190.

192. Hutchings, I. M., Winter, R. E., & Field, J. E. (1976, March). Solid particle erosion of metals: the removal of surface material by spherical projectiles. InProceedings of the Royal Society of London A: Mathematical, Physical and Engineering Sciences (Vol. 348, No. 1654, pp. 379-392). The Royal Society.

193. Stachowiak, G. W., Batchelor, A. W., & Stolarski, T. A. (1994). Engineering tribology: Elsevier, 1993, ISBN 0-444-89235-4, pp 960.

194. Barkoula, N. M., & Karger-Kocsis, J. (2002). Solid particle erosion of unidirectional GF reinforced EP composites with different fibre/matrix adhesion.Journal of reinforced plastics and composites, 21(15), 1377-1388.

195. Yousif, B. F., & El-Tayeb, N. S. M. (2008). Adhesive wear performance of T-OPRP and UT-OPRP composites. Tribology letters, 32(3), 199-208.

196. Chand, N., & Dwivedi, U. K. (2006). Effect of coupling agent on abrasive wear behaviour of chopped jute fibre-reinforced polypropylene composites. Wear, 261(10), 1057-1063.

197. Yousif, B. F., Lau, S. T., & McWilliam, S. (2010). Polyester composite based on betelnut fibre for tribological applications. Tribology international, 43(1), 503-511.

198. Nirmal, U., Hashim, J., & Low, K. O. (2012). Adhesive wear and frictional performance of bamboo fibres reinforced epoxy composite. Tribology International, 47, 122-133.

199. Chin, C. W., & Yousif, B. F. (2009). Potential of kenaf fibres as reinforcement for tribological applications. Wear, 267(9), 1550-1557.

200. Patnaik, A., Satapathy, A., Chand, N., Barkoula, N. M., & Biswas, S. (2010). Solid particle erosion wear characteristics of fibre and particulate filled polymer composites: A review. Wear, 268(1), 249-263.

201. Arjula, S., & Harsha, A. P. (2006). Study of erosion efficiency of polymers and polymer composites. Polymer testing, 25(2), 188-196.

202. Mohanty, J. R., Das, S. N., Das, H. C., Mahanta, T. K., & Ghadei, S. B. (2014). Solid particle erosion of date palm leaf fibre reinforced polyvinyl alcohol composites. Advances in Tribology, 2014.

203. Mishra, P., & Acharya, S. K. (2010). Anisotropy abrasive wear behaviour of bagasse fibre reinforced polymer composite. International Journal of Engineering, Science and Technology, 2(11).

204. Deo, C., & Acharya, S. K. (2009). Solid particle erosion of lantana camaranfibre-reinforced polymer matrix composite. Polymer-Plastics Technology and Engineering, 48(10), 1084-1087.

205. Ruff, A. W., & Ives, L. K. (1975). Measurement of solid particle velocity in erosive wear. Wear, 35(1), 195-199.

206. Sundararajan, G., Roy, M., & Venkataraman, B. (1990). Erosion efficiency-a new parameter to characterize the dominant erosion micromechanism. Wear,140(2), 369-381.

207. Rout, A. K., & Satapathy, A. (2012). Study on mechanical and tribo-performance of rice-husk filled glass–epoxy hybrid composites. Materials & Design, 41, 131-141.

208. Harsha, A. P., & Thakre, A. A. (2007). Investigation on solid particle erosion behaviour of polyetherimide and its composites. Wear, 262(7), 807-818

209. Roy, M., Vishwanathan, B., & Sundararajan, G. (1994). The solid particle erosion of polymer matrix composites. Wear, 171(1), 149-161.

210. Srivastava, V. K., & Pawar, A. G. (2006). Solid particle erosion of glass fibre reinforced fly ash filled epoxy resin composites. Composites Science and Technology, 66(15), 3021-3028.

211. Cantwell, W. J., & Morton, J. (1991). The impact resistance of composite materials—a review. composites, 22(5), 347-362.

212. Edie, D. D. (1998). The effect of processing on the structure and properties of carbon fibers. Carbon, 36(4), 345-362.

213. Luo, X., & Chung, D. D. L. (2001). Carbon-fiber/polymer-matrix composites as capacitors. Composites science and technology, 61(6), 885-888.

214. Bandosz, T. J. (2006). Activated carbon surfaces in environmental remediation (Vol. 7). Academic Press.

215. Adinata, D., Daud, W. M. A. W., & Aroua, M. K. (2007). Preparation and characterization of activated carbon from palm shell by chemical activation with K 2 CO 3. Bioresource Technology, 98(1), 145-149.

216. Ahmad, A. L., Loh, M. M., & Aziz, J. A. (2007). Preparation and characterization of activated carbon from oil palm wood and its evaluation on methylene blue adsorption. Dyes and Pigments, 75(2), 263-272.

217. Marsh, H., & Reinoso, F. R. (2006). Activated carbon. Elsevier.

218. Asakura, R., Morita, M., Maruyama, K., Hatori, H., & Yamada, Y. (2004). Preparation of fibrous activated carbons from wood fiber. Journal of materials science, 39(1), 201-206.

219. Chattopadhyaya, G., Macdonald, D. G., Bakhshi, N. N., Mohammadzadeh, J. S. S., & Dalai, A. K. (2006). Preparation and characterization of chars and activated carbons from Saskatchewan lignite. Fuel processing technology, 87(11), 997-1006.

220. Toles, C., Rimmer, S., & Hower, J. C. (1996). Production of activated carbons from a Washington lignite using phosphoric acid activation. Carbon, 34(11), 1419-1426.

221. Daud, W. M. A. W., & Ali, W. S. W. (2004). Comparison on pore development of activated carbon produced from palm shell and coconut shell. Bioresource Technology, 93(1), 63-69.

222. Cazetta, A. L., Vargas, A. M., Nogami, E. M., Kunita, M. H., Guilherme, M. R., Martins, A. C Tais L. Silva, Juliana CG Moraes, and Almeida, V. C. (2011). NaOH-activated carbon of high surface area produced from coconut shell: Kinetics and equilibrium studies from the methylene blue adsorption. Chemical Engineering Journal, 174(1), 117-125.

223. Hameed, B. H., Tan, I. A. W., & Ahmad, A. L. (2008). Adsorption isotherm, kinetic modeling and mechanism of 2, 4, 6-trichlorophenol on coconut husk-based activated carbon. Chemical Engineering Journal, 144(2), 235-244.

224. Li, W., Yang, K., Peng, J., Zhang, L., Guo, S., & Xia, H. (2008). Effects of carbonization temperatures on characteristics of porosity in coconut shell chars and activated carbons derived from carbonized coconut shell chars. Industrial Crops and Products, 28(2), 190-198.

225. Yang, K., Peng, J., Srinivasakannan, C., Zhang, L., Xia, H., & Duan, X. (2010). Preparation of high surface area activated carbon from coconut shells using microwave heating. Bioresource technology, 101(15), 6163-6169.

226. Donald, J., Ohtsuka, Y., & Xu, C. C. (2011). Effects of activation agents and intrinsic minerals on pore development in activated carbons derived from a Canadian peat. Materials Letters, 65(4), 744-747.

227. Fuchsman, C. (2012). Peat: industrial chemistry and technology. Elsevier.

228. Veksha, A., Sasaoka, E., & Uddin, M. A. (2009). The influence of porosity and surface oxygen groups of peat-based activated carbons on benzene adsorption from dry and humid air. Carbon, 47(10), 2371-2378.

229. Okutucu, C., Duman, G., Ucar, S., Yasa, I., & Yanik, J. (2011). Production of fungicidal oil and activated carbon from pistachio shell. Journal of Analytical and Applied Pyrolysis, 91(1), 140-146.

230. Yang, J., & Qiu, K. (2010). Preparation of activated carbons from walnut shells via vacuum chemical activation and their application for methylene blue removal. Chemical Engineering Journal, 165(1), 209-217.

231. Pereira, M. F. R., Soares, S. F., Órfão, J. J., & Figueiredo, J. L. (2003). Adsorption of dyes on activated carbons: influence of surface chemical groups. Carbon, 41(4), 811-821.

232. Mohan, D., Sarswat, A., Singh, V. K., Alexandre-Franco, M., & Pittman, C. U. (2011). Development of magnetic activated carbon from almond shells for trinitrophenol removal from water. Chemical Engineering Journal, 172(2), 1111-1125.

233. Klasson, K. T., Ledbetter, C. A., Wartelle, L. H., & Lingle, S. E. (2010). Feasibility of dibromochloropropane (DBCP) and trichloroethylene (TCE) adsorption onto activated carbons made from nut shells of different almond varieties. Industrial Crops and Products, 31(2), 261-265.

234. Strezov, V., Patterson, M., Zymla, V., Fisher, K., Evans, T. J., & Nelson, P. F. (2007). Fundamental aspects of biomass carbonisation. Journal of analytical and applied pyrolysis, 79(1), 91-100.

235. El Qada, E. N., Allen, S. J., & Walker, G. M. (2006). Adsorption of methylene blue onto activated carbon produced from steam activated bituminous coal: a study of equilibrium adsorption isotherm. Chemical Engineering Journal, 124(1), 103-110.

236. Linares-Solano, A., Martín-Gullon, I., de Lecea, C. S. M., & Serrano-Talavera, B. (2000). Activated carbons from bituminous coal: effect of mineral matter content. Fuel, 79(6), 635-643.

237. Mochida, I., Kuroda, K., Kawano, S., Matsumura, Y., & Yoshikawa, M. (1997). Kinetic study of the continuous removal of SO x on polyacrylonitrile-based activated carbon fibres: 1. Catalytic activity of PAN-ACF heat-treated at 800° C. Fuel, 76(6), 533-536.

238. Knop, A., & Pilato, L. A. (2013). Phenolic resins: chemistry, applications and performance. Springer Science & Business Media.

239. Dandekar, M. S., Arabale, G., & Vijayamohanan, K. (2005). Preparation and characterization of composite electrodes of coconut-shell-based activated carbon and hydrous ruthenium oxide for supercapacitors. Journal of power sources, 141(1), 198-203.

240. Lin, G. F., Jiang, J. C., Wu, K. J., & Sun, K. (2014). Preparation and characterization of bamboo-based activated carbon by phosphoric acid activation. Carbon, 70, 321.

241. Harsha, A. P., Tewari, U. S., & Venkatraman, B. (2003). Solid particle erosion behaviour of various polyaryletherketone composites. Wear, 254(7), 693-712.

242. Tewari, U. S., Harsha, A. P., Häger, A. M., & Friedrich, K. (2003). Solid particle erosion of carbon fibre–and glass fibre–epoxy composites. Composites Science and Technology, 63(3), 549-557.

243. Tewari, U. S., Harsha, A. P., Häger, A. M., & Friedrich, K. (2002). Solid particle erosion of unidirectional carbon fibre reinforced polyetheretherketone composites. Wear, 252(11), 992-1000.

244. Rattan, R., & Bijwe, J. (2007). Influence of impingement angle on solid particle erosion of carbon fabric reinforced polyetherimide composite. Wear, 262(5), 568-574.

PUBLICATIONS

International journal

1. Ojha, S., Raghavendra, G., & Acharya, S. K. (2014). **A comparative investigation of bio waste filler (wood apple-coconut) reinforced polymer composites**. Polymer Composites, 35(1), 180-185.**(SCI)** (Impact factor: 1.632).

2. Shakuntala, O., Raghavendra, G., & Samir Kumar, A. (2014). **Effect of filler loading on mechanical and tribological Properties of wood apple shell reinforced epoxy composite.** Advances in Materials Science and Engineering, 2014. DOI:10.1155/2014/538651. **(SCI)** (Impact factor: 0.744).

3. Ojha, S., Acharya, S. K., & Raghavendra, G. (2015). **Mechanical properties of natural carbon black reinforced polymer composites**. Journal of Applied Polymer Science, 132(1). **(SCI)** (Impact factor: 1.64).

4. Ojha, S., Acharya, S. K., & Raghavendra, G. (2014). **A novel approach to utilize waste carbon as reinforcement in thermoset composite**. Proceedings of the Institution of Mechanical Engineers, Part E: Journal of Process Mechanical Engineering, 0954408914547118.**(SCI)** (Impact factor: 0.772).

5. Ojha, S., Acharya, S. K., & Raghavendra, G. (2014). **An investigation in to the erosive wear performance of reinforced carbonized coconut shell powder in polymer composites using taguchi approach.** International Journal of Systems, Algorithms & Applications (IJSAA), Volume 2, 2012, pp 77-80.

6. Ojha, S., Acharya, S. K., & Raghavendra, G. (2014). **Fabrication and study of mechanical properties of coconut raw and carbon black reinforced epoxy composite.** International Journal of Systems, Algorithms & Applications (IJSAA), Volume 2, 2012, pp 68-71.

7. Ojha, S., Acharya, S. K., & Gujjala, R. (2014). **Characterization and Wear behavior of carbon black filled polymer composites**. Procedia Materials Science, 6, 468-475.

8. Raghavendra, G., Ojha, S., Acharya, S. K., & Deo, C. R. (2012). **Studying the Parameters of the Solid Particle Erosion and Test Procedure.** Caspian Journal of Applied Sciences Research, 1(13). pp. 176-181.

Article

1. Ojha, S., Acharya, S. K., & Gujjala, R. **Wood apple shell particulates reinforce epoxy composites.**Society of plastic research online. 10, 1002/spepro.005178.

International/ National Conferences:

1. **Ojha, S.,** Acharya, S. K., and Gujjala, R. (2012). **An investigation in to the erosive wear performance of reinforced carburized coconut shell powder in polymer composites using taguchi approach**. International conference on applied science and Engineering (ICASE). July 30th, Taj Deccan, Hyderabad, INDIA.

2. Ojha, S., Acharya, S. K., and Gujjala, R. (2012). **Fabrication and study of mechanical properties of coconut raw and carbon black reinforced epoxy composite.** (ICRASE). November 30th, Taj Deccan, Hyderabad, INDIA.

3. Ojha, S., Acharya, S. K., and Gujjala, R. (2013).**Morphological and mechanical properties of bio waste coconut/bael shell polymer composite**. 7th International Symposium on Feedstock Recycling of Polymeric Materials (7th ISFR), 23th-26th October, New Delhi.

4. Ojha, S., Acharya, S. K., and Gujjala, R. (2013). **Potential of bio waste fibers (coconut-wood apple) reinforcement with polymer composite.** Proceedings of STME-2013 International Conference on Smart Technologies for Mechanical Engineering 25th -26th OCT, New Delhi.

5. Ojha, S., Acharya, S. K., and Gujjala, R. (2014). **A comparative study on erosion wear behavior of bio waste reinforced polymer matrix composites**. ASIATRIB 2014. 17th-20th.

6. Ojha, S., Acharya, S. K., and Gujjala, R. (2014). **Effect on mechanical properties of cocosnucifera shell particles filler polymer composite**. OPJIT, International Conference on Metallurgical & Materials Processes, Products and Applications. January 8th-10th, Raipur.

7. Ojha, S., Acharya, S. K., and Gujjala, R. (2014). **Characterization and wear behavior of carbon black filled polymer composites**.3rd International Conference on Materials Processing and Characterization (ICMPC 2014). 8th-10th March.

National Conferences

1) Ojha, **S.,** Acharya, S. K., and Gujjala, R. (2013). **Tribo potential of coconut shell reinforced epoxy composites.** ENMEA-2013. January 19th-20th, VSSUT, BURLA, ODISHA, INDIA. pp 86

BIBLIOGRAPHY

Mrs. SHAKUNTALA OJHA is a research scholar in the Department of Mechanical Engineering, National Institute of Technology Rourkela (NITR), Rourkela, Odisha India-769008. She has 4 years of research and two year of teaching experience in her field. She did M.E. (Res) in Mechanical Engineering from NIT Rourkela. This dissertation is being submitted for the fulfillment the Ph.D. degree.

The contact address is:

Address:-

C/o Dr. Gujjala Raghavendra
Door no. 8/888/8
Jayanagar colony,
Kalyandurg-515761, Anantapur (D)
Andhra Pradesh.
E mail: Shaku30@gmail.com
Phone: 08093325500(M), 9985803317